When the glacier left the volcano: Behaviour and fate of glaciovolcanic glass in different planetary environments

de Vet, S.J.

Publication date
2013

Document Version
Final published version

Science of fire and ice

Volcano-ice interactions and associated landforms have been studied in Iceland since 1900 and this research gained a new dimension after similar landforms were observed in 1979 on planet Mars. Our current understanding of a volcano's response to the overlying ice mass shows that these eruptions are governed by complex processes that affect the properties of glassy eruption products. Recent observations on Mars show that these types of materials are highly abundant. The aim of this dissertation is to fill gaps in our knowledge of physical erosion properties and transport thresholds of these 'glaciovolcanic glasses'. By combining field and laboratory studies of Icelandic volcanic glass, wind tunnel experiments under low atmospheric pressures and using observations from the Mars Exploration Rovers it becomes possible to determine the fate of these materials in the present-day Martian surface environment.

2013 WHEN THE GLACIER LEFT THE VOLCANO Sebastiaan John de Vet

WHEN THE GLACIER LEFT THE VOLCANO

Behaviour and fate of glaciovolcanic glass in different planetary environments

Sebastiaan John de Vet

When the glacier left the volcano

Behaviour and fate of glaciovolcanic glass in different planetary environments

When the glacier left the volcano

Behaviour and fate of glaciovolcanic glass
in different planetary environments

ACADEMISCH PROEFSCHRIFT

Ter verkrijging van de graad van doctor
aan de Universiteit van Amsterdam
op gezag van de Rector Magnificus
prof. dr. D.C. van den Boom
ten overstaan van een door het college voor promoties ingestelde
commissie, in het openbaar te verdedigen in de Agnietenkapel
op donderdag 27 juni 2013, te 16:00 uur

door

Sebastiaan John de Vet

geboren te Maarssen

Promotiecommissie:

Promotor:	prof. dr. K.Kalbitz
Co-promotor:	dr. L.H. Cammeraat
Overige leden:	prof. dr. ir. W. Bouten
	prof. dr. Ó. Arnalds
	prof. dr. H.F. Henrichs
	prof. dr. W. van Westrenen
	dr. ir. J.H. van Boxel

Faculteit der Natuurwetenschappen, Wiskunde en Informatica

This research was carried out at the Institute for Biodiversity and Ecosystem Dynamics (IBED), Faculty of Science, University of Amsterdam (Amsterdam, The Netherlands).

ISBN: 978-94-91407-11-6 (soft cover)

Available as pdf via the Universiteitsbibliotheek Amsterdam at dare.uva.nl/record/445790

Table of Contents

Wat is wetenschap? Wetenschap is de titanische poging van het menselijk intellect zich uit zijn kosmische isolement te verlossen door te begrijpen.

Willem Frederik Hermans (1921-1995)

physical geographer from the University of Amsterdam and one of three most notable post-WOII writers in The Netherlands. Excerpt from the novel 'Nooit meer slapen' (Beyond sleep) that narrates the ordeals of a PhD student in geology that is trying to find evidence for impact craters in Norway.

What is science? Science is the titanic effort of the human intellect to redeem its cosmic isolation through understanding.

▲ *Glacial ice and volcanic sands meet at the beach near the iceberg lake Jökullsárlón in South-West Iceland.*

Chapter 1
Under the glacier

1. Introduction

Parallels between landscapes in Iceland and those at the surface of planet Mars allow studies of terrestrial landscape processes to be used for characterising Martian landform genetics. One of those landscape parallels is governed by magma-ice interactions that occur during volcanic eruptions underneath ice deposits. The materials created during such eruptions are characteristic for their formation environment and Icelandic volcanic glasses are therefore a unique Mars analogue material for use in process-oriented studies. However, substantial work on the environmental dynamics of these eruption products are lacking for properly understanding erosion, mobility and modification rates on Mars. This dissertation will therefore focus on the post-eruptive transport and the physical modification of glassy eruption products in different planetary environments.

The role of volcano-ice interactions in the formation of fragmental volcanic glass first became apparent in science after the Scottish Geographical Magazine published an article on the topic in 1900. In it, Helgi Pjettursson (1900)[1] accounts his field studies in Iceland during which he discovered "that some rocks of the 'tuff- and breccia formation' may be formed due to the direct interaction of volcanic and glacial forces". Later work by Peacock (1926) showed that basaltic glasses in these breccias were primarily formed by volcanic activity underneath ice sheets or inside lakes. With their observations, Pjettursson and Peacock were among the first to realise that magma-ice contact leads to the formation of a unique type of glassy breccia. The intercalation of these materials in larger landscape features such as steep-sided, table-shaped mountains helped to bolster the hypothesis that their origin was mainly related to subglacial volcanism and the ensuing magma-ice interactions (van Bemmelen and Rutten, 1955). Although the general characteristics of sub-ice and sub-marine eruptions are similar, confinement of eruptions by an ice body distinguishes these eruptions from sub-marine variants in terms of drainage and access of water to the volcanic vent (Moore and Calk, 1991;

[1] *Helgi Pjetturson (1872-1949) was the first Icelandic scholar to graduate with a PhD in Geology in 1905 and published extensively on the geology of Iceland between 1898-1910.*

Smellie 2006). The discovery that pillow lavas are formed during the first eruption stage (Einarsson, 1960) and other units during successive stages (Jones, 1969, 1970) increased the understanding of basaltic sub-ice volcanism in the Icelandic landscape. Studies of rhyolitic subglacial volcanism are scarcer, yet have steadily increased over the past decade (McGarvie, 2009). Numerous studies have since given insight in the similarities and differences between basaltic (e.g. Furnes, 1978; Smellie and Skilling, 1994; Bourgeois *et al.*, 1998; Wilson and Head, 2002; Tuffen, 2007; Smellie, 2008; Skilling, 2009) and rhyolitic subglacial volcanism (e.g. Furnes *et al.*, 1980; Tuffen *et al.*, 2001, 2002a; 2002b; McGarvie, 2009; McGarvie *et al.*, 2006, 2007; Flude *et al.*, 2008). The current state of art focusses on the interrelationships of geochemical and volatile composition with the confining and glaciostatic (or ice overburden) pressure of the overlying ice-mass for reconstructing eruption conditions and past glacial thicknesses (Dixon *et al.*, 2002; Denton *et al.*, 2009; Tuffen *et al.*, 2010, Owen *et al.*, 2012).

This first chapter sets out to review the geological and geomorphological developments reported in studies of subglacial volcanism; it explores the eruption types, resulting landforms and properties of materials in Iceland (paragraph 2). The focus is then shifted to Mars to show that similar glaciovolcanic eruptions occurred throughout the geologic history of the red planet and played an important role in its surface development (paragraph 3). These paragraphs highlight the similarities between eruption styles and the formation of glassy materials that are nowadays being widely observed on both planets. Such parallels justify the use of landforms and materials in Iceland as analogues for field and experimental studies to understand the landform genetics on Mars. With the planetary context set, this chapter continues with defining the relevant research questions and the structure of this dissertation (paragraph 4) and closes with a detailed description of the selected field site in Iceland (paragraph 5).

2. Tuyas, tindars and hyaloclastites

Recognising subglacial volcanic landforms can be quite straightforward in the Icelandic landscape (Fig. 1). Emergent subglacial volcanoes have developed into characteristic table-shaped mountains known as *tuyas* by the melting of magma upward to the ice-atmosphere interface of the glacier. They are by far the most visual illustration of basaltic and rhyolitic eruptions below ice masses during past glacierization of the Icelandic rift zones. Their formation usually starts as a fissure eruption that can develop edifices of considerable dimensions. The largest monogenetic tuya in Iceland (formed during one, possibly multi-phased, eruption) is Eiríksjökull, which has a 77 km^2 footprint and an average height of 1 km (Jakobsson and Gudmundsson, 2008). Although tuyas can be formed over the course of several eruptions such as the Herðubreið tuya (Werner *et al.*, 1996; Werner and Schminke, 1999), their structure always consists of four basic units. A pedestal of (i.) pillow lavas is commonly found at the base, followed by (ii.) layers of glassy breccias and (iii.) a subaerial cap-rock formed when the eruption breached the air interface. These three units are often dissected by (iv.) irregular lava intrusions.

The formation of bedded layers of glassy breccias, also known as *hyaloclastite*, is principally driven by the explosive fragmentation and rapid quenching (thermal contraction and shattering) when erupting magma mixes with meltwater from the surrounding ice. While the historical definitions of hyaloclastite and the Icelandic equivalent *móberg* have been predominantly attributed to describing mafic volcanic glasses (Kjartansson, 1943; Fisher and Schmincke, 1984), the term *glaciovolcanic glass* is used in this dissertation in parallel as a wider

definition to cover all geochemical variations of glass formed during volcano-ice interactions. In the case of basaltic glass the hydrothermal instability makes it easily chemically weathered, which leads to the formation of a palagonite coating on the exterior (Nesbitt and Young, 1984; Gislason and Oelkers, 2003). This coating or 'gel' eventually cements the granular glass into a more cohesive rock compared to the initially loose granular glass. Further chemical weathering of palagonite rinds leads to the formation of secondary clay minerals that in turn causes consolidation and strengthening of these volcanic glass deposits as a result of the filling of vesicles and interparticle pore spaces (Frolava, 2008). Estimates from the Gjálp eruption in 2001 suggest that the entire consolidation process can occur within the first 1-2 years after the eruption (Jakobsson and Gudmundsson, 2008; Jarosch *et al.*, 2008). Under conditions of smaller or variable thermal gradients chemical weathering and consolidation of the outer layers of an edifice can require several thousands of years (Fisher and Schminke, 1984). Basaltic tuyas are transformed by these chemical weathering processes into consolidated formations that are able to resist much of the erosive forces from glacier flow (Jakobsson and Gudmundsson, 2008).

The resistive nature of tuyas makes them potentially powerful palaeo-climatic markers due to the relation of their shape and height with the ice body in which they were formed. The first glacial reconstructions by Walker (1965) used the maximum summit elevations to determine possible ice profiles of past ice sheets. However, recent research indicates that the use of tuyas

Fig. 1 - The extent of glaciovolcanic formations in Iceland. Dark grey features outline the 'Móberg' formation (data from: Jakobsson and Gudmundsson, 2008), adjacent lighter grey areas delineate the Icelandic rift zones (data from: Einarsson and Sæmundsson, 1987) and white regions are present-day glaciers and ice caps (data from: Ahrendt *et al.*, 2012). The dashed area outlines the Torfajökull caldera at the transition between the Eastern Volcanic Zone (EVZ) and the Southern Flank Zone (SFZ). Other volcanic zones in the figure include the Northern (NZV), Snæfellness (SVZ), Western (WVZ) and Öræfajökull (ÖVZ) Volcanic Zones. Black triangles highlight locations of confirmed and suspected rhyolitic subglacial eruptions that are younger than 0.8 Myr (locations from: McGarvie, 2009).

in glacial reconstructions is limited to a minimum ice thickness as the cap rock unit only accurately records the height of the water-air transition zone. This level water accumulating inside the cauldron above the growing edifice was shown to be 150-200 m lower the actual thickness of the surrounding ice (Jakobsson and Gudmundsson, 2008). Detailed dating studies using cosmogenic ^{3}He exposure ages have shown that many tuyas formed during the last deglaciation of Iceland (Licciardi *et al.*, 2007). Temporal clusters of these eruptions were found to coincide with episodes of ice sheet thinning during the Bølling warming (14.5 kyr) and at the end of the Younger Dryas (11.6 kyr) (Licciardi *et al.*, 2007). The effect of a declining ice sheet and the associated isostatic rebound leads to a 30-100 fold increase in the magma supply over a period of 1-2 kyr (Jull and McKenzie, 1996; Slater *et al.*, 1998; Maclennan *et al.*, 2002). The formation of large tuyas therefore benefits from this consistent and continuous volcanic activity for the upward melting through the ice (Jakobsson and Gudmundsson, 2008). Many of the early Holocene flood-lavas in Iceland have been dated to the late Pleistocene and corroborate the effects of lithosphere unloading on increased eruption rates (Jull and McKenzie, 1996; Slater *et al.*, 1998; Maclennan *et al.*, 2002). These feedback mechanisms imply additionally that increased levels of explosive subglacial eruptions can be expected during the next centuries as a consequence of declining ice caps from climate change in Iceland.

Signs of tuya formation have been absent in nearly all recent subglacial eruptions (Jakobsson and Gudmundsson, 2008). These eruptions shared similar eruptions stages as tuyas in the sense that they also contain basal pillow formations and bedded deposits of hyaloclastites. However, they lack the characteristics cap rock layers from the filling of the cauldron with lavas in the subaerial eruption phase (Schopka *et al.*, 2006). Landforms created in such subglacial low-volume fissure eruptions are known as *tindars* and after deglaciation they are recognisable as ridges composed of hyaloclastite (Chapman *et al.*, 2000; Jarosch *et al.*, 2008). Tindars are especially dominant features just north and south of the present ice margin of the Vatnajökull ice cap (Fig. 1) in the in the Northern Volcanic Zone and Eastern Volcanic Zone (Vilmundardóttir, 1997; Jakobsson and Gudmundsson, 2008).

2.1 Recent Icelandic subglacial eruptions

Many eruptions have occurred over the past few decades (Thodarson and Larsen, 2007) and recent examples of subglacial volcanism in Iceland include the eruptions of Eyjafjallajökull in 2010 and Grímsvötn in 2011. Eyjafjallajökull illustrated to the world that subglacial eruptions are still common in Iceland. This particular eruption was intensively studied due to well-developed ground and airborne research infrastructures and this led to various insights into the evolution of the subglacial eruption (Sigmundsson *et al.*, 2010; Matoza *et al.*, 2011; Borisova *et al.*, 2012; Magnússon *et al.*, 2012). The Eyjafjallajökull eruption also clearly illustrated the effects of the eruption environment on the volcaniclastic material properties of the formed eruption products (Donnovan and Oppenheimer, 2011; Gislason *et al.*, 2011; Edwards *et al.*, 2012). The first phase of the eruption sequence started with a subaerial eruption at the Fimmvörðuháls mountain pass from March to April 2010. This eruption formed the Goðahraun lava field with two scoria and spatter cones known by the names Magni and Móði (Edwards *et al.*, 2012). Direct contact of lava with local snow and ice during this eruption was incomparable to the scale of magma-ice interactions of the subsequent eruption-phase. The dike intrusion in the subsurface extended during the eruption at Fimmvörðuháls and formed an eruption conduit underneath the Eyjafjallajökull ice cap. The resulting subglacial eruption had a Volcanic Explosivity Index (VEI) of 4 and started in April with activity lasting until September 2010 (Sigmundsson *et al.*, 2010). Rapid quenching of magma by ice and

abundant meltwater caused considerable spalling and shattering of the magma (Magnússon *et al.*, 2012). Fine glassy ashes were widely distributed across Iceland and carried aloft into European air space where it caused exceptional disruptions of air traffic (Gertisser, 2010). The eruptions at Fimmvörðuháls and under the Eyjafjallajökull glacier were roughly comparable in geochemical composition, yet their eruption environments differed significantly. The substantial differences between the eruption products are illustrated by rock and ash samples collected from the two eruptions (Fig. 2). The high explosivity of subglacial eruptions also makes these forms of eruptions inherently dangerous. The ash production during the magma-

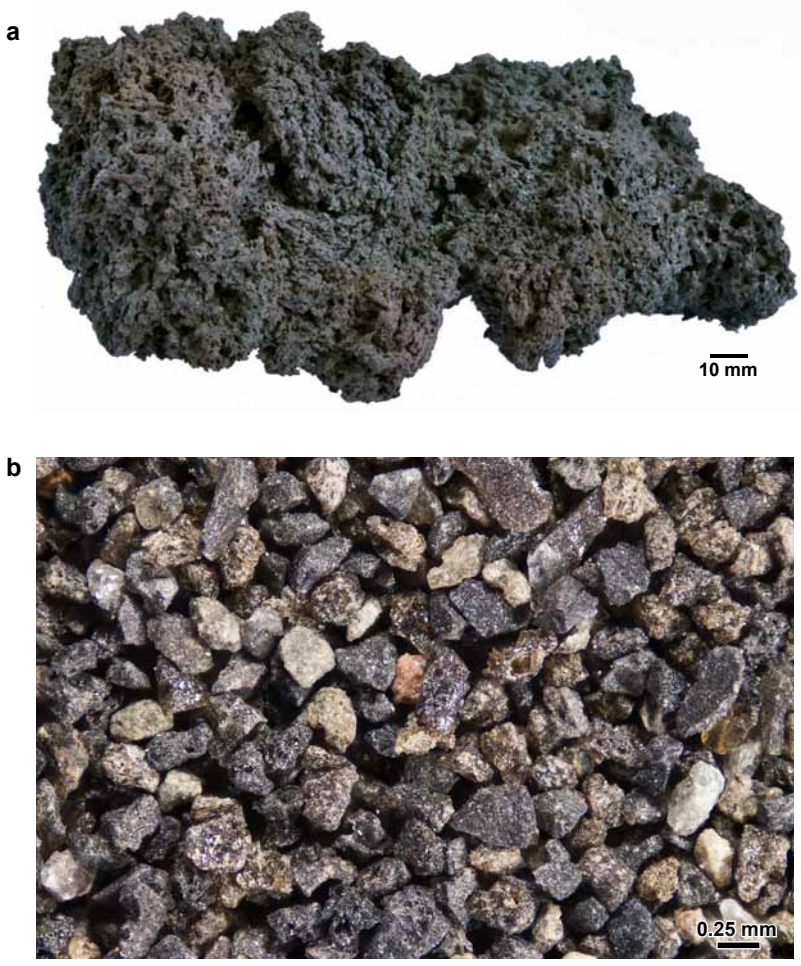

Fig. 2 - Comparison of the material properties of subglacial and subaerial eruption products from the 2010 volcanic eruptions in Iceland. Although the magmatic composition of both eruption products was roughly similar, the scale and properties of the formed materials are clearly different due to the eruption environments. Scoria from the Magni crater (a) illustrates the type of material formed by a subaerial eruption. Ash from the subglacial Eyjafjallajökull eruption (b) shows the end-product of explosive fragmentation and rapid quenching. Scoria samples were collected by the author in 2011 while ash samples were collected by L. Kerstens near Hvosvöller and Mulakot (along the F261 road) four months after the main eruption phase of the Eyjafjallajökull eruption.

ice interactions of the Eyjafjallajökull eruption had detrimental effects on the habitability of the ash-fall affected areas due to the increase in health (Gislason *et al.*, 2011; Gudmundsson, 2011; Carlsen *et al.*, 2012) and environmental hazards (Colette *et al.*, 2011).

2.2 Erosion and redistribution of glass

Throughout the deglaciated Icelandic landscape erosion of subglacially formed landforms and unconsolidated hyaloclastite deposits has led to the modification and redistribution of glassy materials (van Bemmelen and Rutten, 1955; Jones, 1969). Fluvial processes have most frequently been related to the erosion of subglacially formed landforms and can be separated into processes of water-initiated debris flows and landslides (Whalley *et al.*, 1983; Sigurðsson and Williams, 1991; Tuffen *et al.*, 2002a), alluvial fan formation (Schopka *et al.*, 2006) and gully erosion (Hartmann *et al.*, 2003). Catastrophic outburst floods from glaciers (jökulhlaups) are also known for their post-eruptive transport of hyaloclastites into proglacial environments (Bergh and Sigvaldason, 1991; Björnsson, 2002; Carrivick *et al.*, 2004). It may be evident that the environmental conditions in Iceland also drive non-fluvial processes that contribute to the erosion and subsequent redistribution of glassy sediments (Einarsson, 1984). However, studies of the redistribution of hyaloclastites and the postglacial alteration of tuyas and tindars are scarce (Jakobsson and Gudmundsson, 2008). Especially the lack of process studies emphasises the need for research into the post-glacial environmental fate of hyaloclastite materials. Periglacial and aeolian processes involving hyaloclastite sediments have hitherto been neglected, but these may be particularly relevant for understanding the behaviour of similar materials in the unearthly cold and 'hyperarid' periglacial surface environment on planet Mars.

3. A glassy soil on planet Mars

It is well-known on Earth that magma-ice interactions can have a significant influence on the material properties of eruption products and the morphology of subglacially formed landforms. Glaciovolcanism is, strictly speaking, a better term for describing magma-ice interactions as it includes all possible interactions of magma with glacial ice, snow, firn as well as ground ice (Smellie, 2006, 2007). Expansion of the definition is especially relevant in the case of planet Mars. Glaciations on Mars, like on Earth, are driven by orbital forcing. The most recent glacial period occurred 2.1-0.4 Myr ago (Head *et al.*, 2003a) when changes in obliquity have led, for example, to substantial variations in climatic conditions, increased polar ice sheets and glaciated parts of subtropical and tropical latitudes (Carr and Head, 2010). Some argue that these periglacial conditions have been persistent at the surface of Mars (e.g. Gaidos and Marion, 2003), yet others argue in favour of a wetter and warmer Mars with an Earth-like hydrological cycle (e.g. Pollack *et al.*, 1987). An important prerequisite is the stability of water at the surface of Mars. Liquid water may have been stable at some point when surface pressures reached approximately 1 bar, yet it is inherently unstable in the present atmospheric pressures that average only 6 mbar, or 10-15 mbar during periods of high obliquity (>30°) (Kieffer and Zent, 1992; Laskar *et al.*, 2004; Phillips *et al.*, 2011). The majority of water-rich deposits on Mars are therefore found in the form of ice. The largest quantity of ice contained in the Martian cryosphere is currently found at the poles (Clifford *et al.*, 2010) and in the subsurface at lower latitudes (Levy *et al.*, 2010). Irrespective of the exact evolution of the cryosphere, there is ample evidence of glacial and volcanic activity to support the idea that an appreciable portion of volcanism on Mars had a glaciovolcanic nature (Chapman *et*

al., 2000; Head and Wilson, 2007). Outcrops of tholeiitic basalt (rich in silica and iron, poor in aluminium; McSween *et al.*, 2009) at the surface of Mars show that volcanic processes span from the ancient Noachian epochs of >3.5 Gyr ago (Hartmann, 2005; Werner, 2009) to more recent activity in the Early Amazonian epoch, several hundred Myr ago (Neukum *et al.*, 2004). Crater age dating of these volcanic surface features has established that episodic pulses in volcanic activity coincided with periods of increased glacial activity (Neukum *et al.*, 2010). These absolute ages illustrate that conditions for glaciovolcanism have been persistent throughout a significant part of Mars' geologic history and its surface development. Figure 3 links the formation age of several glaciovolcanic surface features to the geologic history and episodes of coinciding volcanism and glaciation.

3.1 Martian tuyas and tindars

Many putative tuyas on Mars were identified by Allen (1979) in the northern lowlands and near the present-day polar ice cap. Due to instrument limitations it used to be impossible to directly observe diagnostic hyaloclastite beddings and generic topographic evidence has therefore been the foremost tool to identify tuyas on Mars. Similar to their analogues in the Icelandic landscape, morphological properties were primarily used for the identification of clear flat-toped features near the Martian North Pole as sub-ice volcanoes (Head and Wilson, 2007; Hovius *et al.*, 2008; Fagan *et al.*, 2010). Many of the Martian tuyas have similar morphologies as Icelandic tuyas, but their slightly lower flank slopes suggests that the relaxation angles of the hyaloclastites may be influenced by effects of the lower gravitational acceleration on Mars (3.71 m s^{-2} vs. 9.81 m s^{-2} on Earth; Kleinhans *et al.*, 2011). Summit heights of North Polar tuyas were used by Fagen *et al.* (2010) to reconstruct the polar palaeo-ice sheets and point to ice thicknesses of 57-610 m. Similar to these features around the North Pole, numerous tuyas have been identified near the Martian South Pole, see appendix A for locations. Features first mapped by Tanaka and Scott (1987) were interpreted as putative subglacial landforms by Ghatan and Head (2002) and a re-evaluation by Fagan *et al.* (2010) corroborated their

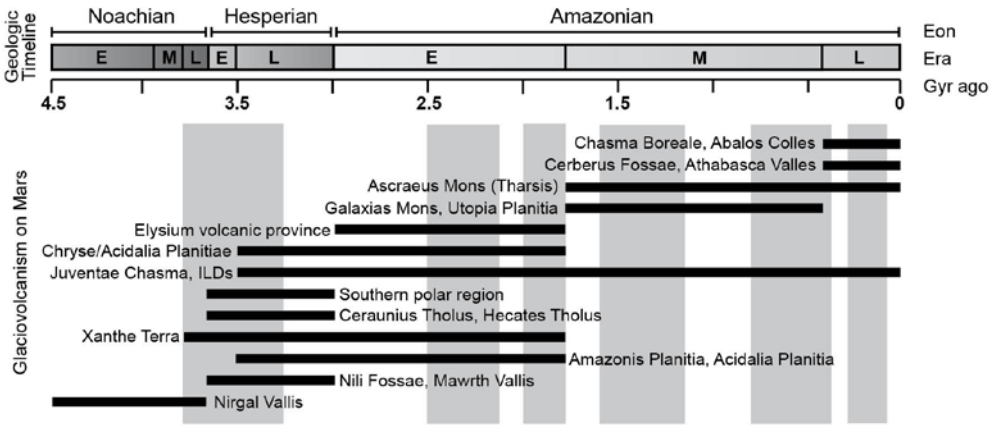

Fig. 3 - Timeline of glaciovolcanism and eruption locations on Mars (locations: Cousins and Crawford, 2011). Magma-ice interactions on Mars are favoured by the coinciding peaks of volcanic and glacial activity (grey vertical bars) at 3.8-3.3 Gyr, 2.5-2.2 Gyr, 2.0-1.8 Gyr, 1.6-1.2 Gyr, 800-300 Myr and 200-100 Myr ago (from: Neukum *et al.*, 2010). Black horizontal bars in the lower part of the figure highlight the estimated periods when glaciovolcanic surface features were formed; they do not reflect the duration of volcanic activity. See appendices B and C for locations on a map.

subglacial formation. The eruptions that formed the south polar tuyas were much more productive compared to the north polar tuyas, and melted through ice sheets of 500-2000 m thick (Fagan *et al.*, 2010). Since then, polar ice margins have retreated to their present-day locations. Numerous studies have shown the relation of such deglaciation with the pulsed release of magma from the lithosphere on Earth (Jull and McKenzie, 1996; Slater *et al.*, 1998; Maclennan *et al.*, 2002). It is not inconceivable that lithospheric unloading of glaciated polar areas has also played a role in the promotion of eruptions on Mars. Similar to the formation of tuyas in Iceland the increased intensity of eruptions during lithospheric unloading may have led to the eruption of sufficient magma volumes for a rapid formation of tuyas (Licciardi *et al.*, 2007). This new and provisional hypothesis provides a better and faster formation mechanism within a plausible regional context compared to the low extrusion rates suggested by Garvin *et al.* (2000) for the formation of volcanic features at the plains around the North Pole.

While ground resolutions of satellite imagery and topographic measurements have improved drastically to sub-metre scales in recent decades, the substantial modification of the Martian surface impedes the identification of the diagnostic units from tuyas (Keszthelyi *et al.*, 2010). Exceptions are locations in Chryse and Acidalia Planetiae, where basic units of tuyas, such as subaerial cap rocks and summit vents, were identified by Martínez-Alonso *et al.* (2011). In contrast to polar areas, glaciovolcanic eruptions at equatorial latitudes are most probably related to dike intrusions into ice-rich subsurface layers from volcanic activity associated to the proposed mantle plume below the Tharsis volcanic province (Head *et al.*, 2003b; Grott and Breuer, 2010). These glaciovolcanic eruptions have led to landforms that resemble Icelandic tindars and are found in Vallis Marineris, Cavi Angusti, Cerebrus Fossae, Marte Vallis and Juventae Chasma (Wilson and Head, 2002; Chapman *et al.*, 2003; Komatsu *et al.* 2004; Zealey, 2009). Appendices B and C show the locations of these and other glaciovolcanic surface features on a map. The massive hydrological networks that drain away from these features, with outwash plains at their terminus in the northern lowlands, suggest that these were carved out by catastrophic floods that resemble terrestrial jökulhlaups. (Mouginis-Mark, 1985; Rice and Edgett, 1997; Carr and Head, 2003; Chapman *et al.*, 2003; Burr, 2010). The large-scale outflow features formed by the hydrological activity in the Hesperian and early Amazonian epochs and the associated geomorphological features are currently best explained by a jökulhlaup hypothesis, induced by sub-ice volcanism (Gaidos and Marion, 2003). Catastrophic outburst floods have therefore been an important driver in the redistribution of glaciovolcanic eruption products and other hydrated minerals across the Martian surface.

3.2 Abundance of glass-rich deposits and parallels in formation

The strongest evidence for the existence of glaciovolcanic eruption products results from the observations by Horgan and Bell (2012a) who used the OMEGA instrument on the European Mars Express satellite. Their detailed spectral analyses of the dark sand seas around the North Pole and the largest dune field Siton Undae in the northern lowlands suggest that 80-90% of these sand fields consist of volcanic glass formed by explosive volcanism, such as glaciovolcanism (Fig. 4). These ratios of glass and crystalline materials are comparable to the materials formed by basaltic and rhyolitic sub-ice volcanism in Iceland (e.g. Jakobssson and Gudmundsson, 2008; Denton *et al.*, 2009). Granular volcanic glass skirting the proglacial areas of the Martian North Pole is primarily sourced from the basal unit below the present ice cap. Sediments from the cross-bedded basal unit were introduced in the circumpolar environment by catastrophic glacial outburst floods, where they are currently redistributed by polar winds (e.g. Fishbaugh and Head, 2002, 2005; Hovius *et al.*, 2008). Catastrophic floods flowing from

tindar features in Chryse Planitia, Valles Marineris and Juventae Chasma and from tuyas in Southern Acidalia may have deposited substantial amounts of granular glass in parts of the Northern Lowlands such as Siton Undae (Martínez-Alonso *et al.*, 2011, Horgan and Bell, 2012a). While the contribution of jökulhlaups in the (re)distribution of these materials is clearly not new, Horgan and co-workers are now finding the first compositional evidence that these large sand seas are sourced from equatorial glaciovolcanic eruptions that occurred in an ice-rich subsurface (Horgan, *personal communication*, 2012). Post-depositional chemical weathering was hypothesised by Horgan and Bell (2012a) to have leached low-valence cations from the glass structure. The formed Fe^{2+} rinds were subsequently removed by the abrasive effects of wind-induced saltation and exposed the leached silica-rich, almost obsidian-resembling, glass that now chemically stabilises these deposits and prevents further dissolution and consolidation (Horgan and Bell, 2012a). The absence of post-depositional cementation causes these glassy materials to be commonly found in aeolian landforms such as dune fields where the glass is affected by present-day transportational and erosional processes. These

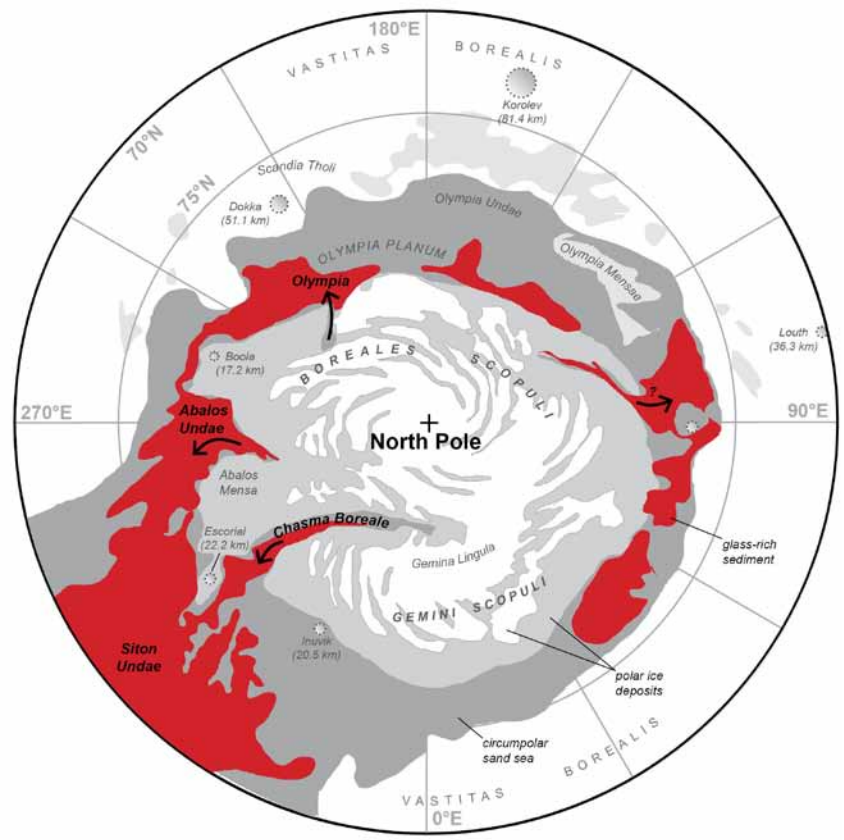

Fig. 4 - Simplified classification map showing areas where volcanic glass is abundant in the polar sand seas and the dune fields of Siton Undae on Mars. The red areas are a combination of the concavity and the 1.2-1.5 micron spectral regions that were interpreted by Horgan and Bell (2012a) as volcanic glass deposits (>80% glass content). Arrows highlight pathways of possible volcanism-driven glacial outburst (e.g. Hovius *et al.*, 2008) that can have deposited the volcanic glass in the circumpolar area. The possible pathways of the catastrophic floods from the equatorial highlands that deposited sands in Siton Undae fall outside the map's extent.

processes drive the migration of dunes (Hansen *et al.*, 2011) and include aeolian abrasion from saltation and wind-induced mass-wasting in the form of granular avalanches on dune slip faces (Horgan and Bell, 2012b).

Determining the physico-mechanical properties of glass particles is still problematic, despite the high abundance of glassy sediments at the Martian surface. Mineralogical properties can be derived from Mars-lander instrumentation and satellite observations (Chevier and Mathé, 2007; Mustard *et al.*, 2008; Horgan and Bell, 2012a), but detailed microscopic observations of Martian particle populations are only limited to incomparable materials at a few lander sites (e.g. Sullivan *et al.*, 2008; Goetz *et al.*, 2010). These observations show that aeolian sediments are well-rounded, which is generally consistent with abrasion from prolonged aeolian transport over geologic time (Keunen, 1960; Greeley and Iversen, 1985). In contrast, glaciovolcanic glasses are characterised by blocky and angular morphologies and have a low degree of vesiculation (Heiken, 1972; Tuffen *et al.*, 2001, 2002a). Scarce field observations (Ayling and McGowan, 2006) and experimental studies (Greeley and Iversen, 1985; Marshall *et al.*, 2012) also show that angular materials such as these glasses are modified at slower rates than other particle types (e.g. Mangold *et al.*, 2011). The discrepancy between the sparse observations of the Martian particle population and known properties of terrestrial glaciovolcanic glasses illustrates the hiatus in our comprehension of glassy materials at the Martian surface. Erosion processes that are involved in the modification of analogue glasses in Iceland can therefore help to increase our understanding of these materials in the environment on Mars. The baseline for such a comparative approach is formed in this dissertation by the parallels in glaciovolcanic eruption environments. These parallels are governed by the ice overburden pressures and the availability of water for the quenching of magma. Both are responsible for controlling the physico-mechanical characteristics of glasses, such as particle size, morphology and degree of vesiculation. Studies of Martian polar ice sheets show that these are mainly composed of water ice with average densities of 1220 kg m^{-3} (Bibring *et al.*, 2004; Zuber *et al.*, 2007; Phillips *et al.*, 2008, 2011). The topographic evidence from Martian polar tuyas establishes that subglacial eruptions occurred under ice thicknesses of 57-2000 m and consequently, based on the known Martian ice properties, confining glaciostatic pressures varied from 0.2-9 MPa. This range in pressure is comparable to the glaciostatic pressure of 2-8 MPa created by 255-960 m thick ice sheets in Iceland, generally composed of a lower-density ice of 850 kg m^{-3}. Refer to appendix D for a comparison of these glacial reconstructions. Subglacial eruptions on Mars and in Iceland are therefore controlled by similar pressure regimes and quenching of erupting magmas by water, forming materials with comparable physico-mechanical properties. Terrestrial hyaloclastites are as such suitable analogue materials for Martian glaciovolcanic glasses. The access to these analogue glasses on Earth allows parameters to be quantified that are of relevance for process-based geomorphological studies to understand glass modification, transport and erosion characteristics. This is where the exploration of Mars brings us back to the Icelandic landscape.

4. Objective and research questions

The objective of this dissertation is to study the behaviour and fate of granular glaciovolcanic glass in different planetary environments. The main aims are to fill a gap in the knowledge of physical erosion mechanisms and transport thresholds of high-silica glaciovolcanic glass and to investigate the role of atmospheric pressure and local environmental conditions in these geomorphological processes. These aims will be addressed by investigating the following research questions:

1. How do landforms composed of glaciovolcanic glass physically weather; which environmental processes are dominant in regulating weathering processes?
2. What is the role of the physico-mechanical properties in the physical weathering of glaciovolcanic glass by wind and ice?
3. What mechanisms permit the mobilisation and transportation of non-cohesive glassy sediments by winds in low atmospheric pressures, such as on planet Mars?
4. Is the fabric of aeolian sediment capable of retaining information on local wind flow conditions and the types of particle transport?

4.1 Outline and structure of this dissertation

Based on the research questions, this dissertation is divided into six chapters. In **Chapter 1**, this chapter, the role of glaciovolcanism in the formation of granular glass has been explored for defining the context, parallels and abundance of this type of material in different planetary environments. **Chapter 2 'Erosion of a subglacial edifice'** sets-out to study which processes affect the modification of hyaloclastites at landscape scales. The underlying aim of this chapter is to understand how the environmental (meteorological) conditions drive various geomorphological processes that are responsible for eroding an edifice. The chapter combines various field observations inside a gorge composed of glaciovolcanic glass in Iceland. A broad approach is applied to the landscape analysis and involves sampling of scree sediments and their source areas to establish if and how dominant transport and erosion processes are reflected in the sedimentary record. The focus in this chapter is then drawn to the contribution of aeolian processes to the erosion of hillslopes and the formation of sedimentary landforms. In reference of the first research question this chapter answers which processes are constructive in the erosion processes at a local scale.

Chapter 3 'Physical weathering of glaciovolcanic glass' takes the analysis of erosion characteristics a step closer to a particle level. While erosion processes at a landscape scale are discussed in chapter 2, this chapter aims at understanding how these erosion processes physically modify particles that compose the friable glassy breccias. The methodology of this chapter is based on environmental laboratory simulations of the two most influential erosion processes that were observed at the field site. Transport of particles after detachment from the matrix was simulated by tumbling sediment non-stop for several months to assess abrasion and textural changes. Freeze-thaw cycles on the other hand were simulated by subjecting larger pumiceous glass particles to diurnal freeze and thaw cycles. Detailed measurements of pores and fracture strengths of the glass give insight in the scale effects of ice growth and glass fracturing during freezing and thawing. In relation to the second research question, this chapter specifically focusses on the role of the material properties in the destructive modification of glaciovolcanic glass. As chapters 2 and 3 are complementary, they provide a 'cause and effect' analysis of the erosion of hyaloclastites at a landscape and particle scale.

In contrast to Iceland, the importance of erosion by flowing water is negligible in the present-day Martian surface environment. Dry erosion processes of hyaloclastites are therefore favoured on Mars and the wind is by far the most shaping geological force, especially when considering that glass-rich sediments are primarily found in dune fields. In order to understand the dependence of aeolian processes in the different planetary conditions, experiments are used to translate these processes to the surface conditions on Mars. The magnitude of atmospheric pressure, the principal 'planetary variable' that affects

these aeolian processes, is therefore used as the variable in the experimental methodology of the 'hypobaric' wind tunnel simulations. In **Chapter 4 'Wind transport at the fluid threshold'** I will examine how glaciovolcanic glass can be transported by winds in the very thin atmosphere of Mars. This focus on aeolian processes is relevant for several reasons. In Iceland aeolian processes are found to play an important role in the modification of textures and sedimentary processes. On Mars the atmospheric pressures are low and the structure of the atmospheric boundary layer is different if compared to Earth. This affects the thresholds for removal and the physical modification of sediments. At the fluid threshold, where particle mobility is initiated by the wind only, rolling is the lowest threshold at which mobility can occur. Experimentally simulating the removal of volcanic glass is achieved by using a special hypobaric (low-pressure) wind tunnel. The ancient age of the surface and limited knowledge on properties of the glassy particle population on Mars makes a comparative approach seemingly difficult. However, due to the parallels in formation environments of glaciovolcanic glasses on Earth and Mars, it is possible to determine a realistic threshold range for particle mobility of glass-rich sediments on Mars. This chapter will therefore address the third research question and assesses how glassy sediments are initially mobilised, thereby triggering saltation and subsequently driving the physical alteration of particles.

Various landers and rovers have shown that aeolian sediments on Mars have been strongly modified by wind transport. Observed particle shapes may represent the 'end state' of particles and the glass detected in dune fields will likely have obtained such well-rounded morphologies due to their aeolian transport over geologic time. In **Chapter 5 'Orientation of particles to wind flow'** I continue the study of wind-induced particle mobility, yet this time *in situ* on Mars. Where the preceding chapter addressed the detachment threshold for setting particles in motion by rolling and saltation, this chapter will focus on how these forms of transport create non-random, preferred orientation patterns in the sediment fabric. Using imagery of non-cohesive sand grains as obtained by the Microscope Imager of the Mars Exploration Rover 'Spirit', I will examine how particles orient themselves and how this orientation can be used to infer local wind flow directions. I briefly trade the landscape in Iceland for that of the Brandenburg Ice Marginal valley in Germany. Here, cover sands and inland dunes composed of laminated sands have been deposited by winds in a periglacial environment during the last glaciation of the area. Palaeowind directions that built these dunes have been inferred in the past from dune morphologies and from the long-axis orientation of sand particles in thin-sections. A new method is developed based on *object-based image analysis*, to segment and reclassify objects in images into polygons that represent the circumferences of individual sand grains. This in turn allows the measurement of sediment statistics such as size distribution and long-axis orientations of individual grains. The method will first be tested and compared to known sediment of the inland dunes and subsequently applied to imagery of sand grains in the Columbia Hills on Mars. In answering the fourth research question, I will show that surficial sediments on Mars have retained patters that represent the wind flows that formed these aeolian features. This new methodology highlights that mobilisation of sand grains can complement pre-existing aeolian analyses that have relied on the analyses of surface features such as dunes, ripples and ventifacts.

Chapter 6 'Synthesis - environmental fate on Earth and Mars', the final chapter of this thesis integrates the conclusions of these preceding chapters to answer the four research questions. This chapter works towards a coherent vision on the behaviour and fate of glaciovolcanic glass and places glaciovolcanic glass in a broader context at the surface of planet Mars. Finally this outline helps in defining future research directions.

4.2 Selection of an analogue glass in Iceland

The research presented in this PhD dissertation is founded on the premise that hyaloclastites in Iceland can be used as an analogue for glaciovolcanic glasses on Mars, as I outlined in section 3.2. Erosion processes and thresholds that drive the environmental behaviour of hyaloclastites are dependent on the material's physico-mechanical properties. Unlike comparative studies that use geochemical analogue materials based on remotely sensed surface mineralogy, selection of an analogue material in this dissertation is based on the physico-mechanical properties of amorphous (non-crystalline) materials that are controlled by the subglacial eruption environment (see Appendix D). The properties of the Icelandic glass analogue therefore need to be well-characterised to understand their interrelationship with various processes outlined in the preceding section. The selection of a single particle population is in this sense vital to exclude mixed materials that would possibly bias the characterisation of the material's physico-mechanical properties. These criteria have led to the selection and use of a rhyolitic hyaloclastite that was formed during the isolated subglacial eruption of Bláhnúkur in the Torfajökull caldera complex (Fig. 5, Fig. 6). Particles in these rhyolitic glass breccias are blocky in shape with a low vesicularity of 5-23% (Tuffen *et al.*, 2001, 2002a; Owen *et al.*, 2012). When the physico-mechanical properties of the Bláhnúkur particle population are compared to basaltic hyaloclastites we see that these glasses are characterised by blocky particle morphologies and vesicularities of 5-30% (Heiken, 1972; Furnes, 1978; Schopka *et al.*, 2006). Weathering of these basaltic hyaloclastites involves cementation from palagonisation, filling of vesicles and as such strengthening. In contrast, rhyolitic (silicic) hyaloclastites appear to be more resistant to such chemical weathering and are generally not well-consolidated (Jakobsson and Gudmundsson, 2008). This also appears to be the case for glass deposits on planet Mars, where leaching of basaltic glass created particles with silicic exteriors that are now detected as chemically-resistant, unconsolidated deposits (Horgan and Bell, 2012a). The excellent accessibility to Bláhnúkur's hyaloclastites has facilitated detailed studies of eruption conditions and hydration properties that are dependent on the subglacial eruption environment (e.g. Tuffen *et al.*, 2001, 2002a; Denton *et al.*, 2009, 2012; Owen *et al.*, 2012). These conditions make the particle population of Bláhnúkur arguably the best-studied example of silicic hyaloclastites. No other basaltic or rhyolitic edifice has been studied to the same extent and provides access to a similar well-characterised material. This is a substantial benefit for the experimental studies presented in this dissertation.

5. Bláhnúkur: a unique field site in Torfajökull, Iceland

5.1 Regional development and subglacial eruptions

The active volcanic zones in Iceland are dated relative to the Brunhes normal magnetic epoch (Sæmundsson, 1979; Jónasson, 2007) and are subdivided into two zonation types: rift zones and flank zones (Sæmundsson, 1974, 1979). Rift zones roughly follow the course of the Mid-Atlantic Ridge through Iceland. Volcanic systems within these zones consist of a central volcano with well-developed fissure-swarms extending several tens of kilometres along the rifts. These systems are frequently composed of tholeiitic basalts (Sæmundsson, 1979). A characteristic property of central volcanoes is that they are often higher in elevation than surrounding terrain. The colder conditions with increasing altitude can nowadays be treacherous for hikers, but it has also led to the development of massive ice sheets during glacial epochs. Their high elevation and exposure enforces an increased likelihood for magma-ice interactions and this contributes to the formation of abundant glaciovolcanic

eruption products in the Icelandic landscape (McGarvie, 2009). In the flank zones however, the volcanic activity is dominated by the >3 cm yr^{-1} spreading rates of the North American and Eurasian plates (Árnadóttir *et al.*, 2009). Consequently, the central volcanoes in these systems are much larger, fissure swarms are lacking or are only poorly developed and some systems are dominated by rhyolitic compositions. Rhyolitic subglacial eruptions in Iceland are currently linked to 23 (suspected) locations with edifices of varying scales (McGarvie, 2009). One prominent example in the southern central highlands is Torfajökull; an area that is recognised as the largest rhyolitic complex in Iceland (Walker, 1966; Jónasson, 2007; Martin and Sigmarsson, 2007) and as the largest on an oceanic crust (Gunnarsson *et al.*, 1998). It has produced roughly two-third of the total erupted rhyolite in Iceland during the past 0.8 Myr, 225 km^3 of the 350 km^3 (Gunnarsson *et al.,* 1998; McGarvie, 2009). The caldera is located at the point where the Easter Volcanic Zone (EVZ) meets the Southern Flank Zone (SFZ) and has been active since the mid-Quaternary. Torfajökull is still considered volcanically active today, as is evidenced by micro-earthquakes from shallow magma

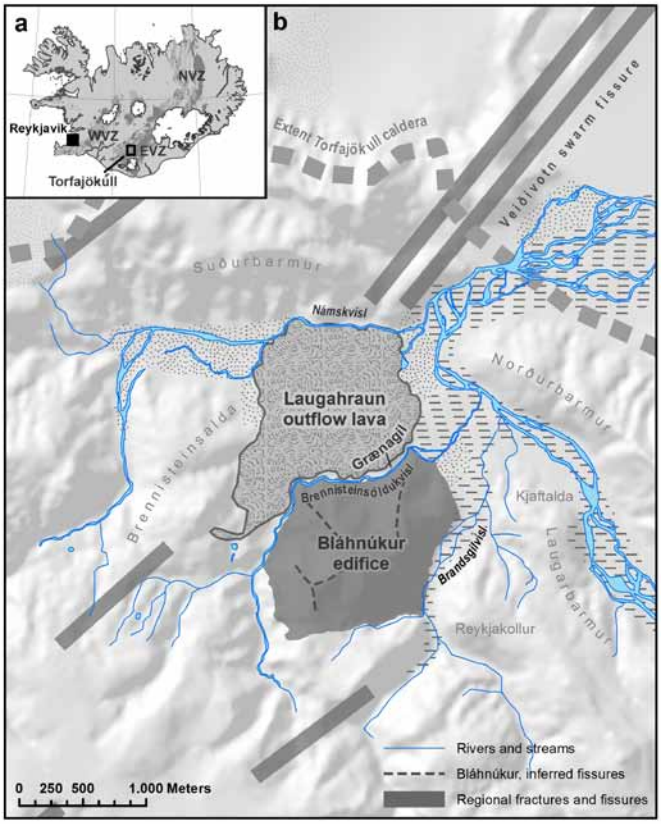

Fig. 5 - Overview map of the Landmannalaugar area (63°59'04" N, 19°3'51" W) where the Veiðivotn swarm fissure intersects the magma chamber of Torfajökull. This section of the Torfajökull region in highlighted by the black box (a) in the southern central highlands of Iceland. The gorge for the field studies in this dissertation is situated between the 1477 AD *Laugahraun outflow lava* and the subglacially formed *Bláhnúkur edifice* (b). Local eruption fissures of Bláhnúkur were inferred by Tuffen *et al.* (2001).

intrusions (Soosalu and Einarsson, 2004; Lippitsch *et al.*, 2005; Soosalu *et al.*, 2006) and large geothermal gradients in the subsurface (Pálmason *et al.*, 1970). The circular depression of the complex is not a caldera in the strict sense of the definition as there is no clear evidence that subsidence of the central area took place. The shape of the caldera was more likely caused by confinement of eruption products underneath the ice that increased the vertical growth of the ring wall during subglacial eruptions (McGarvie, 2009). Subsequent eruptions and geothermal alteration of the eruption products have produced a colourful landscape that is now part of the Fjallabak Nature Reserve (Fig. 6, page 26-27).

The Bláhnúkur edifice near the northern edge of the complex is an example of an isolated small-volume eruption that took place during the last glaciation of Torfajökull between 115-11 kyr ago. It is therefore considered to be the youngest glaciovolcanic landform in the area and consists of a 50 m thick layer of rhyolitic hyaloclastite (Tuffen *et al.*, 2001; McGarvie, *et al.*, 2006). The pyramid-shaped edifice (Fig. 6) was formed by the eruption along four WSW-ENE and NW-SE trending fissures and currently rises 350 m above the surrounding rhyolite plateau to a summit altitude of 945 m.a.s.l. (meters above sea level). The emplacement of the Bláhnúkur hyaloclastites during different eruption stages were first described by Furnes *et al.* (1980) and substantially improved by Tuffen *et al.* (2001). Detailed field studies by Tuffen *et al.* (2001) have shown a complex sequence of volcano-ice interaction where the distance between glacier ice and magma increased during the later eruptive stages and gave room for the emplacement and filling of the subglacial eruption cavern with brecciated ash. This glacial recession destabilised already deposited eruption products and triggered avalanches and debris flows inside the subglacial eruption cavern.

Increased subglacial channelization (Tuffen *et al.*, 2002a) reduced the explosivity of the eruption by draining water from the area around the primary vents. Geologic features and sedimentary strata presently exposed around the edifice reflect a dynamic and well-constrained eruption during which the interaction of magma and ice controlled the material properties of the glaciovolcanic glass (also see Box 1). Degassing of magma during the complex magma-ice interactions also fostered a new approach to studying subglacial eruption dynamics in relation to palaeo-ice reconstructions (Tuffen *et al.*, 2010). The volatiles sequestered in the glass at the time of solidification are considered to follow predictable patterns depending on the glaciostatic pressure (e.g. Tuffen *et al.*, 2010; Owen *et al.*, 2012). In an eruption environment where meltwater from magma-ice interactions dominates the rate of quenching, dissolved H_2O appears to be a suitable, albeit complex, proxy for inferring palaeo-ice thicknesses from subglacial eruption products (Owen *et al.*, 2012). The decrease in water content with increasing sample altitude along the flanks of the edifice showed that Bláhnúkur erupted underneath an ice sheet of 400 metres thickness. This is in line with the thickness inferred from conventional geological methods (Tuffen *et al.*, 2001) and topographic indications from local tuyas (Tuffen *et al.*, 2002b).

Radiometric dating of three tuyas in Torfajökull using ^{40}Ar-^{39}Ar have provided an accurate age (67-278 kyr) and minimum ice sheet thickness for their eruption during past glaciations of the area (McGarvie *et al.*, 2006). These datings show that in contrast to other tuyas in Iceland (Licciardi *et al.*, 2007), tuya-forming eruptions in Torfajökull are likely dissociated from lithosphere unloading during deglaciation (McGarvie, 2009). The promotion of eruptions in this area of Iceland is in fact a likely consequence of the unique architecture in the subsurface where the basaltic (tholeiitic) Veiðivotn fissure swarm intersects the rhyolitic magma chamber of Torfajökull (McGarvie, 1984; Mork, 1984; Gunnarsson *et al.*, 1998; Jónasson, 2007). The Bláhnúkur breccias have basaltic inclusions of several millimetres

to centimetres in size that are indicative for the break-up and mixing of a basaltic body inside the rhyolitic magma chamber (Blake, 1984; Tuffen *et al.*, 2001, 2002a). The presence of these basaltic inclusions also establishes that the eruption of Bláhnúkur was encouraged by the intrusion of a pre-eruptive basaltic magma body in the Torfajökull magma chamber (McGarvie, 1984; Mork, 1984). The adjacent Laugahraun lava flow underwent a comparable fate and outcrops show similar signs for basaltic intrusions prior to the eruption. Although the eruption products from Bláhnúkur and Laugahraun clearly differ and illustrate the effects of the eruption environment (subglacial vs. subaerial), both can be considered as comparable effusive rhyolitic eruptions.

5.2 Hydrological evolution and development to present-day state

After the subaerial eruption of Laugahraun in 1477 AD, local hydrological networks had to re-establish their flow directions due to the blockade of the Landmannalaugar valley by the lava flow (Fig. 5). The gradual evolution of these drainage networks led to the incision of the Brennisteinsöldukvísl stream at the interface between the resistant Laugahraun formation and the less-consolidated Bláhnúkur hyaloclastite. This mainly affected the erosion of the North-western quadrant of the edifice where it caused significant fluvial erosion at the base of Bláhnúkur and undercutting of sections from Laugahraun. The present Grænagil gorge was formed as a consequence of the local hydrological evolution in response to the Laugahraun eruption. Here, green and grey hyaloclastites (see Box 1) are excavated by continuous basal erosion of the stream and by the interaction of local environmental conditions with the exposed slopes. Especially winds are funnelled and aggravated inside the gorge due to the local topographical gradients. The main study area was therefore situated inside the Grænagil gorge (63°59'04" N, 19°3'51" W) due to the occurrence of a large variety of environmental processes that are of interest to this dissertation research. The excellent accessibility and unique geological setting as an isolated subglacial edifice make Bláhnúkur a prime location for studying: (i.) the interaction and effects of local environmental conditions, (ii.) the role of physico-mechanical properties of glaciovolcanic glass in weathering, erosion and transportation processes and (iii.) making the translation of this material's environmental behaviour to the conditions at surface of planet Mars.

Box 1 **50 Shades of green**

The Grænagil gorge is known for its bright-green hyaloclastites that intrigue many hikers and scientists alike. So far, a conclusive explanation for the notable colour has been lacking, while the nature of the green glass may give insights in the eruption and formation conditions of these deposits. Conventional measurements using X-ray diffraction (based on scattering of the radiation by crystalline lettuces, also see chapter 4) show that less than 10% of the glass breccia is composed of minerals such as anorthite, huelandite, mordenite and albite (Denton *et al.*, 2009). None of these minerals are known for their vivid green colours and their abundance is too low to have any contribution to the observed colours by intermixing in the breccia matrix. This colour enigma can be solved by a more detailed study of the glass' geochemical composition and spectral properties. In the production of industrial glasses, colours are created by adding the oxides of transition metals (3d electron shells) or rare-earth metals (4f electron shells) (Shelby, 2005) with ferric and ferrous iron being the most common cause for green hues in glasses. High ferrous-ferric ratios typically produce blue-green colours, while yellow tinges occur in glass mixes with a more ferric ratio. The bulk of such glass fragments may in fact appear black at a greater viewing distance, while still having these green or yellow

Box 1 - continued

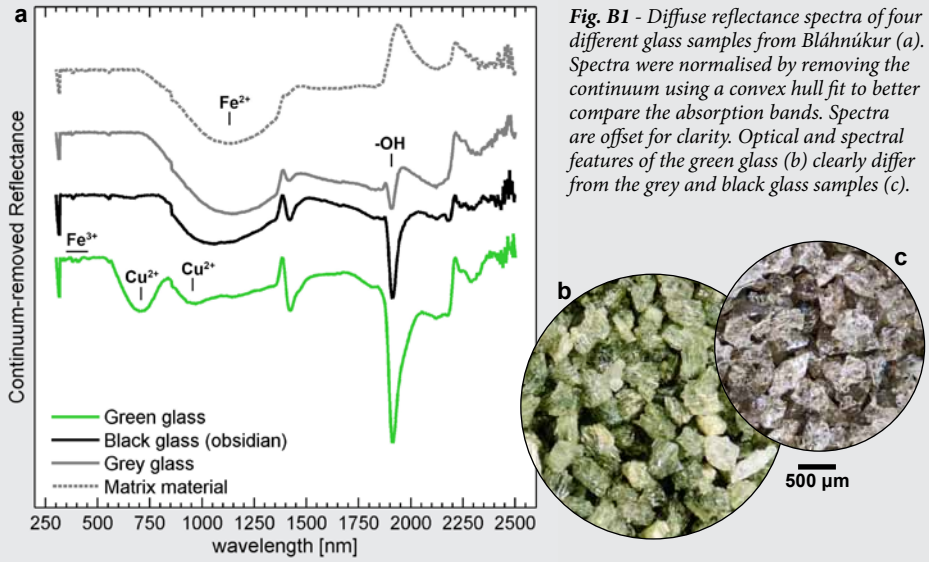

***Fig. B1** - Diffuse reflectance spectra of four different glass samples from Bláhnúkur (a). Spectra were normalised by removing the continuum using a convex hull fit to better compare the absorption bands. Spectra are offset for clarity. Optical and spectral features of the green glass (b) clearly differ from the grey and black glass samples (c).*

tinges on closer inspection (compare Fig. 6 with Fig. 26). These optical properties are also reflected in the names given to the edifice and its features; Bláhnúkur translates from Icelandic to '*blue peak*', while Grænagil translates to '*green gorge*'. It would thus be logical to attribute the green colour of the glassy breccias to the ferrous-ferric ratios of the various formations. However, other ions can have similar colouring effects and are also known to produce green glass, such as copper (Cu^{2+}), and multivalent chromium (Cr^{2+}, Cr^{3+}, Cr^{6+}). Spectral properties of several Bláhnúkur glasses were measured using a Lamda 900 UV/VIS/NIR spectrometer with integrating sphere from Perkin Elmer. Green, grey and black (obsidian) glass samples were milled to a fine powder and measured from 300-2500 nm at a scan speed of 450 nm per minute. The diffuse spectral reflectance was then normalised by removing the continuum with a convex hull fit (the line connecting the peaks on top of the original graph) for a better comparison. A notable absorption feature for the green glass occurs at 700 nm that absorbs red, orange and yellow, giving the glass a green appearance. This broad feature and a smaller feature at 900 nm are most consistent with Cu^{2+}. The high Fe^{2+} absorption at 1050 nm seen at the other samples and stronger absorption features of Fe^{3+} around 400 nm for the green glass indicate that the green glass is more oxidised than the other three samples. The higher oxidation of the green glass is most likely the cause of steam activation (e.g. Starokon *et al.*, 2003) associated with hot steam filtering through the glass breccias when the material of the green outcrop avalanched down-slope (see Tuffen *et al.*, 2001). The colour at the entrance of the Grænagil gorge is therefore associated to proposed mass wasting processes inside the hot and steamy subglacial cavern during the formation of Bláhnúkur. ▪

***Fig. B2** - Entrance of the Grænagil gorge in Iceland. Veins in the exposed rock face were proposed by Tuffen et al. (2001) to have formed by filling of cracks with fines mobilised by steam filtering through the breccias during avalanching of these deposits inside the hot subglacial eruption cavern.*

Fig. 6 - The Bláhnúkur edifice in Torfajökull (see Fig. 5 for the regional context), viewed from the flank of the Brennisteinsalda towards the northeast. The edifice is roughly pyramidal in shape with a summit altitude of 945 m above sea level (350 m above the valley floor). A 50 m thick layer of silicic hyaloclastite drapes an older pre-existing rhyolite core. Towards the left border of photo, between the Laugahraun lava flow and Bláhnúkur, is the entrance to the Grænagil gorge. *Photo courtesy of Daniel Bergmann, used by permission.*

▲ *Slumping and break-up of scree deposits in the Grænagil gorge as a result of water-saturation.*

Chapter 2

Erosion of a subglacial edifice

Abstract

Scree cones and slopes are common sedimentary landforms created by rock fall and rock particle fall in mountainous environments. These formative processes are attributed to various weathering and particle detachment mechanisms. However, the aeolian contributions to the weathering of rock faces and formation of scree sediments are poorly understood and often underestimated. A case study in the southern highlands of Iceland provided a geological setting in a subarctic environment where the contribution of various erosion and deposition mechanisms to the development of scree deposits could be studied. Here, moderately-cohesive subglacial volcanic eruption products are continuously undercut by local streams, creating exposed and steep-sided canyon walls where scree cones and slopes are formed by dominant influences of freeze–thaw cycles and the wind on rock particle fall. The stratigraphy and the morphometry of these sedimentary landforms indicate that wet formative processes can contribute but are not as dominant. Avalanching of accumulated material occurs in dry conditions and creates distinct stratified sediments. The aeolian contribution to the scree development was studied by determining the physical requirements of particle detachment using wind tunnel simulations. Simulated threshold wind speeds of the removal of fines show that these wind and gust conditions are common in these areas in Iceland. A detailed particle analysis of the sediment from an isolated scree cone and the contributing rock face showed that sediments were depleted in the silt fractions. Field observations confirmed the influence of deflation where fine material is removed by the wind from exposed sediments whereas larger particles are excavated by the deflation of the surrounding matrix on the overlying rock face. The outcomes highlight the role that aeolian processes can fulfil in subarctic environments. As similar glassy materials are also found on other planets, the studied processes can for example offer insights in hillslope processes at the surface of planet Mars.

This chapter is based on: *De Vet, S.J., Cammeraat, L.H., 2012. Aeolian contributions to the development of hillslopes and scree sediments in Grænagil, Torfajökull, Iceland. Geomorphology, 175-176, 74-85, doi:10.1016/j.geomorph.2012.06.023*

1. Introduction

Scree cones and slopes are common sedimentary landforms in mountainous environments across the world. They are formed by the accumulation of material of varying particle sizes which are delivered by rock fall (large boulders, >35 m^3 yr^{-1}) and rock particle fall (<pebble sized particles, <5 m^3 yr^{-1}) from overlying slopes (Whalley, 1984; Selby, 2000). Studies focussing in detail on rock particle fall are still relatively scarce, whereas more is known about the evolution of debris cones or talus slopes in various environments (e.g. Sass and Krautblatter, 2007). Processes driving rock particle fall are attributed to weathering mechanisms of rock faces as a result of: (i.) freeze-thaw interactions, (ii.) shrinkage and swelling processes driven by wetting and drying, or (iii.) due to salt weathering (Selby, 2000). In addition to these, other contributing mechanisms are also reported and include plant root penetration and mechanisms involving rapid snow melt, rain storms and earthquakes (Wieczorek *et al.*, 1995; 2000).

When liberated particles are eventually concentrated in sedimentary landforms, the internal angle of friction of the accumulated sediment influences the slope angle. This is an important empirical property which allows the discrimination between formation environments and deposition processes. This approach is illustrated for many geomorphological phenomena on Earth and even on other planetary bodies. For example, at the surface of Mars slope angles are the foremost means for inferring the formation conditions of a particular landform. Distinctions on Mars can be made between alluvial processes, dry mass wasting and aeolian distributed sediments (e.g. Kleinhans, 2010) on the basis of these morphometric properties. On Earth, auto-organisation of particles occurs during avalanching of freshly deposited sediments and results in segregation (slope length-wise sorting) and stratification (layering perpendicular to the slope and avalanche flow direction). These processes occur in various subaerial and subaqueous sedimentary landforms such as immersed deltaic foresets (Kleinhans, 2005), in dry sand-blown dunes (Hunter, 1977; Bristow *et al.*, 2000) or in mountain slope deposits (Sass and Krautblatter, 2007). Lubrication of these avalanches by the interstitial medium influences the morphometry of such sedimentary landforms (Bertran and Texier, 1999). Forceful conclusions about the formation environments of a particular sedimentary landform can therefore be drawn from a combination of the stratigraphy and morphometry (Steijn *et al.*, 1995). For stratified slope deposits we can differentiate between dry rock fall-derived scree cones (30-40° slope angle) (Rapp, 1959; Sass and Krautblatter, 2007), debris flow dominated deposition (<30° slope angle), frosted granular flow (<28° slope angle) and alluvial deposits with characteristic solifluction-lobes and incised stream beds (3-25° slope angle) (Blair and McPherson, 1994; Steijn *et al.*, 1995). However, the contribution of aeolian processes to rock particle fall and erosion in cold mountainous environments has not been extensively studied or reported for these sedimentary landforms, even though the wind is widely recognised to influence the development and modification of landforms in various environments, especially in the subarctic Icelandic sandy deserts (Arnalds, 2000; 2010; Arnalds *et al.*, 2001). Aeolian erosion of rock walls has been more commonly associated with abrasion by coarse-textured materials (Laithy, 2009) rather than with deflation and entrainment of finer textures from the rock face. We observed aeolian processes contributing to the formation of foot slopes below rock faces of subglacially-formed volcanic glass in a dry environment in Iceland. Local winds and gusts deflated the silt and clay fractions from rock faces, making the coarser fractions instable which induced rock particle fall and which in turn contributed to the formation of scree deposits at the valley bottom. Our aim was to study the physical requirements for

deflation of small particles and determine the possible contribution of aeolian mechanisms to the stratigraphy and morphometry of the sedimentary landforms. We hypothesise that stratified sediments with slopes angles >30° and deprived of fine particles are indicative of a predominantly cold and dry formation environment in which aeolian deflation contributes to the formation of scree deposits.

2. Regional setting and material properties

Our field observations of aeolian contributions to scree formation were made in a geological context unique to Iceland. Here, subglacial, subaerial and submarine volcanic eruptions are widespread. Subglacial eruptions have produced a great variety of distinctive landforms and materials that include tuyas, hyaloclastite sheets and ridges that have come to dominate the present-day post-glacial landscape (e.g. Bourgeois *et al.*, 1998; Gudmundsson, 2000; Wilson and Head, 2002; Schoka *et al.*, 2006; Thodarson and Larsen, 2007; Jarosch *et al.*, 2008; Smellie, 2008; McGarvie *et al.*, 2006; McGarvie, 2009). This landscape is currently influenced by various geomorphological processes which include mass wasting, periglacial, fluviatile and aeolian processes. The volcanic sequences found within the Torfajökull area in the southern highlands resulted from the magmatic activity within the Veiðivotn swarm fissure and the activity in the Torfajökull magma chamber (Lippitsch *et al.*, 2005; Gunnarsson *et al.*, 1998; Jónasson, 2007). The highly dissected rhyolite plateau of Torfajökull, currently part of the Fjallabak Nature Reserve, features remnants of quaternary glacial environments such as subaerially formed rhyolites, subglacially formed rhyolitic hyaloclastites and some minor traces of fluvioglacial sediments. The area measures roughly 18x12 km and with a volume of an estimated 225 km^3 it is considered to be the largest and most active rhyolite core on an oceanic crust (Gunnarsson *et al.*, 1998).

The Bláhnúkur edifice (Icelandic for 'blue peak') is the youngest subglacial eruption in the area around Landmannalaugar (Tuffen *et al.*, 2001). Bounding Bláhnúkur to the north is the subaerial rhyolitic Laugahraun formation that was formed as a post-glacial subaerial lava flow which currently fills a major part of the valley bottom (Blake,1984; Thordarson and Larsen, 2007). These two adjoining formations illustrate well how different eruption environments influence the material properties found in the present-day landscape (Fig. 7). The lithofacies and formation mechanisms of subglacial rhyolitic hyaloclastites within the surrounding area of Bláhnúkur have been extensively studied by Tuffen *et al.* (2001, 2002a). These subglacial eruption products were formed during the last glaciation and are deposited on top of the older rhyolite topography, adding an estimated +50 m to the local elevation (Tuffen *et al.*, 2001). The flanks of Bláhnúkur consist of one type of hyaloclastite deposited by different emplacement processes at the time of the formation (Tuffen *et al.*, 2001). The hyaloclastite are considered to have been formed by spalling of brittle lobes of erupted lava under contact with water and ice in the subglacial eruption cavity (Tuffen *et al.*, 2001). The resulting blocky and charded particle morphology has a moderate vesicularity which favours the interpretation of an effusive eruption environment with slow discharge rates <5 $m^3\ s^{-1}$ at high basal pressures (Tuffen *et al.*, 2001, 2002a; 2008). The formation that dominates the area of interest are breccias which have been interpreted by Tuffen *et al.* (2001) as collapse remnants. The composition of this facies consists of breccias with a green to greyish ash matrix containing volatile-rich pumiceous obsidian (Tuffen *et al.*, 2001; Denton *et al.*, 2009); lending the name 'Grænagil' (green gorge) to the area of interest. These eruption products have been deposited during the early stages of the subglacial eruption

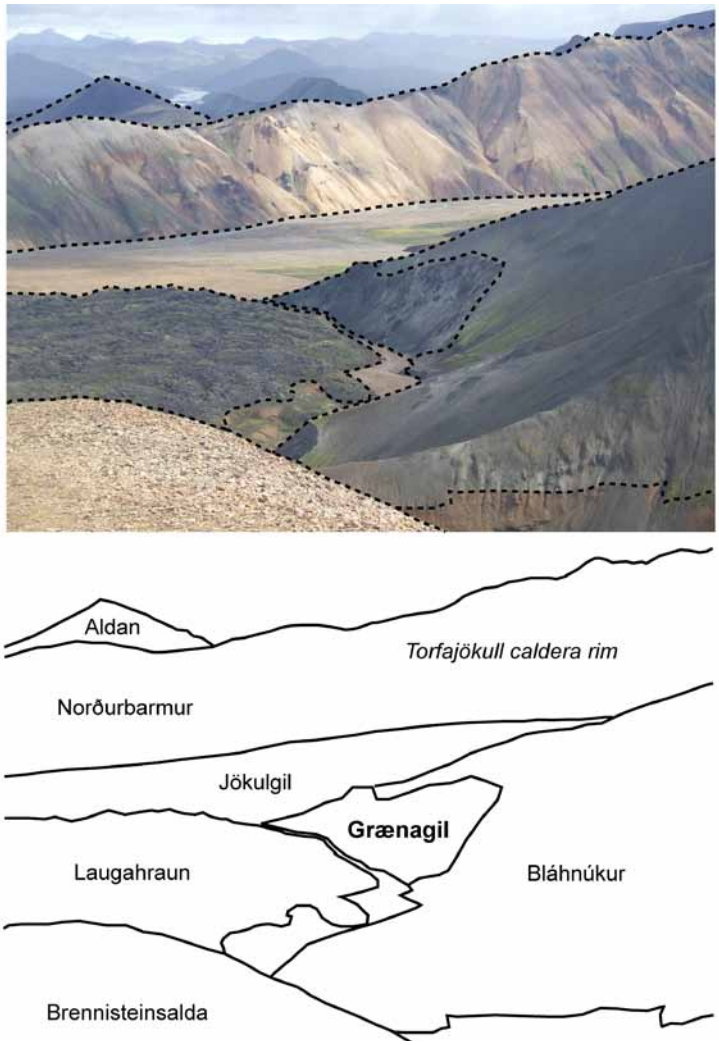

Fig. 7 - The area of interest in Torfajökull, viewing towards the northeast from the flank of the Brennisteinsalda (+855 m). Clearly visible is the colourful rhyolitic pre-glacial topography that lines the caldera rim. Towards the right, darker subglacially formed hyaloclastites mark the flanks of the Bláhnúkur edifice. Directly next to Bláhnúkur is the subaerial outflow lava Laugahraun ('bathing lava' in Icelandic, referring to the active geothermal hot springs on the far side of the formation).

and can best be interpreted as the remnants of debris avalanches and sections remobilised by slumping. Both processes occurred subglacially in the eruption cavity (Tuffen *et al.*, 2001). The resulting well-drained and moderately-cohesive deposits are found across the entire area of interest and have a predominant coarse-grained sandy texture that is also characteristic for other rhyolitic ashes in the area (Heiken, 1972; Tuffen *et al.*, 2001; Denton *et al.*, 2009). The Bláhnúkur edifice and Grænagil gorge hence provide a unique geological setting with material properties that are favourable for studying aeolian influences on hillslope weathering and scree cone development.

3. Methodology

A geomorphological field inventory focused on establishing dominant sedimentary landforms within the Grænagil gorge (63°59'04" N, 19°3'51" W, 620 m.a.s.l). Previously reported geological sequences and observed development of geomorphologic features over a five year period (2007-2011) were combined to reconstruct the landscape evolution of the area of interest. The stratigraphy and morphometry of distinguishable sedimentary landforms such as scree and alluvial deposits inside the Grænagil gorge were determined and allowed us to infer and link the formation environments to the measured properties. Ten undisturbed cubic decimetre (1 L) rock samples were collected on various locations on the rock face of Bláhnúkur above the Grænagil gorge (henceforth called the 'source areas'). These samples were used to determine the abundance of deflatable fractions (<150 μm). Collected samples were homogenised prior to further analyses to compensate for sorting processes during transport. Particle-size analyses were carried out for the fraction ≤4.8 mm for each of the obtained samples according to the preparation and sieving protocols described by Gee and Bauder (1986). The 150-2000 μm fraction was processed by sieving the samples over eight ½ φ fractions. The texture of the silt and very fine sand fraction (<150 μm) was measured using a Micromeritics Sedigraph 5100, which uses X-ray to determine grain-size distributions by measuring the settling velocity of particles. The GRADISTAT utility of Blott and Pye (2001) was used for describing and summarizing the particle-size distributions following the arithmetic methods of moments (Friedman and Sanders, 1978).

3.1 Meteorology and wind tunnel simulations

Wind tunnel simulations were carried out in order to measure the physical requirements for the removal of fine hyaloclastites by the wind. Four of the size fractions (<212 μm) were sampled with a repetition of $n = 3$ and were used for simulations inside a recirculating wind tunnel according to a fixed protocol (Merrison *et al.*, 2007; 2008, also see chapter 4 for more details on this method). Threshold wind speeds (u) and friction velocities (u_{*ft}) were measured for dry (70°C air-dried) samples for an atmospheric pressure of 1024 mbar at 20-25°C. Saltation mechanisms for wind-driven removal of particles may be more difficult to achieve on steep slopes and the contribution of gravity-driven saltation impact is difficult to quantify. Using the method of Merrison *et al.* (2007) we therefore exclusively measured the detachment threshold (particle removal which includes rolling and sliding) by excluding the influence of wind-induced saltation impact.

Meteorological observation of hourly wind speeds, precipitation rates and temperature were used in conjunction with the measured threshold wind speeds for particle removal to assess the occurrence of favourable weather conditions for wind erosion and the contribution of other processes. We assessed the vulnerability of the hyaloclastite material for shallow mass movements in wet conditions, which could contribute to the formation of the foot slope sediments. Rainfall intensities and durations were therefore compared to empirical thresholds for landslides, debris flows and soil slips from other studies (Caine, 1980; Innes, 1983; Clariza *et al.*, 1996 and Guzetti *et al.*, 2008) for our 5-year observation period. Due to the lack of long-term meteorological records in the surrounding area of Landmannalaugar, we used data from the two closest automated meteorological stations located at Vatnsfell (64°11'39" N, 19°2'51" W, 539 m.a.s.l., 24 km distance) at a heading of 2 degrees N and the station Lónakvísl (64°5'53" N, 18°36'50" W, 675 m.a.s.l. at 26 km distance) at a heading of 60 degrees NE from Bláhnúkur.

3.2 Comparing grain-size distributions

One scree cone was selected as a case study to measure if the physical conditions required for removal of fine fractions by the wind were reached often enough to affect and modify the texture of the sediment. We tested our hypothesis for a well-defined representative scree cone in the gorge where deflation of the overlying rock face was observed in the field and which had a distinguishable source area of ~50 m^2 and a defined supply route (chute) that channelized all forms of rock particle fall from different erosion and transport mechanisms to the studied scree cone. Twelve cubic decimetre (1 L) samples were collected in-situ from the upper 10 cm of scree along three transects running from the feed mouth down to the base of the scree cone.

The grain-size distributions of the scree sediment samples were then compared to the overlying source area to determine the selection and depletion of size-ranges in the sediment that could be indicative of aeolian influences. A Pearson's X^2 test for independence (Davis, 2002) was used to statistically test the equality of the distributions of the primary source area above the sampled scree cone and the samples obtained from the scree cone itself. A Pearson's X^2 test is the sum of the squared differences between the observed (O) particle distribution and the expected (E) distribution in each particle-size class, divided by the expected distribution ($X^2 = \Sigma((O-E)^2/E)$). The null-hypothesis (H0) that we used for this statistical comparison was the assumption that the distribution of the parent rock in the source area (E) matched the distribution of the scree sediment (O). In other words: erosion and transport processes do not modify the texture of the sediment. Using the Pearson's X^2 test we could falsify the H0 hypothesis by showing that the sediment distribution of the scree sediment was significantly different from the parent material. We tested the null hypothesis (E and O are similar) at the 0.01 significance level.

4. Results

The eruption of Laugahraun in 1477 AD and the subsequent blockade of the valley plays an important role in the geomorphological and hydrological development of the present-day area. The hydrological networks that established after the eruption incised into the less-resistant hyaloclastites at the interface with the Laugahraun outflow lavas. The geomorphology of the area of interest (Fig. 8) is therefore dominated by the narrow incision of the Brennisteinsöldukvísl stream between the resistant outflow lavas and the softer subglacially deposited Bláhnúkur hyaloclastites. The continuation of these hyaloclastites underneath the Laugahraun outflow lavas is only well exposed at the entrance of Grænagil, although remnants can also be found underlying Laugahraun at other locations inside the gorge. From the present morphology we can infer that the stream undercut the hyaloclastites positioned underneath Laugahraun, which caused partial collapses along the southern edge of the formation. Presently, the Laugahraun formation can be characterised as a fairly inert formation and it does not show significant forms of physical weathering, aside from the occasional rock fall. Resistant rock formations of Laugahraun and lava lobes in the hyaloclastites pinch the stream at various locations at the bottom of the gorge. The stream has a wider bed at other sites where the gravely substrate and large surplus in sediment gives the stream a modest braided character. The continuous migration of the streambed causes undercutting and abrasion of the foot slopes is the most active geomorphological processes inside the Grænagil gorge. These processes uphold the conditions for the formation of foot slopes below the steep-sided rock faces inside the gorge.

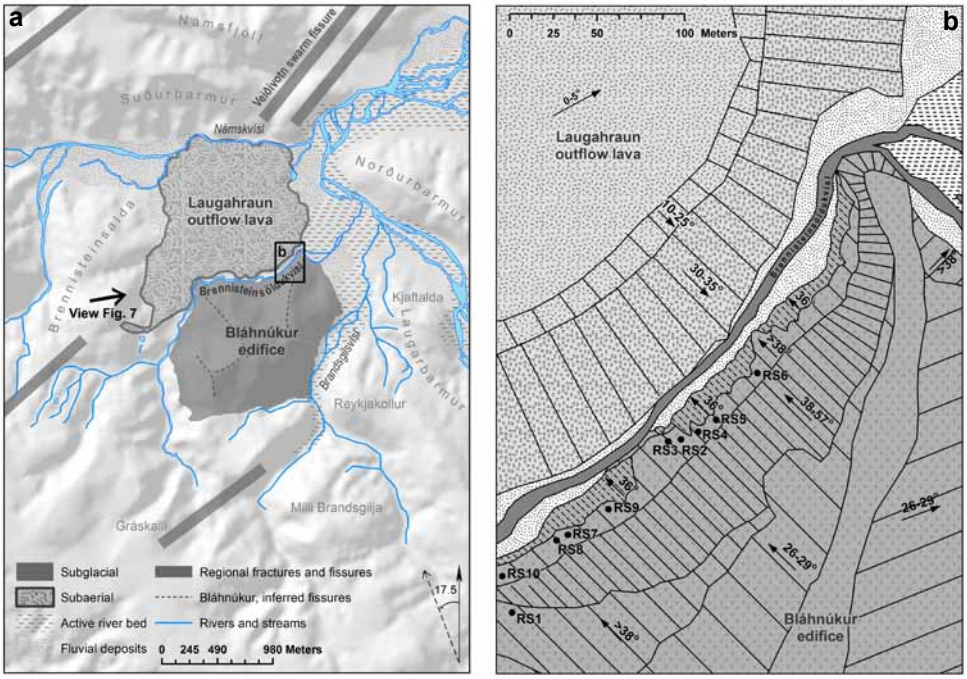

Fig. 8 - Geomorphological overview of the Grænagil gorge. A shaded-relief map shows the setting with the Laugahraun and Bláhnúkur formations delineated in grey (a). The simplified geomorphological map of the Grænagil gorge illustrates the processes and landforms of the area of interest (b). Collected rock samples (RS01-RS10) are marked. Sample RS3 is located inside the source area of the studied scree cone.

Above the valley floor, the hyaloclastite slopes of Bláhnúkur described by Tuffen *et al.* (2001) show a higher magnitude of geomorphological activity compared to Laugahraun. The flanks from the summit down to the valley bottom of Bláhnúkur can be generalised into three main sections. A low inclination (26-29°) top plane leads from the main summit down to a spur situated above the steep-sided rock face overlying Grænagil. The inclined furrowed rock face resides close to, or above the maximum angle of repose (>38°) and is interlaced with numerous chutes with more resistant protruding lava lobes. Various steep-sided subvertical parts of the rock faces extend to an altitude that varies from 40-70 meters above the valley floor. The development of these slopes is strongly influenced by the undercutting at the foot by the Brennisteinsöldukvísl stream and backwards erosion of rills and gullies at the nick-point of the rock face and top plain. Sedimentary deposits are formed directly underneath the rock face. A small number of distinguishable scree cones with slope angles of 36±1.3° (n = 7) have been formed at the foot of the green and grey-coloured rock faces (calibrated Munsell-scale colours of dried samples range from 2.5G 5/2 to 8/10Y). Fluvial influences on the deposition of material is shown by well-developed rills and gullies in the top plain of Bláhnúkur and these features continue into the morphology of the furrowed rock faces. Contrary to the abundance of rills and gullies only one distinct alluvial fan has been formed from these systems in 5 years of field observations inside the gorge (Fig. 9a-b). The morphometry of alluvial landforms consisting of hyaloclastites was characterised by <25° slope angles, which clearly differed from the slope angles of the dominant scree deposits inside the gorge. The low abundance of sedimentary landforms formed by fluvial processes suggested that transport and deposition

of material by water does not take place at a large scale. These contributions may only be active during torrential events and rapid large-scale seasonal snow melt in spring and early summer. Shallow mass movements were observed in various scree deposits that have been initiated by oversaturation with water. It is common to see slumping near the interface of the scree with the rock face as a direct result of overland flow or lateral rain (Fig. 9c). Sliding of sediment was found in close proximity to these slumping regions, where a typically 30 cm thick layer is oversaturated with water and drives the sliding across a slipface of predominant gravely strata, which eventually breaks-up of the slope's face (Fig. 9d). Characteristic layering was mostly absent in the alluvial fan of Fig. 9a-b whereas stratified sediments were more commonly found in the abundant scree deposits. This layering with sharp boundaries is well-exposed at various locations such as in the sampled scree cone (Fig. 10a, 10c) and in adjacent scree slopes. Liberated and excavated particles created discontinuous avalanches of sediment that formed lobes of material and progressively changed the surface texture from small particles at the top of the scree cones to larger particles at the foot of the cone. Erosion occurs as a result of this stratification when the overlying layers are destabilised in dry conditions by undercutting of the stream and experience sliding on the contact surface of the coarse gravely strata.

Due to absent meteorological records inside the area itself, snow cover conditions have been inferred from the accessibility of the F208 road leading directly to Landmannalaugar (Torfajökull) from 2007-2011 (Table 1). More general meteorological records (Einarsson, 1984) also show that slopes in the area have a snow cover ~60-70% of the year with a snow-free period typically from June to September. The thin blanketing layers of fall deposits and sheltering of snow in steep valleys allow ice lenses to survive into the heart of the summer at places, which have preserve records of these processes (Fig. 11).

4.1 Meteorology and wind tunnel simulations

The two nearest meteorological stations allow some speculation about the meteorological conditions controlling the observed types of particle-removal. Measurements of the meteorological conditions at Vatnsfell and Lónakvísl have been summarised in Table 1. The mean annual temperature for both sites is close the freezing point and illustrates the importance of the frequently occurring freeze-thaw cycles in these regions. Although there is some spatial variation in the precipitation, we find that the majority of rainfall events in the summer period (June - September) fall below the thresholds for initiating shallow mass movements (Fig. 12). Within this snow-free season (June - September) wind speeds varied between 8-11 m s^{-1} while maximum gusts during violent storm evens reached wind speeds in excess of 45 m s^{-1}.

Entrainment of substantial amounts of fine material (silt particles) has been observed during episodes of dry and windy weather where larger particles were excavated and subsequently rolled down-slope where they accumulated in the scree sediments (see Fig. 13 and the video material included in the online appendices). Meteorological records indicate that during the observed deflation the average wind velocities and gusts ranged from 11-17 m s^{-1} from a north-north-easterly (NNE) direction. Wind tunnel simulations showed that threshold wind speeds required for removal of these hyaloclastites by the wind varied from 5 m s^{-1} for >200 μm sandy particles to 10 m s^{-1} for finer silt fractions (Fig. 14) in dry conditions. The field conditions are well over the critical threshold wind speeds required for removal of silt and sand-sized particles.

The locations of the obtained samples inside the gorge have been marked in Fig. 8 and the spatial arrangement for sampling of the scree cone is provided in Fig. 10a. From the stratigraphic column (Fig. 10c), it can be inferred that sampling of the upper 10 cm of the sediment provides an average sediment distribution of 4-5 consecutive avalanche events. The results of the texture analyses have been visualised in Fig. 15 and a complete overview of all the samples is included in appendix E. The scree sediments were typically poorly-sorted platycurtic distributed coarse sands (D50 = 821 μm, D90 = 2855 μm) whereas the primary source area was classified as poorly-sorted mesokurtic medium to fine sands (D50 = 297 μm, D90 = 1255 μm). The Sedigraph analyses of the deflatable fractions (<150 μm) of the rock matrix show that the source areas were dominated by a high percentage of coarser silt (10-70 μm) and a small amount of clay-sized particles. A notable difference between the source and deposition areas was identified in the silty size range. The overall distribution of the primary source area has a silt fraction in the order of 5-10% whereas the scree sediments only have a 0.3-0.6% silt content. An opposite trend is found in the larger textures. Source areas contained coarse to very coarse sands in the order of 8-20%. The similar fractions in the scree sediments showed a notable enrichment of which the contribution varies between 21-73% (40% on average).

A statistical comparison of the particle-size distributions using the Pearson's X^2 test shows that the distributions of twelve scree cone samples collected from the one scree

Table 1 - Overview of meteorological conditions from 2007-2011. Values for the stations Vatnsfell and Lónakvísl are calculated from hourly measurements.

Meteorological conditions	Year				
	2007	2008	2009	2010	2011
Vatnsfell					
Average wind speed [m s^{-1}]	7.7	7.7	8.0	7.7	8.4
Average gust [m s^{-1}]	11.0	11.0	11.4	11.0	11.9
Maximum gust [m s^{-1}]	42.8	48.1	49.6	45.5	51.2
Mean annual precipitation [mm]	925	699	681	639	776
Summer precipitation sum [a] [mm]	291	356	218	264	178
Mean annual temperature [°C]	1.1	1.1	1.8	1.8	1.8
Days of freezing	159	165	130	144	106
Freeze-thaw cycles	144	62	117	86	116
Lónakvísl					
Average wind speed [m s^{-1}]	6.9	6.7	6.3	6.2	7.1
Average gust [m s^{-1}]	10.9	10.6	10.0	9.8	11.0
Maximum gust [m s^{-1}]	54.0	47.5	44.5	46.1	44.9
Mean annual precipitation [mm]	1465	1444	1379	1182	- [b]
Summer precipitation sum [a] [mm]	369	694	373	574	- [b]
Mean annual temperature [°C]	0.6	0.3	0.7	1.0	0.6
Days of freezing	167	173	153	151	158
Freeze-thaw cycles	127	67	125	93	129
Melting of snow cover [c] [day-month]	7-6	29-6	5-6	2-6	21-6
New snow cover [c] [day-month]	- [b]	- [b]	30-9	- [b]	- [b]

[a] *June 1st - September 30th summer period*
[b] *Not measured or no data available*
[c] *F208 road access to Landmannalaugar, data from: Vegagerðin (Icelandic Road Administration)*

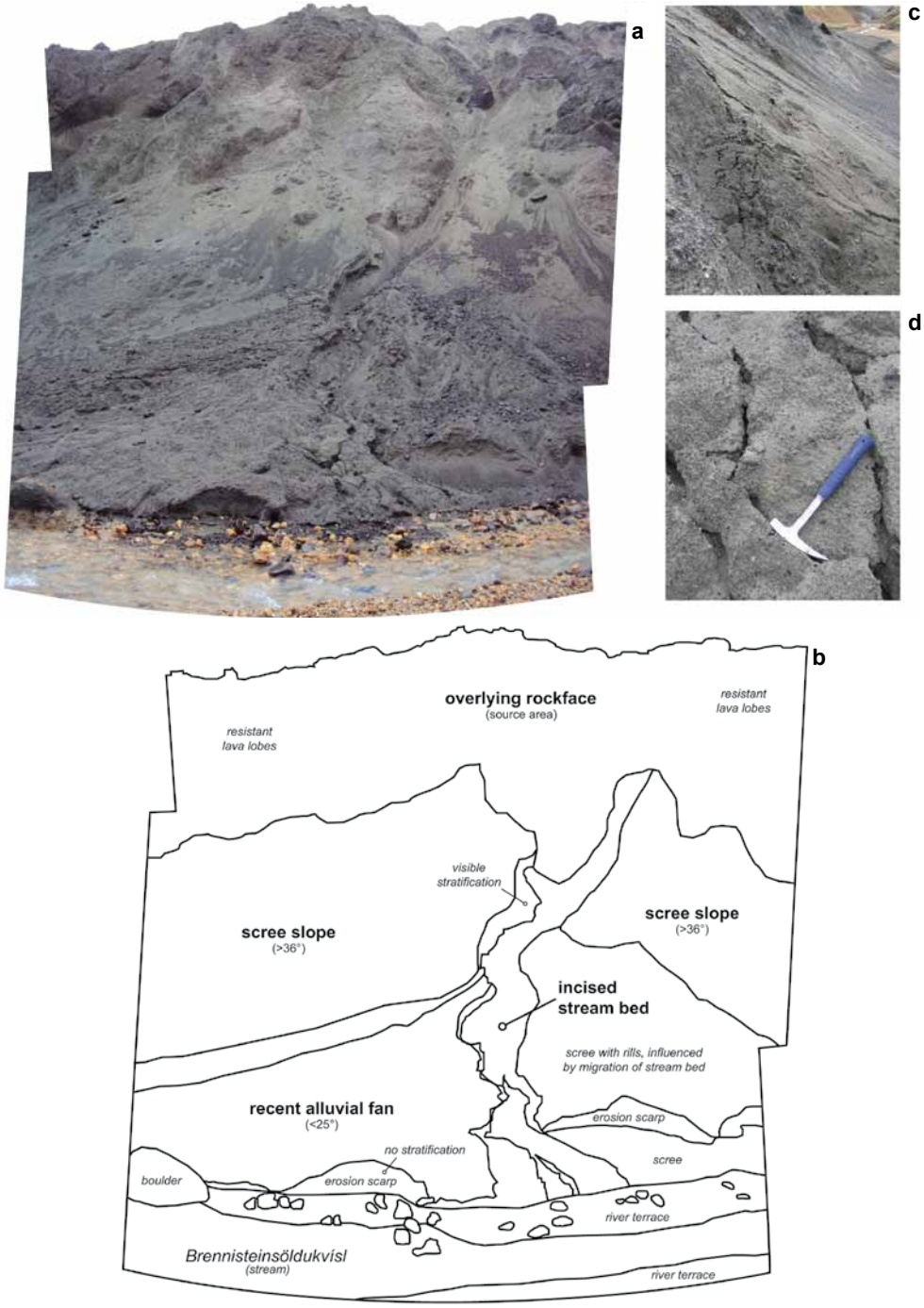

Fig. 9 - Wet geomorphological processes. In five consecutive years of field observations, snow melt and local rainfall conditions have been able to produce one distinct alluvial fan inside the Grænagil gorge (a). Differences in angles of repose are found between scree and alluvial deposits, clearly resulting from the two different formation environments (b). Excessive water saturation of scree deposits by overland flow across the rock face creates mass movements in the form of slumping with distinct back-rotations (c) and sliding of oversaturated deposits across coarse gravely layers (d).

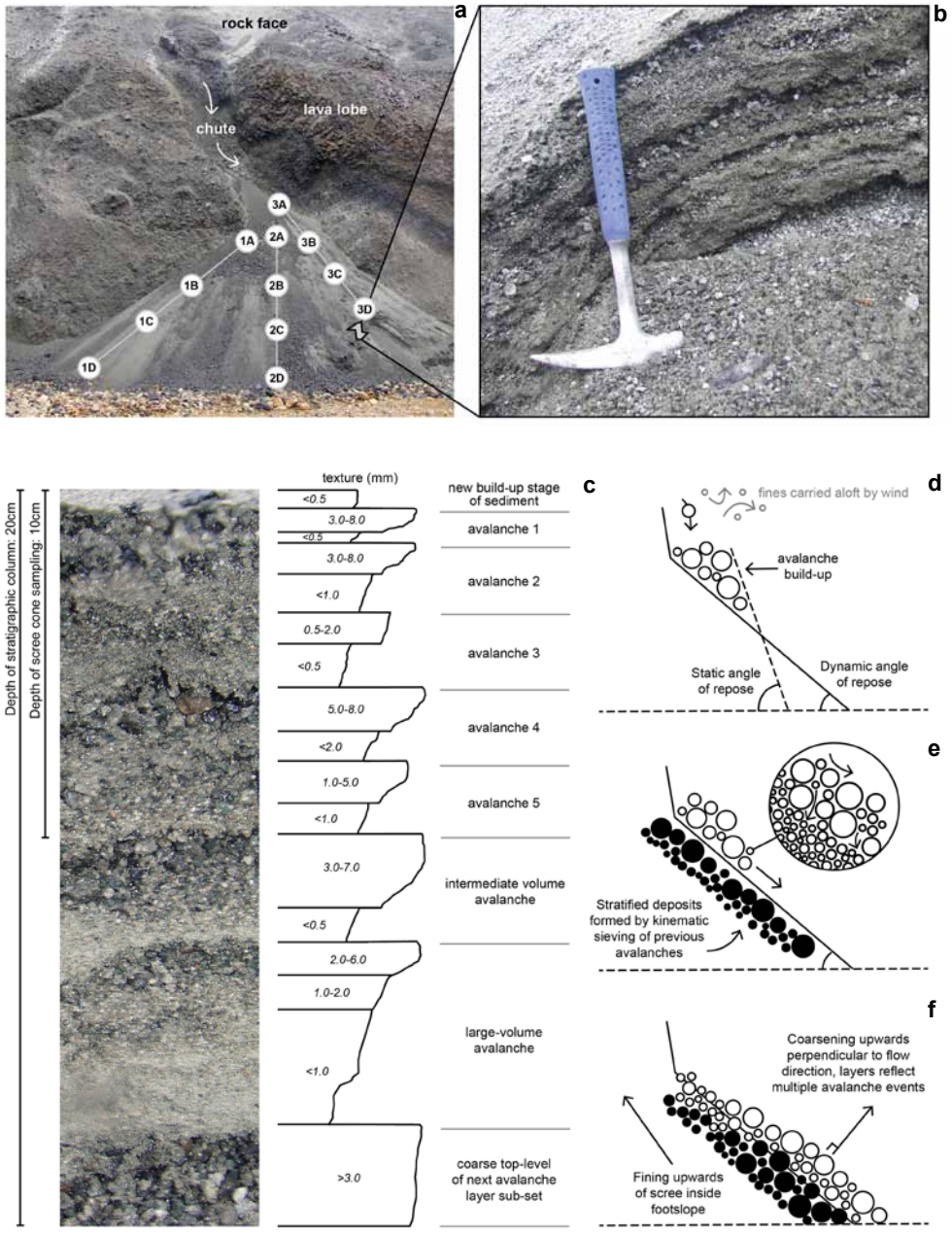

Fig. 10 - Dry geomorphological processes. Sampling transects over the face of the scree cone (see text) run under a ~36° slope angle from the 1 m wide feed mouth down to the foot of the slope (6.1 m slope length, 12.3 m circumference) (a). Clear stratification is visible inside the scree cone (b). The stratigraphic column shows distinct coarsening upwards within layers which reflects individual avalanche events (c). Stratification is attributed to sorting processes during avalanching of sediment when the maximum static angle of repose is exceeded (d). Kinematic sieving then causes a separation in grain-size where small particles sieve through the coarser particles (e). Fining upwards occurs along the slope length of the scree cone and coarsening upwards is found perpendicular to the flow direction of each individual avalanche (f) (d-f adapted from: Kleinhans, 2005).

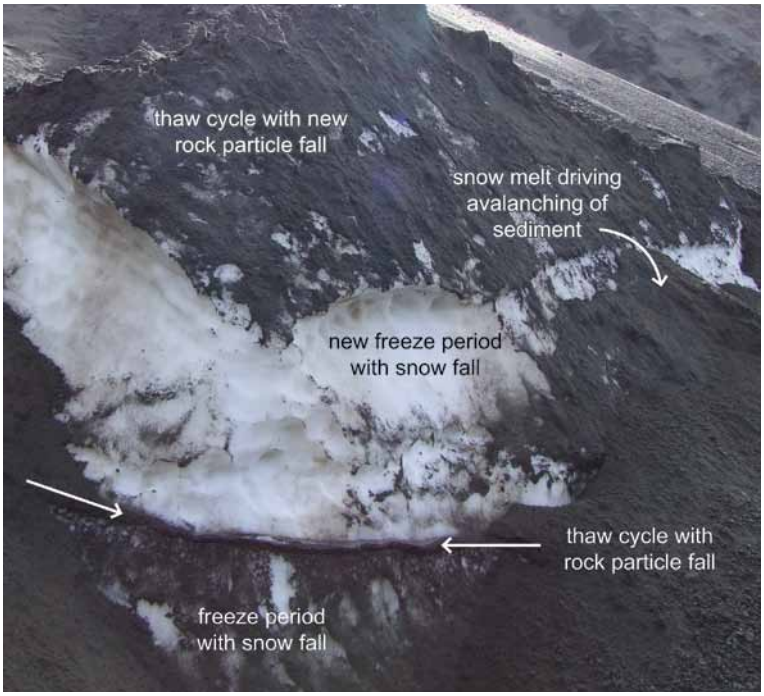

Fig. 11 - Icy geomorphological processes. An ice lens preserved in Grænagil on the foot of a northwestwardly exposed scree slope which survived into late-summer of 2009. Two major snow periods illustrate the accumulation of material excavated by freeze and thaw cycles and subsequent avalanching of the sediment.

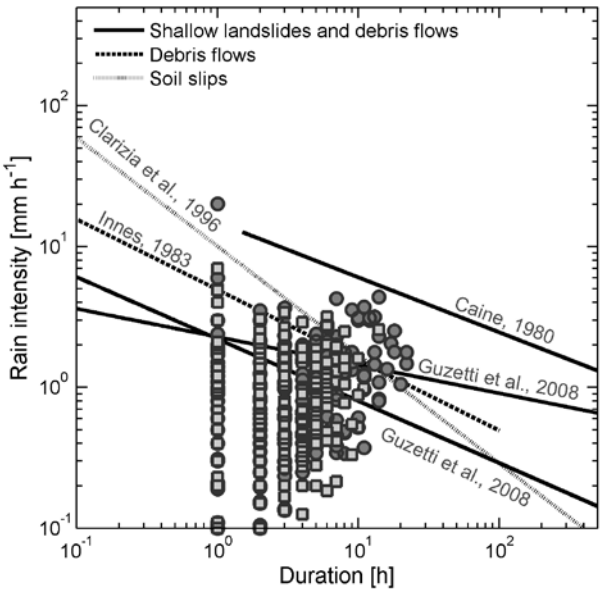

Fig. 12 - Rainfall intensity-duration (ID) plot showing that the majority of rain events at Lónakvísl (circles) and Vatnsfell (squares) over a 5 year period are below the observed thresholds for debris flows and shallow landslides from other studies.

Fig. 13 - In-situ observation of deflation inside the Grænagil gorge. Fine silt from the Bláhnúkur hyaloclastites is carried aloft by the prevailing wind gusts while being deposited elsewhere in the area. At the time of these observations (15th August 2007) winds and gusts in the southern highlands of Iceland varied between 11-17 m s^{-1} from predominantly north-north-easterly (NNE) directions.

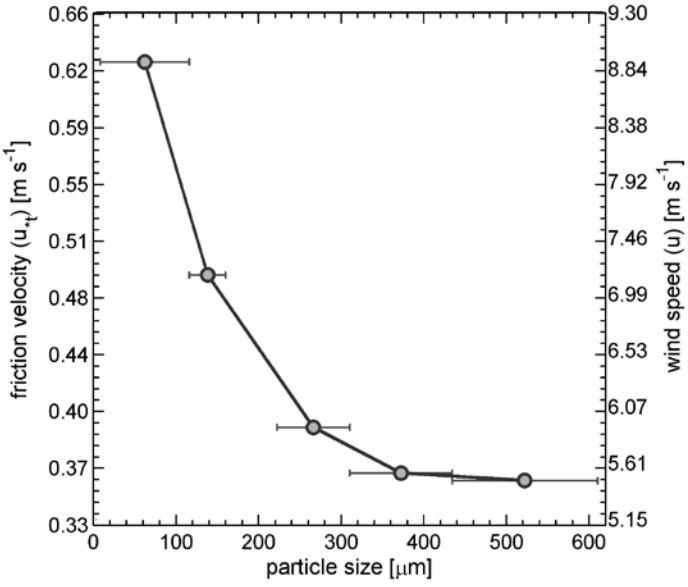

Fig. 14 - Threshold shear stress measured in wind tunnel simulations for the detachment of dry samples of different textures of Bláhnúkur hyaloclastites. Simulations were carried out at an atmospheric pressure of 1024 mbar at 20-25°C. The error-bars on the x-axis represent the size-range of each fraction.

cone were significantly different from each other (X^2 = 146, df = 49, $p \leq 0.001$). The average distribution of these scree sediments has been calculated to produce a spatially averaged value to compare the scree sediment with the expected distribution of the primary source area that was concentrated in the scree cone. This comparison showed a statistical difference between the source and deposition areas with (X^2 = 34, df = 11, $p \leq 0.0003$). A broader spatial comparison of the particle-size distribution of ten different locations of the Bláhnúkur hyaloclastites (including the primary source area) shows that the distributions of these source areas are comparable throughout the Grænagil gorge (X^2 = 43, df = 63, $p \leq 0.97$), as H0 (i.e. distributions are similar) is not rejected by the Pearson's X^2 test.

5. Discussion

The regional landscape evolution has played an important role in creating the favourable conditions for the development of the rock face and the formation of scree deposits by a multitude of processes throughout the seasons. Studies of geomorphological and sedimentary processes involving the modification and transport of friable glassy hyaloclastites are scarce and comparisons to other studies are therefore difficult. Deposits that resemble the texture of the studied sediments in Iceland in similar cold environments are Grèze-Litée sediments (hillslope sediments with alternating layers of coarse and fine shales) commonly formed in alpine periglacial environments (van Steijn *et al.*, 1984; 1995). The stratigraphy and morphometry of these fine-grained deposits have been studied more intensively and thus provide a reference for comparing and inferring the contributions for various erosion and deposition processes to the sedimentary landforms inside the Grænagil gorge.

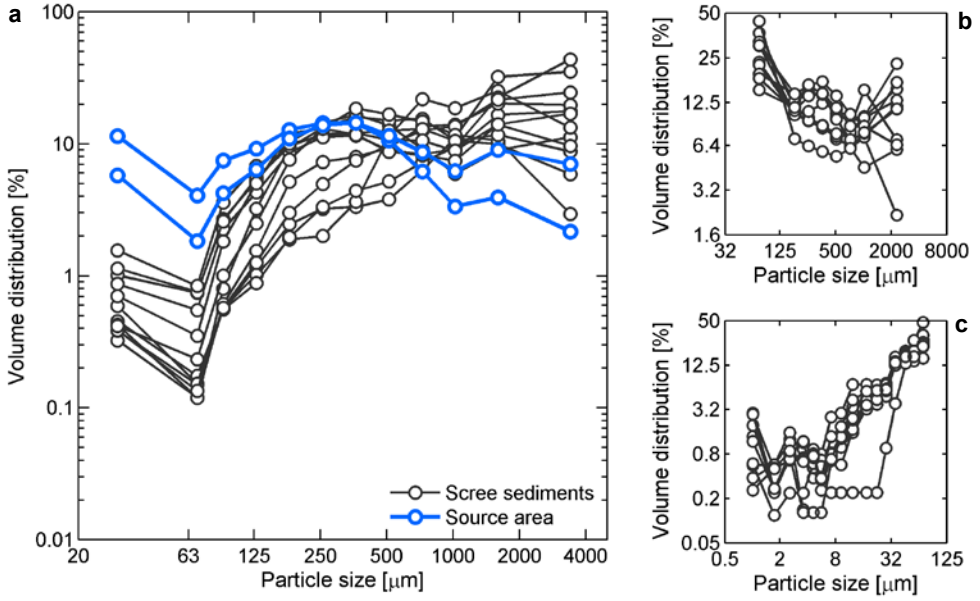

Fig. 15 - Overview of the distribution analyses of sampled source areas and scree sediments in Grænagil. The main graph (a) compares the primary source area (RS03) and another source area 100 meters further down the gorge (RS08) with the sediment sampled in the scree cone. Sediment distribtions are comparable for the samples source areas (b) while silt and clay contents are nearly identical thoughout the gorge (c).

5.1 Processes driven by flowing water

The rainfall intensity-duration conditions during the 5-year observation period show that the vast majority of rainfall events is below the threshold for shallow mass movements (Fig. 12). When taken together with the permeable nature of the hyaloclastite material it suggests that such processes are rare, which is supported by the low occurrence of alluvial landforms in the studied gorge. However, other forms of erosion and transport by overland flow of water could still have occurred. The particle morphology of hyaloclastites and their observed random orientation in the layers exclude the role of (melt)water-related transport processes such as nivation. This view is supported by the questionable contribution of nivation on slopes of flaky Grèze-Litée where particle-orientation is often more pronounced than for these blocky hyaloclastites (van Steijn *et al.*, 1984; 1995). Similarly, slush avalanching (Caine, 1969) during thaw periods from overlying slopes would play a minimal role as indications from oriented particles are absent. The required conditions for this process on the high-angle scree slopes would only occur very infrequently during spring, while being absent throughout the remaining seasons. These processes therefore do not provide sufficient explanation for the abundant stratification of the scree sediments. In wetter conditions overland flow or slope wash, perhaps driven by lateral rain or rapid snow melt on the overlying rock face or on top of top plain, is illustrated by the numerous rills and gullies. However, the amount of water and stream velocity required to move the coarser particles found in the sediment would more likely create incised streambeds and alluvial landforms during torrent events (van Steijn and Hétu, 1997). The straight upper slope in combination with absent concave tailing, incised stream beds and levées also support the exclusion of wet debris flows (Statham, 1973; Blissenbach, 1954; van Steijn *et al.*, 1995). Furthermore, the morphometry of the observed alluvial fan disputes an alluvial formation environment for the scree deposits due to their higher slope angles (van Steijn and Hétu, 1997). These morphometric differences are in line with observations of Rapp (1959) who concluded that in periglacial conditions sedimentary landforms of fine materials below 25° should be derived by other mechanisms than rock particle fall. Alluvial landforms are very scarce in the area and water-related effects are more commonly found in the form of localized slumping of the upper scree slopes and sliding by the oversaturated mass. An alternative hypothesis involving a wet formation environment which could explain the difference between the parent rock and sediment involves eluviation of fine particles through the sediment column. However, we can argue against such processes due to the observed sharp boundaries in the stratigraphy of the sediment (Fig. 10c). Other studies have also questioned similar influences in other geological settings with fine-grained sediments due to sharp sediment boundaries (van Steijn *et al.*, 1984). If in the most optimum case, clay from the sediment column is indeed lost with percolating water, this mechanisms would not be able to sufficiently explain the reduced coarser silt content in the scree sediment. Overall, we do not exclude the influence of wet processes but we find little support for large-scale contributions of rain and snow-melt driven processes to the formation of scree sediment inside the gorge.

5.2 Freeze and thaw cycles

Similar to conditions in other periglacial environments, freeze and thaw cycles are an important process for the physical weathering of Bláhnúkur. Throughout the year some 100 cycles occur as the mean annual temperature in the area is close to the point of freezing. Cyclic loading of the rock face occurs mainly from the weeks after first snow fall (September) until thaw in the following spring (May-June). The friable tuffaceous nature of the hyaloclastites

and the frequent occurrence of freeze-thaw cycles suggest that gelifraction (water infiltrating in the vesicles of the volcanic material, expanding upon freezing and fracturing the material) could be important. However, a larger amount of fines should be present in these sediments which is not the case. It is more likely that expanding ice in interparticle pore spaces leads to physical weathering of the rock matrix which excavates material rather than fracturing into smaller particles. Intact larger particles in the strata (Fig. 10c) of the scree deposits support the notion that these sediments are derived by excavation rather than the gelifraction of larger clasts. Snow covers the slopes some 60-70% of the year (Table 1) and in the middle of winter the limited insolation, combined with the low elevation of the sun, a north-westerly exposure and the nearly continuous below-freezing temperatures would only cause significant rates of frost weathering on the overlying rock face. The accumulation of excavated materials on the snow blanket creates a temporal form of sediment storage. The persistent snow cover of these scree slopes during winter therefore prevents avalanching of sediments. After thawing of the snow and ice, the accumulated material during contributes directly to the build-up stage of new avalanches. A significant contribution of semi-frozen materials or frosted granular flow is excluded as this process is inhibited by the continuous snow cover and the observed slope angles exceed the known maximum range for this process (slope angles <28°). Avalanching of the accumulated material therefore occurs presumably in dry conditions, due to the high slope angles measured for these scree slopes.

5.3 Dry avalanching

In the local of the study site environment, discrete avalanching of sediment over the slope face is crucial *in lieu* of driving (i.) sorting of larger grain sizes along the slope and (ii.) distinct coarsening upward of the sediment perpendicular to the slope. Clear effects of these processes are found in the stratigraphy (Fig. 10c) and point towards a combination of kinematic sieving and length-wise sorting inside each granular avalanche (Fig. 10d-f) (van Steijn *et al.*, 1995; Makse *et al.*,1997; Aranson and Tsimring, 2006; Sass and Krautblatter, 2007). Dry avalanching processes are therefore considered to be common for the studied high (>36°) slope angle scree deposit. While the sediment build-up takes place continuously, avalanching of the accumulated sediments is limited to dry conditions which creates the characteristic layering.

5.4 Contributions of aeolian processes

Aeolian influences on the development of fine scree deposits are often underestimated and usually associated with the removal of larger clasts in extreme events such as blizzards or by moderate gale force winds (>14 m s^{-1}) (van Steijn *et al.*, 2002). In other studies the aeolian influence on fine sediments is usually of niveo-aeolian origin, whereas only few putative examples are known where wind-induced erosion of overlying rock faces contribute directly to the liberation of coarser materials and clasts (van Steijn *et al.*, 2002). Based on our field observations and wind tunnel simulations of the removal of the volcanic glass we find that this material can be removed by a moderate to fresh breeze (<10 m s^{-1}) and such conditions occur frequently in the southern highlands of Iceland (Table 1). Although the velocities and flow turbulence of the wind may be aggravated by the local topography, both meteorological stations show similar wind conditions over the 5 year observation period in favour of a high occurrence of the observed deflation processes. We therefore believe that the given records in Table 1 reflect the region's meteorological conditions, which allows the use of this data for the research field site.

Analyses of the scree sediments and the source areas showed a clear numerical and statistical

differences between the distributions. The scree cone sediment (D50 = 821 μm, D90 = 2855 μm) is depleted in the silt and enriched in larger sands in comparison to the source area on the overlying rock face (D50 = 297 μm, D90 = 1255 μm). The notable enrichment of large particles and depletion in silt particles suggests a highly selective mechanism to influence the distribution and formation of the scree cone sediments. Aeolian deflation of the rock face and sediments offers a plausible mechanism that is sufficiently explaining the observed differences between the particle-size distributions, whereas fluviatile processes must be less important. Silt is easily carried aloft and away from the hillslopes by prevailing winds and gusts. The transport length of excavated material along the steep rock face further increases this effect by injecting clay and silt fractions into even modest winds. Larger particles are gradually excavated and transported down-slope under the influence of gravity by which they dominate the particle-size distribution of the scree sediments. As such an aeolian deflation mechanism permanently modifies the texture of the sediment by the selective removal of the fine textures. Favourable conditions for aeolian contributions may indeed be limited throughout the year, but their effects during single events can be much stronger compared to other processes which only redistribute the sediment. The contribution of this aeolian deflation mechanisms to the development of the scree slopes is corroborated by field observations during dry and windy conditions (Fig. 13).

Overall, we can conclude that individual rock particle fall and avalanching of accumulated sediment in dry conditions (deposited by a multitude of processes that includes aeolian excavation) control the observed morphometry and stratigraphy of the scree deposits. Aeolian deflation permanently modifies these sediment either in-situ or during transport which explains the observed textural differences between the scree and the original parent rock. Although the deflation mechanism proposed here has not previous been reported, more work is still required to fully understand the scale of these processes in the development of stratified slope deposits of friable volcanic ash in subarctic environments.

5.5 Planetary occurences of the Icelandic field processes

Volcanic glass such as the Bláhnúkur hyaloclastites in Iceland are an interesting analogue material for Mars due to the parallels between the formation of subglacial eruption products on Earth and the eruption mechanisms in contact with (sub)surface ice bodies on Mars (Allen *et al.*, 1981; Bishop and Pieters, 1995). With some constraints we can use the aeolian mechanism proposed here (deflation of fines by the wind followed by excavation, transport and sedimentation of sands under the influence of gravity) as a model for the recently active gully-systems observed on various crater walls on Mars (Balme *et al.*, 2006). Several hypotheses have been put forward for either dry or wet out-flow forming processes inside these gullies (Hartmann *et al.*, 2003; Hugenholtz, 2008; Pelletier *et al.*, 2008; Coleman *et al.*, 2009). We propose an alternative, erosive aeolian mechanism parallel to depositional aeolian mechanisms suggested for example by Treiman (2003). The micro-topography of pre-existing rills and gullies (formed during past climates) can sufficiently increase the turbulence and shear stress in the present atmosphere of Mars to entrain fine textures from the regolith by processes such as dust-electrification (Merrison *et al.*, 2007; 2011). Larger particles excavated from the regolith then become available for transport down-slope while being channelized through the existing chutes (gullies), analogue to parts of the steep-sided walls in Grænagil on Iceland. Sufficient sediment build-up at intermediate storage areas inside gullies on Martian hillslopes and crater walls can then create localised avalanching when the static angles of repose of the accumulating sediment is exceeded. Triggering of such granular avalanches

from within the gullies on Mars can easily be initiated by winds which are also capable of mobilising larger sand particles in the present environment (Silvestro *et al.*, 2010; Bishop, 2011; Bridges *et al.*, 2012a).

6. Conclusions

Subglacial and post-glacial volcanism have played a prominent role in landscape evolution of the present-day surroundings of Bláhnúkur. The regional development is driven by the basal erosion of the hyaloclastite rock face and undercutting of scree sediments by the Brennisteinsöldukvísl stream inside the Grænagil gorge. Scree sediments are formed by alternating erosion processes on the overlying rock face throughout the seasons, which eventually results to avalanching of sediments in dry conditions across the pre-existing slope deposits. Although we do not exclude the influence of the other depositional processes, agents involving water or other forms of interstitial lubrication lack a morphometric and stratigraphic proof in the sedimentary record. Based on this stratigraphy and morphometry we cannot reject our hypothesis as we found dominant contributions of freeze-thaw cycles in the snow record and influences from the wind which both contribute to the development and modification of these landforms. The influence of the wind is highly relevant in dry conditions when it drives the deflation of fine material in accumulated scree sediment and it causes larger particles to be excavated from the overlying rock face. The threshold conditions required for particle removal in wind tunnel simulations agree with the range of frequently occurring winds in the region. Although the processes involved in the presented case study occur in a specific Icelandic environment, we suggest that deflation processes acting on hillslopes with a moderately-cohesive rock matrix are more widespread in dry and cold environments than presently understood and recognized. We propose that these mechanisms can therefore also occur in the present climatological conditions found on planet Mars.

▲ *Rhyolitic hyaloclastites with obsidian fragments exposed at the slopes of Bláhnúkur, Torfajökull*

Chapter 3

Physical weathering of glaciovolcanic glass

Abstract

Fragmental volcanic glass or 'hyaloclastite' is a common glaciovolcanic eruption product that occurs in basaltic and rhyolitic variants. These types of material are often found in Iceland in periglacial environments where they are susceptible to various forms of physical weathering and particle modification. This includes ice growth during freeze-thaw cycles and abrasion during aeolian transport. Physical weathering of rhyolitic volcanic glasses differs from basaltic glass due to the lack of edifice strengthening and consolidation. However, these materials are much rarer and they have been less studied and this emphasises the need for characterising the various facets of their mechanical modification. In this study we measured the weathering properties of rhyolitic hyaloclastites from the Bláhnúkur edifice in Torfajökull (Iceland) using simulations of freeze-thaw cycles and low-energy aeolian transport. Nearly identical particle size distributions were formed in the freeze-thaw simulations as in brittle fracturing experiments when glass was subjected to uniaxial stress. Brittle fracturing from frost weathering and compressive loading produced similar particle distributions. This comparable behaviour suggests that ice crystallisation and volumetric expansion has the strongest effect on pumiceous particles with vesicles and interparticle pore spaces >1000 μm. In contrast, abundant surface pores >1 μm (measured by high-pressure mercury intrusion) may only contribute to surficial crack propagation. Compared to the effects of ice weathering, particle abrasion during simulations of wind-induced transport was found to be a very slow-going process. Non-stop tumbling of 300-600 μm samples for 15 weeks, or 578-715 km of transport, only led to textural alterations at the limit of detection. Physical weathering of shards and pumiceous particles marginally increased the portion of <10 μm particles, which may increase the risk to health hazards after chronic exposure by inhalation. The experiments presented in this study illustrate too that accessible techniques can be applied to understand fracturing dynamics and the contribution of physical weathering to the formation of new and potentially hazardous respirable sediment textures.

This chapter is based on: *De Vet, S.J., Mittelmeijer-Hazeleger, M.C., Braakhekke, J.J.M., Cammeraat, L.H., 2013. Physical weathering and fracturing of a rhyolitic hyaloclastite in Iceland. (Submitted to: Bulletin of Volcanology)*

1. Introduction

Fracturing of glassy subglacial eruption products (known as hyaloclastite or as 'móberg' in Icelandic) results from the initial magma-ice and magme-melt water interactions during formation and from post-eruptive environmental processes. Recent eruptions from the Eyjafjallajökull have given insights in the eruption evolution (Sigmundsson *et al.,* 2010; Borisova *et al.,* 2012; Magnússon *et al.,* 2012) and deposition of these types of eruption products (Donnovan and Oppenheimer, 2011; Edwards *et al.,* 2012). Such glaciovolcanic eruptions have received much attention due to immediate syneruptive environmental effects (Colette *et al.,* 2011) and health hazards (Gudmundsson, 2011; Carlsen *et al.,* 2012), but these eruptions only illustrated the syneruptive effects of glass fracturing. The Icelandic landscape is littered with examples of deglaciated subglacial edifices where these eruption products are currently being modified. Suspension of ash from recent eruptions (Leadbetter *et al.,* 2012), wind-induced transport in glass-rich sandy deserts (Arnalds *et al.*, 2001, 2012; Baratoux *et al.,* 2011) and contributions of freeze-thaw and aeolian processes to the erosion of hillslopes from subglacial landforms (de Vet and Cammeraat, 2012) exemplify some of the environmental processes that affect glaciovolcanic glasses. Weathering of the basaltic glass often leads to rapid edifice strenghtening and reduces effects of physical erosion, while rhyolitic glasses hardly consolidate at all (Jakobsson and Gudmundsson, 2008). The physical modification of this silisic type of glass is primarily driven by mechanical forces created by microscopic (Scherer, 1999) and macroscopic ice growth (Jackson and Chalmers, 1958) and wind-induced transport of sand-sized fractions (Greeley and Iversen, 1985). These processes are especially important in cold periglacial environments where rates of chemical weathering are much lower (Peltier, 1950).

Our understanding of the post-eruptive environmental fate of rhyolitic glaciovolcanic glasses is still poor and emphasises the need for further study. The aim of our study is to understand the scales and contributions of frost-weathering and wind-induced transport to the modification of rhyolitic glaciovolcanic glass. We therefore focus on a specific eruption product from a well-studied subglacial rhyolitic edifice in Torfajökull (Iceland).

1.1 Fracturing by ice

There are different pathways in which the permeable glassy deposits of tindars (hyaloclastite ridges) and tuyas (emergent sub-ice volcanoes which become table mountains after deglaciation) can weather. Most frequently ice wedging and thermal stress produce sufficient mechanical forces inside the rock matrix to promote crack propagation, fracturing and particle excavation. Effects from thermal gradients that exceed 2°C min^{-1} are much less relevant for the fracturing at the fine particle scale of the granular glass that we consider here (Simmons and Cooper, 1978; Hall, 1999). Ice nucleation in pores therefore occupies a prominent role in the mechanical weathering of these materials (Walder and Hallet, 1986; Scherer, 1999). Since the semantics of the term 'pore' differs per discipline, we distinguish here between two scales. The finest scale covers the nanometre-sized surface pores that are present at the surface of individual particles. Interparticle pores on the other hand are the vesicles and voids between packed particles which cover the micrometre to millimetre size range. Especially surface pores are ideal nucleation sites for starting ice growth as these pores maximize the surface area and contact with the growing ice crystal (Scherer, 1999; Scherer and Valenza, 2005). Encroaching ice can entrap water inside pores >100 nm and eventually generate a pressurisation stress that is sufficient for superficial fracturing (Scherer, 1999; Scherer and Valenza, 2005). This mechanism applies to weathering of all granular materials such as eruption products and

industrial materials such as concretes (Scherer, 1999). In contrast, volumetric expansion of ice pressing against the glass matrix during its formation is the dominant process inside much larger voids. Forces generated by the growing ice are strong enough to segregate material, heave particles (Jackson and Chalmers, 1958; Walder and Hallet, 1986; Scherer, 1999) and they can even shatter the toughest granitic rocks (Matsuoka and Murton, 2008).

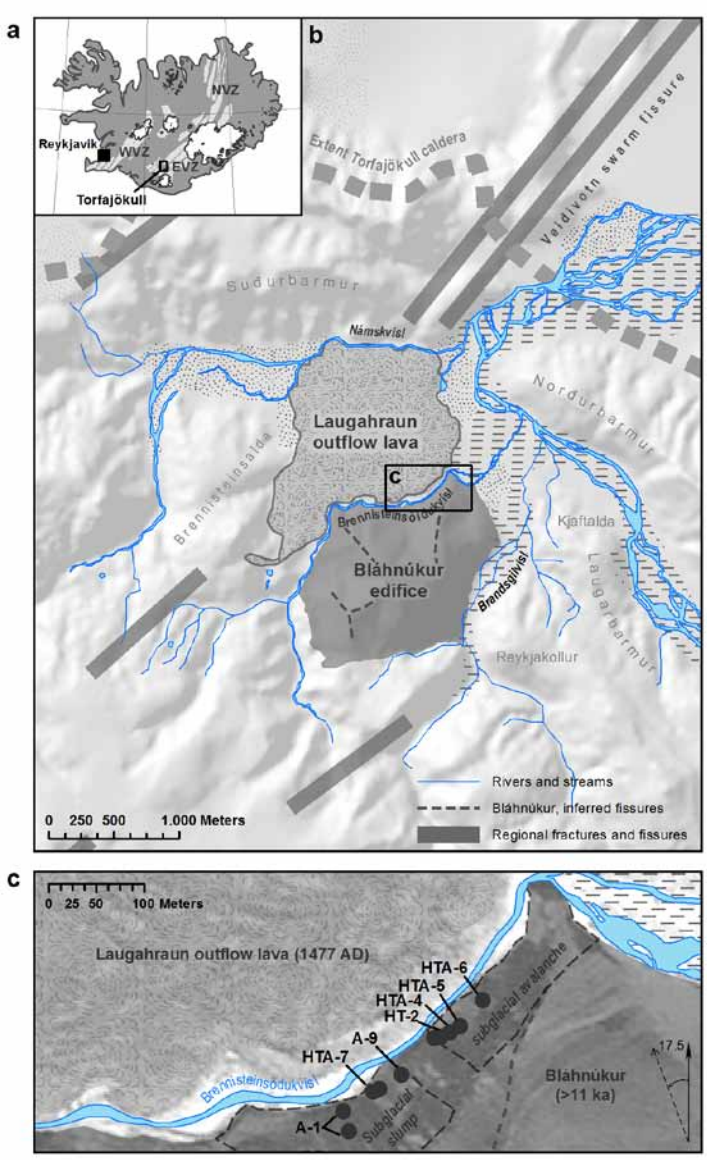

Fig. 16 - Overview of the Bláhnúkur region near the intersection of the Torfajökull caldera and the Veiðivotn fissure swarm on the edge of the Eastern Volcanic Zone (EVZ) and Southern Flank Zone (SFZ) in Iceland (a), fissure data: Einarsson and Sæmundsson (1987). The study area in the southern central highlands (b) is dominated by migration of local hydrological networks and the narrow incision of the stream after the Laugahraun eruption. Fissures and emplacement units were inferred by Tuffen *et al.* (2001). Sampling sites of hyaloclastites are indicated (c), letters highlight the use of each sample in the experiments in this study; H = high-pressure mercury intrusion, T = Tensile strength testing, A = abrasion experiments. Maps modified from chapter 2.

1.2 Abrasion by wind

Loosely bound granular volcanic glass can also be modified during aeolian transport. Repetitive impacts create cracks and are dependent on the impact velocities from both low-energy rolling and reptation, or from high-energy saltation of particles. Particle morphology and impact velocity therefore dictate the type of surface fracturing (Marshall *et al.,* 2012). Impacts from rounded particles have been shown to produce circular 'Hertzian' fractures, while impacts by angular grains with sharp edges produce 'Boussinesq' crack systems (Marshall *et al.,* 2012). The latter is mostly relevant for glaciovolcanic glass due to the angular particle morphology. Boussinesq cracks consist of intersecting plains of radially extending fractures from the impact point and lateral pseudo-conchoidal cracks (Greeley and Iversen 1985; Marshall *et al.,* 2012). Shards removed in these fracture zones expose new surfaces which can be chemically reactive and create mineralogical alterations of the sediment over time (Merrison *et al.,* 2010; Mangold *et al.,* 2011). The particle surface therefore preserves a record of the environmental conditions, rates of modification and the maturity of the aeolian system (Heiken and Wohletz 1985; Marshall *et al.,* 2012).

Both mechanical processes discussed above create new materials which are often fine enough to be inhaled. In simulated saltation experiments by Merrison *et al.* (2010) respirable fractions <10 μm (PM_{10}) increased by 10%. Chronic exposure to such fractions can lead to inflammatory responses in the respiratory pathways and even asthma (Horwell and Baxter, 2006; Gudmundsson, 2011). So far, no distinction has been made between the origins of fine respirable fractions and possible mechanisms that introduce them in the environment. Shedding light on the general contribution of physical weathering to the availability of respirable fractions is therefore also valuable for assessments of respiratory health hazards.

2. Bláhnúkur in Torfajökull, Iceland

Bláhnúkur is one of the youngest glaciovolcanic landforms in the Torfajökull caldera complex, which is presently part of the Fjallabak Nature Reserve. It is located in the southern central highlands of Iceland at the intersection of the Veiðivotn fissure swarm and the caldera complex (Fig. 16). The hyaloclastite layer formed during the effusive eruption of Bláhnúkur is only a few tens of meters thick and covers an older rhyolitic core (Tuffen *et al.* 2001; McGarvie *et al.*, 2006). The pyramid-shaped edifice rises some 350 meter above the surrounding rhyolite plateau to a summit altitude of 945 m.a.s.l. Local palaeo-ice sheet thicknesses at the time of eruption have been inferred using geologic features, magma degassing and nearby similarly aged tuyas. These features indicate that the area was once covered by an ice sheet of at least 350-400 m thick during the Weichselian and it was confirmend by magma-degassing studies (Owen *et al.*, 2012). The erupted volumes at Bláhnúkur and adjacent Laugahraun show signs of partial mixing of rhyolitic magmas from Torfajökull with basaltic sources (Blake, 1984; Tuffen *et al.,* 2001, 2002a), which is illustrated by millimetre to even centimetre-sized basaltic inclusions in the matrix of the rhyolitic hyaloclastites. Emplacement mechanisms of the subglacial eruption products and lava lobe-hyaloclastite facies are well-described by Furnes *et al.* (1980) and Tuffen *et al.* (2001), who propose that mass movements (i.e. sliding and slumping) in the subglacial cavern contributed to the morphogenesis of diagnostic features and strata presently exposed in some of the gorges around the edifice. In this study we focus on the freshly excavated materials inside Grænagil, a roughly NE-SW trending gorge on the north flank of Bláhnúkur. Weathering of the deposits in the gorge is promoted by local meteorological conditions that create ~100 freeze-thaw cycles at an average year temperature of 0.5-1.5°C above freezing (Table 2). Deflation of fine materials on scree sediments and

the overlying steep rock face takes place by moderate winds and gusts during the snow-free months in summer. These two forms of physical weathering are prominent and contribute to the overall erosion of the bright green and grey hyaloclastites exposed inside the gorge (Fig. 17; de Vet and Cammeraat, 2012). The accessibility and geological setting make Bláhnúkur and its eruption products globally the best-studied rhyolitic subglacial edifice. This provides a well-defined basis to use it as a case study for which we can study the physical weathering properties of rhyolitic hyaloclastites driven by local environmental conditions.

3. Experimental simulations of physical weathering

Analogue to the conditions observed in the field we discriminate in our experiments between the two mechanisms that actively contribute to the erosion and modification of the Bláhnúkur hyaloclastites: (i.) the compressive and expansive forces of ice nucleation in relation to fracturing of glasses during freeze-thaw cycles and (ii.) the effects of wind transport on the abrasion and textural modification of sand-sized materials. As these weathering processes are closely linked to particle size, we used only the particle diameters that are involved in these processes in the field. Gravel-sized pumiceous glass particles (2-32 mm in diameter on the Wentworth scale) contain pores of both scales defined in the introduction and these particles were therefore used for understanding the effects of expanding ice in freeze-thaw cycles. Finer glass shards sieved over 300-600 μm mesh were used in the wind abrasion experiments as these are, contrary to the large pumiceous particles, easily mobilised by local winds.

Eight Bláhnúkur hyaloclastite samples were collected from the walls of the Grænagil gorge (Fig. 16c). Rock outcrops of moderate consolidated breccias with pumiceous glass fragments were sampled to depths of 10 cm, where according to Hinkel (1997) the largest effects of freeze-thaw cycles are expected as a result of thermal diffusion and water infiltration. Four samples were collected from a slope section formed by slumping in the subglacial eruption cavern, whereas the other four were taken from a formation formed by sliding (Fig. 16c). These sections correspond with the detailed descriptions of breccias B and C in Tuffen *et al.* (2001).

Table 2 - Overview of the thermal conditions at nearby meteorological stations located in Vatnsfell and Lónakvísl in the central highlands of Iceland. Table modified from: de Vet and Cammeraat (2012).

Meteorological conditions	Year				
	2007	2008	2009	2010	2011
Vatnsfell					
Mean annual temperature [°C]	1.1	1.1	1.8	1.8	1.8
Minimum recorded temperature [°C]	-16.9	-21.8	-16.1	-17.3	-17.9
Maximum thermal gradient [a] [°C min^{-1}]	0.13	0.13	0.17	0.19	0.05
Days of freezing	159	165	130	144	106
Freeze-thaw cycles	144	62	117	86	116
Lónakvísl					
Mean annual temperature [°C]	0.6	0.3	0.7	1.0	0.6
Minimum recorded temperature [°C]	-19.0	-21.8	-19.2	-20.2	-20.3
Maximum thermal gradient [a] [°C min^{-1}]	0.15	0.09	0.16	0.16	0.10
Days of freezing	167	173	153	151	158
Freeze-thaw cycles	127	67	125	93	129
Melting of snow cover [c] [day-month]	7-6	29-6	5-6	2-6	21-6
New snow cover [c] [day-month]	- [b]	- [b]	30-9	- [b]	- [b]

[a] *From hourly temperature measurements*
[b] *Not measured or no data available*
[c] *F208 road access to Landmannalaugar, data from: Vegagerðin (Icelandic Road Administration)*

3.1 Ice-induced fracturing

In experimental simulation of freeze-thaw cycles a trade-off needs to be made between either field-analogue conditions (e.g. Potts, 1970), or by constraining the parameters influencing the freeze-thaw (e.g. Matsuoka and Murton, 2008). The foremost aim was to distinguish between internal damage (pore pressurisation) and external damage (volumetric ice expansion) that causes the glass to fracture during freezing of water inside pumiceous glass particles. Five of the eight sampled locations contained sufficient material of the size fractions for the experiments described below. Three different experiments were set-up, where the latter two were used to interpret the fracturing behaviour in the first experiment:

1. **Environmental laboratory simulations:** tubes were filled with 1.5 grams of 1-3 cm^3 sized pumiceous particles and 1.0 ml water was added to saturate the particles by capillary rise in vesicle networks or by full immersion. Sealed tubes (with a repetition of n=12 per sample site) were frozen to -19°C over a period of 16 hours to reach similar temperature extremes as in the field (Table 2) and subsequently thawed over 8 hours at +5°C. After 10 cycles the individual particles fractured to finer particles of various grain sizes. The residue <1400 µm in the 12 tubes was homogenised into a single sample for each site, pre-treated with an $Na_4P_2O_7{\cdot}10H_2O$ dispersing solution (Eshel *et al.,* 2004) and then measured using a Sympatec HELOS laser-diffraction particle sizer to measure the grain-size variation produced by ice-induced fracturing.
2. **Surface porosity of the glass:** the porosity of bulk samples consisting of ten ~0.25 cm^3 particles were measured using high-pressure mercury intrusion at pressures up to 400 MPa (with n=9, independent repetitions) for each of the 5 sampled locations. These measurements were made using a PASCAL 440 porosimeter from Thermo and allowed us to measure the pore diameters at the glass surface and the bulk density. Together with the measured vesicle-free skeletal densities (ρ_{He}) we obtained the degree of porosity on the exterior of the particle that is accessible to ice. Peaks of modal pore diameters were statistically tested using an analysis of variance (n-way ANOVA) to analyse if these are a common property of the Grænagil particle population or dependent on the sampled location, measurement repetition or the combination of these two.
3. **Brittle fracturing from ice expansion:** ice expanding inside vesicles exerts a force and as such a deflection of the thin glass walls inside the pumiceous particles. When the deflection reaches a critical level it causes fracturing of the glass. Measuring the deflection at which the glass experiences brittle deformation is made possible by uniaxial loading of samples using a tensile strength test bench M359-20CT from Testometric. Similar pumiceous glass particles as in preceding experiments were compressed between two rigid plates to 80% of their original height (also with n=9 independent repetitions). Measurements of the forces were obtained with an accuracy in the range of 10^{-2} N per compression step of ~5.8 µm. As these pumiceous particles are very friable, it was not possible to produce a standardised test volume and contact surface for a conventional stress-strain analysis. Fast-Fourier-Transform (FFT) analyses of the compression data were therefore used to calculate the critical deflections at which the material fractured. Peaks representing these critical deflections were extracted from the periodograms produced by the FFT analyses. The cumulative distributions of fracture distances were compared to establish if the deflection for brittle deformation is a collective property for all the sampled locations. Grain-size distributions of the residue <1400 µm were measured for a comparison to the freeze-thaw experiments.

3.2 Aeolian transport simulations

Abrasion of granular sediments during transport can be experimentally simulated using continuous axial tumbling. Such set-ups have been used for understanding interactions and abrasion of particles in pyroclastic density currents (Kueppers *et al.,* 2012), volcanic and fluviatile debris flows (Kaitna and Rickenmann, 2007; Caballero *et al.,* 2012), textural alterations from simulated saltation impacts and subsequent mineralogical alteration of the sediments (Merrison *et al.,* 2010). We studied the abrasion of the angular glass particles using six rubber-covered drums with a 10 cm diameter that rotated at 50 rpm (300 °/s). Fig. 18 shows a schematic description of the set-up. In rotational set-ups unmixing effects from axial segregation (Aranson and Tsimring, 2006) would bias larger particles over smaller particles in their transported distance over time. We filled the drums below the axis of rotation (a_r) to overcome this problem and ensure continuous mixing. We use this set-up as a model for low-energy transport of sediment in summer months by rolling and reptation below saltation thresholds. Reptation is a process in which particles are liberated by (high-energy) saltation impacts that in turn hit the surrounding substrate at much lower impact velocities. Such low-energy aeolian processes account for the majority of mobilised sediments (Kok *et al.,* 2012). The size range of 300-600 µm inside the drums represents a size fraction that is most susceptible to the effects of such low-energy interactions from rolling and reptating particles (Kok *et al.,* 2012). Indications from past tumbling experiments with vesiculated materials suggest that the highest degree of fracturing occurs in the first week or even hours (Kueppers *et al.,* 2012). We therefore had a weekly sample rate during the first five weeks of tumbling and continued the experiment for a total of 15 weeks. After each week of tumbling a ~15 g subsample was extracted from the bulk and treated according to the same protocols as in the other experiments. The measured size distributions were evaluated using Pearson X^2 tests to assess if significant changes to the material and particle distributions had occurred.

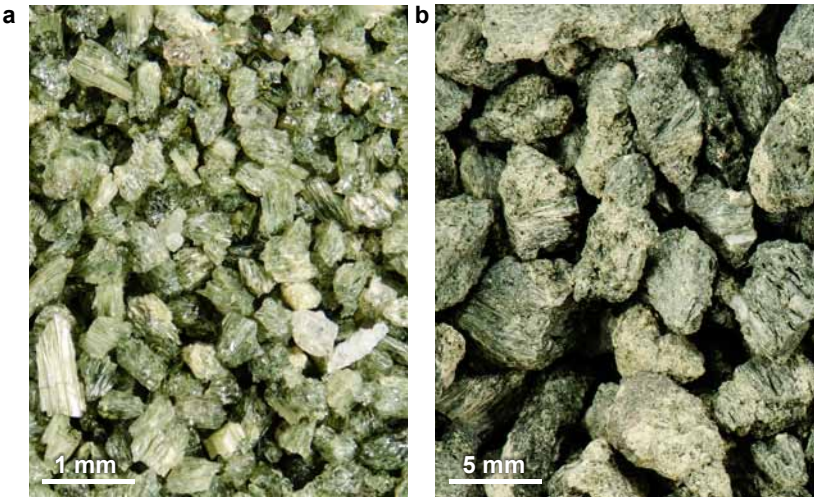

Fig. 17 - Focus-stacked microscope images show examples of particle morphologies of (a) 300-600 µm granular glass fragments and (b) gravel-sized pumiceous particles that comprise the Bláhnúkur hyaloclastites at sample site HTA-6. Visible are the voids and vesicles and the numerous sharp edges of the particles at different particle scales. These properties play a role in the weathering pathways of these materials under the influence of ice and wind. Note the scale difference between the two images.

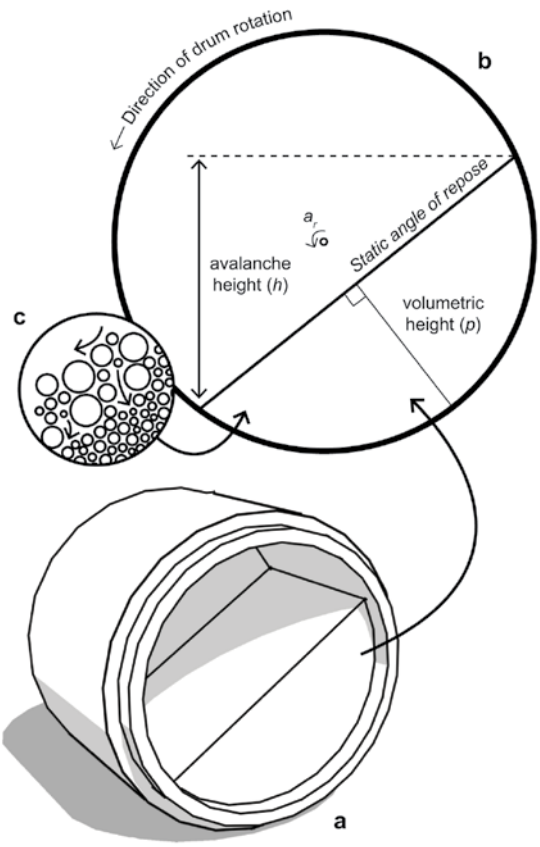

Fig. 18 - Schematic rendering of a rubber covered drum used in the tumbling experiments with the slope of sediment at the static angle of repose (a). Parameters used to translate the axial tumbling and random positioning laboratory experiments to aeolian transport in the field are shown in (b). In rotating systems, axial segregation results from particle size differences and kinematic sieving during each discrete avalanche (c). These effects were minimised by keeping the volumetric height p below the axis of rotation a_r.

4. Results

The particle size distributions formed by the fracturing of the original centimetre-sized particles during the 10 freeze-thaw cycles are shown in Fig. 19 (black lines). The damage from ice growth during freezing most notably created sandy textures. Due to distinct scale effects in ice-induced weathering, porosity measurements and uniaxial loading may allow the interpretation of the measured particle size distributions to determine the type of fracturing.

Brittle fracturing of particles during uniaxial compression tests (Fig. 20) shows numerous small peaks. Each peak represents a build-up of force which is suddenly released when the glass fractures. This highly variable signal of successive fracturing events is superimposed on a longer frequency, larger amplitude signal that may represent the effects of the changing contact area during compression (Fig. 20a). Frequency analyses allowed us to extract the recurring critical distances at which fracturing took place, visible as peaks in the periodograms (Fig. 20b). After normalisation we extracted these peaks based on a relative threshold of 0.01% with surrounding data points. The interquartile range (middle 50%) of critical deflections cover a

range of 25-75 μm (Fig. 20c). Inspection of the peak distribution of the five sample sites shows that the notches of the box plots and medians overlap. The range in critical deflections are therefore not significantly different between the sampled locations and can be considered as a collective material property. Particle sizes formed by brittle fracturing are shown in Fig. 19 (blue lines) and are very comparable to the distributions formed by ice-growth during freeze-thaw cycles.

Effects of surficial fracturing by ice can also result from the pressurisation of surface pores. Results of high-pressure mercury intrusion measurements to obtain these pore diameters are shown in Fig. 21. The pore diameters are highly comparable per sampled field location, although at first sight some spatial variability appears to be present between the different locations. On closer inspection the modal pore diameters appear to be of the same order of magnitude and coincide with the distinct peaks present in all the intrusion measurements (compare peaks in e.g. Fig 21b and 21c). Using an analysis of variance we established that the higher abundance of pores with those diameters is not an effect dependent on the sampled location, repetition of measurement or an interaction of both (with p = 0.12, 0.79 and 0.86 respectively).

Abrasion by low-energy particle collisions of wind-blown sediments was simulated by continuous axial tumbling for several weeks on end. The experiment parameters and covered distances of the sediment per drum are shown in Table 3. After 15 weeks of tumbling (or 578-715 km of transport, see table 3) the distributions of particle sizes show only minute shifts to smaller textures (Fig. 22). These changes are not statistically significant on the whole of the size distribution with a Pearson's X^2 test and often fall within the measurement accuracy.

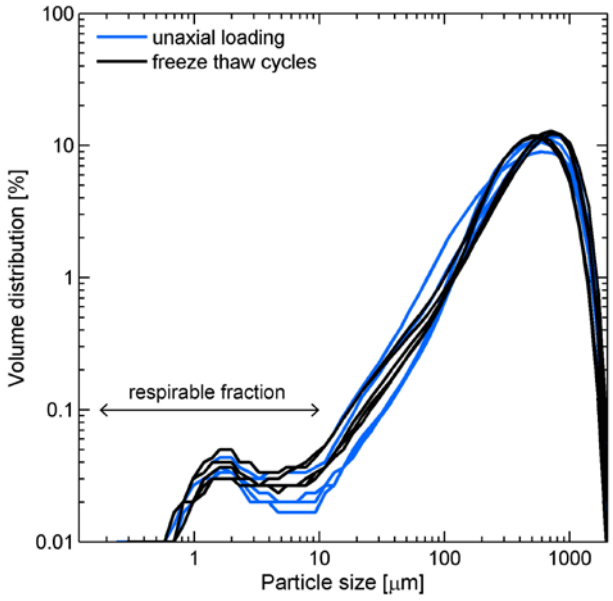

Fig. 19 - Size distribution of the sediment produced by the fracturing of single pumiceous particles (d >10 mm). Nearly identical particle size distributions are produced after 10 freeze-thaw cycles from ice-induced fracturing (in black) and during brittle fracturing from uniaxial loads (in blue). Pumiceous particles used in the experiments were taken from sampled locations HT-2, and HTA-4 through to 7. Similar-sized particles were used for the physico-mechanical measurements presented in Fig. 20 and Fig. 21.

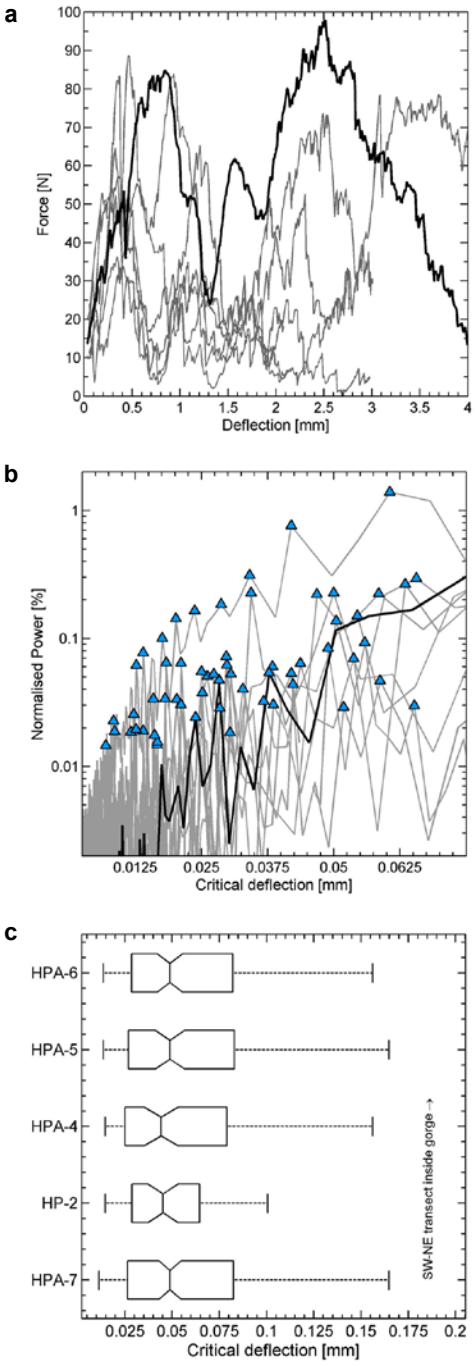

Fig. 20 - Frequency analyses from the uniaxial loading of gravel-sized pumiceous glass particles with a tensile-test bench. Figure (a) shows the raw data of the measured force at a given deflection for nine different pebble-sized particles from location HT-2 during the compression of an individual particle. Figure (b) shows the dominant periods (peaks marked with blue triangles) of recurring deflection steps at which fracturing takes place, as determined using Fast Fourier Transform analyses. Figure (c) shows boxplots of these critical deflections when brittle fracturing occurs for each of the 5 sample sites inside the gorge (see Fig. 16 for their locations in a map).

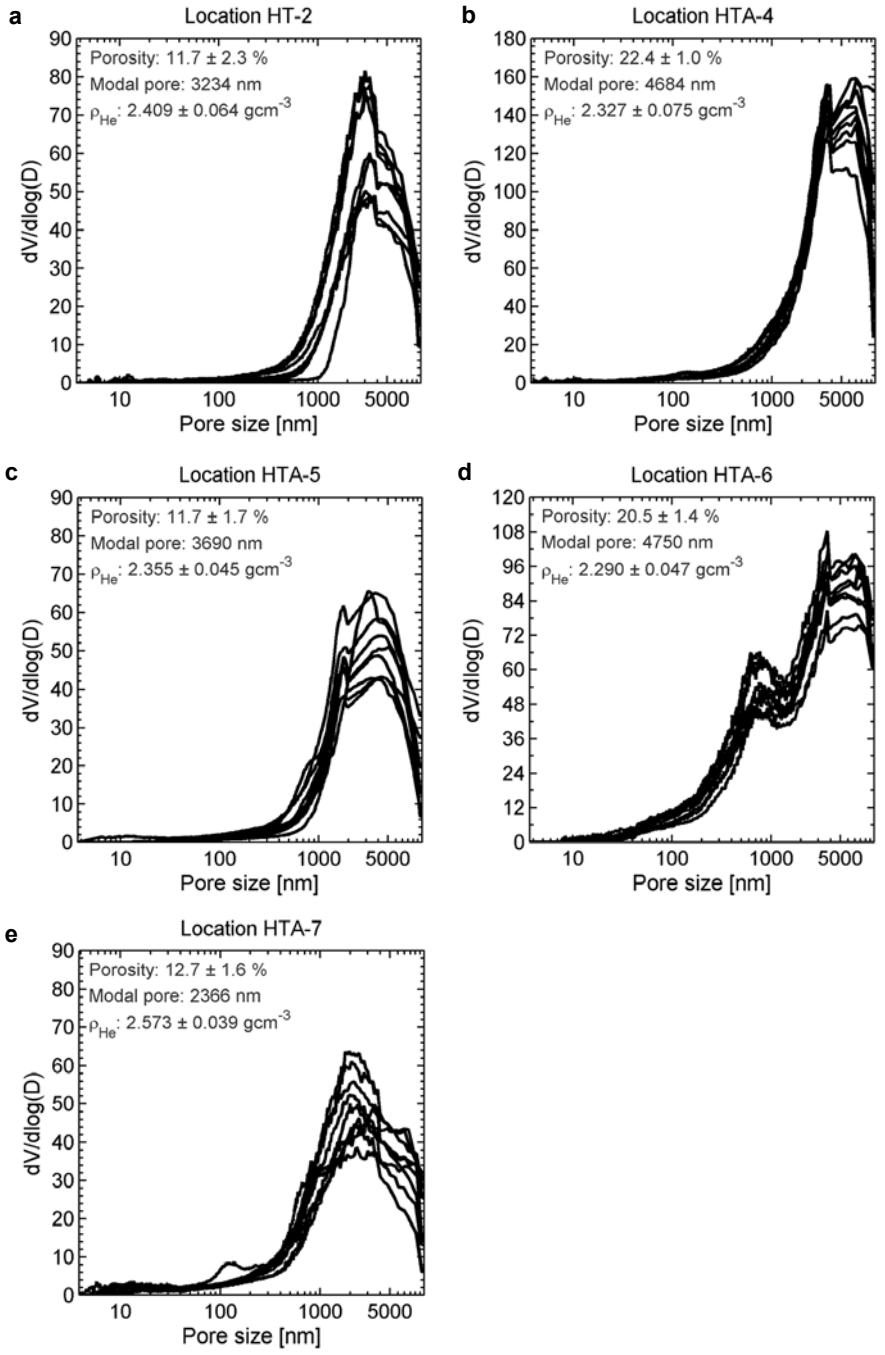

Fig. 21 - Porosimetry data measured using high-pressure intrusion of mercury for 5 different sampled locations. Each line in the graph was measured for ten pumiceous glass particles and each graph therfore shows nine independent repetitions (n=9). Values for skeletal densities (ρ_{He}) and porosity in each graph are the site-specific averages. All samples with the exception of sample HTA-7 are deposited in a subglacial hot avalanche (see Fig. 16).

However, the peak of respirable fractions <10 μm shows some change by broadening and increased contribution to the sediment. Comparing the surface below the graph of the <10 μm fraction before and after 15 weeks of tumbling using a paired *t*-test shows that the quantity of respirable fractions significantly increased by 0.03-0.07% ($p \leq 10^{-3}$). This is equivalent to a production of 0.7-1.6 kg of respirable dust per m^3 of mobilised sediment, assuming an average skeletal density from data in Fig. 21 of 2.4 g cm^{-3}.

5. Discussion

Common basaltic hyaloclastites are a hydrothermally unstable and physically weak type of volcaniclastic rock, which makes them easily chemically weathered by water and heat (Frolava, 2008). Studies of 2-2.5 Ma old basaltic glasses have shown that over time vesicles are filled with secondary minerals which changes physico-mechanical characteristics such as porosity and permeability (Frolava, 2008; Franszon *et al.,* 2010). In contrast, rhyolitic glass is known to be more resistant to chemical weathering than basaltic glass (Jakobsson and Gudmundsson, 2008) and experiences no consolidation or strengthening. No clear indications are visible in microscope images of the material that strong chemical weathering has affected the Bláhnúkur hyaloclastites in Grænagil, although some chemical weathering has led to the formation of clays and zeolites (Denton *et al.*, 2009). Vesicles of the Bláhnúkur glass were prominently clear from filling and cementation by these minerals (see Fig. 17) and this illustrates that little resistance is offered by chemical weathering to physical erosion. Physical weathering processes are therefore especially relevant for modifying rhyolitic glass deposits.

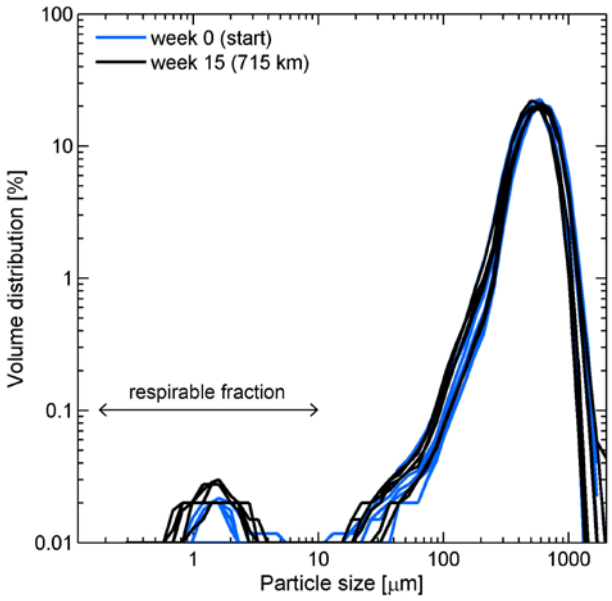

Fig. 22 - Particle size distribution following low-energy abrasion before (in blue) and after 15 weeks or 500-700 km of continuous axial tumbling (in black) using sands from sampled locations HTA-4 through to 7, A9 and A1 (also see Table 3). Modification rates at intermediate stages were insignificant after 1-5 weeks of tumbling and have therefore been omitted in the graph for clarity.

Table 3 - Data overview of the tumbling experiments and the conversion to field conditions. We assumed that each grain participated in at least one avalanche per revolution of the drum for determining the transport distance.

Sample	Tumbling experiments				Field
	Mass (g)	Height, *p* (cm)	Slope length (cm)	Duration (days)	Transport (km)
HTA-4					
week 1	178.2	3.9	9.7	6	43.1
week 5	132.1	3.2	9.3	34	233.7
week 15	120.1	3.0	9.2	107	715.2
HTA-5					
week 1	192.1	3.9	9.7	6	43.1
week 5	143.2	3.1	9.2	34	232.8
week 15	130.8	2.9	9.1	107	708.1
HTA-6 [a]					
week 1	58.2	1.9	7.8	6	34.7
week 5	58.2	1.9	7.8	34	191.7
week 15	48.5	1.7	7.6	107	588.6
HTA-7					
week 1	228.6	3.9	9.7	6	43.1
week 5	169.8	2.7	8.9	34	229.5
week 15	155.9	2.5	8.6	107	681.4
A-3 [a]					
week 1	74.7	1.9	7.8	6	34.7
week 5	74.7	1.9	7.8	34	191.7
week 15	61.8	1.6	7.4	107	578.2
A-1					
week 1	193.1	3.9	9.7	6	43.1
week 5	134.8	3.0	9.2	34	232.0
week 15	125.9	2.8	9.0	107	702.0

[a] *Sampled in week 0, 5 and 15 due to availability of size fraction in field samples*

5.1 The effects of ice inside vesicles and surface pores

Bláhnúkur hyaloclastites are dominated by a fine-grained matrix that contains larger pumiceous particles. The dominance of small particle sizes reduces particle fracturing from high thermal gradients, which is further diminished by insulating properties of snow blankets. Measured thermal gradients in the field were found to be below the 2°C min^{-1} gradients of the fracturing threshold (Table 2) and show that the weathering and modification of these materials requires an additional agent such as infiltration of water. In sub-freezing conditions, ice nucleation occupies a prominent role in the weathering of the Bláhnúkur hyaloclastites as shown by effects of frost heave (ice expansion in pores between particles) in the excavation of particles during winter (de Vet and Cammeraat, 2012). At the level of individual particles, the influence of nucleating ice will differ depending on particle size. The friable and vesiculated nature of the pumiceous glass is instrumental for the fracturing by volumetric ice expansion and will likely affect only the large particles in the breccias. As the distributions formed by freeze-thaw cycles in Fig. 19 are very comparable with the distributions formed uniaxial loading, it leads us to conclude that the distributions in the freeze-thaw experiments are primarily the result of brittle fracturing of the pumiceous glass matrix. Ice expansion is known to generate forces of sufficient magnitude to cause this type of brittle deformation (Matsuoka and Murton, 2008). As water expands 9% in volume during freezing (Potts, 1970) brittle fracturing may result from ice nucleating inside vesicles, but also from the outside of a particle in the interparticle pore spaces. In the latter case this will require pores with a minimum diameter of 1000 μm to produce the 25-75 μm deflection of the glass matrix to cause the same wide-spread brittle

fracturing as in the uniaxial loading experiments. Ice-induced weathering of pumiceous glass particles in the hyaloclastite matrix is therefore the most prominent mechanisms for producing new sandy textures (d<700 μm). These fracturing effects can potentially be higher for the more vesiculated (20-70%) rhyolitic eruption products found elsewhere in Torfajökull (Tuffen *et al.*, 2008) as these particles contain more pores and vesicles for ice nucleation.

For smaller particle diameters, where vesicles are absent, other types of frost weathering may contribute to particle modification. Superficial fracturing of a particle's surface only occurs if the diameter of the surface pore in which stress is being generated, exceeds the size of nearby flaws in the glass (Scherer, 1999). Detailed mercury intrusion measurements show that the modal pore diameters in Fig. 21 are a common property of the Grænagil particle population, characterised by surface pores >1000 nm. Above 100 nm ice is capable of growing from the outside into pores, which closes the pore and pressurises the water inside it to cause superficial fracturing. Pore pressurisation during freezing of the Grænagil glasses is therefore favoured by the μm-sized surface pores that can exceed many small surface flaws. Remarkably, no wide-spread superficial fracturing was observed during pore pressurisation with pressures up to 400 MPa using mercury intrusion (well-above the hydrostatic pressures created by ice encroaching into surface pores). We also see no clear contributory effects of surficial fracturing expressed in the particle size distributions after the freeze-thaw cycles (Fig. 19). Pore-pressurisation may therefore be of minor relevance for the modification of glass fragments in the Bláhnúkur hyaloclastite. This may signify that the glass surface lacks appropriately-sized surface flaws in respect to the measured pore diameters. Rhyolitic volcanic glasses therefore require a prior history of chemical weathering (perlitisation) to obtain flaws that contribute to internal damage during freezing (Denton *et al.*, 2009; 2012). The formation of new surface flaws at the glass surface can also result from physical processes such as aeolian and gravitational transport, which we will discuss in the next paragraph.

Various lines of geomorphological and geological evidence indicate a subglacial formation of Bláhnúkur and these include orientations of columnar joints, glass hydration and perlitisation and the presence of subglacial till deposits (Tuffen *et al.*, 2001). Measured particle properties such as a porosity of 10-20% (Fig. 21) also indicates a phreatomagmatic eruption environment (Mueller *et al.,* 2011) that agrees with an eruption in a melt-water dominated subglacial cavity where rapid degassing, spalling and shattering led to the formation of the Bláhnúkur hyaloclastites. As the volatile content of Bláhnúkur glasses has been shown to depend on the subglacial cavity pressure (e.g. Tuffen *et al.,* 2010; Owen *et al.,* 2012), it suggests that some control is exerted on the chemical parameters that influence the viscosity and strength to syneruptive fragmentation. Surface porosity of glass particles is influenced by degassing of the magma and may therefore follow predictable patterns based on the confining glaciostatic pressure of the overlying ice mass. Such a common property is shown by the comparable peaks of measured surface pore diameters (Fig. 21). This is not unlike quantitative models derived for the relation between much larger vesicles morphologies and pressure by e.g. Macpherson (1984). Although the subglacial setting appears to have been favourable in controlling vesicle formation and fragmentation, parameterisation of these processes has been difficult in experimental settings (Martel *et al.,* 2000). Samples used in this study represent only one 'pressure depth' and further scrutiny is required to establish if surface porosity is indeed related to degassing under the eruption cavity pressure and a such the associated palaeo-ice thickness, or whether it represents a property related to post-eruptive chemical weathering processes.

5.2 Simulated aeolian abrasion

Impacting sand grains during saltation produce up to 10 grains that subsequently impact the surrounding surface by reptation and rolling (Cooke *et al.,* 1993). While these high-energy impacts from saltation are far more efficient in reaching favourable impact regimes for particle modification, these interactions are less abundant on the steep slopes if compared to the amount of low-energy interactions from e.g. wind- and gravity-induced rolling down-slope (de Vet and Cammeraat, 2012). Low-energy particle interactions from creep, roll and reptation therefore encompass a substantial part of the impacts during aeolian mobilisation of sediments at Bláhnúkur (Kok *et al.,* 2012). Simulations of granular avalanches inside similar rotating drums as our experiments show that avalanche velocities reach avalanche velocities that create particle collisions of 0.3 m s^{-1} (Yang *et al.,* 2008). These impact velocities are well below the impact regime of 1-10 m s^{-1} for saltating grains (Marshall *et al.,* 2012) and clearly show that the results of these experiments are reflecting the material's response to low-energy transport processes in the field. The studied glaciovolcanic glass has been remarkably resistant to this form of abrasion. After 578-715 km of simulated aeolian transport, changes in the sediment's texture are only noticeable by a marginal broadening of the <10 µm peak. As the Grænagil gorge is ~2 km long, these required distances for noticeable effects exceed the possible travel distances in the field. Similar to the outcomes of our abrasion experiments, no significant abrasion of glass particles was observed for volcanic glasses in other periglacial environments, where transport below and above wind mobilisation thresholds did modify other sediment types (Ayling and McGowan, 2006). Prolonged low-energy aeolian transport clearly lacks the power to substantially change sediments, even when these impacts are the most common type of particle interaction in the field. We therefore conclude that frequent low-energy transport of hyaloclastites by wind or gravity is incapable of significantly altering particle shapes and textures. Modificaion by frost weathering therefore seems most prevalent for the weathering and modification rhyolitic glasses.

Fig. 23 - The abrasion of the particle surface by impacts of angular grains in many ways resembles the damage caused by stones hitting the windshield of a car, as shown in this image. In amorphous materials such as glass, these 'Boussinesq' crack features are common at all scales of glass fracturing. Clearly visible are lenticular cracks radiating away from the impact point and lateral pseudo-conchoidal fractures where small chips of glass have been removed or are prone to removal by ice infiltration. (Windshield courtesy of W. and N. Remijn)

As shown by the changes in sediment texture, low-energy particle impacts may form minute Boussinesq fractures (illustrated in Fig. 23) in which shards can be removed from the particle surface. Even when the quantity of intersecting fracture zones is insufficient for removing shards at substantial rates, physical weathering by ice benefit from the production of these fractures. The formation of new flaws thus increases crack propagation whenever stress is being generated by pore pressurisation and ice expansion during freezing. This ultimately suggests that over time, aeolian and gravitationally transported eruption products in deglaciated environments are more susceptible to combinations of physical weathering processes, compared to eruption products being weathered *in situ*.

5.3 Physical weathering and health

Conditions favourable for large-scale dust suspension occur frequently and are notorious in the coastal areas and the glass-rich sandy deserts in Iceland (Arnalds, 2010; Leadbetter *et al.,* 2012). These suspension events show that the abundance of fine dust in the environment exceeds the rates of chemical weathering and soil uptake that would otherwise inhibit further distribution. Ashes of the eruptions of Eyjafjallajökull and Grímsvötn in Iceland have raised several health concerns (Gudmundsson, 2011; Carlsen *et al.,* 2012). Reflecting more broadly on the behaviour of basaltic and rhyolitic volcanic glass poses the question at which rate physical weathering contributes to the post-eruptive formation of new respirable fractions in these cold periglacial environments. During the 2010 Eyjafjallajökull eruption glassy ash particles of 300-600 μm were deposited as far as 20 km from the eruption site (Gudmundsson *et al.,* 2012), allowing particle modification by wind-induced abrasion to introduce new respirable fractions into local settlements. However, from our abrasion experiments we find no evidence to support the hypothesis that materials are subject to high-rate secondary fracturing from frequent low-energy aeolian transport. Perhaps only under extremely windy conditions when saltation transport of these materials can occur, surficial fracturing can lead to the production of respirable fractions on sufficiently large rates for detrimental health effects. This view is supported by experimental studies that have shown that abrasion of angular material, even by saltation, is a very lengthy and gradual process (e.g. Greeley and Iversen, 1985). Much more important may be the influences of seasonal interactions in local periglacial conditions as discussed in the preceding section. By freezing of gravel-sized particles alone, more respirable material <10 μm is formed compared to aeolian transport. Since physico-mechanical properties of volcanic glasses vary from eruption to eruption, event-specific experimental simulations would be required to properly assess these physical weathering processes. Similar to other assessment methods for particle sizes (Horwell, 2007), the methods explored here are well-accessible. They can potentially be used to complement health assessments, which so far have structurally overlooked the long-term contribution of physical weathering of glassy eruption products in subarctic or high-alpine periglacial environments.

6. Conclusions

In constrast to basaltic volcanic glasses, rhyolitic hyaloclastites are not consolidated by chemical weathering. This makes these glass deposits much more susceptible to physical weathering and promotes different pathways for the geomorphological development of landforms composed of rhyolitic glass. Laboratory simulations have allowed us to assess the scale-dependency and effects of physical weathering for a rhyolitic glaciovolcanic glass (summarised in Table 4). Measurements of the physico-mechanical properties can be used to understand the aptitude

of glaciovolcanic glass to various physical weathering mechanisms. Fracturing by ice growth clearly drives the formation of new sandy textures in pumiceous glass deposits on relatively short time scales. These processes are favoured by the large surface pores and vesicles formed initially by the subglacial eruption conditions. Modification rates by aeolian transport of glass shards that dominate the bulk of these breccias is near to neglectable. However, pre-existing micro-cracks and the formation of new micro-cracks at the particle surface from aeolian particle transport potentially increase the total rate of modification in combination with frost weathering. These processes highlight the importance of seasonal interactions and the interdependency of physical weathering mechanisms that affect glaciovolcanic eruption products in periglacial environments.

Table 4 - Effects and scales of mechanisms contributing to physical weathering and modification of a rhyolitic volcanic glass, based on laboratory experiments and the physico-mechanical characteristics of the studied rhyolitic glaciovolcanic glass.

Mechanism	Location	Affected particle size (µm)	Process scale (µm)	Effects
Ice nucleation				
volumetric expansion *(external damage)*	pumiceous glass, large vesicles, interparticle pore space	>5000	>25	maximum deflection sustainable by glass walls of vesicles is exceeded, brittle fracturing occurs, leads sandy textures
hydrostatic pressure *(internal damage)*	surface pores	>10	>1	crack propagation, superficial fracturing
Aeolian abrasion	exposed particle surface	300-600	<10	chipping, lateral cracks, mineralogical alterations, textural change

▲ *View down-wind in the hypobaric (low-pressure) wind tunnel before the start of a new experiment.*

Chapter 4

Wind transport at the fluid threshold

Abstract

Sands are actively transported in the present surface environment of Mars. Recent observations show that volcanic glass is an important component in active dune systems and other aeolian sediments. The mobility of these sediments may benefit from rolling induced by aeolian drag forces. In this study we experimentally determined detachment thresholds for volcanic glass that include the removal by rolling. Discrete heaps of particles were subjected to wind shears of 0.1-0.6 N m^{-2} under atmospheric pressures of 240-1024 mbar inside a wind tunnel simulator. The observed flat threshold for larger particle diameters (>150 μm) was best explained using a semi-empirical model that includes detachment by rolling. This model produced a much better fit to the data than models that describe saltation. Using a residual analysis of the variability in measured particle properties we evaluated the obtained model fit and found no dependencies on variations in particle properties that affected the fitting accuracy. The model could therefore be validly applied to the detachment threshold of volcanic glass and was therefore used to predict the removal on Mars. These model predictions show that volcanic glass with larger particle diameters can be detached by rolling from existing surface wind shears. As rolling is further enhanced by the thick laminar sublayer, it provides a possible mechanism for the initial mobilisation of particles by the wind. A wide morphological variety and range in particle diameters is found to be susceptible to this form of removal at wind speeds than are lower than fluid thresholds for saltation. Recent sand mobility may therefore have benefited from rolling as a contributing or as a saltation triggering process.

This chapter is based on: *De Vet, S.J., Merrison, J.P., Mittelmeijer-Hazeleger, M.C., Van Loon, E.E., Cammeraat L.H., 2013. Effects of rolling on wind-driven detachment thresholds of volcanic glass on Mars (submitted to: Icarus)*

1. Introduction

Surface wind flow drives aeolian processes and the erosion of surface features on Venus, Earth, Mars and Titan (Iversen and White, 1982; Arvidson *et al.*, 1983; Bourke *et al.*, 2010; Kok *et al.*, 2012). On Mars, various aeolian landforms appear to be much more active in the present-day surface environment than previously thought possible (Silvestro *et al.*, 2010; Hansen *et al.*, 2011; Bridges *et al.*, 2012a; Gardin *et al.*, 2012; Horgan and Bell, 2012b). Sand mobility is observed to be fairly common (e.g. Bourke *et al.*, 2008, 2010; Fenton, 2006; Sullivan *et al.*, 2005, 2008; Chojnacki *et al.*, 2011; Silvestro *et al.*, 2011) and sand fluxes of dune systems can be comparable to dunes on Earth (Bridges *et al.*, 2012b). The geomorphologic evidence of these processes implies that active saltation of sand-sized particles occurs in the present low-pressure (6-10 mbar) surface environment. However, wind speeds in the atmospheric boundary layer measured by Mars lander instrumentation (Hess *et al.*, 1977; Sutton *et al.*, 1978; Schofield *et al.*, 1997; Magalhães *et al.*, 1999; Holstein-Rathlou *et al.*, 2010) and predictions from global atmospheric circulation models (e.g. Haberle *et al.*, 2003; Michaels and Rafkin, 2008) show that winds above 10 m s^{-1} are very rare on Mars. Much higher wind speeds are required to reach the *fluid* or *static threshold* when particles are lifted from the bed by the force of the wind (Greeley *et al.*, 1974, 1980; Iversen and White, 1982; Greeley and Iversen, 1985). The apparent contradiction of saltation on Mars is solved to some extent by results from numerical simulations that have shown that saltation can be sustained by splashing and reptation of particles by much lower wind speeds at the *impact* or *dynamic threshold* (Kok 2010a, 2010b; Kok *et al.*, 2012). For this to be possible, particles still need to be mobilised at a much higher fluid threshold first. Beneficiary contributions to the mobilisation of particles may result from rolling by aeolian drag, which is known to occur for larger particle diameters at lower fluid thresholds than saltation (Cleaver and Yates, 1973; Nickling, 1988; Manukyan and Prigozhin, 2009).

This work focuses on experimentally quantifying fluid thresholds that include detachment of particles by rolling as one of the possible processes that can contribute to the observed sand fluxes and the onset of saltation on Mars. Experimental simulations of aeolian processes can be carried out in Martian atmospheric conditions using specialised low-pressure (hypobaric) wind tunnels (e.g. Greeley *et al.*, 1974; Greeley and Iversen, 1985; Merrison *et al.*, 2008). Simulations under atmospheric pressures higher than those on Mars are also possible as these can be normalised for the difference in atmospheric density using empirical relations (Merrison *et al.*, 2007; Kok *et al.*, 2012) and this approach is used in the presented study (more details are discussed in section 2). Simulating particle removal under Martian gravity (g = 3.71 m s^{-2}) is cumbersome and is only possible during partial-gravity parabolic flights (White *et al.*, 1987) or by using gravitationally-adjusted particles in ground-based hypobaric wind tunnels (e.g. Merrison *et al.*, 2007). Many studies of particle mobility on Mars have therefore relied on semi-empirical models to extrapolate results of wind tunnel simulations in terrestrial gravity to the gravitational or atmospheric conditions on Mars.

Obtaining results in wind tunnel simulations that are applicable for the Martian particle population is dependent on the selection of a proper analogue material. Recent spectral observations show that volcanic glass is an important component of aeolian sediments and the massive dune fields in the Northern highlands and polar sand seas (Horgan and Bell, 2012a; Carrozzo *et al.*, 2012) where wind-induced erosion and transport of glass-rich material is actively taking place (Hansen *et al.*, 2011; Bridges *et al.*, 2012a; Horgan and Bell 2012b). While this type of glass can be produced by various forms of explosive volcanism (Wilson and Head, 2007), the localised and concentrated deposits bare striking resemblances to glass-rich sediments that are formed in Iceland during glaciovolcanic eruptions (Horgan and Bell, 2012a).

Crater surface dating shows that peaks of glacial and volcanic activity coincided throughout Mars' geologic history, which increased the likelihood for magma to encounter ice during eruptions (Neukum *et al.*, 2010). The abundance of Martian magma-ice interactions capable of producing glassy sediments is further evidenced by a wide variety of surface features. These features include *tuyas*; emergent sub-ice volcanoes that melted upward through an ice sheet (Allen, 1979; Ghatan and Head, 2002; Head and Wilson, 2007; Hovius *et al.*, 2008; Fagan *et al.*, 2010; Martínez-Alonso *et al.*, 2011) and features that resemble subglacially formed volcanic ridges known as *tindars* (Wilson and Head, 2002; Chapman *et al.*, 2003; Komatsu *et al.*, 2004; Zealey, 2009; Pedersen *et al.*, 2010). As these types of volcanic eruptions are commonly dissociated from erupting in subaerial conditions, physico-mechanical properties of the formed glass particles are controlled by the glaciostatic (ice overburden) pressure of the overlying ice mass and the explosive fragmentation of quenching by melt water. The formative conditions of Martian glasses were therefore well-comparable to the glasses that consitute similar landforms in Iceland (van Bemmelen and Rutten, 1955; Wilson and Head, 2002; Schopka *et al.*, 2006; Thodarson and Larsen, 2007; Jarosch *et al.*, 2008; Smellie, 2008; McGarvie, 2009).

As physico-mechanical particle properties cannot be distilled from orbital measurements such as those made by Horgan and Bell (2012a), important clues can be obtained from their terrestrial analogues. In the absence of any superior characterisation of Martian volcanic glass at this point in time, we have used an unaltered volcanic glass (meaning not modified by aeolian transport or other physical modification processes) as an analogue material for studying the aeolian behaviour of particles in glass-rich Martian dunes. The particle properties of the selected analogue glass allowed us to determine a realistic upper limit for particle detachment by rolling due to their irregular shape. Fitting of a semi-empirical model for rolling from Merrison *et al.* (2007) to obtained experimental data, combined with a residual analysis of the model fit with the variability of particle properties made it possible to assess the sensitivity and validity of the new model for predicting the removal of these volcanic glass by winds on Mars. This study therefore complements earlier wind tunnel simulations by addressing the fluid threshold regime that includes rolling, while using a material that is comparable to a significant portion of aeolian sediments at the surface of Mars.

2. Theory of particle detachment in a low-pressure atmosphere

2.1 Paradox of particle removal on Mars

Atmospheric density plays a vital role in promoting or limiting particle mobility on Mars. The force exerted by the wind on a surface, or shear stress, is directly proportional to the product of the fluid mass density of the atmosphere (ρ) and the friction velocity (u_*) of the flow squared ($\tau = \rho u_*^2$). The atmospheric density is most strongly affected by variations in atmospheric pressure and large variations have occurred in the geologic past of Mars. Simulations of atmospheric evolution show that Martian surface pressures once peaked around 500-1000 mbar, which was similar to conditions on Earth and as such favourable for aeolian processes (Kass and Yung, 1995; 1996). Erosion of the atmosphere from interactions with solar winds led to a rapid decline early in Mars' history (Kass and Yung, 1995; Dennerl, 2006; Dennerl *et al.*, 2006; Bhardwaj *et al.*, 2007). The present surface pressures of 6-10 mbar are only considered to increase to 10-15 mbar during periods of higher obliquity (Kieffer and Zent, 1992; Laskar *et al.*, 2004; Phillips *et al.*, 2011). This persistent low-density state of the Martian atmosphere causes diurnal winds to infrequently exceed the fluid threshold ($u_{*\mathrm{ft}}$) for saltation of sand particles (Sullivan *et al.*, 2005). In rare cases threshold conditions have been

observed in dust devils with wind speeds in excess of 10-20 m s^{-1} (e.g. Ringrose *et al.*, 2003; Greeley *et al.*, 2006) and during the dust storms in which the Viking landers measured gusts as high as 25-30 m s^{-1} (Arvidson *et al.*, 1983). Friction velocities derived from these surface measurements and reconstruction from ripples and dune systems are in good agreement with each other and give a maximum range of $u_{*ft} \approx$ 2-4 m s^{-1} for the highest winds on Mars (Sullivan *et al.*, 2005; Parteli and Herrmann 2007a, 2007b; Kok *et al.*, 2012). The main reason why saltation on Mars is effective for mobilising sediment is that once particles are injected in the airstream, they will hop higher and farther as a result of the low atmospheric pressures and the lower Martian gravity (Claudin and Andreotti, 2006; Almeida *et al.*, 2008; Kok *et al.*, 2012). This substantially increases the final impact velocity of a saltating particle and lowers the impact threshold (u_{*it}) to ~10% of the initial fluid threshold (Kok, 2010a; 2010b). Saltation at the impact threshold is therefore easy to sustain on Mars once it has been set in motion due to the large ratio of the impact and fluid thresholds. However, getting an aeolian system to this

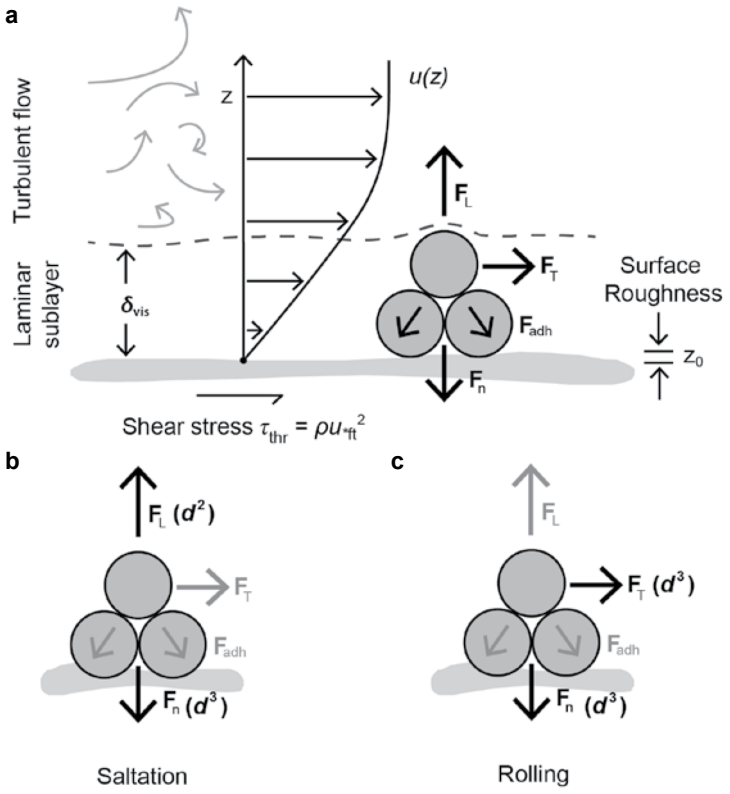

Fig. 24 - The forces and flow properties involved in the detachment of particles with diameter *d* by wind. The atmospheric boundary layer is subdivided in a turbulent flow and a viscous laminar sublayer (with thickness δ_{vis}). The threshold wind speed (*u*) at a given height (z) can be normalised for measurement height ($u_{*_{ft}}$) and in combination with the atmospheric density (ρ) they define the shear stress exerted by the wind. Forces acting on a particle at the moment of detachment include a lift force (F_L) and a rotational force created by the aeolian drag of the particle (F_T). These have to overcome the interparticle adhesion forces (F_{adh}) and particle weight (F_n) for detachment. Threshold scaling for saltation (b) is dominated by the lift force for lifting a particle completely off the bed. In the case of detachment by rolling (c) the linear increase in shear stress from the surface produces a rotational force (torque) that removes particles with diameters above ~150 μm without leaving the bed. This difference in scaling with particle diameter causes the threshold shear stress for rolling to be lower than the threshold for saltation (modified from: Merrison *et al.*, 2007 and Melosh, 2011).

state is also inherently more difficult due to the higher fluid thresholds in the low-pressure environment (Kok *et al.*, 2012). Bagnold (1954) was one of the first to realise that saltation at the fluid threshold is often preceded by rolling, which was confirmed by observations of others (e.g. Chepil, 1959). On Mars the contribution of rolling can be enhanced due to the structure of the atmospheric boundary layer. Very close to the surface, viscous forces resulting from the friction of the flow with the surface create a laminar sublayer. The thickness of this layer (δ_{vis}) is approximated by $5\mu/(\rho \cdot u_{*ft})$, where μ is the dynamic viscosity of the atmosphere (Kok *et al.*, 2012; White, 2006). With 2 mm the laminar layer on Mars is roughly 5 times thicker than on Earth due to differences in kinematic viscosity (Kok *et al.*, 2012) and fully engulfs sand-sized particles ($63 \leq d \leq 2000$ μm). Particles are shielded by this laminar sublayer from the turbulence of the upper part of the boundary layer, which prevents the removal by saltation; a property that adds to the paradox of saltation on Mars (Greeley, 2002). As particles are subjected to the aeolian drag from the flow inside the laminar sublayer, the structure of the Martian atmospheric boundary layer promotes the removal by rolling without leaving the surface. This makes sediment mobility possible at lower fluid thresholds than saltation (Cleaver and Yates, 1973; Nickling, 1988).

2.2 Thresholds for saltation and rolling

Aeolian field studies and experimental simulations have focussed primarily on the fluid thresholds of saltation for understanding wind-induced sediment fluxes (e.g. Bagnold, 1954; Greeley *et al.*, 1974, 1980; Greeley and Iversen, 1985). Much advancement has been made in the development of semi-empirical models for describing saltation by e.g. Iversen and White (1982) and the subsequent improvement and simplification by Shao and Lu (2000). These semi-empirical models show that threshold friction velocities scale proportional to the particle diameter (d), with $d^{-0.5}$ for small particles and $d^{0.5}$ for large particles (Shao and Lu, 2000). The scaling of thresholds expressed in terms of the shear stress (τ) can be illustrated using the force balance in Fig. 24a, where forces resulting from the wind flow, such as a lift force (F_L) and the torque (F_T) created by the drag of a particle, have to overcome the impeding properties of the particle. These particle forces include the normal load (F_n) resulting from the weight of the particle in the terrestrial (or Martian) gravity field and an adhesion force (F_{adh}) between particles from compositional interactions, surface friction or moisture adhering to the particle's surface (Ziskind *et al.*, 1995). For small particle diameters (<100 μm) the force balance is dominated by adhesion forces and removal is primarily governed by the lift force. Fluid thresholds for larger particle diameters (>100 μm) are dominated by the particle's weight. Simplistically, fluid thresholds for saltation (Fig. 24b) of larger sand-sized particles scale with d^3/d^2 as the regime is dominated by the lift force (scaling with d^2) that has to overcome the impeding force of gravity from the particle's weight (scaling with d^3) to lift the particle off the bed. When rolling is included (Fig. 24c) particles are not required to be lifted from the bed. Mobilisation is therefore dominated by aeolian drag force acting on the particle as it protrudes into the boundary layer, here the shear stress increases linearly with height above the surface (i.e also with grain size) leading to a rotational force (torque) which scales as d^3. Since the force of gravity also scales with d^3 the fluid threshold for detachment including rolling therefore scales with a dimensionless constant (d^3/d^3) for larger particle diameters and the threshold shear stress will be lower than the threshold for saltation. In this work we will refer to fluid thresholds that include detachment by rolling as the *detachment threshold* for clarity. Merrison *et al.* (2007) developed an experimental method and a semi-empirical model for detachment of spherical glass particles that includes

rolling (Eq.1). It integrates the forces in the force balance, where lift ($F_L = C_L \cdot \rho \cdot u_{*ft}^2 \cdot d^2$) and torque ($F_T = C_T \cdot \rho \cdot u_{*ft}^2 \cdot d^3$) have to overcome the normal load ($F_n = \pi \cdot d^3 \cdot g \cdot \rho_{He}/6$) and a simplified adhesion term ($F_{adh} = C_{adh} \cdot d$) for particle removal. Solving these terms for the threshold condition for particle detachment $F_L + F_T \geq F_n + F_{adh}$ gives the threshold shear stress (τ_{thr}):

$$\rho \cdot u_{*ft}^2 = ((\pi/6) \cdot g \cdot \rho_{He} \cdot d^3 + C_{adh} \cdot d) \,/\, (C_L \cdot d^2 + C_T \cdot d^3) \qquad \text{[Eq.1]}$$

Using the fluid mass density (ρ) of the atmosphere makes it is possible to calculate the shear stress (τ_{thr}) at a given threshold friction velocity (u_{*ft}). This fluid mass density is given by the relation $\rho = p \cdot m/\kappa \cdot T$, with the atmospheric pressure (p), molecular weight (m), Boltzmann-constant (κ) and temperature (T). The threshold friction velocity (u_{*ft}) can be derived from the turbulent wind speed (u_{RMS}), which was the measured dependent variable in our wind tunnel simulations (see section 3.3). The particle diameter (d) and the particle's skeletal density (ρ_{He}) are known independent variables. The lift (C_L), torque (C_T) and adhesion (C_{adh}) fitting parameters reflect various particle properties in each term of the force balance approach. Fitting eq. 1 to obtained experimental data (for g = 9.81 m s^{-2}) can therefore be used to predict detachment thresholds on Mars (with g = 3.71 m s^{-2}).

3. Approach to wind tunnel simulations

3.1 Analogue glass and particle properties

Post-depositional chemical weathering of volcanic glasses on Mars has leached mobile cations and produced a high-silica, almost obsidian-resembling, particle exterior (Horgan and Bell, 2012a). In order to obtain analogue glass grains with a similar high-silica exterior that were also formed in a subglacial volcanic environment, we sampled the volcanic glass formed during the subglacial eruption of the Bláhnúkur volcano in Torfajökull, Iceland (Tuffen *et al.*, 2001; de Vet and Cammeraat, 2012). These fragmental rhyolitic volcanic glasses are characterised by blocky particle morphologies with a low vesicularity of 10-20% and were formed under glaciostatic pressures of 2-4 MPa (Tuffen *et al.*, 2001; Owen *et al.*, 2012). The fresh and unaltered properties make the Bláhnúkur glass a suitable physico-mechanical analogue for determining an upper detachment limit for rolling of glassy sediments on Mars. Samples were collected on recently excavated slopes and eight ½ φ fractions ≤1200 μm (size-ranges included in appendix G) were extracted according to the soil preparation and sieving protocols of Gee and Bauder (1986). Various particle properties of these fractions were measured for understanding how the variability in the particle properties affects the fitting of the semi-empirical model. In the force balance (Fig. 24, Eq.1) the terms for lift and torque are expected to be influenced by the particle morphology, adhesion is mostly driven by particle surface properties and the composition of the material, whilst the gravitational term can differ as a result of minute mass density variations. Several techniques were therefore used to quantify various physico-mechanical properties. Mineralogical compositions were measured using established techniques (listed below, point 1-2) and we explored other techniques to quantify particle surface properties and shape parameters (points 3-5). This suite of particle property characterisations included:

1. **bulk mineralogy**, using X-ray powder diffraction (XRD) with an x-ray diffractometer and Cu(Kα) radiation. Full scans were made for a 2θ range of 5°-70° at a scan speed of 0.02° 2θ/s. Reflection patterns were analysed and compared using the X'Pert HighScore Plus mineralogical reference database.

2. **major element ratios**, measured by means of spot-measurements using Energy Dispersive X-ray (EDX) at 20.0 keV with a Hitachi S3500N scanning microscope on polished cross-sections of randomly selected glass particles (n=10).

3. **specific surface area** (S_a), measured using adsorption of N_2 (at 77 K) on the particle surface (Rouquerol *et al.*, 1999) with a Thermo Scientific Surfer. The specific surface area per weight-unit was calculated with the BET (Brunauer-Emmet-Teller) 2-parameter equation from the measured isotherm.

4. **skeletal densities** (ρ_{He}), obtained using gas displacement pycnometry with a Micromeretics 1305 pycnometer (Bielders *et al.*, 1990) for several repetitions per size fraction (n=9).

5. **shape properties**, measured using the object-based image analysis software eCognition, which segmented microscope imagery of particles into individual polygons using scale, shape and compactness parameters of respectively 50, 0.4 and 0.5. The created polygons were classified and extracted from the imagery (n=50) and automatically described using eight different shape-describing algorithms (Trimble, 2011).

3.2 Hypobaric wind tunnel simulations

Wind tunnel simulations with Icelandic volcanic glass were carried out inside the AWTS-I hypobaric wind tunnel, which is described in detail in Merrison *et al.* (2008). A schematic illustration of the wind tunnel is inculded in appendix F. A horizontal test surface was placed inside the tunnel's unobstructed airflow to exert a quantifiable shear stress by the flowing wind onto an array of samples. The aim here was to determine the shear stress (τ_{thr}) required for particle removal by measuring the threshold friction velocity (u_{*ft}) at a given fluid mass density (ρ). Experiments were carried out for four different fluid mass densities using atmospheric pressures at 240, 480, 920 mbar (where the fluid mass density of the atmosphere doubled with each step) and 1024 mbar using ambient air within a temperature-range of 298-303K. We followed the approach of Merrison *et al.* (2007) where discrete heaps of granular material ('pellets') were placed inside the wind tunnel and photographed from above while the wind speed was increased until the material was removed. Pellets with a 10 mm diameter and a 1 mm thickness were created using an aluminium mask to reproduce a consistent volume per pellet. During each wind tunnel run, four different size-fractions (with three replicates, n=3) were placed on a rough surface to inhibit sliding and to provide a realistic sand bed. We used sand paper with a 45 μm grain-size for the small fractions (≤212 μm) and 254 μm grain-size for the coarser fractions (≥212 μm) to be roughly comparable with the particle diameter. Fractions were evenly distributed across the width of the test section to determine the mean detachment shear stress and to average the ~10% flow gradient due to non-uniformity of the flow inside the tunnel.

3.3 Photometry and data analyses

Images of particle removal were pre-processed to reduce noise and preserve pellet edges using a median filter with 15x15 and 25x25 kernels for the two respective substrates. The reflectivity of a pellet was used to evaluate particle removal by extracting the average spectral histogram of the image measured across the pellets (L1) and removing the background in front (L3) and behind (L2) the pellets. A 75 pixel-wide mean around the centre of the pellet was used and the reflectivity was normalised from beginning to full removal by the

wind (steps summarised in Fig. 25). The threshold shear stress (τ_{thr}) was then calculated from the measured flow turbulence (u_{RMS}) for the condition when >90% of the pellet was removed by the wind using the relation $\tau_{thr} \approx \rho u_{*ft}^2$, where the friction velocity is given by $u_{*ft} = u_{RMS} / 2.1$ (Merrison *et al.*, 2008). Based on the force balance (Fig. 24) where particles are positioned on top of particle comparable in size, we used two different surfaces with a comparable particle size to create realistic torque conditions for removal of the last particles in the pellet. A disadvantage of this approach was the need to compensate for a difference in surface roughness (z_0) affecting the upwind flow turbulence in the boundary layer when comparing the two surfaces. We therefore added a 212-300 µm reference pellet to the sample array on the fine substrate and a 150-212 µm reference pellet on the coarse substrate. The relative difference between the removal of the two reference pellets on the two different substrates was then used to adjust the observed threshold shear stress of the coarse fractions (>212 µm).

The data analyses for the fitting of the semi-empirical model to the observed threshold data from the wind tunnel simulations consisted of two steps. In the first step, the relation between particle size and threshold shear stress from Eq.1 was evaluated by fitting it to the

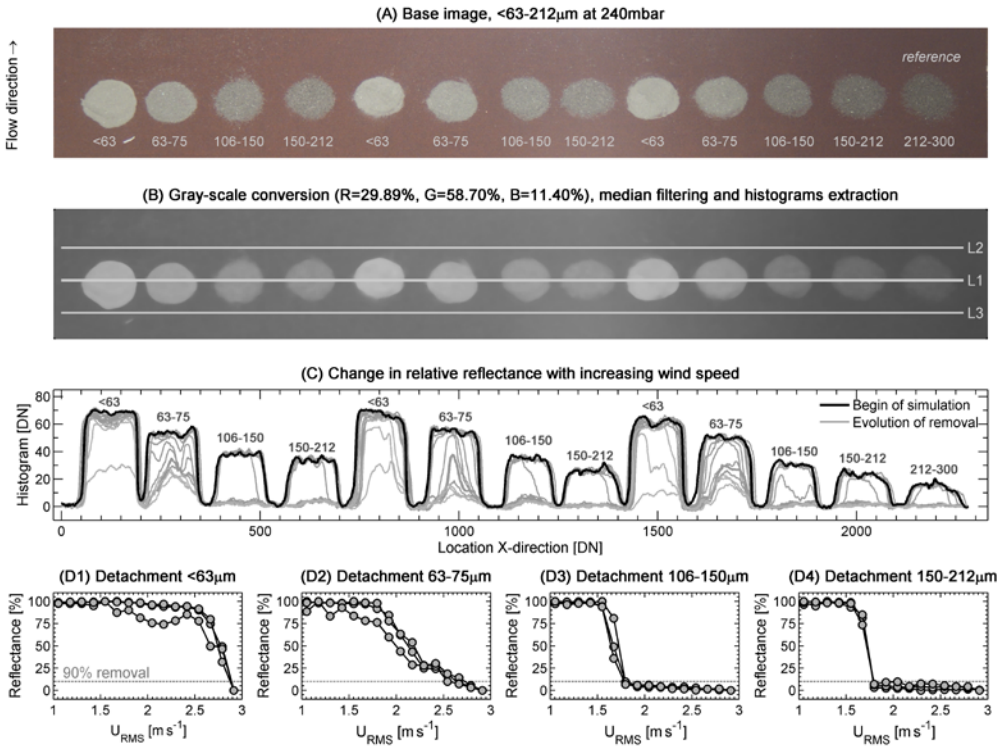

Fig. 25 - Steps in data processing for the fine fractions (≤212 µm). From the original photo (A) a grey-scale conversion averaged the three spectral bands and was followed by median-filtering (B). This procedure was repeated for each step-wise increase of the wind speed to obtain the relative reflectance of pellets in each image (C) by extracting the average reflectivity of the image background (L2, L3 in subset B) from the reflectivity measured across the pellets (L1). The reflectance per size fraction was then normalised in order to extract the flow turbulence (u_{RMS}) for a 90% detachment threshold (D1-D4). Refer to section 3.3 for further details.

data. Optimal values for C_T, C_L and C_{adh} were found by applying a nonlinear weighted least-squares criterion using the nls function in *R* (R Development Core team, 2011), which uses the *nl2sol* algorithm (Dennis *et al.*, 1981). In the second step, the unexplained variance was investigated by evaluating relationships between model residuals and the various particle properties of the volcanic glass. Specifically, Spearman correlations between the model residuals and each mean and standard deviation of the measured particle properties (see appendices F and G) were estimated and tested. In case a significant relation between the model residuals and any of these particle properties is found, the material property could be proposed as a parameter for improvement of the semi-empirical model in addition to the particle diameter and particle mass density. Finally, the most significant model is used to predict the threshold for removal by rolling of particles in the surface conditions on Mars.

4. Results

The blocky and low-vesicular morphology of the Icelandic volcanic glass used in the wind tunnel simulations is shown in the focus-stacked microscope images (Fig. 26). The extraction of various shape properties with eCognition (appendix G), identified minute variations in shape for the eight size fractions. Increasing trends for the elliptic fit, radius enclosed ellipse and rectangular fit with particle diameter were found, while decreasing trends of the asymmetry, border index, radius inclosing ellipse, length/width ratio and roundness with particle diameter occur (mathematical definitions can be found in Trimble, 2011). The gradients in particle shape suggests that the angular and asymmetric silt and fine-sand sized fractions differ in shape compared to more rounded and blocky large fractions, but the variability in shape also created a large standard deviation from these trends.

Skeletal densities of the individual size-fractions had a pronounced non-linear relation with the particle diameter (Fig. 27) that is indicative of the presence of vesicles and closed-porosity and, to a minor extend, small compositional differences. The latter was evidenced by EDX measurements of the major element ratios in individual glassy particles (appendix H). Most notable are the high carbon levels that are indicative of dissolved carbon dioxide in these hyaloclastites. The bulk mineralogy of the material was dominated by a broad reflection features extending from 2θ = 15°-40°, which is consistent with amorphous volcanic glass (Fig. 28). Only minor sharp features on top of the refractograms indicate the low abundance (<10%) of primary feldspathic minerals such as anorthite and albite. The contribution of these crystalline particles varies with particle diameter and is below the detection limit for some size fractions.

A particle property of relevance for the adhesion term in the force balance is the specific surface area. Isotherms of N_2 sorption (Fig. 29) show so-called type-II isotherms (Rouquerol *et al.*, 1999), which are characteristic for a weak interaction of the adsorbent with the amorphous particle surface. Although these type-II isotherms did not allow us to differentiate between a non-porous or macro-porous surface, macroporosity (>50 nm) is expected to result from outgassing of the magma and fracturing of the volcanic glass. This in turn affects the shape, surface roughness and friction between particles that relates to the shape parameters with particle diameter. BET-2 parameter fitting of the data indicates that the fractions have small specific surface areas (Fig. 27), ranging from 1.51 m^2/g for the smallest fraction (<63 μm) to 0.53 m^2/g for the largest fraction (850-1190 μm). These measurements illustrate that surface properties do not scale predictably with d^{-1} for particles from a natural environment.

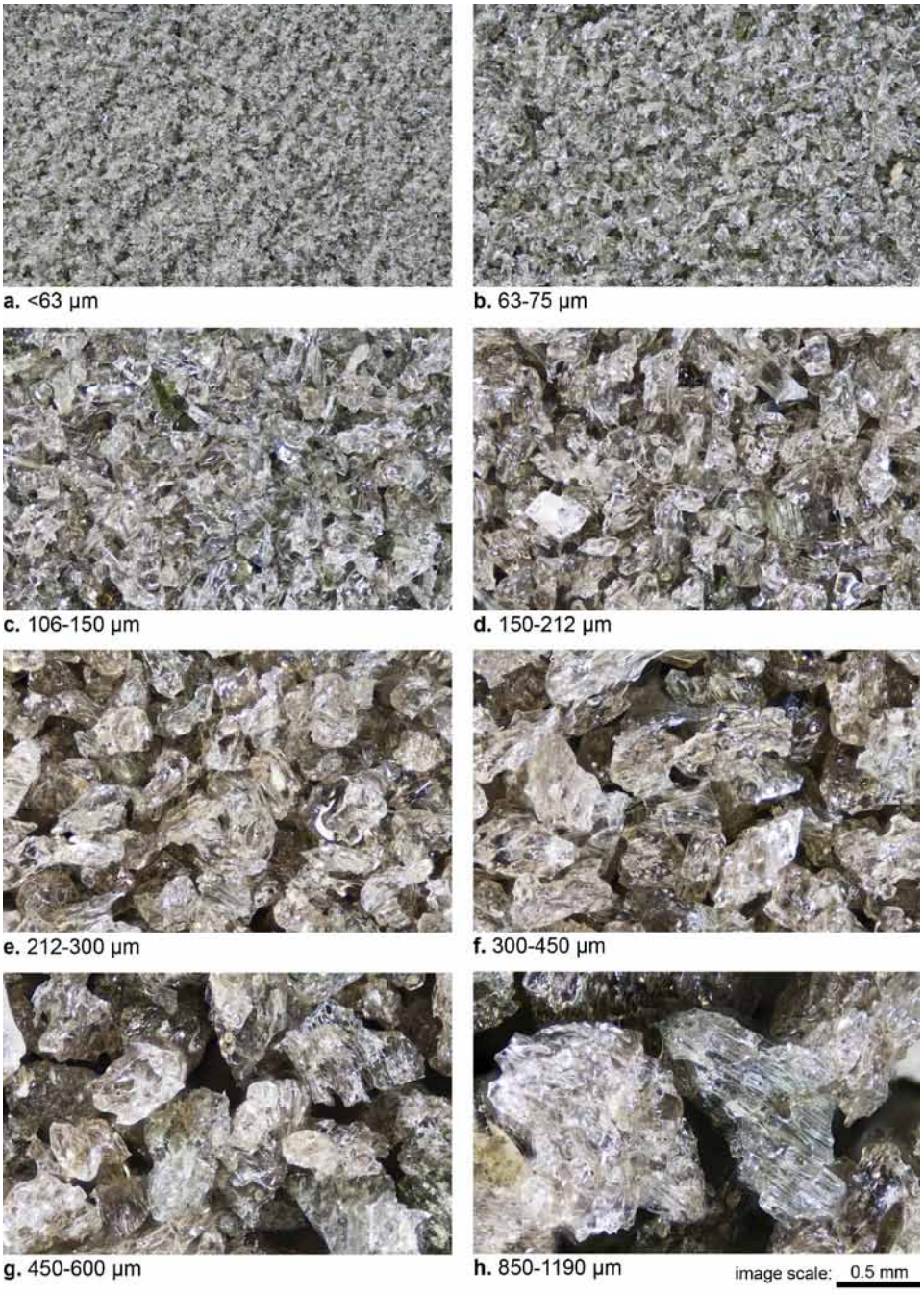

Fig. 26 - Focus-stacked microscope photographs of the volcanic glass used in the wind tunnel simulations. Small fractions show predominantly asymmetric angular particles considered to be the end-members of particle and vesicle fracturing at the time of the subglacial formation (a-d). The mid-range fractions (c-e) have the largest skeletal densities >2.34 g cm-3 whereas vesicularity and closed porosity (gas bubbles trapped inside particles) are more dominant at the larger fractions (f-h). Scale bar applies to all images.

The removal of the small heaps of sand in the wind tunnel simulations showed a threshold-dominated response when pellets are subjected to wind shear (Fig. 25). Heaps of volcanic glass were typically removed in only two or three steps by which the wind speed was increased. The evolution of the pellet diameter (Fig. 25c) showed that detachment of the 63-75 μm fraction is an exception and spans several steps in wind speed. A comparison of the 4 obtained thresholds clearly illustrated that higher friction velocities (u_{*ft}) are required in environments with lower atmospheric pressures due to the lower fluid mass density (Fig. 30), as $u_{*ft} = (\tau/\rho)^{0.5}$.

A more convenient comparison of thresholds in different atmospheric pressures was shown by the shear stress that normalises the observed thresholds for the fluid mass densities (Fig. 31). Good agreement was seen between the threshold measurements made at four different pressures once plotted against shear stress. A fit of the semi-empirical model to the observed threshold shear stress (blue line, Fig. 31) was achieved by imposing non-negativity bounds on all three fitting parameters (C_T, C_L and C_{adh}). The lower detachment threshold for the <63 μm fraction is presumably caused by low-density dust aggregate formation and to a minor extent by artefacts in image processing resulting from non-removable silt between the grains of the used grit paper (Fig. 25). A weighted least-squares scheme was therefore used, where the weight for the <63 μm size-fraction was set to 1% compared to the weights for the other size-fractions due to the 'unrepresentativeness' of the threshold (relative to the model in Eq.1) at this small size-fraction. The resulting fitting parameter values produced a significant fit to the data. The parameter values are listed in Table 5 (fifth column). A residual analysis, using the Spearman correlation between the model residuals and the measured material properties, did not lead to the identification of any pattern in the residuals that could be explained by the measured grain properties. The analysis for example showed no significant correlation

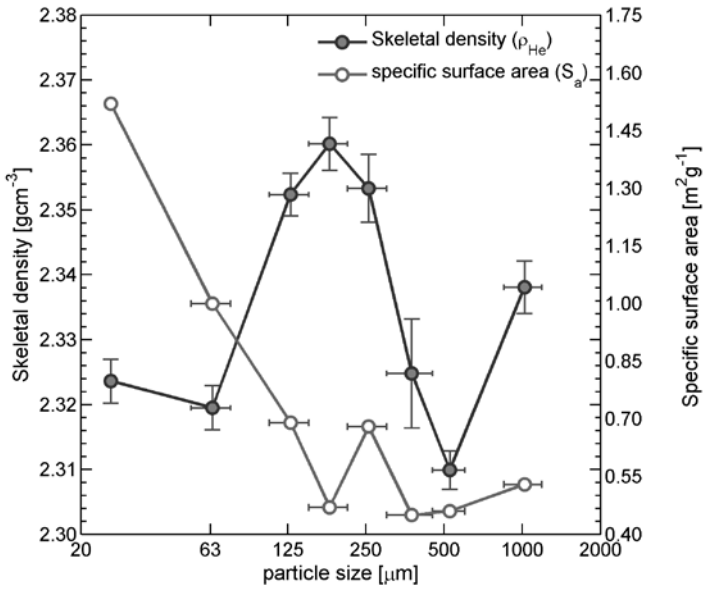

Fig. 27 - Non-linear variations of the skeletal density (ρ_{He}) and specific surface area (S_A) of the particles measured using N_2 sorption for each of the size fractions. Horizontal error bars reflect the ½ φ sieving steps used to separate the Icelandic glass samples into usable fractions (Gee and Bauder, 1986).

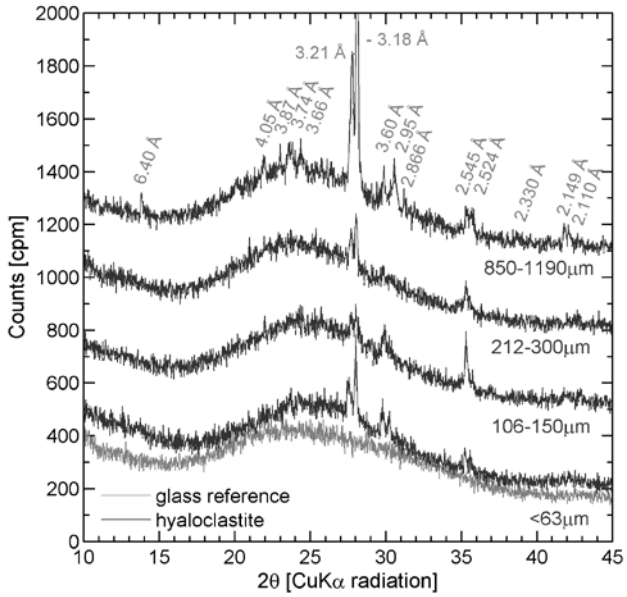

Fig. 28 - XRD powder diffraction patterns from 10°-45° 2θ at a scan speed of 0.02° 2θ/s, given for four of the eight volcanic glass fractions and industrial glass beads for reference purposes. Reflection patterns are offset by 300 counts for comparison and d-values (in Å) are given for the most prominent features and highlight the low abundance of crystalline particles in the amorphous matrix of the used volcanic glass.

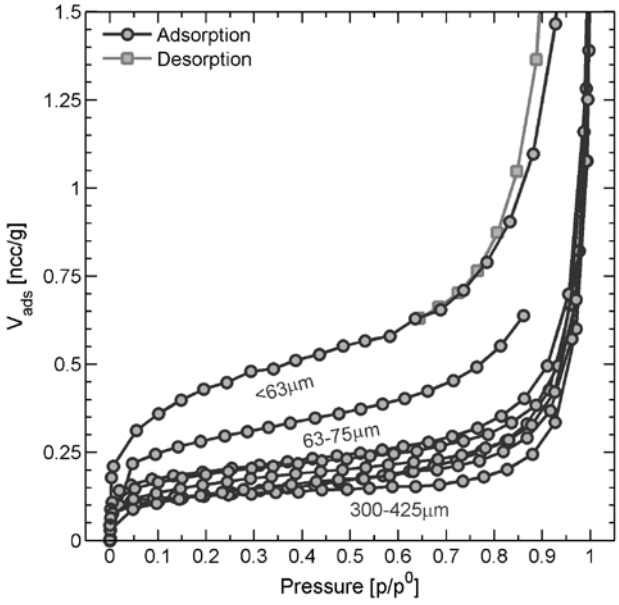

Fig. 29 - Isotherms of the N_2 sorption on the volcanic glass surface. Isotherms were used to determine the specific surface area (S_a) for each of the size fraction used in the wind tunnel simulations. A larger adsorbed volume (at low relative pressures) equals a larger specific surface area. The desorption isotherm for the <63 µm fraction is given as a reference.

coefficients for the morphological variables (n=8) or the mineralogical variables (n=5). When assuming a real correlation of 0.6 and a significance of 0.05, the power of these analyses is low: 0.33 for the morphological variables and 0.16 for the mineralogical variables. After the residual analysis the semi-empirical model was used without any modification with the newly found values for the fitting parameters to predict the threshold for rolling of volcanic glass particles on Mars (Fig. 32). A comparison of the detachment threshold is also given for the spherical glass particles from Merrison *et al.* (2007), which shows that the differences between the threshold of irregular-shaped volcanic glass and spherical glass particles are quite significant and most pronounced for particle diameters <200 μm.

5. Discussion

5.1 Volcanic glass on Earth and Mars

Parallels in formation processes of volcanic glass during glaciovolcanic eruptions on Earth and Mars make it possible to use Icelandic volcanic glass as analogue material. While Wilson and Head (2007) show that subaerial eruptions in low atmospheric pressures create highly vesiculated materials, Horgan and Bell (2012a) argue, based on geographic occurrence, abundance and possible emplacement mechanisms that the detected glass deposits on Mars may have been formed by magma-ice interactions during sub-ice eruptions. Explosive fragmentation during such magma-ice interactions does not take place under low atmospheric pressure and the formation of glassy eruption products is therefore controlled by the glaciostatic pressures of the overlying ice body (e.g. Tuffen, 2007; Jakobsson and Gudmundsson, 2008). The glaciostatic pressure (p_{ice}) is given by $p_{ice} = \rho_{ice} \cdot g \cdot h$, with ρ_{ice} the ice

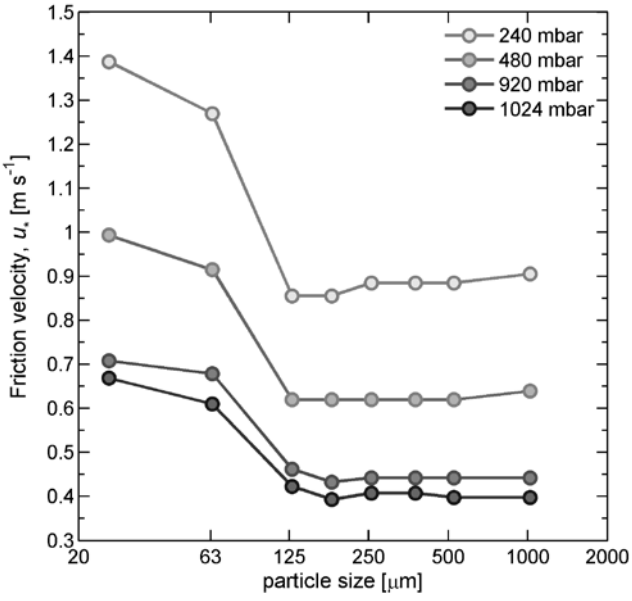

Fig. 30 - Threshold friction velocity u_{*ft} (m s^{-1}) for removal of volcanic glass by rolling under hypobaric pressures of 240, 480, 920 and 1024 mbar. For Mars these pressures are purely palaeobarometric in nature, but they served as four independent experiments for fitting of the semi-empirical model to the calculated shear stress (a value independent of the atmospheric density, see Fig. 31). Note the 'flat', horizontal threshold for removal of particles >150 μm.

density, *g* the gravitational acceleration and *h* the overlying ice thickness (also see appendix D). Based on glacier reconstructions using the summit heights of Martian tuyas (Fagan *et al.*, 2010) and ice densities of 1220 kg m^{-3} (e.g. Zuber *et al.*, 2007), eruptions on Mars may have occurred under glaciostatic pressures of 0.2-9 MPa. This range is comparable to the pressures of 2-8 MPa under past Icelandic ice sheets of 255-960 m thick with ice densities of 850 kg m^{-3} (Licciardi *et al.*, 2007). While variability may occur depending on the conditions under the glacier, physico-mechanical particle properties of Martian volcanic glass are generally comparable to glassy materials in Iceland, as others have proposed before (e.g. Allen *et al.*, 1981; Bishop and Pieters, 1995; Chapman and Tanaka, 2002).

5.2 Evaluation of threshold models

Models are widely used for describing and predicting aeolian processes on Earth and the other terrestrial planets (Bagnold, 1954; Iversen and White, 1982; Greeley and Iversen, 1985). Recent developments in the field of aeolian studies show that simple boundary layer models are incomplete as turbulent processes occur with different dependencies on physical parameters such as the particle properties discussed in this work (Ibrahim and Dunn, 2006; Nino *et al.*, 2003). Simple standard models of Iversen and White (1982) and Shao and Lu (2000) do not account for such dependencies and are also based on sparse empirical measurements that validate their results. Compared to these studies, some differences in the magnitude of thresholds are found with our work in the form of an offset on the vertical axis. Put in terms of the friction velocity: particles were removed at minimum friction velocities of 0.2 m s^{-1} in other studies (e.g. Bagnold, 1954; Iversen and White, 1982), while the jagged volcanic glass used here requires a minimum of 0.4 m s^{-1} (at 1024 mbar, Fig. 30). The systematic offset in friction velocity could be explained by empirical difference in the experimental approach. Specifically due to the different design and type of wind tunnel and the different experimental technique used to determine removal of particles, different approximations have been made for the complex conversion of measured turbulent wind speed into friction velocity (and shear stress) compared to e.g. Greeley and Iversen (1985). The magnitude of friction velocity is dependent on the particle and sand-bed properties, surface roughness and flow turbulence, which in this work differs from previous studies. As the obtained results are realistic values for the removal of these particles, a factor of two difference in absolute magnitude (scaling) of the friction velocity is arguably acceptable based on the experimental approach and considering the inherent turbulent (stochastic) nature of particle removal.

Models developed by Iversen and White (1982), Greeley and Iversen (1985), Shao and Lu (2000) and the model in this study are all semi-empirical in nature and fitting parameters in these models can therefore be adjusted to fit any new data set for different materials. This has to occur within the predefined bounds of fitting parameters to obtain physical results for valid application. In order to evaluate the goodness of the obtained model fit in our study, we conducted a residual analysis where the residual of our null-model was related to the residuals in the model fit and the available compositional, particle surface and shape properties of the volcanic glass. Only univariate correlations between model residuals and the particle properties were considered due to the available sample size in our study. This approach was motivated by the structure that was observed in the residuals of the model fit in Fig. 31; an under-estimation in the 200–400 μm particle range while the model slightly over-estimates the observations at the remaining particle diameters. We therefore aimed at determining if the variability in particle properties could explain the observed structure in the residuals

Table 5 - Parameter values for C_T, C_L and C_{adh} of Eq. 1 with the predicted range from theory and measured values for spherical glass particles (Merrison *et al.*, 2007). The last columns give the least squares parameter estimates for the model fit in this study to threshold data for volcanic glass, with DoF = 29, R^2-adjusted = 0.030.

Parameter	Units	Predicted range	Spherical glass	Volcanic glass			
				Estimate	Std.Error	t-value	Pr(>|t|)
C_L	-	1-10	1.45	11.04	5.346	2.065	0.0480
C_T	m^{-1}	-*	$4.4 \cdot 10^{4}$	$4.382 \cdot 10^{4}$	$7.520 \cdot 10^{3}$	5.827	$2.56 \cdot 10^{-6}$
C_{adh}	N m^{-1}	10^{-5}-10^{-4}	$2.7 \cdot 10^{-5}$	$3.383 \cdot 10^{-4}$	$1.408 \cdot 10^{-4}$	2.402	0.0229

** lacks a relevant experimental framework to define a range*

of the model fit. It turned out that none of the correlation coefficients differed significantly from zero. As the significant model fit is not dependent on the variation in particle properties per particle diameter, the obtained fitting parameters for C_T, C_L and C_{adh} are therefore valid for describing the wind-induced removal of irregular-shaped volcanic glass. The obtained fitting parameters are also comparable to what Merrison *et al.* (2007) found for spherical particles. The torque is of a similar magnitude and the lift parameter is a factor of 8 higher but still reasonably close to the predicted range of 1–10. The adhesion term differs by a factor of 16 compared to spherical glass particles, but the high value is within the expected range of 10^{-5}–10^{-4} N m^{-1} (Merrison *et al.*, 2007).

While our results conform to other studies and the values of the fitting parameters fall within the predicted ranges (Table 5), it is also evident from Fig. 32 that there are clear differences in threshold scaling compared to spherical glass particles that can be attributed to the effects of the different particle properties. The most pronounced difference of the threshold compared to spherical particles occurs for particles <212 μm, where adhesion is much more important in the force balance due to the smaller particle mass. In this size range the adhesion force can be up to 100 times stronger than the gravitational force from the particle's weight and thresholds therefore depend largely on the properties of the particle surface (Shao and Lu, 2000). The simplified adhesion term in the used model may benefit from further parameterisation to explain the observed difference in the thresholds of irregular and spherical particles. The specific surface area (S_a) could potentially be a powerful proxy for adhesion properties as it depends on the particle's surface roughness, which in turn results from the surface microtopography from asperities, macroporosity and micro-fractures. Such surface properties have a considerable influence with decreasing particle diameter on the adhesion and pull-off forces required for particle mobilisation at the threshold condition (Jones *et al.*, 2002; Katainen *et al.*, 2006).

We expect that if particle properties could be varied independently for different samples of glass particles, a better parameterisation could be found for the fitting parameters in order to filter out the effects of specific particle properties on each of the terms in the force balance. Alternatively, if collinearity between different particle properties appears to be inevitable, collecting a much larger sample size may also help to achieve improvements in the parameterisation. Further experimental simulations and research will thus be required to enhance our understanding of the interrelationship of fluid thresholds that include rolling and the physical particle properties of natural materials. This requires wind tunnel simulations where the particle diameter is varied independently from the (relevant) adhesion and shape

parameters with sufficient independent replicates. While such well-constrained materials are not readily available, natural particles with a suitable variety in physical properties could be obtained from edifices with different subglacial eruption conditions, as currently found in Iceland.

Overall, no evidence results from our experiments and residual analysis that, in addition to average particle diameter and mass density, other particle properties are required for describing thresholds that include rolling at the fluid threshold. The semi-empirical model of Merrison *et al.* (2007), originally developed for wind removal of *spherical* glass particles, is therefore also valid for describing the threshold of *natural* glass particles and predicting the removal in the environmental conditions on Mars.

5.3 Particle removal by rolling and the application on Mars

Detachment thresholds measured in our experiments are 'flat' (the curves approximate the horizontal) for larger particle diameters and scale independent of the particle diameter (Fig. 30). This threshold behaviour from around >150 μm agrees with what is expected for fluid thresholds that include detachment by rolling and it is unlike the threshold scaling for saltation that is dominated by lift (e.g. Greeley and Iversen, 1985; Shao and Lu, 2000). This is also illustrated when our model is used to simulate detachment by only lift (with $C_T = 0$), which then causes the model to explain the observed data very poorly (Fig. 31, thin blue line). As expected, Eq.1 gives

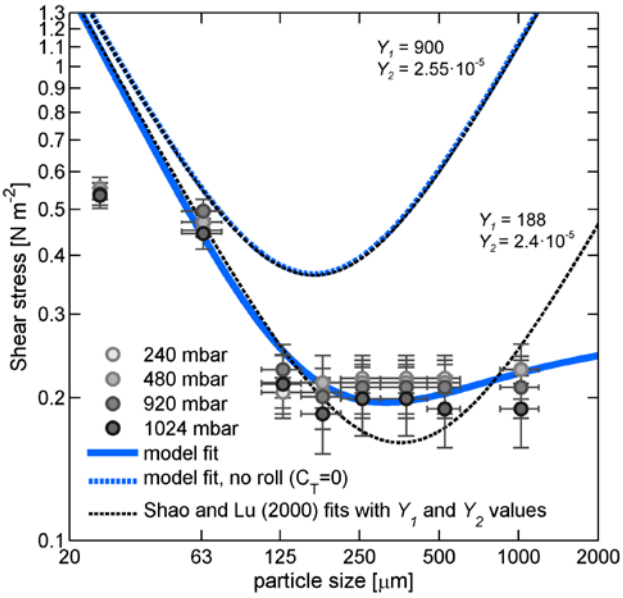

Fig. 31 - Shear stress required for detachment of volcanic glass by rolling. Measurements of removal in the wind tunnel are plotted against the shears stress under four different atmospheric pressures and are modelled by the best fit (solid blue). The importance of rolling in explaining the flat, horizontal threshold is illustrated when the torque term in the model fit is set to zero (dashed blue) and by the inability of saltation models (dashed black) to fit well to the data for the larger particle diameters (>150 μm). Thresholds are given for a 1g (9.81 m s^{-2}) environment and error bars on the x-axes of these figures show the steps of ½ φ sieving (Gee and Bauder, 1986), while the error bars on the y-axes reflect the step size in the wind speed between two consecutive photos.

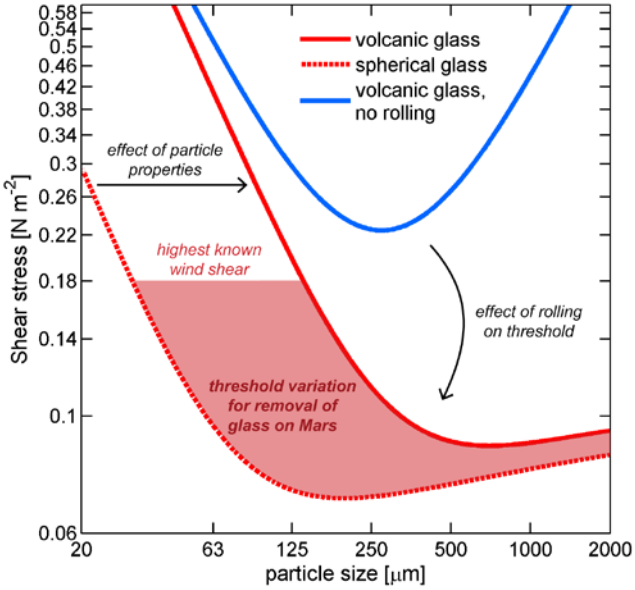

Fig. 32 - Model predictions of the thresholds for wind-induced removal of volcanic glass on Mars (g=3.71 m s^{-2}). As spherical particles provide the easiest morphology for detachment by rolling (dashed red; fit from Merrison *et al.*, 2007), the angular volcanic glass from this study detaches with more difficulty and provides the maximum expected threshold (solid red) for volcanic glass with mass densities of 2.34 g cm^{-3}. The highest measured and inferred wind shears on Mars (see section 2.1) average at 0.18 N m^{-2} for ($u_* \approx$ 3.0 m s^{-1}) and the red area therefore defines the threshold variation for removal of volcanic glass particles on Mars. The effect of removal by rolling of larger particle diameters is clearly visible compared to the modelled threshold that only includes lift.

the same result as other saltation models when the torque from aeolian drag is excluded (Fig. 31, upper dashed line). Using the same method to find the best parameter fit of Eq.1, we also fitted Shao and Lu's model ($\tau_{thr} = \rho \cdot Y_1 \cdot d + Y_2 / d$, where Y_1 and Y_2 are empirical fitting parameters) to obtain the best fit to the data with Y_1 = 188, $Y_2 = 2.4 \cdot 10^{-5}$ (or A_N = 0.099 and $\gamma = 2.94 \cdot 10^{-3}$ in Shao and Lu's less-simplified model). The relative goodness of fit (AIC) of this saltation model is much lower than a model fit that includes rolling (AIC values of 472 vs. 443, where a difference of 2 is already significant; Burnham and Anderson, 2002). Saltation models can therefore be rejected as an alternative explanation for the observed 'flat' threshold data for larger particle diameters. The fact that the minimum threshold in the best saltation model fit has been shifted so far to larger particle diameters, requiring a much bigger relative adhesion force to achieve this, is in itself also an indication that a different removal process is occurring. This strongly supports the interpretation that spherical and jagged volcanic glass particles are indeed removed by rolling above diameters of ~150 μm and it allows our model to be used for predicting this behaviour.

The modelled detachment threshold on Mars (Fig. 32) predicts a minimum shear stress of 0.09 N m^{-2} to permit rolling of volcanic glass with a mass density of 2.34 g cm^{-3}. The highest known friction velocities of 2-4 m s^{-1} on Mars (Sullivan *et al.*, 2005; Parteli and Herrmann 2007a, 2007b; Kok *et al.*, 2012) are capable of producing shear stresses of 0.08-0.3 N m^{-2}. The obtained threshold values fall within this range and existing surface winds can therefore mobilise these particles. The threshold also allows us to assess the variability in shear stress required for detachment of volcanic glass. The lower limit of this range is given by the model

fit from Merrison *et al.* (2007) for the removal of non-cohesive spherical particles that detach most easily. The upper limit is given by the data from this work that defines the upper threshold for a material that is mobilised with more difficulty due to the irregular particle properties. This variation in thresholds (solid area, Fig. 32) is applicable to a wide variety of glassy materials that includes everything between the well-rounded particles observed in certain aeolian sediments (Sullivan *et al.*, 2008; Goetz *et al.*, 2010) and fresh volcanic glass that has undergone little modification from aeolian abrasion. While there is still some debate on the exact diameters of saltating particles (Kok *et al.*, 2012) we find evidence for wind-induced mobility of larger sandy particles in ripples and dune systems (e.g. 700-1800 μm particles observed in the 'Eldorado' outcrops, Sullivan *et al.*, 2008) by rolling at threshold conditions that are roughly comparable to those of smaller particle diameters (~200 μm). Larger grains in surface sediment can therefore still play a role in present-day aeolian processes, rather than reflect the deposition in past climates (Sullivan *et al.*, 2008).

Various other processes have also been proposed for explaining the behaviour of aeolian sediments on Mars. Current resolutions of global circulation models are unable to accurately simulate the much higher winds that are created by topographic forcing of the wind flow and convective processes (Fenton and Michaels, 2010). Favourable winds at the fluid threshold may thus occur very locally and this is probably part of the solution of the saltation paradox (Kok *et al.*, 2012). Other mechanisms for aeolian activity focus on the emission of dust and include processes that are based on thermal gradients from solar insolation, 'thermophoresis' (Wurm *et al.*, 2008), and electrostatic interactions that lead to low-density dust aggregates that are easily detached by modest winds (Merrison *et al.*, 2007, 2011; Sullivan *et al.*, 2008; Bridges *et al.*, 2010). Emerging views on sand mobility also propose favourable effects of grain electrification on particle trajectories and increased sand fluxes, but still have to be studied in further detail (Renno and Kok, 2008; Rasmussen *et al.*, 2009). Other effects dependent on the mobilisation history of an aeolian system, or hysteresis, may be suitable too for explaining particle mobility at lower friction velocities (discussed in more detail by Kok, 2010a). While these processes are viable for explaining the high sand fluxes on Mars, they are based on a state in which particles are already set in motion. We consider the contribution of rolling vital for the initial mobilisation of sediment by surface winds on Mars. As a rolling particle gains kinetic energy, it becomes easier to entrain it into the turbulent flow. Nickling (1988) showed that gradual transitions occur from rolling to saltation of particles. On Mars these transitions may play an important role in sediment mobility and as a potential trigger for saltation. The thickness of the laminar sublayer on Mars is beneficiary for the detachment of particles by rolling as the sublayer reduces the contact with flow turbulence to drive saltation. These benefits are only applicable in flow conditions before the onset of saltation as the laminar sublayer will most probably be disturbed when saltation starts and vertical mixing between the two layers occurs (Kok *et al.*, 2012).

In this study we have focussed primarily on the quantification of the detachment threshold for removal of larger sand-sized particles by rolling in turbulent flow conditions. As our experiments in the hypobaric wind tunnel did not fully simulate the effects of the laminar sublayer, further research into the behaviour of particles inside a well-developed laminar sublayer (one that is several times thicker than the average particle diameter) may be vital for characterising the full contribution of rolling in aeolian systems on Mars.

6. Conclusions

The paradox of saltation on Mars draws much attention but so far lacks a mechanistic framework for achieving saltation from an idle state at the fluid threshold. In this experimental study we focussed on the contributions of rolling as a possible means for mobility of coarser sediments at lower fluid thresholds than saltation. Glassy materials were recently identified as an important constituent of sand dunes and other aeolian sediments on Mars. We therefore used an unaltered, fresh volcanic glass from Iceland to experimentally determine an upper threshold for wind-induced detachment for this type of sediment. Observed removal of large particles in wind tunnel simulations was not consistent with saltation thresholds and it was only well-explained by rolling. As the particle properties in glass-rich sediments on Mars may vary from fresh (angular) to highly abraded (spherical), depending on their eruption age and transport history, we were able to delineate the possible variation in detachment threshold of glass-rich sediment on Mars. We showed that a large size-range and morphological variety of particles can be removed by rolling at the fluid threshold in winds that occur in the present surface environment. Due to the thicker laminar sublayer, rolling from aeolian drag may also be much more important on Mars if compared to Earth. It could therefore by a viable process that contributed to the recently observed aeolian mobilisation of sands.

Box 2 Atmospheric density and buoyancy effects

Physical models and experiments are important didactic tools in education. For atmospheric density, a compelling experiment is the Dasymeter ('*Daah-zea-meter*') that was invented in 1650 by Otto von Guericke. The experiment consists of a light-weight glass sphere that is suspended on a balance for showing the principle of Archimedes in gasses. A counterweight is shifted along the arm to reach equilibrium with the buoyancy forces acting on the sphere immersed in the atmosphere. Inside a vacuum the reduced gas density decreases the buoyancy forces that act on the sphere, thereby offsetting the balance. ESA-astronaut Tim Peak took a Dasymeter with him during the NEEMO 16 mission on board the Aquarius dive station off the coast of Key Largo (Florida, USA). The experiment was part of the 'Science Under Pressure' programme where followers were challenged via social media to hypothesise about the outcomes of the experiment. The experiment in the denser 2.5 bar atmosphere illustrated how the buoyancy increases in the denser atmosphere. Similarly, the lift term (F_L) in Eq.1 also incorporates buoyancy effects for particle detachment. ▪

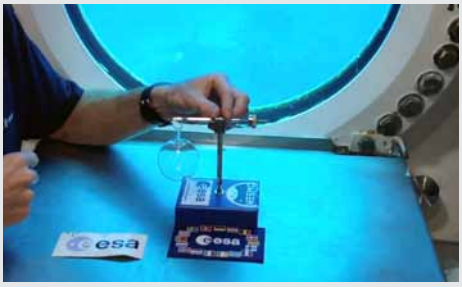

Fig. B3 *Equilibrium position 1 bar, 'topside'*

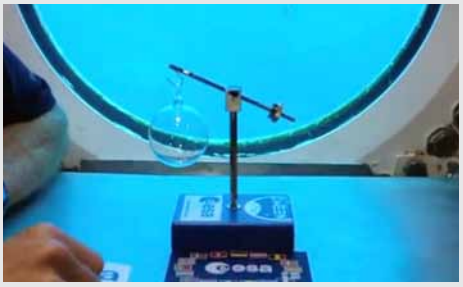

Fig. B4 *Equilibrium 2.5 bar, inside Aquarius*

▲ *Wheel tracks on sol 706 when Mars rover Spirit entered the 'El Dorado' dune field in the Columbia Hills.*

Chapter 5

Orientation of particles to wind flow

Abstract

Long-axis orientation of particles in unconsolidated sediments harbours information on particle mobility in aeolian systems as it reflects the orientation to dominant wind directions. We developed a method using object-based image analysis (OBIA) to measure the orientation of sand grains. This method was first developed and validated using thin-sections of well-studied and oriented sediments in terrestrial inland dunes where it increased the available sample size, reduced operator bias and improved the analysis of grain orientation compared to pre-existing techniques. As the developed method was found to work well for terrestrial thin-sections, it was subsequently applied to images of aeolian sediments on Mars. These images were obtained using the Microscope Imager of the Mars Exploration Rover 'Spirit'. We detected non-random particle orientations in fine-grained sediments at the El Dorado and Winter Haven sites that we interpret to be caused by orientation to local winds. The flow directions inferred from these sediments seem to agree with the flow directions that formed other aeolian features in the vicinity, such as bedforms, ventifacts and wind tails. Although particle orientation occurs during saltation of particles, some degree of orientation may also reflect orientation to flow conditions below the fluid threshold. The detection of preferred long-axis orientations using the newly developed OBIA method can improve pre-existing thin-section studies of aeolian sediment on Earth and it potentially provides a new form of wind flow data that may be of interest to aeolian studies at the surface of Mars.

This chapter is based on: *De Vet, S.J., Anders, N.S., De Boer, W.M., 2013. Near-surface wind directions recorded by particle orientation in Mars' aeolian sediments (Submitted to: Journal of Geophysical Research - Planets)*

1. Introduction

Long-axis orientation of particles by flowing media can be used to study flow patterns. This application is well exemplified in aquatic environments where 'imbrication' is used to study turbidites (Spotts, 1964), shearing deltaic sediments (Hamilton *et al.*, 1968), costal sands (Curray, 1956) and gravelly deposits (Major, 1998). Atmospheric orientation of particles also occurs, yet it is less pronounced compared to aquatic environments (Rusnak, 1957; Schwan 1989). Inferring near-surface flow conditions from particles that have been mobilised or transported by winds is therefore infrequently applied, in spite of potential benefits to aeolian studies on Earth or surface investigations on other planetary bodies. Orientation of particles in aeolian sediments is dependent on the transport regime and as such, particle diameter. At the *static* or *fluid threshold* (Bagnold, 1954) several transport regimes can be identified depending on particle diameter. These regimes cover suspension (<20 μm), short term suspension (~20-70 μm), saltation (~70-500 μm) and reptation (>500 μm) (Kok *et al.*, 2012). A-axis orientation from long-axis streamlining of particles (Fig. 33a) occurs almost instantaneously after entrainment of ~70-500 μm grains by saltation into the turbulent boundary layer (Schwan, 1989). The resulting type of particle orientation is observed in a wide variety of aeolian sediments that vary from non-cohesive wind-blown sand deposits (Sindowksi, 1957) to lithified cross-beddings preserved in sandstones (Wayland, 1939; Schwarzacher, 1951; Martini, 1971). Other forms of particle mobility that result to preferred orientation are made possible by rolling transport at wind speeds below the fluid threshold (e.g. Nickling, 1988). Rolling traverses the long-axis (A-axis) of the particle perpendicular to the flow direction of the wind ('AB-plane' orientation, Fig. 33b). Similar AB-plane orientations may result from individual particles rolling downslope which orients the rolling axis parallel to the strike of the slope (Dapples and Rominger, 1945). Grain orientation therefore harbours valuable information on the type of particle mobility and recent near-surface flow conditions (Schwan, 1989) that can be used *de facto* to reconstruct the wind directions that deposited local cover sands and dunes (De Boer, 1992, 1996).

The interaction of the atmosphere with non-cohesive sediments also leads to the formation of aeolian dunes and ripples on Mars. These processes take place in atmospheric conditions that are different compared to Earth. Present-day atmospheric pressure averages around 6 mbar and higher pressures of 10-15 mbar are only created during periods of higher obliquity (Kieffer and Zent, 1992; Laskar *et al.*, 2004; Phillips *et al.*, 2011). The small amounts of wind speed data in the boundary layer, obtained using meteorological instrumentation on surface landers (Hess *et al.*, 1977; Sutton *et al.* 1978; Schofield *et al.*, 1997; Magalhães *et al.*, 1999; Holstein-Rathlou *et al.*, 2010) and estimates from global atmospheric circulation models (e.g. Haberle *et al.*, 1999; Michaels and Rafkin, 2008) both show that winds in excess of 10 m s^{-1} are very rare. In spite of low atmospheric pressures and infrequent threshold wind speeds, sand mobility is observed to be common (e.g. Sullivan *et al.*, 2005, 2008; Fenton 2006; Bourke *et al.*, 2008, 2010; Silvestro *et al.*, 2011; Chojnacki *et al.*, 2011). Evidence for saltation of sand in aeolian systems such as dunes and ripples occurs more widely than previously assumed (Silvestro *et al.*, 2010; Hansen *et al.*, 2011; Bridges *et al.*, 2012a) and their sand fluxes are comparable to dune systems on Earth (Bridges *et al.*, 2012b). At the global scale mid-latitudinal Martian dune fields reflect unidirectional or multidirectional winds and their orientation seems to correspond to present-day atmospheric circulation (Gardin *et al.*, 2012). Since saltation is the main process driving the preferential particle orientation in aeolian sediments, observational evidence on surface processes on Mars suggest that favourable

wind conditions exist to produce these patterns in aeolian sediments on Mars. However, this assumption is debatable. The low atmospheric density may hamper, for example, airborne streamlining to produce A-axis imbrication. On the other hand, imbrication resulting from *in situ* orientation to the wind flow can potentially be more common on Mars due to the thickness of the laminar sublayer. This layer close to the surface is several times thicker than sand-sized particles, which prevents particles from being detached by saltation into the upper turbulent boundary layer (Greeley, 2002; Kok *et al.*, 2012). Combined with the well-rounded particles of Martian aeolian sediments (Sullivan *et al.*, 2008; Goetz *et al.* 2010) this boundary layer property can promote the rolling of particles across the surface. If A-axis and AB-plane orientation of sand grains from wind flow indeed occurs in surficial sediments, quantification of these sediment property provides valuable information on particle mobility in the present-day atmospheric boundary layer on Mars.

The aim of this work is to develop a method for extracting sand grain orientations from imagery and provide a proof-of-concept for determining near-surface wind flow conditions using sediments on Mars. We used *object-based image analysis* for extracting individual sand grains from imagery data and calculating particle properties such as size, length-width ratio and the orientation of the individual sand grains. The method was developed by testing it for two case studies: (i.) thin-sections made from aeolian deposits with known grain orientations from pre-existing studies in two dune fields in Southern Brandenburg (Germany); and (ii.) lander imagery of non-cohesive surficial sand deposits in the Columbia Hills on Mars.

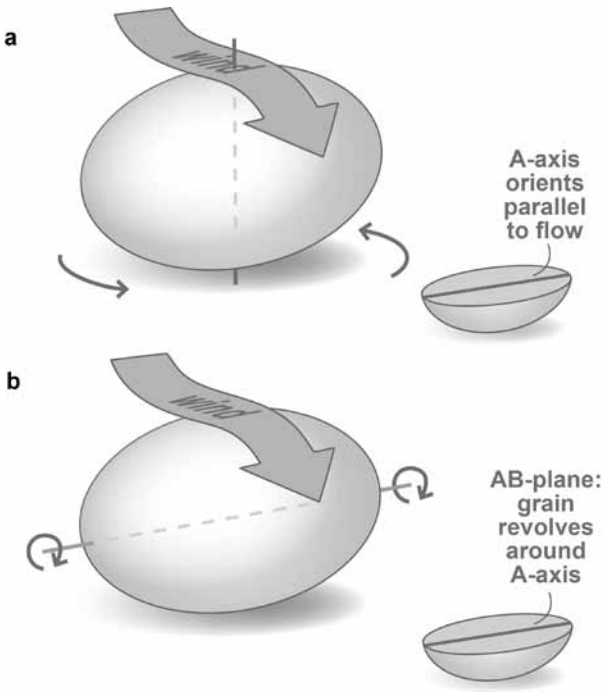

Fig. 33 - Illustration of orientation processes that result to preferred orientations of 'imbrication' of aeolian sediments. Airborne A-axis orientation (a) occurs during saltation when an ellipsoid sand grain (here slightly exaggerated) pivots around the short axis and streamlines the long-axis (A-axis) to the local wind flow. AB-plane orientation results from rolling when the particle revolves around the A-axis, induced by either wind forces acting on the sand grain (b), or from gravity-induced rolling over an inclined surface.

2. Background on extracting long-axis orientation of sand grains

Methods for measuring long-axis orientation of elongated quartz grains in unconsolidated or lithified aeolian sediments have focused primarily on analysing thin-sections made parallel or perpendicular to the bedding of the sediment fabric (Martini, 1971). Using the rotation method for cross-polarised microscopy developed by Bonham and Spotts (1971), required the manual selection and the optical measurement of several hundred suitable quartz grains per thin-section. These lengthy procedures were improved using video-based processing software and hardware to count and measure a variety of grain parameters (Jenkinson, 1989). Several studies successfully used these techniques for the detection of grain orientation in thin-sections (Schwan, 1989; De Boer, 1992). However, in order to obtain sufficient contrast and image data, thin-sections needed to be viewed under polarised or cross-polarized light over 16 axes, or 'ferrets' (Fitzpatrick, 1980). More complexity is introduced in such video-based orientation measurements by the need to exclude boundary pixels in a sand grain due to irregular changes of the pixel values during the rotation under crossed polars. The applicability of this technique at a given image resolution therefore reduces drastically for smaller particle diameters. These boundary effects and the small forms of overlap between two adjacent grains at their boundaries (Heilbronner and Pauli, 1993) required small grains to be avoided in these types of measurements (Passchier and Trouw, 2005). Meanwhile, software developments of image processing tools have shown that similar results as in manual thin-section analysis methods can be obtained, with and without the use of the rotation between crossed polars, at much faster and automated rates compared to the methods used in previous studies (Heilbronner, 2000; Zaniewski, 2001; Fueten and Goodchild, 2001; Sime and Ferguson, 2003, Li *et al.*, 2008; Hassanpour, 2011).

A recent development that allows similar orientation data to be extracted from imagery of sand grains is Object-Based Image Analysis (OBIA; see Blaschke, 2010, for an extensive review). OBIA is based on the automatic clustering of image grid cells into objects or polygons (more information on OBIA is presented in section 3.1). In geosciences OBIA has been previously applied to various gridded datasets, including airborne or satellite imagery data and elevation data. In aeolian or sedimentological research thin-sections under cross-polars provide sound imagery data for OBIA analyses due to the high contrast between individual grains and the background. OBIA can therefore be applied to imagery of thin-section to isolate individual sand grains and measure long-axis orientation, as well as other sediment statistics (e.g. Urbanski *et al.*, 2011). For obvious reasons it is not possible to produce thin-sections from sediments at the Martian surface. However, the versatility of the OBIA method lends itself for application to conventional imagery of sand grains in aeolian sediments in order to measure sediment properties and infer long-axis orientations of grains on Mars. This planetary application benefits from the pre-existing cadre of well-established thin-section studies on Earth. We therefore used thin-sections of horizontally laminated sediments in terrestrial inland dune as a test bed to develop a general method to extract particle orientations.

3. Methods

This section is divided into three parts. The first part (3.1) describes the general procedure of sand grain extraction from imagery data and the subsequent granulometric analysis. The second part (3.2) describes the case study from the Schöbendorf and Klein Zieschte dune complexes in Southern Brandenburg (Germany). Here we validated the automated procedure with an existing and well-studied dataset of sand deposits formed by comparable

unidirectional wind flow conditions as the present-day surface winds on Mars. The third part (3.3) presents the case study where we finally applied the OBIA method to imagery data of aeolian sediments in the Columbia Hills, obtained by the Mars Exploration Rover 'Spirit'.

3.1 Extracting sand grain properties from imagery data

As noted, the method on extracting sand grain properties is based on Object-Based Image Analysis (OBIA) techniques. OBIA consists of two main concepts, namely image segmentation and object classification. Image segmentation is the process of clustering grid cells into homogenous groups or 'objects', based on values of gridded data sets. These objects are subsequently categorized into classes using criteria related to; (i.) object statistics (e.g. mean, standard deviation, range) of enclosed grid cell values; (ii.) shape properties (e.g. main direction, length-width ratio, size, roundness) and/or; (iii.) topological relationships between objects or (geo)spatial context. Any type of gridded data set can be used as input for object-based analyses technique, such as aerial photography and multi/hyperspectral satellite imagery (e.g. Burnett and Blaschke, 2003; Blaschke, 2010) and digital elevation data (e.g. Van Asselen and Seijmonsbergen, 2006; Anders *et al.* 2011), or even MRI, X-Ray, and microscope images in medical disciplines.

The concept of OBIA is implemented in the commercially available software package eCognition (Trimble, 2011). The multi-resolution segmentation (MS) algorithm (Baatz and Schape, 2000) is a widely-used region-growing algorithm to formulate homogeneous objects based on 'colour' values (i.e. grid cell values). The algorithm allows the definition of a shape parameter (a dimensionless value ranging from 0-1) to prevent generating very irregularly

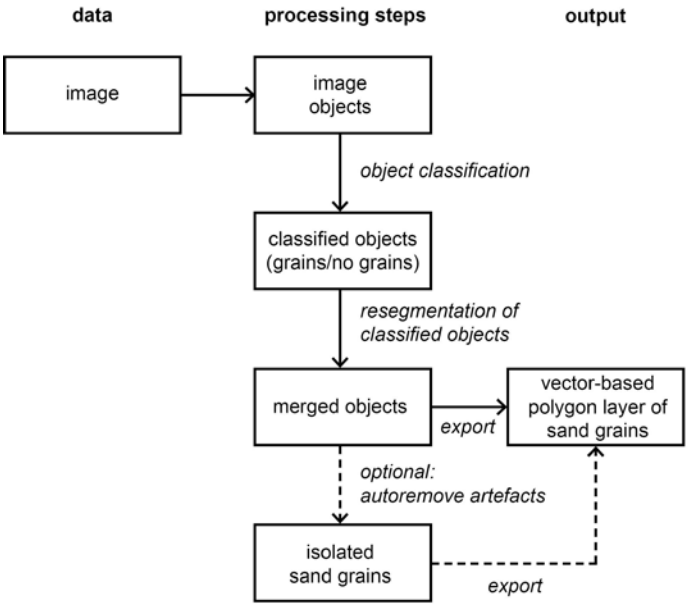

Fig. 34 - Work flow of the object-based image analysis strategy. The flow is divided into three phases where (i.) objects are obtained by segmentation of the original image, (ii.) subsequent object classification and reclassification leads to the identification of individual sand grains that are then (iii.) exported as polygons with an appended attribute table that contains their features such as surface area, length-width ratio and orientation of the long-axis. Fig. 37 shows a visual reference of the three consecutive steps.

shaped objects. When a higher shape parameter is defined (close to 1), less weight is assigned to colour values in the process of object delineation. In this research presented here the shape parameter was set to an average value of 0.5 to prevent the generation of very irregularly shaped objects, but allow colour values to drive the general object shape. The additional scale parameter in the algorithm influences the size of the objects and is closely related to the image quality (blurred images require smaller scale parameters for equally sized objects) and spatial resolution (images with smaller grid cells require larger scale parameter values for equally sized objects). The scale parameter was iteratively determined to obtain the most optimal value to accurately enclose individual sand grains in the image. Once segmented, sand grains were classified to differentiate between foreground elements (sand grains) and background noise (i.e. organics, interparticle pore spaces and dust). The actual procedure used for the processing of thin-section imagery and Mars rover imagery data, as depicted in Figure 34, was as follows:

1. **Image segmentation** to create small objects. The individual grains are oversegmented (one grain consists of multiple objects) to prevent oversized objects where grains are mixed with background noise. Depending on the quality of the imagery data the first step was preceded by an edge-preserving median filter with a 3x3 moving window (kernel) to enhance the contrast of the image (this was essential for the imagery data of surficial sediments on Mars).
2. **Classification of objects** to differentiate between sand grains and background noise.
3. **Resegmentation of objects** that were classified as 'sand grain' with a larger scale parameter value to merge the oversegmented objects. After this step individual objects represent entire sand grains.
4. **Removal of segmentation artefacts** by excluding objects with a roundness larger than 1.2.
5. **Exportation of objects** classified as 'sand grains' as polygons to a vector-based shape file with an appended attribute table containing polygon properties (e.g. area, length, width) that were automatically calculated by eCognition. This vector-layer formed the basis of the subsequent orientation and granulometric analyses.

The processing steps and their corresponding parameter values are summarised in Table 6. All thin-section data could be processed with a single rule set. The Martian surficial deposits images used the same extraction strategy, but with different parameter settings due to different spectral conditions of the images (more information on this matter is found in the following subsections). Individual shape properties were determined for each of the polygons representing extracted sand grains and included the main orientation direction, length-width, and surface area. Length-width ratios were computed due to the effect of different ratios on the calculated degree of imbrication and its use to select a suitable sample subset to infer the wind flow directions from the sediment fabric. Schwan (1989) defined a set of suitable parameters for describing the long-axis orientation of aeolian sediments. The most notable is the mean resultant length (R) as a measure for the overall fabric strength. This parameter is a relative value between 0 and 1 for the concentration (variation) around the mean orientation of the sediment fabric and it is calculated for eighteen 10° intervals using:

$$R = \{(C/n)^2 + (S/n)^2\}^{0.5} \text{ , with } C = \sum_{i=1}^{18} f_i \cdot \cos 2\alpha_i \text{ , } S = \sum_{i=1}^{18} f_i \cdot \sin 2\alpha_i$$

Here, n is the total amount of measured sand grains, f_i the amount of grains per interval and α_i the mid-class point of the interval (with α_i = 5°, 15°, 25°, …, 175°). As the preferred

Table 6 - Process parameters used in the object-based image analysis (OBIA) strategy. Images were analysed using the commercially available software eCognition, according to the workflow in Fig. 34 with the use of the set of parameters specified below.

Process	Parameter	Brandenburg	Mars		
			Shadow	*King George Isl.*	*Troll*
Median filter	-	-	3	3	3
Segmentation	Layer	RGB	median	median	median
	Scale	20	10	10	35
	Shape	0.5	0.5	0.5	0.5
Classification	Mean Red	> 120	-	-	-
	Mean median value	-	> 300	> 1200	> 1200
	Roundness	> 1.5	> 1.15	> 1.15	> 1.15
	Length/width	-	< 1.6	< 1.6	< 1.6
	Area	-	-	-	< 250
Segmentation	Layer	RGB	median	median	median
	Scale	80	25	25	50
	Shape	0.5	0.5	0.5	0.5
Remove artefacts	Roundness	> 1.2	-	-	-

orientations of grains is measured in a 2D plane, the long-axis orientations is strictly non-vectorial such that inferred directions are either in $x°$ or $x°+180°$. The mean of the preferred orientation direction of grains (x) is then defined by:

$$x = 0.5 \cdot \tan^{-1}(S/C) + K \cdot 90°\text{, with } K = 0, 1 \text{ or } 2$$

Here, K is a value used to calculate the preferred orientation per quadrant due to the asymptotes occurring every 90° in a tangential function. In addition to parameters for describing the preferred long-axis orientation, object properties such as the particle surface area were used to calculate more general sediment properties such as particle diameter distribution (Urbanski *et al.*, 2011).

3.2 Case study 1: Thin-sections of Schöbendorf and Klein Ziescht, Germany

The thin-sections used in this study were made from laminated aeolian sediments exposed in the sandpits near the village of Schöbendorf and a comparable depost at Klein Ziescht (see Fig. 35). The area is located in the Central Glogów (Glogau)-Baruth ice-marginal valley. The Baruth valley was the main discharge channel that drained the meltwater of the Brandenburg ice-margin (maximum Brandenburg advance at about 24 kyr BP, Litt *et al.* 2007 to about 20-21 kyr BP, Heine *et al.*, 2009). Schöbendorf and Klein Ziescht are located on the oldest of the river terraces that were formed by at least four consecutive discharge events (Juschus, 2001). The Baruth ice-marginal valley is part of the Brandenburg young moraine landscape ('Jungmoränenlandschaft'), which was formed during the Weichselian glacial stage when the area was devoid of vegetation. Aeolian processes were the dominant agent for mobilising and transporting cover sands and the subsequently formation of several (up to 25 m high) inland dunes, mainly in the form of longitudinal, transverse, hummocky and parabolic dunes. These dunes consist for more than 95% of sand-sized (63-630 µm), well-rounded quartz grains (De Boer, 1992) and were formed by winds from roughly westerly and southerly headings (De

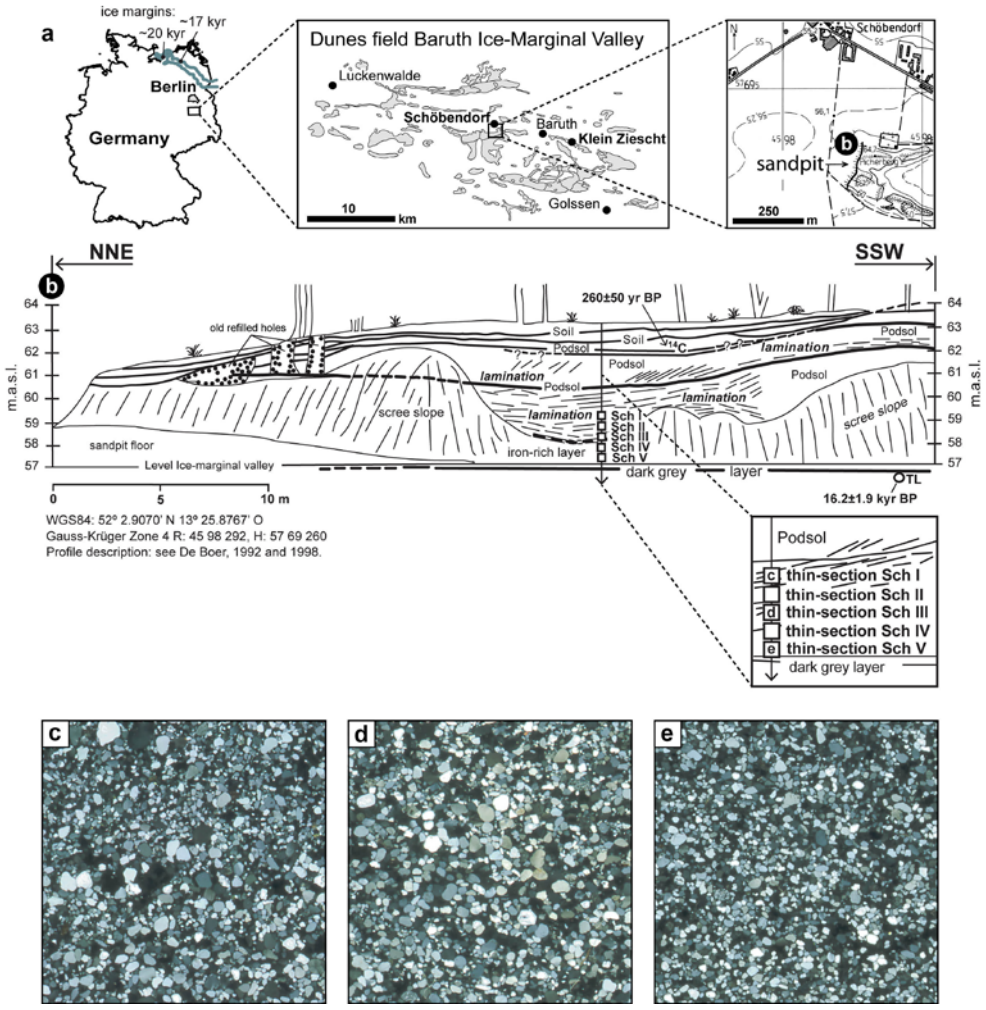

Fig. 35 - Aeolian sediment exposed in the Picherberge quarry near Schöbendorf (a, modified from: De Boer, 1992, 1998, glacial margins are based on: Ehlers *et al.*, 2011; Brandes *et al.*, 2012). The illustration (b) shows the subsurface structure in the north-north-westerly exposure of the Picherberge complex. The geomorphological setting of the Klein Zieschtdune is nearly identical to the Schöbendorf dune and samples were obtained from similar strata. Excerpts of the thin-sections (10x10 mm) were made from undisturbed laminae and are shown here between crossed-polars (c-e). The grain morphology and the conditions of the late-Weichselian genesis of these dunes, in dry periglacial conditions devoid of vegetation, are comparable to the conditions in which well-rounded aeolian sediments are currently being transported on Mars.

Boer, 1996). The similarities in particle diameter and morphology of these sand deposits with the well-rounded sand grains in aeolian sediments on Mars (Sullivan *et al.*, 2008; Goetz *et al.*, 2010) allowed us to use these inland dunes as a test-bed to develop a strategy for application of the OBIA method to aeolian grains on Mars. The goal of the first stage in our study was therefore to demonstrate the effectiveness of the OBIA method within a small but well-studied dataset of aeolian sediments with the purpose of validating the developed method with results from pre-existing thin-section analysis techniques. We used the same thin-sections of the Schöbendorf and Klein Zieschtprofiles that were used in the study of De Boer (1992), which

were sampled roughly plane-parallel to horizontal laminae. Thin-sections were scanned with a pixel resolution of 9 μm between crossed-polarisation filters to increase the optical contrast (Fig. 35c-e).

Table 6 summarizes the OBIA processing steps and parameter values used for the processing of the thin-sections. Objects have been formed based on their Red, Green, and Blue (RGB) colour values in the original thin-section images. In this case only the red colour band was sufficient to differentiate between the sand grains and the background noise. A final step before exporting the sand grains to a polygon layer was required to remove segmentation artefacts, which have been identified based on their irregular shape. The 'roundness' property was used to automatically identify these irregularly shaped objects. Roundness is a standard property that can be derived from objects in eCognition software, and describes how well an object fits into an elliptic shape. Roundness is calculated by the difference of the outer ellipse and the inner ellipse (Trimble, 2011). Objects with a roundness value higher than 1.2 were considered irregularly shaped and were therefore removed from the final collection of classified sand grains. With the obtained polygon layer other sediment statistics such as grain size distribution can be calculated. For the purpose of comparing the OBIA method to earlier research by De Boer (1992), we have limited the analysis to comparing the frequency distributions of long-axis orientations and fabric strength properties using the methods described in section 3.1.

3.3 Case study 2: Surficial sands in the Columbia Hills, Mars

Images from sand grains at the surface of Mars were obtained during the primary mission phase of the MER B, or 'Spirit' rover, using the Microscope Imager located at the end of the robotic arm (Herkenhoff *et al.*, 2003). This fixed-focus CCD camera is used for extreme close-ups of rocks and soils and has a field of view of 31x31 mm with a pixel resolution of 30 μm. Images made by the Microscope Imager (MI) are taken plane-parallel to the surface to obtain a consistent focus across the image. The projected surface of the grain therefore reflects the morphology of axes that have oriented to the local wind flow. Particles with a minimum surface area of 20 pixels contain sufficient object data for segmentation with eCognition, which means that grain orientation in Martian sediments can be detected to a lower size limit of 100-150 μm. This detection limit is well in line with the sand-sized particle diameters that are regularly mobilised by aeolian processes and the estimated particle sizes of aeolian sediments in the Columbia Hills (Sullivan *et al.*, 2008; Kok *et al.*, 2012). By multiplying or 'rotating' the state vector (1 0 0) with the quaternion of each image (a vector composed of 4 complex numbers for describing orientations and motion in a 3D space) we obtained the pointing vectors of the camera, which were then decomposed into an azimuth and elevation to determine grain orientations relative to true north. Due to the shallow 6 mm deep focus, the camera had to be positioned plane-parallel to the imaged surface. The calculated tilt of the image plane could therefore be used to determine if the slope angle of the deposit has been favourable for rolling and as such particle orientation parallel to the strike of the slope (Land, 1964; Rees, 1968). Other preferred orientations were therefore interpreted the primary orientation axis that reflects the local wind flow direction.

Suitable images of undisturbed sediments were obtained on sol 707, 1034 and 1085 during Spirit's traverse of the Columbia Hills (a 'sol' is the mission's Martian day number starting at landing). Other studies have extensively explored the sand-mobility in this area and inferred the local wind flow patterns from aeolian features such as bedforms, ventifacts, wind tails and

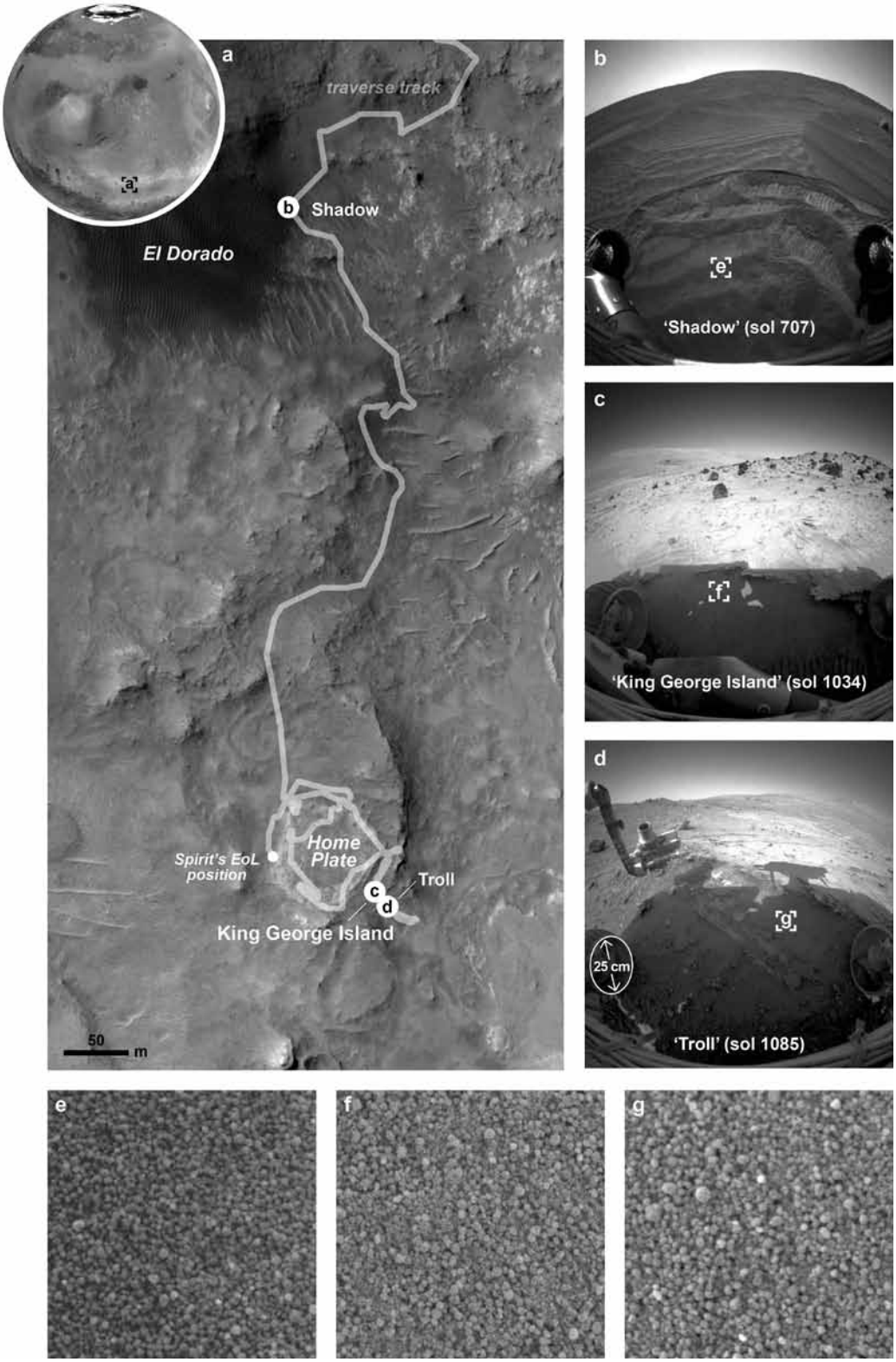
a
traverse track
b Shadow
El Dorado
Home Plate
Spirit's EoL position
Troll
c
d
King George Island
50 m
b
'Shadow' (sol 707)
c
'King George Island' (sol 1034)
d
25 cm
'Troll' (sol 1085)
e
f
g

dust streaks (Greeley *et al.*, 2008; Sullivan *et al.*, 2008; Thomson *et al.*, 2008). This provides a well-documented setting for understanding and explaining preferred orientations observed in the used imagery. The selected locations at the El Dorado dune field and two sand deposits SE of Home Plate are composed of similar-sized, well-rounded mafic sand grains free from interstitial dust (Fig. 36). Overlapping images of sands at the 'King George Island' (KGI) target at the Winter Haven site (Fig. 36c) were first used to establish if the developed technique would give the same result for images of the same grains but with different pointing vectors of the camera. The segmentation strategy was then applied to a comparable sand drift located a few meters away at 'Troll' (Fig. 36d). As both sites are impeded sand drifts pinned down between the same resistant platy layers (Arvidson *et al.*, 2008), the comparable flow conditions over these two sites are ideal for detecting and discriminating between A-axis orientation from saltation and possible AB-plane orientation from rolling of particles down-slope. Finally, orientations of particles in the 'Shadow' ripple at El Dorado served as an independent site to study preferred particle orientations and flow directions in an area with a topographically more complicated bed.

A similar OBIA procedure as for the thin-sections was applied to the images of the Martian aeolian sands, though with different parameter values. Table 6 summarises the used rule set and parameter values for the images in the three locations. Due to high ISO noise in some areas in the images a median filter was required to enhance the suitability of the images for segmentation. The edge-preserving median filter with a 3x3 moving window (kernel) slightly blurred the images and removed the high ISO noise in the image. This allowed a more accurate delineation of individual sand grains. The digital colour or brightness value differed notably between the images due to different light conditions during surface imaging operations (the 'Shadow' area was imaged in deep shade, in contrast to highly exposed images at the King George Island and Troll targets. The quality of the images also influences the scale parameter values; the image in the Troll area being slightly sharper than the other areas. Similar to the processing of the thin-sections, digital representations of the sand grains were exported to a vector-based polygon layer to calculate granulometric properties such as length-width ratio, surface area, and orientation. The detected orientations in the sediment fabric were then compared to local hillslope angles and wind directions that were inferred from local aeolian features such as dunes, ripples and ventifacts along the traverse of the Colombia Hills (Greeley *et al.*, 2008; Thomson *et al.*, 2008) to understand the contextual relation of the three studied sites with the local flow patterns.

4. Results

4.1 Thin-sections of Schöbendorf and Klein Ziescht

The increased contrast from thin-sections under crossed-polars made the segmentation of the imagery straight forward as grains are easily separated from dark background in the image (Fig. 37). The excerpt of the original image and the classification results (Fig. 37) illustrated that a large quantity of sand grains with different particle diameters can be classified using this method for thin-section analysis (n_{tot} in Table 7). Based on the calculated length-width

Fig. 36 (left) - Traverse map of the Spirit rover in the Columbia Hills, spanning from the El Dorado dune field to Home Plate (a). Locations used for the object-based image analysis include the 'Shadow' ripple located 8 m inside the El Dorado dune field (b) and two sand drifts at the 'Winter Haven' site SE of Home Plate where grains are perched on slopes below the exposed resistant lava layers at 'King George Island (c) and at the 'Troll' ridge (d). Diameter of the rover wheel is given for size. The 10x10 mm excerpts of MI imagery (e-g) show the comparable well-rounded morphologies of 100-300 μm sand grains that have no appreciable bonding to other particles in these deposits.

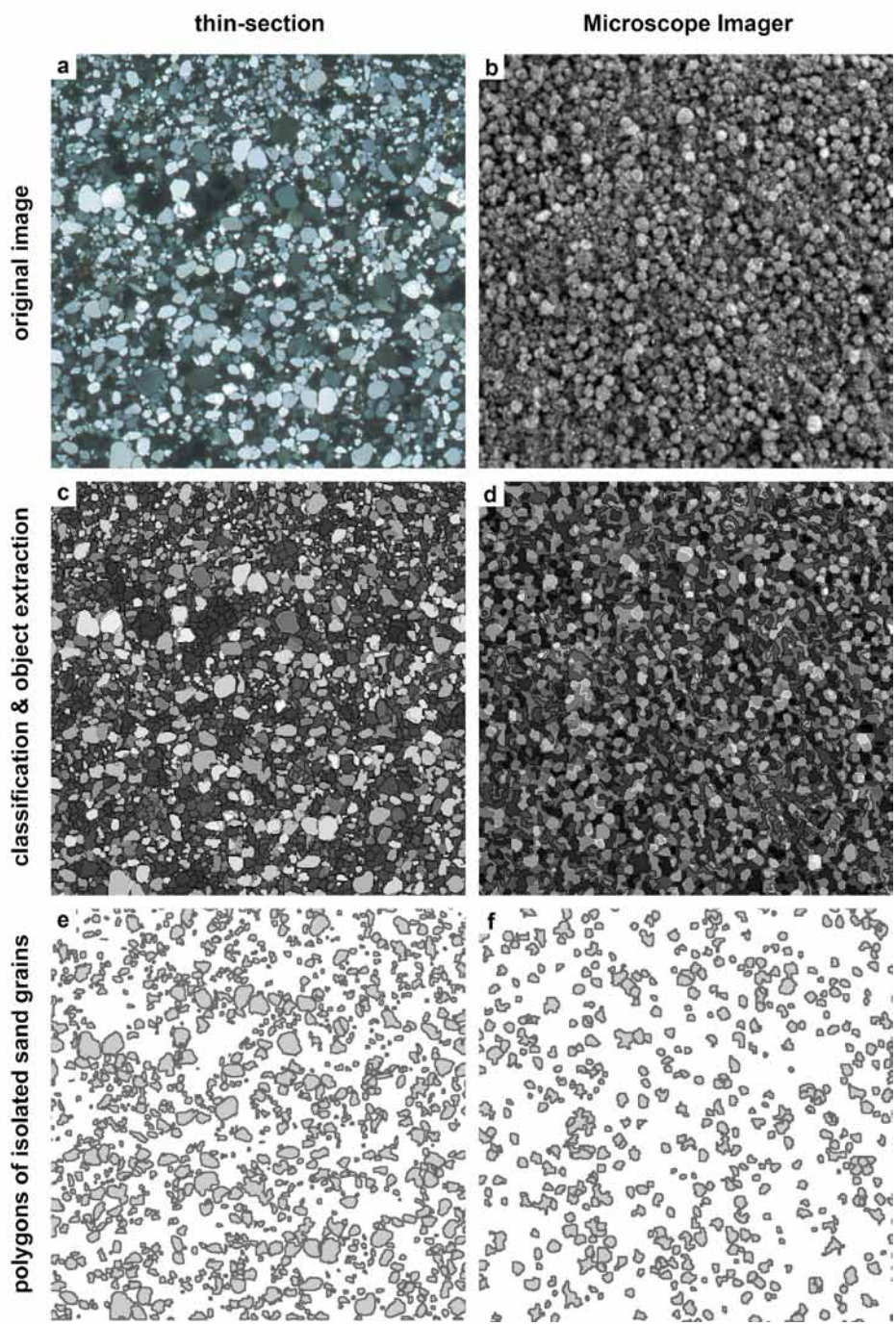

Fig. 37 - Steps in the object-based analysis shown for 10x10 mm excerpts of the original images. Steps show how the original image (a,b) is decomposed (segmented) into polygons of similar pixel data (c,d) and classified to obtain the eventual polygons that reflect the outline of individual grains (e,f). The same strategy was used for the objected-based image analysis for thin-sections and imagery obtained by the Microscope Imager on Mars. Comparable polygons are produced and this highlights the ability of object-based image analysis to produce similar sediment statistics, independent of the type of sand-grain footage.

ratios a subset was selected containing particles with a length-width ratio of >1.5, similar to De Boer (1992). While not all grains in the thin-sections were identified based on the used rule-set (some of the darkest grains are omitted), or eventually included on the basis of their length-width ratios, the amount of grains used in the calculations is still 3-6 times more than those manually selected in pre-existing studies (compare the $n_{>1.5}$ values in Table 7). The selected subset allowed the frequency distribution of the long-axis orientations and fabric strengths to be calculated with the parameters as summarised in Table 7. Rose diagrams (Fig. 38) show bimodal headings with a preferred and a transverse heading. Average headings of the preferred orientations are illustrated in the wind roses by blue (x) and green lines (x_a) and they are compared to pre-existing measurements (in red) in Fig. 38. Preferred orientations were found to be very consistent throughout the depth of the profile (sample depths shown in upper left-hand corners of the wind roses) and they are also very comparable between the two sites. Despite the spatial separation of 7 km, both sites indicate wind directions oriented along an azimuth of (N)NE-(S)SW. These headings are in good agreement with pre-existing studies, although SCH I and SCH III show a deviation of 5-28°.

4.2 Surface images on Mars

The same processing method as for the terrestrial thin-sections was used for the imagery of surficial sediments on Mars. However, low exposures, image contrast and increased ISO noise (Fig. 36e-g) required the adaptation of the process parameters in the rule-set to compensate for these differences in imagery data, which yielded comparable results as in the analysis of the thin-sections (Fig. 38 vs. 39). Obtained polygons of sand grains in the MI imagery are clearly affected by the pixel-resolution of the CCD camera (30 μm) and grains therefore generally appear jagged compared to the higher-resolution of the thin-sections (9 μm). This did not interfere with the computation of sediment statistics as the majority of particles exceeded the minimum required object size of 20 pixels, or particle diameters of 100-150 μm (Fig. 39, first column). The algorithm was first applied to the overlapping images at the drift sand of 'King George Island'. In spite of the different pointing vectors of the MI camera, orientations of grains measured in both images and their orientation relative to true north are in good agreement (Fig. 39). Processing and analysis of the obtained data from the 'Troll' and 'Shadow' targets produced comparable results for headings and fabric strengths (Table 8). In contrast to terrestrial aeolian sediments, particles were found to be highly spherical as they did not exceed length-width ratios of 1.7 (Fig. 39, second column). Further selection with a higher minimum length-width ratio amplified the orientation pattern, yet also rapidly reduced the amount of particles for calculating orientation patterns and other sediment properties. Due to the large pixel scale, rose diagrams were made using a length-width ratio larger than 1.1 such that only very spherical particles were excluded. Bimodal frequency distributions of long-axis orientations were detected for all of the three sites (Fig. 39). Based on the calculated tilt of the camera (Table 8) one of the headings was excluded as a possible orientation axis caused by rolling parallel to the strike of the slope (red lines, Fig. 39) and the second orientation heading was inferred as the wind-induced orientation (blue lines, Fig. 39). The wind-induced headings are very comparable for the targets at Home Plate and good agreement was also found for the wind quadrants of the calculated orientations (x). A comparison of the preferred orientations was also made with the orientation of aeolian features at the El Dorado and Home Plate sites (Fig. 40). The long-axis orientation of grains in the sediment fabric were found to align well with the directions of other aeolian features. The most notable deviation with local aeolian features was found at the Shadow ripple in El Dorado.

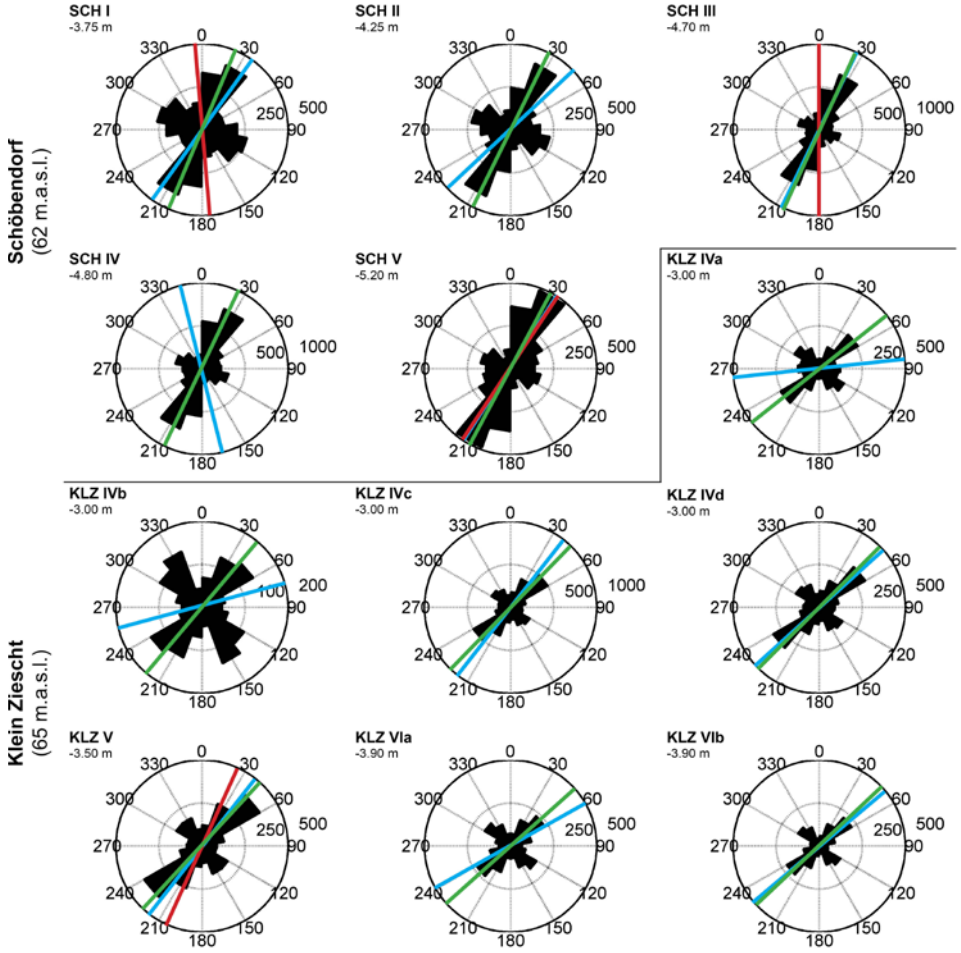

Fig. 38 - Preferred orientation of grains in thin-sections of aeolian sediment at the Schöbendorf and Klein Zieschт dune complexes. Rose diagrams show the long-axis orientations for all particles with a length-width ratio of >1.5. The average heading relative to true north (x° or x°+180°) is shown for data obtained using video-based analysis (in red), the OBIA method from this study (in blue) and arithmetic means calculated for the preferred orientation (in green). Orientations related to gravity-induced rolling are absent, as thin-sections were made from horizontal laminae. Weak signals in nearly all thin-sections orthogonal to the main heading are examples of wind-induced rolling.

5. Discussion

5.1 Detecting preferred long-axis orientations in thin-sections

5.1.1 Comparison of the OBIA method with pre-existing techniques

Relating preferred orientation of grains in thin-sections to local flow conditions is a method that has been around for several decades. Studies by Schwan (1989) and those pre-dating his work relied mostly on the manual extraction of grain properties. Orientations and length-width ratios of quartz grains were therefore estimated by hand using a micro-ruler in the eye-piece of the microscope. These measurements were repeated a minimum of 8 times per grain by rotating the thin-section under crossed polars, until the best measurement was obtained when the grain had the strongest translucence. Improvements using video-based image analysis

Table 7 - Grain orientations in thin-sections Schöbendorf and Klein Ziescht using particles with a length-width ratio of 1.5 and larger, based on the developed object-based image analysis (OBIA) method and pre-existing video-based image processing (De Boer, 1992). Comparisons can be made between the amount of particles ($n_{>1.5}$), orientation relative to true north (x) and the fabric strength (R). The latter is a measure of the concentration around the mean orientation (x). A value closer to 1 indicates a stronger preferred orientation of grains in the sediment fabric. Other sediment properties include the total amount of detected particles (n_{tot}) and the arithmetic mean of the orientation distribution (x_a).

Thin-section	Video-based analysis			OBIA using eCognition				
	$n_{>1.5}$	x (°)	R	n_{tot}	$n_{>1.5}$	x (°)	x_a (°)	R
Schöbendorf								
SCH I	624	175.2	0.0864	6641	2213	35.6	22.9	0.0154
SCH II	-	-	-	5549	1914	227	26.3	0.0717
SCH III	760	0.1	0.1252	7348	2678	26.0	24.7	0.2425
SCH IV	-	-	-	8900	3117	166	25.6	0.1731
SCH V	344	33.7	0.0561	5635	1998	32.9	28.2	0.2456
Klein Ziescht								
KLZ II	261	126	0.0229	-	-	-	-	-
KLZ IVa	-	-	-	3347	1224	264	51.6	0.1056
KLZ IVb	-	-	-	2387	847	75.4	40.3	0.0837
KLZ IVc	-	-	-	6577	2258	38.1	44.3	0.1203
KLZ IVd	-	-	-	3987	1333	48.0	45.0	0.0941
KLZ V	232	24.5	0.0807	4815	1606	38.1	42.9	0.1650
KLZ VIa	-	-	-	3422	1193	60.7	48.3	0.0444
KLZ VIb	-	-	-	2853	978	50.0	46.8	0.0844

were made possible with equipment such as the Quantimet 970 from Cambridge Instruments (De Boer, 1992). This development reduced potential operator bias as the hardware could automatically detect grains and calculate properties such as area, length, breath (width) and long-axis orientation at pixel resolutions of 1.3 µm. Contrast issues still required the circumference of many grains to be manually traced with an 'image pen' during post-processing steps, if the contrast was insufficient to automatically separate a grain from its surroundings.

Compared to these pre-existing methods, the OBIA method automates the first two steps in a thin-section analysis (grain detections and the quantification of grain properties) and eliminates possible operator bias in these steps and during post-processing of grains. Although the OBIA method still requires some operator intervention to optimise the scale parameter for obtaining satisfactory segmentation and classification results, the quality and quantity of delineating grains are equal if not better than those from other pre-existing methods (e.g. Table 7). Furthermore, the workflow of the OBIA method is much less complex compared to recent GIS-based image processing methods that still rely on the rotation of thin-sections between crossed polars (e.g. Hassanpour, 2011).

Processing of cross-polarised thin-sections is always sensitive to contrast variations that result from the diversity in mineralogical properties (some minerals have a dark colour) and the dependence of grain translucency on the relative orientation between the crossed polars. This is the foremost reason for the inclusion of the rotation stage in pre-existing thin-sections methodologies. The resolving power of the OBIA method at pixel-scales allows such low contrast grains to be detected too, irrespective of their particle diameter. With the

exclusion of thin-section rotation, the OBIA method also cuts down on total processing time with several orders of magnitude (minutes of processing datasets versus days). However, the analysis is based on a rule-set that causes some portion of darker grains not to be detected and classified as they fall outside the specified contrast criteria. Conversely, some irregular shaped objects are erroneously classified as grains due to the low contrast effects. Such artefacts were substantially reduced by including the roundness parameter in the work flow (see Table 6), but a small degree of artefacts is still present in the final classification result. This is illustrated by a closer inspection of Fig. 37. Further refinement of the OBIA method steps is therefore possible, as shown by parameter optimisation in other applications of OBIA strategies (e.g. Anders *et al.*, 2011). Taking these considerations into account, the quantity of detected grains with this method is still much larger and more time-efficient than what can be achieved by hand and eye. The most important prospect of the OBIA method may therefore be this increase in particle detection (several thousand per thin-section), which causes measurements of particle orientations to better reflect the actual state of the sediment fabric. At the same time, large amounts of particles also allow further refinements in the orientation analysis by using different length-width ratios (e.g. 1.0-1.5, 1.5-1.7 or all particles with >1.7) whilst still retaining a statistically sound sample size. This kind of versatility and the level of maturity of multi-resolution segmentation algorithms as implemented in the software suite eCognition (Baatz and Schape, 2000) allow the OBIA method for thin-sections to potentially supersede the analytical performance of other thin-section analysis methods.

5.1.2 Relation of detected orientations to wind flow patterns

The applicability of wind-induced particle orientation data is ultimately determined by how well the measurements made of the sediment fabric relate to (in this case) the local palaeowind directions. In this discussion we will first briefly consider the timing and regional conditions that formed the sampled laminae in Germany to understand how the detected orientations relate to local flow processes at the time of their deposition, and then we will focus on the performance of the OBIA method.

The position of the Schöbendorf and Klein Zieschte dunes in the central Baruth ice-marginal valley relate their maximum TL/OSL ages (16.2±1.9 kyr) to the early formation period of the ice-marginal valley terraces in the Weichselian Lateglacial (Hilgers, 2007). In this period the deposition of initial cover sands was mainly driven by katabatic winds from northerly and easterly quadrants (De Boer, 1992). Thin-sections of the Schöbendorf and Klein Zieschte profiles were sampled from laminated sediments that were part of this initial period of cover sand deposition. While wind regimes driven by oceanic flow patterns from the west are considered to be highly unlikely at this time (Zeeberg, 1998), changes in atmospheric circulation eventually caused a radical shift of dominant winds to westerly and southerly quadrants. This shift is well-reflected by the orientation of the superposed parabolic dunes that post-date the laminae sampled in this study. Rejecting one of the two types of atmospheric flow conditions (katabatic NNE vs. oceanic SSW) is difficult due to the non-vectorial nature of 2D orientation measurements, but we can argue for NNE-winds on the basis of age, climate and proximity of the glacial margin at the time these cover sands were formed. Similar unidirectional katabatic flow patterns have been hypothesised further eastward along the glacial margin on the basis of global circulation models (Zeeberg, 1998).

We used the same thin-sections in this study as in previous studies and the inferred quadrants are in general agreement. However, Fig. 38 and Table 7 also show a 5-28° offset in the average headings (x) calculated using video-based and object-based image analyses of the same thin-

sections. This poses the question which of the two methods is correctly reflecting the wind flow conditions. Data obtained with the OBIA method show a very pronounced orientation in both sampled profiles along the azimuth (N)NE-(S)SW, based on 3-6 times the amount of sand grains than those in the study by De Boer (1992). As the inferred headings are also consistent throughout the depth of the profile and may have benefited from the reduction in operator bias or measurement errors, we consider the observed difference in headings between the methods to be a consequence of the larger sample size. A similar interpretation applies to the generally higher fabric strength (*R*) as the larger quantity of particles also gives a better reflection of this sediment property. The re-analysis of the aeolian sediments at Schöbendorf and Klein Ziescht illustrates that the OBIA method seems to be a valid approach for measuring preferred particle orientation patterns that allows wind flow conditions at the time of sediment deposition to be inferred.

5.2 Wind directions at the Martian surface

Aeolian features and the behaviour of wind-mobilised sediment along Spirit's traverse of the Columbia Hills have been extensively studied by Greeley *et al.* (2008), Sullivan *et al.* (2008) and Thomson *et al.*, (2008). The contextual interpretation of inferred wind directions in our study is therefore largely based on their extensive landscape analyses. The imaged sediments consist of mafic 100-300 µm sands that are common in the Columbia Hills and represent the saltation-capable fraction from the regolith in Gusev crater (Sullivan *et al.*, 2008). Transport of these fine sands occurred initially by sporadic storm events from the NNW and SSE that winnowed the regolith to form the local sand deposits at El Dorado and the ripples and sand drifts at Home Plate. As orientations of aeolian ripples are related to the net transport rate, their orientation can be used to infer the local wind direction (Rubin and Hunter, 1987; Andreotti *et al.*, 2006). Ripples in the Columbia Hills are no exception and were formed primarily by saltation, based on the measured particle diameters in these ripples (see Sullivan *et al.*, 2008 for an authoritative review of particles, particle mobility and the relation to bedforms in this area). As preferred orientations of sand grains are formed principally by saltation, we can validly assume that detected orientations (Fig. 39) are directly associated to saltation and as such local wind flow directions. Wide-spread migration of sand drifts and ripples composed of particles similar to the imaged grains in this study was observed during sol 1260-1265 when a storm swept the area around Home Plate and caused up to 2 cm down-wind displacement (Sullivan *et al.*, 2008). Unfortunately, damage was sustained to the optics of the MI during this storm event, hampering the application of the developed OBIA strategy to images postdating the storm. Only images were used that pre-date this event. The orientations detected in the sediment fabric therefore reflect the most recent high-energy wind event, probably related to the storm on sol 417-420. This event mobilised sands and trapped particles on the rover deck before it entered the Columbia Hills (Sullivan *et al.*, 2008). Local wind flow patterns were inferred by Greeley *et al.* (2008) and Thomson *et al.* (2008) by combining surface observations of Spirit's cameras with high-resolution orbital footage of oriented aeolian features. Their analyses focussed on wind-blown ripples and dunes, ventifacts formed by the scouring action of particle impacts during saltation and wind tails of sand deposited on the lee-side of flow obstacles. We have therefore compared the dominant long-axis orientation of particles to this very detailed set of observations of near-surface wind directions along Spirit's traverse of the Columbia Hills.

Imaged particles along the traverse are generally well-rounded, as shown by the length-width ratios in Fig. 39. A benefit of the OBIA method is that grain orientations can be

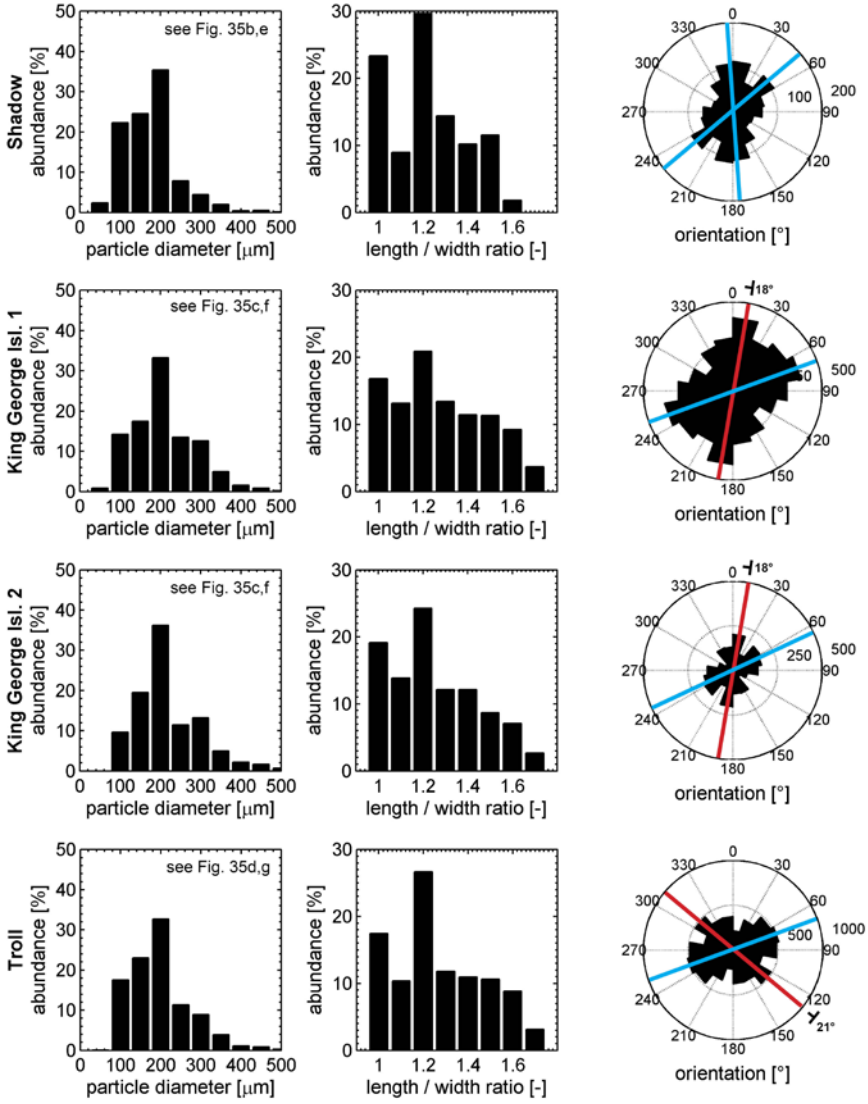

Fig. 39 - Overview of measured sediment properties on Mars. The first and second columns show the particle size distributions and the length-width ratios. Rose diagrams in the third column show the preferred long-axis orientation of particles with a length-width ratio larger than 1.1. Red lines identify the heading from probable rolling and avalanching of particles down-slope (based on the tilt of the image); blue lines are inferred as the A-axis orientations and reflect the heading of local wind flow. The different orientation of the red line at Troll orthogonal to that of King George Island may indicate an avalanche orientation, considering the same orientation of the dunes.

quantified for very low length-width ratios and this makes the method well-suited to analyse imagery of such aeolian grains. Compared to the studied horizontal laminae of terrestrial covers sands, the analysis of orientations patterns in ripples on Mars is more complicated. Sediments fabrics at all three surface targets were found to exhibit a moderately bimodal 'x-type' pattern where the two headings are not oriented perfectly orthogonal to each other. This rules out that both were formed by wind flow, as identified in some of the terrestrial

Table 8 - Overview of the orientation data derived from the MI images of sediments on Mars. The image orientation was derived by multiplying the pointing vector of the camera with the quaternion of each image. The obtained orientation in x, y, z was then decomposed into the azimuth and tilt. The number of particles (*n*), orientation relative to true north (*x*° or *x*°+180°) and fabric strength (*R*) of the sediment were then calculated for particles with a length-width ratio larger than 1.1.

Location	Sol	Image orientation					Sediment properties		
		x	*y*	*z*	Azimuth (°)[a]	Tilt (°)[b]	*n*	*x* (°)	*R*
El Dorado									
Shadow	707	0.24501	0.96923	0.02366	75.8	1.4	714	356	0.1717
Home Plate									
King George Isl. 1	1034	0.14423	0.93840	0.31401	81.3	18.3	2820	359	0.1289
King George Isl. 2	1034	0.18342	0.93164	0.31369	78.9	18.3	1194	359	0.1585
Troll	1058	0.49406	0.79336	0.35565	58.1	20.8	3662	28	0.1061

[a] *azimuth is calculated using atan2(y,x)*

[b] *tilt is calculated using atan2(z,$(x^2+y^2)^{0.5}$)*

laminae (Fig. 38). Dapples and Rominger (1945) showed that when multiple particles are involved in a granular avalanche, their long-axis orientation traverses towards the sediment source, while down-slope rolling of individual particles produces orientations orthogonal to the avalanche direction. The highest slope angles of the stoss sides of ripples and the angles of repose of sand drifts in the Columbia Hills vary between 19-36° (Sullivan *et al.*, 2008). One of the detected headings was interpreted and excluded using the image tilt (Table 8) as a possible preferred orientation related to rolling or avalanching down-slope (red lines in Fig. 39). This non-aeolian rolling interpretation is further supported by the deviating azimuth of these headings with local aeolian features (e.g. Thomson *et al.*, 2008). The other heading was therefore interpreted as an A-axis orientation caused by airborne streamlining during saltation (blue lines in Fig. 39). These headings are in excellent agreement with flow directions reflected by other aeolian processes in the area (Fig. 40). The fabric of aeolian sediments on Mars may thus harbour valuable information on the up-wind source of these sediments after their deposition.

At El Dorado the interpretation of wind flow patterns is more complicated than at Home Plate due to the sinuous nature of ripples at the edge of this contiguous sand deposit (Fig. 36b). Asymmetry of the cross-sectional profile of the largest (T_1) ripples show that these bedforms were likely formed by regional winds from the WSW (Sullivan *et al.*, 2008). In this case T_n is the classification used for the largest bedform, with T_{n+1} being a superposed bedform (Warren and Kay, 1987). Smaller T_2 ripples with wavelengths of 10 cm are formed inside the 2-3 m wide troughs, often at right angles to the trough axis and interwoven with subtle T_3 ripples consisting of fine dust (Sullivan *et al.*, 2008). The orientation of the T_2 ripples indicates that wind directions inside the troughs are approximately NNW-SSE oriented, although it should be noted that these flow directions can be highly variable due to the discontinuity of the T_1 ripples in the area visited by Spirit. Flow-modification resulting from the ripple topography is known to produce radically different flow patterns in the troughs of ripples (Bourke *et al.*, 2004). These flow modification processes have also been proposed for the orientation of other bedforms in the Columbia Hills by Thomson *et al.* (2008). As the low tilt of the MI camera indicates a low gradient of the surface (Table 8), it eliminates a clear gravity-induced rolling direction in this part of the trough area (Fig. 36b) and bimodal orientation pattern therefore seem to have an aeolian origin. As imagery of Shadow was taken from a T_2 ripple, there

can be two hypotheses for the headings along NNW-SSE and ENE-WSW; (1.) the bimodal orientation result from the same wind flow were the orientation pattern is a blend of saltation in bedform-modified winds and the unmodified flow; or (2.) a portion of the particles has been mobilised by a different mode of transport such as rolling, which (partly) oriented the axis to the ENE-WSW heading. Bimodal distributions may indicate two wind regimes at the time of deposition. However, hypothesis 1 is inherently complex and seems to be rejected by the orientation of secondary ripples that clearly reflect the net-transport direction of bedform-modified winds inside the troughs (Sullivan *et al.*, 2008). It is not unlikely that the bimodal orientation pattern was formed only by this bedform-modified flow when considering that different modes of particle transport are possible. Wind tunnel simulations have shown that sand-sized particles >100 µm can indeed be detached and transported by rolling, which can take place at lower wind speeds than what would be required for saltation at the fluid threshold (Merrison *et al.*, 2007). Rolling of particles may also be promoted by the thick laminar sublayer on Mars that engulfs sand-sized particles and to some extent prevents saltation transport (Greeley, 2002; Kok *et al.*, 2012). It is therefore conceivable that some degree of the observed orientation at El Dorado reflects particle mobility at sub-threshold conditions due to the complex interaction of wind flow with the bed. No extensive imaging campaign of other undisturbed sediments at El Dorado was undertaken that would allow us to decisively prove or disprove this interpretation, but it defines a topic that may require further scrutiny by surface investigations elsewhere on Mars or by wind tunnel simulations to understand this type of aeolian behaviour.

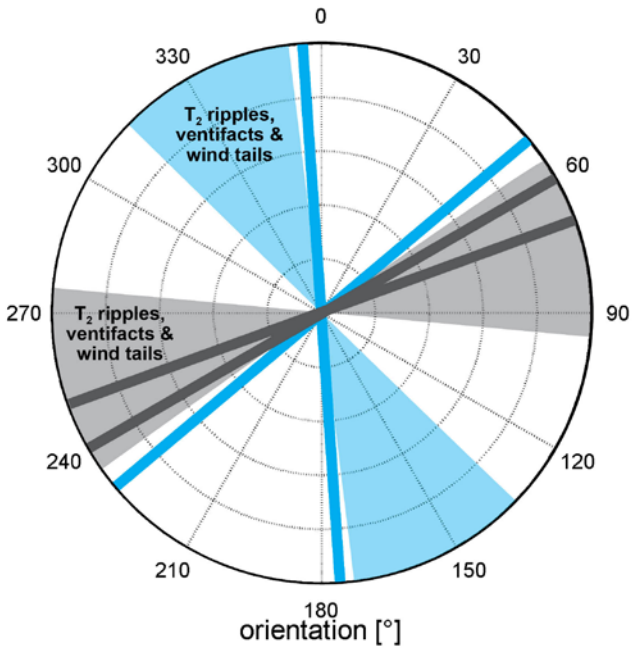

Fig. 40 - Rose diagram summarising wind directions in the Columbia Hills. Sectors with solid colours are wind directions inferred from ventifacts, wind tails and 2nd-order bedforms (T_2) from photographic interpretation of these aeolian features by Greeley *et al.* (2008) and Thomson *et al.* (2008). Solid lines are the preferred orientations of particles measured in the sediment fabric of the three surface targets in this study. Blue sectors and lines correspond to El Dorado; those in grey give the headings for Home Plate.

5.3 Saltation conditions, implications and outlook

Saltation of sands on Mars is one of the most elusive surface processes as atmospheric conditions seem unfit to achieve favourable conditions for this process, in spite of the abundant geomorphic evidence showing that saltation takes place. It has been proposed by Sullivan *et al.* (2008) that the mobilisation of sands in the Columbia Hills is highly dependent on the complex interaction of infrequent storm events with the local topography, rather than the persistent seasonal variations in wind flow suggested by Greeley *et al.* (2008). The formation of aeolian features in the Columbia Hills by high-energy wind events is further evidenced by the observed A-axis orientation in the sediment fabric that only results from airborne streamlining during saltation. Although these wind flow conditions occur sporadic on Mars, several authors have argued that GCM models are unable to resolve the much higher wind speeds at smaller local scales due to the low resolution of these models (Fenton and Michaels, 2010; Kok *et al.*, 2012). Process simulations at much finer scales have recently shown that saltation at the dynamic threshold can indeed be sustained by splashing (reptation) of particles at much lower wind speeds that occur more commonly on Mars than infrequent storm events (e.g. Kok, 2010a, 2010b; Kok *et al.*, 2012). Gusts or topographic forcing of the wind flow can therefore provide the initial 'push' at fluid threshold conditions to set particles in motion, leading to the high rates of observed bedform migration (e.g. Bridges *et al.* 2012a; 2012b) and the preferred orientation of particles in the sediment fabric. Interestingly, these preferred orientations can potentially contribute to wind-induced particle mobility. Once an elongated particle has obtained a preferred (flow-induced) orientation, often with a negative angle of attack dipping into the sediment fabric, the increase in aeolian drag and lift create a resultant force from below the particle that can cause it to flip upward, detach and migrate downwind (Rusnak, 1957). When saltation is achieved, the low air density and gravity causes saltating particles to hop higher and farther down-wind compared to Earth and this leads to a much larger acceleration of the particle (Kok *et al.*, 2012). The range in fabric strengths on Mars (0.1-0.17) varies somewhat compared to Earth (0.01-0.24). Lower fabric strengths of aeolian sediment on Mars may be a likely consequence of the much higher impact velocities of saltating grains that result from this airborne acceleration (Greeley, 2002; Almeida *et al.*, 2008). The disruption of the sediment fabric by particle impacts and the reptation (splashing) of nearby grains therefore causes a much larger loss of preferred orientation compared to Earth. This in turn causes a higher randomisation in long-axis orientation and produces an even larger difference in the fabric strength compared to those of well-oriented fluvial sediments (Rusnak, 1957; Schwan, 1989). The degree of particle orientation in lithified sedimentary facies can thus be used as a powerful tool to discriminate between wet or dry formative conditions of sedimentary rocks on Mars.

We have focused in this study primarily on the 'qualitative' aspects of wind-induced orientation of particles on Mars. Object-based analyses of sediment images on Mars is still in its infancy, but for the application of measuring long-axis grain orientation it has great potential for aeolian surface studies. Measurements of wind speeds in combination with imaging provide further information on the near-surface flow conditions, perhaps even allowing grains to be used as passive flow indicators on multi-sol research stations. While the MER rover Spirit did not have any meteorological instrumentation, the Mars Science Laboratory rover 'Curiosity' is equipped with an environmental sensor suite (Gómez-Elvira *et al.*, 2012) that can be used to correlate *in situ* measurements of wind speeds and directions with observations of grains using the Mars Hand Lens Imager (MAHLI) (Edgett *et al.*, 2012). The developed OBIA method was based on the use of monochromatic imagery of the Microscope

Imager. A benefit of the panchromatic MAHLI camera over the MI camera is the smaller pixel scale of 14 μm and availability of colour channels that increase the information available for the OBIA algorithm, allowing more accurate detection and extraction of aeolian grains from the imagery. Measuring wind flow directions using the sediment fabric can therefore give additional insights in particle mobility on more common diurnal or seasonal scales and during sporadic storm events.

6. Conclusions

The orientation of aeolian grains in the fabric of sedimentary facies provides information on local near-surface wind flow directions, independent of profile depth or degree of consolidation. The developed Object-based Image Analysis (OBIA) method shows that sediment statistics such as particle size distributions, particle orientations and fabric strength can be obtained irrespective of the type of sand grain imagery by adapting the criteria of the OBIA strategy. This allows a rapid detection of large quantity of grains in traditional analyses of thin-sections under crossed polars and it improves the accuracy for inferring palaeowind directions. Our analyses have been based on a limited amount of thin-sections and further work is needed to underpin the applicability of this very promising technique in local and regional wind flow reconstructions. The same OBIA strategy can be applied to extreme-close up imagery of sand grains on Mars, providing a similar granulometric analysis of aeolian sediment such as with well-established methods that are based on the analysis of thin-sections. Mars lander and rover cameras with pixel-resolutions of several tens of micrometres therefore provide sufficient image data to allow the detection of preferred grain orientations and infer the directions of the most recent high-energy wind flow event. Particle orientation on Mars occurs mainly in non-cohesive aeolian deposits that consist of well-rounded sand grains, winnowed from fine dust. A much larger fraction of preferred long-axis orientations on Mars can be caused by gravity and wind-induced rolling compared to the portion oriented by saltation in local winds on Earth. Contextual analyses of surficial sediments therefore provide insights in the characteristics and types of particle mobility. With the present focus of lander instrumentation on the geochemical characterisation of surface materials, the method also allows the characterisation of physical particle properties of Martian soils. Ultimately, this form of *in situ* analysis of local wind flow can be a valuable new resource to surface studies of aeolian features on Mars.

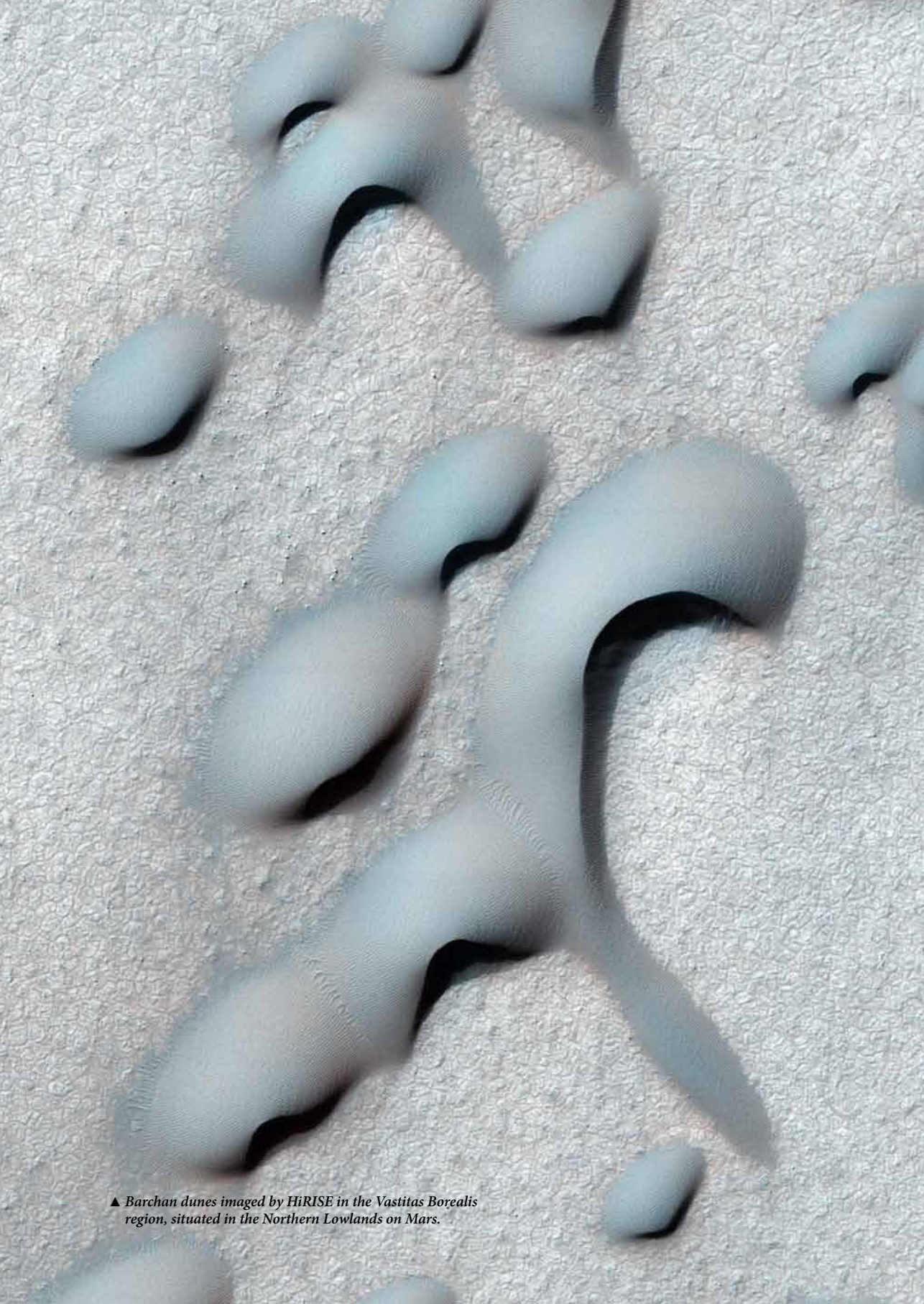

▲ *Barchan dunes imaged by HiRISE in the Vastitas Borealis region, situated in the Northern Lowlands on Mars.*

Chapter 6

Synthesis - environmental fate on Earth and Mars

1. Synthesis

The final chapter of this dissertation provides a synthesis of the preceding chapters. The first section aims at discussing the environmental fate of volcanic glass on Earth and those found at different latitudes on Mars. The second section provides a more general conclusion of this dissertation and gives a tabular summary of the individual answers to the research questions, based on the chapter conclusions and synthesis. In the third and final section of this chapter, new directions are proposed for future research into the environmental behaviour of glaciovolcanic glass on Earth and Mars.

1.1 Glaciovolcanic glass in Iceland

During the eruption of volcanoes underneath or in contact with ice, magma shatters explosively and this result to the formation of fine-grained glassy breccias. This is certainly the case for the hyaloclastites of Bláhnúkur, whose formation was fully subglacial. The edifice is an a-typical *tindar* in the sense that it did not form from the start as a fissure eruption, but rather erupted along fissures through a pre-existing rhyolite core. Although chemical weathering (perlitisation) of rhyolitic glass takes place and leads to the formation of zeolites and clays (Denton *et al.*, 2009), silicic glasses are generally found to be metastable and no consolidation and strengthening by their weathering products occurs. This is the key-difference between chemical weathering of basaltic and rhyolitic glasses. The lower cohesion of Bláhnúkur's rhyolitic glass outcrops causes the edifice to be actively modified by local environmental processes. Weathering of these outcrops is largely controlled by the granular nature of glass breccias that are composed of various particles diameters, creating different weathering pathways due to different physico-mechanical properties per particle size. The fine-grained glass matrix of Bláhnúkur also contains much larger centimetre-sized fragments of pumiceous glass. Yearly average temperatures in these central highlands are close to freezing and create large amounts of freeze-thaw cycles in the material. The availability of liquid water from precipitation and snow melt drives the cryogenic weathering of these large pumiceous glass particles when temperatures fluctuate around zero. The expansion of freezing water drives

frost heave which is an effective mechanism for detaching a wide range of sand-sized particle diameters from the breccia matrix. Ice expanding inside the vesicles of the centimetre-sized pumiceous glass particles is especially important as it is the primary process for the post-eruptive formation of new sandy textures. The physical weathering of the Bláhnúkur glass during freeze-thaw cycles in the exposed top layer of the rock face ultimately decreases the cohesive strength of these deposits and makes the outcrops more susceptible to erosion by water and wind. The latter was found to be the most noticeable geomorphic agent inside the gorge as the local topography acts as a 'wind tunnel' and aggravates local winds to well above the threshold for detachment of particles. Although the loose sandy weathering products can be persuaded to roll down-slope by modest wind speeds, strong gusts cause significant deflation and winnowing of fines from the rock face and scree sediments (chapter 2). These winds carry large quantities of silt and clay off-site and the most appreciable differences in the textures of sediments and the original rock face occur in the range of these small particle diameters. The deflation of natural present respirable fines and those additionally formed by fracturing during weathering increase the risk to respiratory health hazards, although the many thousands of hikers that visit the site yearly will certainly experience no adverse effects due to the very low exposure rates. From the physical weathering experiments (chapter 3) it becomes clear that the combined influences of aeolian and cryogenic processes on volcanic glasses in general can create respirable fines, making these conclusions relevant to other areas that are composed of large amounts of basaltic and rhyolitic glaciovolcanic glass.

While the majority of studies of subglacial landforms performed to date have focussed on the abundant basaltic hyaloclastite (*móberg*) formations in Iceland, many rhyolitic subglacial locations have been identified and await further exploration (Fig. 1; McGarvie, 2009). Geomorphological processes set in these rhyolitic hyaloclastites are driven by the interaction of the environment with the unique physico-mechanical properties of eruption products. However, one important difference with basaltic edifices is that these silicic glasses experience lower rates of chemical weathering (Jakobsson and Gudmundsson, 2008). The resulting lack of consolidation and vesicle filling changes the hydrological properties and causes the physical erosion of rhyolitic features by environmental processes to differ substantially from their basaltic (tholeiitic) counterparts. In this dissertation a well-studied and well-accessible edifice was the focus of process-based studies and I have addressed the erosion characteristics on landscape and particle scales. Although it has given new insights in the physical weathering of silicic glass deposits, further study is still needed to understand how weathering of these rhyolitic tindars compares to basaltic edifices. As other geomorphological studies of tuya and tindar weathering with a process-oriented approach are scarce, it is clear that there is a bright future for further research.

1.2 Volcanic glass in different surface environments on Mars

Silicic volcanism has not occurred on planet Mars, or at least no evidence for it has been found so far (McSween *et al.*, 2009). Properties of observed volcanic glasses resemble terrestrial silicic eruption products due to their high-silica, almost obsidian exterior (Horgan and Bell, 2012a). This property certainly does not have a magmatic origin, but it is rather a product of the chemical weathering of basaltic glass. Not only makes this the chemical signature of the particle exterior comparable to rhyolitic glasses in Iceland, but it also creates deposits that are not cemented and therefore easily eroded or mobilised by environmental processes. Large quantities of glaciovolcanic glasses with silicic exteriors are presently found in large sand seas in the Northern Lowlands and the circumpolar erg (Lancaster and Greeley, 1990),

covering an estimated 10 million km^2. A large segment of the erosion of volcanic glass on Mars therefore occurs from transport by mostly unidirectional winds (Hayward *et al.*, 2008), rather than from in-situ weathering of local outcrops. Two observations become immediately apparent. Volcanic glasses on Mars are found in cold periglacial conditions and secondly, glass is contained in aeolian landforms ('glass dunes') which make aeolian and cryogenic processes prevalent in the transport and modification of the material. A clear distinction can therefore be made on Mars based on the latitude of their occurrence. Observations of the polar areas shows that dunes and other high-latitude landforms are frosted and defrosted with yearly cycles (e.g. Bourke *et al.* 2008; Smith *et al.* 2001). This occurs primarily by CO_2 and H_2O ice deposition from the atmosphere onto the surface of particles. The minute quantities of water-ice were observed during seasonal changes in the North polar environment, mostly in the form of wind-mobilised frost that caused brightening of dunes (Pommerol *et al.*, *in press*). Although water-ice deposition certainly occurs, it is highly improbable that sufficiently large rates of water are released during thawing in the present environment to initiate water-based debris flows that have been postulated by some authors on other places on Mars (Costard *et al.* 2002; Christensen, 2003; Lanza *et al.*, 2010). The small portion of this seasonal frost plays an important role in the chemical weathering of the observed glass-rich sand deposits. Leaching of soluble cations after melting of deposited water-ice from the atmosphere was proposed by Horgan and Bell (2012a) as an explanation for the high-silica spectral signatures once aeolian abrasion removed iron-rich rinds from the particle. As a much larger portion of the seasonal ice deposition is CO_2 ice (Hansen *et al.*, *in press*). The build-up of this ice on the particle surface and inside pores will not result to the same type of cryogenic erosion that is observed in the field environment in Iceland. Cryogenic erosion by the expansion of freezing of water is in this respect quite unique as only water is known to expand by 9% during crystallisation (chapter 3). Carbon dioxide ice does not possess this property and even though it contributes to the destabilisation of dunes (Hansen *et al.*, 2011; Horgan and Bell, 2012b), it is incapable of fracturing materials. The seasonal CO_2 layer also plays an important role in a new geomorphic process that was recently discovered during defrosting when gas is trapped below the ~60 cm thick ice layer, causing outbursts of gas and particles through cracks in the ice (Hansen *et al.*, *in press*; Portyankina *et al.*, *in press*). Although particles are transported only for short distance in this fashion, it is highly dependent on the seasons and the contribution to particle erosion will be minimal. The seasonal ice layer is therefore mostly effective as a form of '*cryogenic induration*' that inhibits all other forms of sands mobility throughout ~70% of the Martian year. Modification of glass-rich sediments is therefore limited in circumpolar dune systems to the abrasive effects of short-lived aeolian transport in unfrosted conditions.

The occurrence of this cryogenic induration differs across the planet as seasonal frosting and defrosting only occurs in this extent near the poles. It is of much lesser importance in the northern lowlands as the seasonal ice layer only extents down to latitudes of ~70°N (Hansen *et al.*, *in press*). Horgan and Bell (2012a) detected glass-rich deposits at lower latitudes than 70°N, well outside the influence sphere of seasonal polar ice deposits. The absence of seasonal frosting and cryogenic induration at lower latitudes causes aeolian processes to prevail. This makes the glass-rich sediments at these latitudes much more susceptible to wind-induced modification throughout the Martian year. Dune complexes in the lowlands were shown to be aeolian active (e.g. Hansen *et al.*, 2011) and observations by Bridges *et al.* (2012a) seem to indicate that migration rates of dunes are much higher at more temperate latitudes than those near the pole. The introduction of the slope angle shifts the force balance by a relative lowering of the normal load (Eq.1), which lowers the thresholds compared to particle detachment on

horizontal surfaces (Rasmussen *et al.*, 1996). The comparable migration rates of dunes to those on Earth (Bridges *et al.*, 2012b) may in part be sustained by the mobilisation by winds on the inclined surface of the stoss side of sand dunes. Once saltation is triggered by wind-induced rolling of particles and sustained, it can drive the migration of dune systems, causing high impact velocities that inflict substantial damage to particles (e.g. Greeley and Iversen, 1985; Marshal *et al.* 2012).

1.3 Timing and latitudinal dependency of modification rates on Mars

Explosive fragmentation of magma causes volcanic glass particles to be very irregular in shape directly after their formation. Physical weathering processes then cause the material to lose its irregular morphology. However, conditions may not always be favourable in the present surface environment to drive the transport and modification of aeolian grains on Mars. Wind shear stress measured at the Phoenix landing site during defrosted conditions (the lander was destroyed by ice encroachment in the next season) were below the measured threshold conditions in chapter 4, required for detachment of particles by rolling (Holstein-Rathlou *et al.*, 2010). The absence of dune and ripple-forming winds in the area suggest that surface conditions can indeed be unfavourable to transport particles at sufficiently large rates to cause substantial modification. Combined with the seasonal reduction of aeolian activity by cryogenic induration it is conceivable that glasses formed in more recent subglacial eruption near the poles, shown by Fagan *et al.* (2010) and Hovius *et al.* (2008), are likely less-weathered than glass grains sourced and reworked from the basal unit under the present polar ice cap. The lower modification rates of geologically young glass particles may potentially have preserved physical properties and volatile signatures that reflect their formation conditions. Polar glaciovolcanic glasses may therefore be ideal materials for geochemical palaeo-ice reconstructions of Martian eruption environments. Overall, the weathering of volcanic glasses over very long periods of geologic time appears to be highly dependent on geographic location as a consequence of the environmental conditions at different latitudes on Mars. This is notably different from Earth as the latitudinal extent of volcanic glass is much smaller in Iceland and therefore confined to less-prominent differences in environmental conditions.

1.4 Relating particle observations to particle behaviour

Observations of single, well-rounded dark particles (allegedly dark mafic glass) seem to support the notion that the environmental fate of volcanic glass on Mars is mainly driven by aeolian modification (Goetz *et al.*, 2010; Horgan and Bell, 2012a). However, this observation at the Phoenix landing site represents only one sand grain and its relevance is therefore highly debatable. This touches on a sensitive topic with respect to the paradigm of current surface explorations on Mars. Over the past decades abundant orbital observations have been made, while only few Mars landers have explored the properties of granular sediment in great detail. Lander instrumentation has frequently been designed to determine geochemical properties rather than physical particle properties that control the threshold of aeolian mobilisation. Especially physical properties are quintessential for understanding the process dynamics of planet-wide sands mobility on Mars, which is the most active process in the present surface environment. Obtaining physical particle properties is therefore limited to the analysis of extreme-close up images. Of the sparse observations that have been obtained, there is a general tendency to present these observations as more 'general properties' in spite of the known difficulties of linking remote-sensed imagery to properties of sediment (e.g. Sullivan *et al.*, 2008). Observed sediment properties may undoubtedly share properties that are common

for Mars' global particle speciation, but data on observed grain properties should still be used conservatively. I have used available imagery of well-rounded mafic grains in the Columbia Hills on Mars as a substitute for abraded volcanic glass for study how well-rounded materials respond to the local wind flow at the surface of Mars. The detachment of particles by rolling (chapter 4) and transport by saltation causes sediment to reflect the local wind flow at the scale of individual particles. Assuming that well-rounded morphologies are indeed a common environmental 'end-state' of surficial sediments shows that the method developed in chapter 5 can be more generally applied to various aeolian sediments on Mars. This kind of aeolian behaviour of sand grains has to date not been detected and documented at the surface of Mars and potentially marks a new development in the surface exploration of Mars.

1.5 Are there possibly more glaciovolcanic edifices on Mars?

I have focussed this dissertation primarily on the context of glass-rich sand dunes in the Northern lowlands on Mars. These volcanic glasses on Mars are most likely produced by glaciovolcanism. Surface features formed by glaciovolcanic eruptions appear to be abundant on planet Mars, yet diagnostic bedded glass deposits still escape detection (e.g. Chapman 1994, Keszthelyi *et al.*, 2010). Morphometric properties are therefore invaluable for determining whether a landform was created by sub-ice volcanism or not. In terrestrial sub-ice eruptions the hyaloclastite beddings are formed by granular avalanches of glass particles. The lower angles of repose of tuya flanks on Mars relative to those in Iceland (Fagan *et al.*, 2010) illustrate that gravity effects may be involved in the deposition of these hyaloclastites, as shown by recent experiments (Kleinhans *et al.*, 2011). As the morphometric properties of tuya are likely dependent on the lower gravity of Mars, the identification of glaciovolcanic landforms needs to account for these gravity-dependent differences if they are identified in the basis of terrestrial morphometry. Perhaps many more glaciovolcanic edifices may exist, but now escape detection due to their 'incompatible' landform morphometry.

2. Main conclusion and summary related to the research questions

In this dissertation I have discussed the environmental fate of glaciovolcanic glasses on Earth and Mars. While the latitudinal extent and environmental extremes are much larger on Mars than in Iceland, the processes affecting the modification are not dissimilar on Mars and reflect well how these materials are transported on Mars, albeit on differing time-scales. Glaciovolcanic glasses on Mars are observed and identified primarily in aeolian landforms such as dune systems, highlighting that the environmental fate is mainly driven by the interaction of the material with the atmosphere. The modification of these materials progresses from an initial irregular state via physical and chemical weathering to aeolian sediments that are primarily detected on the basis of silicic particle exteriors. Near the North Pole on Mars, these glasses are sourced from the basal unit of the current polar ice cap and their weathering history in the present environment is largely dependent on how they entered the circumpolar environment via subglacial floods. Some of the detected glass may be a product of more recent subglacial volcanism that formed the North Polar Tuyas and high-angle Crater Cones, making these glasses geologically younger than the glass sourced from the basal unit and reworked in the present environment. The lower alteration state results from the cryogenic induration of aeolian sediments by seasonal ice that covers vast areas in the circumpolar environment. These particles may therefore have retained the physico-mechanical and geochemical signatures that are indicative of their eruption environments. In contrast to the seasonal dependence of the transport and erosion of glaciovolcanic glasses

near the pole, glasses in the Northern lowlands are probably derived from glaciovolcanic eruptions in Acidalia Planetia and in the Chasma and Valles of the Tharsis volcanic province. These geologically old glasses experience weathering throughout the Martian year and can be characterised as highly abraded from aeolian transport over long geologic time. Comparing this fate on Mars to that on Earth shows that glaciovolcanism occurred at a much wider range in latitudes on Mars by which there difference in latitude also causes a larger variety in weathering pathways. In the environmental 'end-state', glass particles will have obtained a well-rounded morphology most commonly from long-term aeolian abrasion. These particles are then capable of reflecting the local wind directions from transport by rolling or saltation. The sediment fabric of aeolian deposits thus harbours detailed information on Mars' aeolian activity.

Table 9 – Overview of the main chapter conclusions.

Research question	Earth	Mars	
	Iceland	*North Pole (>70°N)*	*Northern Lowlands*
Regulating environmental processes on weathering?	Freeze-thaw cycles with water, wind erosion in dry conditions. Influences of water to lesser extent.	Seasonal frosting causes induration of sediment while cryoventing redistributes sands. Wind erosion occurs only in defrosted conditions.	Mainly by winds at threshold conditions, more particle mobility than at pole due to lack of cryogenic induration by seasonal ice.
Influence physico-mechanical properties on weathering?	Expansion of freezing water in vesicles causes fracturing of larger particles. In spite of angular particle shape, little abrasion occurs during rolling.	If vesiculated, no fracturing due to predominant CO_2 ice from atmospheric deposition.	General lack of seasonal ice; no effects from ice deposition or water-ice induced fracturing.
	Particle diameter and density determine thresholds of wind transport. This dictates particle abrasion during aeolian transport (low-energy rolling vs. highly-abrasive saltation) and leads to well-rounded sediments over time.		
Means of particle mobilisation and transport by wind?	Deflation; fine particles carried away in suspension from outcrops by moderate winds. Large particles are excavated and roll down-slope	Detachment by rolling. For large particles this mobility is possible at a lower threshold than saltation and may be promoted by the presence of a thick laminar sublayer in a low-pressure atmosphere. As such, rolling is important as a trigger to initiate the mobility and transport of sands by saltation.	
Information on particle mobility retained in the sediment fabric?	Saltation drives long-axis orientation that allows wind directions during last glacial period. Object-based image processing improves interpretation of palaeowind flow.	Long-axis orientation occurs during saltation of well-sorted aeolian sediment (100-300 μm), but much orientation is lost due to high impact velocities. Based on slopes and contextual interpretation, other modes of transport include gravity and wind-induced rolling. Fabric strength measurements using e.g. OBIA can be used to discriminate between wet and dry sedimentation.	

3. Directions for further research

The age differences of the glassy material on the two planets are quite substantial (Fig. 3, chapter 1), but the chemical stability from the silicic particle exterior of these glasses on Mars (Horgan and Bell, 2012a) makes them long-lived and in some ways comparable to the materials

studied in the southern central highlands in Iceland. However, the erosion characteristics of glaciovolcanic eruption products are still a poorly studied topic in Iceland and on Mars. This is quite notable as these landforms have the potential to yield valuable insights in the palaeoclimatic conditions and they have the added dimension on Mars as potential habitats to sustain microbial life due to the presence of liquid water and higher temperatures (Cousins and Crawford, 2011). As the collective of putative glaciovolcanic locations on Mars will encompass a wide variety of materials with different exposure ages and weathering histories, the glasses on Mars vary from potential fresh to 'end stages' after several Myr-Gyr of exposure to erosion processes in various surface environments.

In this dissertation I have discussed several questions surrounding the behaviour of volcanic glasses on Mars, and by no means have I been able to discuss all relevant questions. In this final section I will highlight a few new challenges that I consider to be most important for the continued study of the environmental fate to these materials. These suggestions cover proposed experiment to study the state and degree of modification of particles in Martian glass-rich aeolian sediments, and secondly, the need for understanding how the variation in particle properties relates to mobilisation thresholds.

3.1 Unifying transport rates with particle modification and spectral properties

Rolling of sediment has been shown in chapter 4 to occur in the surface environment of Mars, and this mode of transport may occur frequently as it encompasses a substantial part of wind-induced sediment mobilisation (Kok *et al.,* 2012). While it was found that rolling does not lead to significant alteration of sediments, more energetic saltation inflicts significant damage that causes textural and morphological modifications of wind-blown sediments. Observations of well-rounded glassy grains at the Phoenix landing site (Goetz *et al.*, 2010) therefore raise two questions. First, if these glassy particles were originally blocky and vesiculated as a result of their eruption environment (Heiken, 1972; Wilson and Head, 2007), then these particles must have been transported over prolonged periods and distances to obtain their rounded morphology. It is generally accepted that these rounded particle morphologies on Mars are formed by aeolian transport. However, no decisive values of modification rates for Mars exist. While the validity of the aeolian abrasion mechanism for the observed particle shape is certainly not questioned here, it does raise several questions on the exact path of this modification. The required time and distances may be troublesome for very locally confined glass deposits, considering the unidirectional wind patterns from the atmospheric circulation that is reflected in many of the low-latitude dune fields (Gardin *et al.,* 2012). In other words, particle modification has to be united with the probable ages of the sediments and migration flux (travelled distances) of these sediments through time, taking into consideration the invariant or perhaps time-dependent variance in wind patterns. Secondly, if these particles have a silica-rich exterior from leaching of elements in acidic environments making them chemically stable as proposed by Horgan and Bell (2012a), then the chemical weathering inferred from these spectral properties may be difficult to unify with the reworking by post-depositional abrasive transport. These glassy deposits are found in massive dune fields formed by saltation, but were initially introduced by catastrophic floods. If iron-bearing rinds were formed directly after deposition, than transport may have plausibly led to chipping of the exterior and removed any existing pre-existing rinds to expose the now high-silica exterior. As these rinds are only thin, several micrometres at best, much more chipping would be required to obtain the well-rounded morphology of particles for which such rinds were tentatively observed (Goetz *et al.*, 2010). From an initial blocky shape, the

amount of chipping required to obtain well-rounded particles may in fact be so high that it also removes much of the leached high-silica glass. In other words, if we observe high-silica particles on Mars, than these particles may either still be fresh morphology-wise, or acidic leaching occurred that postdates an episode of substantial aeolian modification. In the polar areas this sequencing of abrasion and leaching may perhaps be favourable due to the highly variability in the extent of seasonal polar ices and the deposition of water ice from the atmosphere. Solving this conundrum may be possible using aeolian transport simulations with experimentally leached glasses that cover the high-energy impact regimes, such as in the study of Merrison *et al.* (2010) or Marshall *et al.* (2012). This may be instrumental for understanding the depositional and weathering timeline. In conjunction with these abrasive and chemical weathering processes, the 'jökulhlaup' type deposition in the northern lowlands would also causes substantial mobilisation of sediment predating the emplacements events. Unmixing analyses of sediments (e.g. Prins *et al.*, 2007) from the glass-rich sandy deserts in Iceland may give insight in how catastrophic floods and post-depositional redistribution of sediments by winds influences the signature of current glass-rich deposits in Iceland and similar deposits on Mars.

3.2 Hypobaric wind tunnel simulations in hypogravity

Semi-empirical models developed for removal of particles have reached a mature explanatory level for aeolian processes on Earth and Mars. However, filtering out the effects of material properties on the raising of thresholds, as shown in chapter 4, is still difficult. Future studies may use analogue glass deposits for which the eruption environment has also been well-established as in Torfajökull. This undoubtedly hefty sampling effort in Iceland may allow further characterisation of upper thresholds for sediment behaviour in glass-rich dune fields

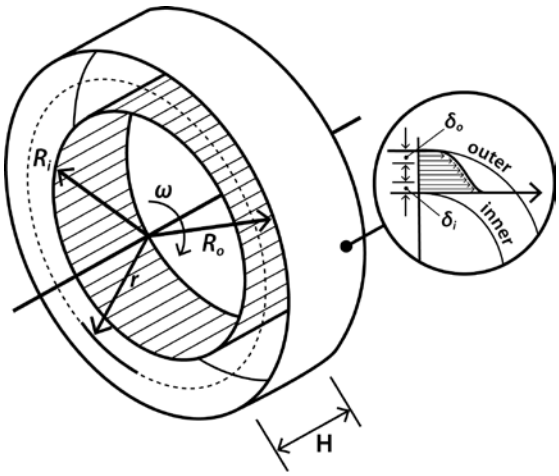

Fig. 41 - Illustration of a carousel-type wind tunnel, modified from White *et al.* (1987). The outer drum rotates to achieve a desired gravitational acceleration (e.g. 3.71 m s^{-2} for Mars) while the inner drum rotates at a much higher speed (ω>500 RPM) to achieve a boundary layer between the inner and outer walls (Taylor, 1935). The inset shows the two opposing boundary layers (δ_i and δ_o) created by the rotation of the inner drum with radius R_i, relative to the outer drum with radius R_o. Successful particle removal experiments were carried out during parabolic flights and testing shows that valid flow parameters at a given height above the surface (r) can be obtained (White *et al.,* 1987). Not shown in the illustration are the anti-vortex vanes required to minimize secondary flow patterns.

on Mars. The most notable effects of particle properties were observed for small particle diameters where adhesion dominates the threshold. This allows new directions in wind tunnel simulations to be defined. Potential experiments can involve comparable detachment experiments at fluid threshold conditions by employing a magnetic field to artificially increase the magnitude of adhesion forces based on ferromagnetic and paramagnetic particle properties. This approach is comparable to the use of magnetism to increase adhesion forces in the experiments of Hutton *et al.* (2004) to understand the role of interparticle forces in granular avalanching of sediments. Much more efficient is the use of a variable pressure, carousel-type wind tunnel during parabolic flight that provides a practical solution to fitting a wind tunnel in small-volume space such as an aircraft (Fig. 41). Initial pilot-studies have shown that great refinement in the understanding of adhesion forces can be achieved from particle removal studies in hypogravity (Greeley and Williams, 1987; White *et al.,* 1987). The shift in the force balance towards the interparticle forces in hypogravity thus allows further parameterisation of the 'simple' adhesion term (see Fig. 32 and Eq.1 in chapter 4) and subsequently the parameterisation of other model fitting parameters as well. The type of wind tunnel is ideal for studying the detachment of particle by rolling as the rotational components of the tunnel requires no complex conversions of particle trajectories and inertial systems, compared to the use of this tunnel for saltation studies (White *et al.,* 1987). While it was shown in chapter 5 that particles can orient to the local wind flow by saltation, it remains unclear to what extent particles can orient *in situ*, without ever leaving the bed. Experimental simulations using the proposed carousel-type wind tunnel may provide an excellent opportunity for studying *in situ* particle mobility to give valuable insights in flow-orientation processes.

3.3 Triggers of sub-ice eruptions

Glaciovolcanism on Mars appears to have benefited from coinciding peaks of volcanism and glaciations (Neukum *et al.*, 2010). I have outlined a possible new hypothesis for the promotion of these subglacial eruptions in the introduction of this dissertation. Lithosphere unloading might have been a trigger on Mars due to the absence of distinct plate tectonics and the dominance of plume-based volcanism. The volcanic features around the North Pole would make it possible to determine if temporal clusters exist where some of the tuya features (Appendix A) are related to post-glacial (subaerial) eruptions. Impact crater dating (Hartmann and Neukum, 2001) of these features can be complicated due to the scale of individual edifices, but it may be possible using the relative age differences of the area surrounding tuyas or other volcanic features (e.g. from Fagan *et al.,* 2010). Regional palaeo-ice reconstructions applying known parameters of the rheology and composition of the Martian polar ice caps (Bibring *et al.*, 2004; Zuber *et al.*, 2007; Phillips *et al.*, 2008, 2011) can be used to determine the possible extent of the ice during these eruptions. This would give a contextual analysis for testing the proposed hypothesis as the eruption trigger of the polar volcanic features and tuyas.

This dissertation aimed at characterising the environmental behaviour of glaciovolcanic glass in Iceland and on planet Mars. Several new insights in the behaviour of glass on Mars have been obtained within the research framework of this dissertation. Local erosion, transport and modification of volcanic glass have been studied and new niches for further research have been proposed. The combined study of volcanism and ice on Earth and Mars shows that the geomorphological understanding of the environmental fate of glaciovolcanic glasses benefits from the characterisation of its material properties with dedicated experiments.

References

Allen, C.C., 1979. Volcano-ice interactions on Mars. J Geophys Res 84:8048–8059.

Allen, C.C., Gooding, J.L., Jercinovic, I.M., Keil, K., 1981. Altered Basaltic Glass: A Terrestrial Analog to the Soil of Mars. Icarus 45, 347-369.

Ahrendt, *et al.*, 2012. Randolph Glacier Inventory (v2.0): A Dataset of Global Glacier Outlines. Global Land Ice Measurements from Space, Boulder Colorado, USA. Digital Media.

Almeida, M.P., Parteli, E.J.R., Andrade jr., J.S., Herrmann, H.J. 2008. Giant Saltation on Mars. P. Natl. Acad. Sci. USA., 105(17), 6222-6226.

Andreotti, B., Claudin, P., Pouliquen, O., 2006. Aeolian sand ripples: experimental study of fully developed states Phys. Rev. Lett. 96, 028001, doi: 10.1103/PhysRevLett.96.028001

Anders. N.S., Seijmonsbergen, A.C., Bouten, W., 2011. Segmentation optimization and stratified object-based analysis for semi-automated geomorphological mapping. Remote sensing environ. 115, 2976-2985.

Árnadóttir, T., Lund, B., Jiang, W., Geirsson, H., Björnsson, H., einarsson, P., Sigurdsson, T., 2009. Glacial rebound and plate spreading: results from the first countrywide GPS observations in Iceland. Geophys. J. Int. 177, 691–716., doi: 10.1111/j.1365-246X.2008.04059.x

Arnalds, O., 2000. The Icelandic 'Rofabard' soil erosion features. Earth Surf. Process. Landf. 25, 17-28.

Arnalds, O., 2010. Dust sources and deposition of aeolian materials in Iceland. Icel. Agric. Sci. 23, 3-21.

Arnalds, O., Gisladottir, F.O., Sigurjonsson, H., 2001. Sandy deserts of Iceland: and overview. J. Arid Env. 47, 359-371.

Arnalds, O., Gisladottir, F.O., Orradottir, B., 2012. Determination of aeolian transport rates of volcanic soils in Iceland. Geomorphology 167-168, 4-12. doi: 10.1016/j.geomorph.2011.10.039

Aranson, I.S.,Tsimring, L.S., 2006. Patterns and collective behavior in granular media: Theoretical concepts. Rev. Mod. Phys. 78, 641-692.

Arvidson, R.E., Guinness, E.A., Moore, H.J., Tillman, J., Wall, S.D., 1983. Three Mars years: Viking lander 1 imaging observations. Science 222, 463–468.

Arvidson, R.E., *et al.*, 2008. Spirit Mars Rover Mission to the Columbia Hills, Gusev Crater: Mission overview and selected results from the Cumberland Ridge to Home Plate. J. Geophys. Res. 113, E12S33, doi:10.1029/2008JE003183.

Ayling, B.F., McGowan, H.A., 2006. Niveo-Eolian Sediment Deposits in Coastal South Victoria Land, Antarctica: Indicators of Regional Variability in Weather and Climate. Arctic Antarct. Alpine. Res. 38, 313-324.

Baatz, M., Schäpe, A., 2000. Multiresolution segmentation—An optimization approach for high quality multi-scale image segmentation. Angewandte Geographische Informationsverarbeitung XII. Beiträge zum AGIT-Symposium Salzburg, 200, 12–23.

Bagnold, R.A., 1954. The physics of blown sands and desert dunes, Methuen and Co. Ltd., London.

Balme, M., *et al.*, 2006. Orientation and distribution of recent gullies in the southern hemisphere of Mars: Observations from High Resolution Stereo Camera/Mars Express (HRSC/MEX) and Mars Orbiter Camera/Mars Global Surveyor (MOC/MGS) data, J. Geophys. Res. 111, E05001

Baratoux, D., Mangold, N., Arnalds, O., Bardintzeff, J-M., Platevoët, B., Grégoire, M., Pinet, P., 2011. Volcanic sands of Iceland - Diverse origins of aeolian sand deposits revealed at Dyngjusandur and Lambahraun. Earth Surf. Proc. Land. 36, 1789–1808.

Bergh, S.G., Sigvaldason, G.E., 1991. Pleistocene mass-flow deposits of basaltic hyaloclastites on a shallow submarine shelf, South Iceland. Bull. Volcanol. 53, 597–611.

Bertran, P., Texier, J.-P., 1999. Facies and microfacies of slope deposits. Catena 35, 99-121.

Bhardwaj, A., *et al.*, 2007. X-rays from solar system objects. Planet. Space Sci. 55, 1135-1189.

Bibring, J-P., *et al.*, 2004. Perennial water ice identified in the south polar cap of Mars. Nature 428, 627-630, doi:10.1038/nature02461

Bielders, C. L., De Backer, L. W., Delvaux, B., 1990. Particle Density of Volcanic Soils as Measured with a Gas Pycnometer. Soil Sci. Soc. Am. J. 54, 822–826.

Bishop, B.A., 2011. Aeolian scours as putative signatures of wind erosion and sediment transport direction on Mars. Geomorphology 125, 569–574.

Bishop, J.L., Pieters, C.M., 1995. Low-temperature and low atmospheric pressure infrared reflectance spectroscopy of Mars soil analog materials. J. Geophys. Res. 100, 5369-5379.

Björnsson, H., 2002. Subglacial lakes and jökulhlaups in Iceland. Global. Planet. Change. 35, 255-271.

Blair, T.C., McPherson, J.G., 1994. Alluvial fan processes and forms. In: Abrahams, A.D., Parsons, A.J. (Eds.), Geomorphology of Desert Environments. Chapman and Hall, London, pp. 354–402.

Blake, S., 1984. Magma mixing and hybridization processes at the alkalic, Silicic Torfajokull central volcano triggered by tholeiitic Veidivötn fissuring, south Iceland. J. Volcanol. Geotherm. Res. 22, 1-31.

Blaschke, T., 2010. Object based image analysis for remote sensing. ISPRS Journal of Photogrammetry and

Remote Sensing, 65(1), 2–16.
Blissenbach, E., 1954. Geology of alluvial fans in semiarid regions. Geol. Soc. Am. Bull. 65, 175-190.
Blott, S.J., Pye, K., 2001. GRADISTAT: a grain size distribution and statistics package for the analysis of unconsolidated sediments. Earth Surf. Proc. Land. 26, 1237–1248.
Bonham, L.C., Spotts, J.H., 1971. Measurement of clay orientation. In: R.E. Carver (Eds.), Procedures in Sedimentary Petrology. Wiley, New York, N.Y., pp. 285-312.
Borisova, A.Y., Toutain, J-P., Stefansson, A., Gouy, S., De Parseval, P., 2012. Processes controlling the 2010 Eyjafjallajökull explosive eruption. J. Geophys. Res. 117, B05202. doi:10.1029/2012JB009213.
Bourgeois, O., Dauteuill, O., Vliet-Lanoë, B. van, 1998. Pleistocene subglacial volcanism in Iceland: tectonic implications. Earth Planet. Sci. Lett. 164,165-178.
Bourke, M.C., Bullard, J.E., Barnouin-Jha, O.S., 2004. Aeolian sediment transport pathways and aerodynamics at troughs on Mars. J. Geophys. Res., 109, E07005, doi:10.1029/2003JE002155.
Bourke, M.C., Edgett, K.S., Cantor, B.A., 2008. Recent aeolian dune change on Mars. Geomorphology 94, 247-255.
Bourke, M.C., Lancaster, N., Fenton, L.K., Parteli, E.J.R., Zimbelman, J.R., Radebaugh, J., 2010. Extraterrestrial dunes: An introduction to the special issue on planetary dune systems. Geomorphology 121, 1–14.
Brandes, C., *et al.*, 2012. Activity along the Osning Thrust in Central Europe during the Lateglacial: ice-sheet and lithosphere interactions. Quart. Sci Rev. 38, 49-62, doi:10.1016/j.quascirev.2012.01.021
Bridges, N.T. *et al.*, 2010 Aeolian bedforms, yardangs, and indurated surfaces in the Tharsis Montes as seen by the HiRISE Camera: evidence for dust aggregates. Icarus 205 165–82.
Bridges, N.T., *et al.*, 2012a. Planet-wide sand motion on Mars. Geology 40, 31-34.
Bridges, N.T., Ayoub, F., Avouac, J-P., Leprince, S., Lucas, A., Mattson, S. 2012b. Earth-like sand fluxes on Mars. Nature 485, 339-342.
Bristow, C.S., Bailey, S.D., Lancaster, N., 2000. The sedimentary structure of linear sand dunes. Nature 406, 56-59.
Brown, I., Ward, R., 1996. The Influence of Topography on Snowpatch Distribution in Southern Iceland: A New Hypothesis for Glacier Formation? Geogr. Ann. Ser. A, Phys. Geogr. 78, 197-207.
Burnham, K.P., Anderson, D.R., 2002. Model selection and multi-model inference - A practical information-theoretic approach. 2nd ed., Springer, New York. 488 p.
Burnett, C. and Blaschke, T. 2003. A multi-scale segmentation / object relationship modelling methodology for landscape analysis. Ecological Modelling 168(3), 233-249.
Burr, D.M., 2010. Palaeoflood-generating mechanisms on Earth, Mars, and Titan. Global Planet. Change 70, 5-13, doi:10.1016/j.gloplacha.2009.11.003
Caballero, L., Sarocchi, D., Borselli, L., Cárdenas, A.I., 2012. Particle interaction inside debris flows: Evidence through experimental data and quantitative clast shape analysis. J. Volcanol. Geoth. Res. 231-232, 12–23
Caine, N., 1969. A Model for Alpine Talus Slope Development by Slush Avalanching. J. Geol., 77, 92-100.
Caine, N., 1980. The Rainfall Intensity: Duration Control of Shallow Landslides and Debris Flows. Geogr. Ann. Ser. A, Phys. Geogr. 62, 23-27.
Carlsen, H.K., *et al.*, 2012. A survey of early health effects of the Eyjafjallajökull 2010 eruption in Iceland: a population-based study. BMJ Open 2012;2:e000343. doi:10.1136/bmjopen-2011-000343
Carr, M.H., Head, J.W., 2003. Basal melting of snow on early Mars: a possible origin of some valley networks. Geophys Res Lett 30, doi:10.1029/2004GL018575.
Carr, M.H., Head, J.W., 2010. Geologic history of Mars. Earth Planet. Sci. Lett. 294, 185–203.
Carrivik, J.L., Russell, A.J., Tweed, F.S., 2004. Geomorphological evidence for jökulhlaups from Kverkfjöll volcano, Iceland. Geomorphology 63, 81–102.
Carrozzo, F. G., F. Altieri, G. Bellucci, F. Poulet, E. D'Aversa, and J.-P. Bibring (2012), Iron mineralogy of the surface of Mars from the 1 μm band spectral properties, J. Geophys. Res. 117, E00J17, doi:10.1029/2012JE004091
Chapman, M.G., 1994. Evidence, age, and thickness of a frozen paleolake in Utopia Planitia, Mars. Icarus 109, 393-406.
Chapman, M., *et al.*, 2000. Volcanism and ice interactions on Earth and Mars. In: Zimbelmann, J., Gregg, T., (Eds.), Environmental Effects on Volcanic Eruption: From the Deep Oceans to Deep Space, Kluwer Academic/ Plenum Publishers, New York, 39–73.
Chapman M.G., Tanaka K.L., 2002. Related Magma–Ice Interactions: Possible Origins of Chasmata, Chaos, and Surface Materials in Xanthe, Margaritifer, and Meridiani Terrae, Mars. Icarus 155, 324–339.
Chapman, M.G., Hare, T.M., Russell, A.J., Gudmundsson, M.T., 2003. Possible Juventae Chasma subice volcanic eruptions and Maja Valles ice outburst floods on Mars: Implications of Mars Global Surveyor crater densities, geomorphology, and topography, J. Geophys. Res. 108(E10), 5113, doi:10.1029/2002JE002009
Chepil, W.S., 1959. Equilibrium of soil grains at the threshold of movement by wind. Proc. Soil. Sci. Soc. 23, 422-428.
Chevier, V., Mathé, P.E., 2007. Mineralogy and evolution of the surface of Mars: A review. Planet. Space Sci. 55, 289-314.
Chojnacki, M., Burr, D.M., Moersch, J.E., Michaels, T.I., 2011. Orbital observations of contemporary dune activity in Endeavor crater, Meridiani Planum, Mars. J. Geophys. Res. 116, E00F19, doi: 10.1029/2010JE003675
Christensen, P.R., 2003. Formation of recent Martian gullies through melting of extensive water-rich snow

deposits. Nature 422, 45-48.
Clarizia, M., Gullà, G., Sorbino, G., 1996. Sui meccanismi di innesco dei soil slip. International conference. Prevention of hydrogeological hazards: the role of scientific research. 1, 585–597 (in Italian).
Claudin, P., Andreotti, B., 2006. A scaling law for aeolian dunes on Mars, Venus, Earth, and for subaqueous ripples. Earth Planet. Sci. Lett. 252, 30–44.
Cleaver, J.W., Yates, B., 1973. Mechanism of detachment of colloidal particles from a flat substrate in a turbulent flow. J. Colloid and Interface Sci. 44, 464-474.
Clifford, S.M., Lasue, J., Heggy, E., Boisson, J., McGovern, P., Max, M.D., 2010. Depth of the martian cryosphere: revised estimates and implications for the existence and detection of subpermafrost groundwater. J. Geophys. Res. 115, doi:10.1029/2009JE003462.
Coleman, K.A., Dixon, J.C., Howea, K.L., Roe, L.A., Chevrier, V., 2009. Experimental simulation of martian gully forms. Planet. Space Sci. 57, 711-716.
Colette, A., *et al.* 2011. Assessing in near real time the impact of the April 2010 Eyjafjallajökull ash plume on air quality. Atmos. Environ. 45, 1217-1221.
Cooke, R., Warren, A., Goudie, A., 1993. Desert Geomorphology. University College Press, London.
Costard, F., Forget, F., Mangold, N., Peulvast, J.P., 2002. Formation of recent Martian debris flows by melting of near-surface ground ice at high obliquity. Science 295, 110-113.
Cousins, C.R., Crawford, I.A., 2011. Volcano-Ice Interaction as a Microbial Habitat on Earth and Mars. Astrobiology 11, 695-710, doi:10.1089/ast.2010.0550
Curray, J.R., 1956. Dimensional grain orientation studies of recent coastal sands. Bull. Am. Ass. Petrol. Geol. 40(10), 2440-2456.
Dapples E.C. and Rominger, J.F. 1945. Orientation Analysis of Fine-Grained Clastic Sediments: A Report of Progress J. Geol., 53, 246-261
Davis, J.C., 2002. Statistics and data analysis in geology (3d ed.). John Wiley and Sons, New York.
de Boer, W.M. 1992. Äolische Prozesse und Landschaftsformen im mittleren Baruther Urstromtal seit dem Hochglazial der Weichselkaltzeit. PhD Dissertation Humboldt-University, Berlin. pp.144 (in German with an English summary) http://nbn-resolving.de/urn:nbn:de:kobv:11-100206153
de Boer, W.M. 1996. Paläowindrichtungen in Brandenburg – Feststellungen anhand geologischer und geomorphologischer Daten. Biologische Studien, 25, 29-32 (in German) http://nbn-resolving.de/urn:nbn:de:kobv:11-100179346
de Boer, W.M. 1998: Aeolian landforms in the Baruth Ice-Marginal Valley and the dune profile in the Picher Berge near Schöbendorf (Brandenburg). In: dunes and fossil soils of Vistulian and Holocene age between Elbe and Wisła. - In: Guide book of Excursions. - Poznań, p. 17-21.
de Vet, S.J., Cammeraat, L.H., 2012. Aeolian contributions to the development of hillslopes and scree sediments in Grænagil, Torfajökull, Iceland. Geomorphology 175-176, 74-85. doi:10.1016/j.geomorph.2012.06.023
Dennerl, K., 2006. X-rays from Mars. Space Science Rev. 126, 403-433.
Dennerl, K., *et al.*, 2006. First observations of Mars with XMM-Newton; High resolution X-ray spectroscopy with RGS. Astronomy & Astrophys. 451, 709-722.
Dennis, J.E., Gay, D.M. and Welsch R.E., 1981. NL2SOL - An adaptive nonlinear least-squares algorithm. ACM Trans. Math. Softw. 7(3), 369-683.
Denton, J.S., Tuffen, H., Gilbert, J.S., Odling, N., 2009. The hydration and alteration of perlite and rhyolite. J. Geol. Soc. 166, 895–904.
Denton, J.S., Tuffen, H., Gilbert, J.S., 2012. Variations in hydration within perlitised rhyolitic lavas—evidence from Torfajökull, Iceland. J. Volcanol. Geotherm. Res. 223-224, 64-73.
Dixon, J.E., Filiberto, J.R., Moore, J.G., Hickson, C.J., 2002. Volatiles in basaltic glasses from a subglacial volcano in northern British Columbia (Canada): implications for ice sheet thickness and mantle volatiles. in: Chapman, M.G. (Eds.), The geology of Mars – Evidence from Earth-based analogues, Cambridge University Press, Cambridge, pp.255-271.
Donnovan, A.R., Oppenheimer, C., 2011. The 2010 Eyjafjallajökull eruption and the reconstruction of geography. Geograph. J. 1771, 4–11. doi: 10.1111/j.1475-4959.2010.00379.x
Edgett, K.S., *et al.*, 2012. Curiosity's Mars Hand Lens Imager (MAHLI) Investigation. Space Sci. Rev. 170 (1-4), 259-317, doi: 10.1007/s11214-012-9910-4
Edwards, B., Magnússon, E., Thodarson, T.,Guðmundsson, M.T., Höskuldsson, A., Oddson, B., Haklar, J., 2012. Interactions between lava and snow/ice during the 2010 Fimmvörðuháls eruption, south-central Iceland. J. Geophys. Res. 117, B04302. doi:10.1029/2011JB008985
Ehlers, J., Grube, A., Stephan, H.-J., Wansa, S., 2011. Pleistocene glaciations of North Germany e New results. In: Ehlers, J., Gibbard, P.L., Hughes, P.D. (Eds.), Quaternary Glaciations - Extent and Chronology - A Closer Look. Developments in Quaternary Science, vol. 15, pp. 149-162.
Einarsson, Th., 1960. Geologie von Hellisheidi (Sudwest-Island). Sonderver. Geolog. Inst. Univ. Köln 5, 55 pp.
Einarsson, M.Á., 1984. Climate of Iceland. In: H. van Loon (Eds.), World Survey of Climatology: 15: Climates of the Oceans. Elsevier, Amsterdam, pp. 673-697.
Einarsson, P., Sæmundsson, K., 1987. Earthquake epicenters 1982–1985 and volcanic systems in Iceland map. In: Sigfússon, I. (Eds.), Í hlutarins eðli, Festschrift for Þorbjörn Sigurgeirsson. Menningarsjóður, Reykjavík

Eshel, G., Levy, G.J., Mingelgrin, U., Singer, M.J., 2004. Critical Evaluation of the Use of Laser Diffraction for Particle-Size Distribution Analysis. Soil. Sci. Soc. Am. J. 68, 736-743.
Fagan, A.L., Sakimoto, S.E.H., Hughes, S.S., 2010. Formation constraints on Matian north polar volcanic edifeces. J. Geophys. Res. 115, E07013, doi:10.1029/2009JE003476
Fenton, L.K., 2006. Dune migration and slip face advancement in the Rabe Crater dune field, Mars. Geophys. Res. Lett. 33, L20201, doi:10.1029/2006GL027133.
Fenton, L.K., Michaels, T.I., 2010. Characterizing the sensitivity of daytime turbulent activity on Mars with the MRAMS LES: early results. Mars 5, 159–171.
Fishbaugh, K.E., Head III, J.W., 2002. Chasma Boreale, Mars: Topographic characterization from Mars Orbiter Laser Altimeter data and implications for mechanisms of formation. J. Geophys. Res. 107, E3, 5013, 10.1029/2000JE001351
Fishbaugh, K.E., Head III, J.W., 2005. Origin and characteristics of the Mars north polar basal unit and implications for polar geologic history. Icarus 174, 444–474
Fisher, R.V., Schmincke, H.-U., 1984. Pyroclastic rocks. Springer Verlag, Berlin, 472 pp.
Fitzpatrick, E.A.,1980. The Micromorphology of Soils. Department of Soil Science, University of Aberdeen, Scotland.
Flude, S., Burgess, R.,McGarvie, D.W., 2008. Silicic Volcanismat Ljósufjöll, Iceland: insights into evolution and eruptive history from Ar–Ar dating. Bull. Volcanol. 169, 154–175.
Franszon, H., Guðfinnsson, G.H., Helgadóttir, H.M., Frolava, J., 2010. Porosity, density and chemical composition relationships in altered Icelandic hyaloclastites. In: Birkle & Torres-Alvarado (Eds.), Water-Rock Interaction, Taylor & Francis Group, London
Friedmann, G.M., Sanders, J.E., 1978. Principles of Sedimentology. John Wiley and Sons, New York, pp. 78-81.
Frolava, Y.V., 2008. Specific Features in the Composition, Structure, and Properties of Volcaniclastic Rocks. Mosc .Univ. Geol. Bull. 63, 28-37.
Fueten, F., Goodchild, J.S. 2001. Quartz c-axis orientation determination using the rotating polarizer microscope. J. Struct. Geol. 23, 895–902.
Furnes, H., 1978. Element mobility during palagonitization of a subglacial hyaloclastite in Iceland. Chem. Geol. 22, 249-264.
Furnes, H., Fridleifsson I.B., Atkins, F.N., 1980. Subglacial volcanics: on the formation of acid hyaloclastites. J. Volcanol. Geotherm. Res. 8, 95–110.
Gaidos, E., Marion, G., 2003. Geological and geochemical legacy of a cold early Mars. J Geophys Res 108, doi:10.1029/2002JE002000.
Gardin, E., Allemanda, P., Quantina, C., Silvestro, S., Delacourt, C., 2012. Dune fields on Mars: Recorders of a climate change? Planet. Space Sci. 60, 314-321.
Garvin, J.B., Sakimoto, S.E.H., Frawley, J.J., Schnetzler, C., Wright, H.M., 2000. Topographic evidence for geologically recent near-polar volcanism on Mars. Icarus 145, 648–652.
Gee, G.W., Bauder, J.W., 1986. Particle-size analysis.. In: Klute, A. (Eds.), Methods of Soil Analysis, Part 1. Physical and Mineralogical Methods. Agronomy Monograph No. 9 (2ed). American Society of Agronomy/ Soil Science Society of America, Madison, WI, pp. 383-411.
Gertisser, R., 2010. Eyjafjallajökull volcano causes widespread disruption to European air traffic. Geology Today 26, 94-95.
Ghatan, G.J., Head, J.W., 2002. Candidate subglacial volcanoes in the south polar region of Mars: Morphology, morphometry, and eruption conditions. J. Geophys. Res 107, 1-21.
Gislason, S.R., Oelkers, E.H., 2003. Mechanism, rates, and consequences of basaltic glass dissolution: II. An experimental study of the dissolution rates of basaltic glass as a function of pH and temperature. Geochem. Cosmochim. Acta. 67, 3817-3832.
Gislason, S.R., *et al.* 2011. Characterization of Eyjafjallajökull volcanic ash particles and a protocol for rapid risk assessment. PNAS, 108, 7307-7312.
Goetz, W., *et al.*, 2010. Microscopy analysis of soils at the Phoenix landing site, Mars: Classification of soil particles and description of their optical and magnetic properties, J. Geophys. Res., 115, E00E22, doi:10.1029/2009JE003437.
Gómez-Elvira, J. *et al.*, 2012. REMS: the environmental sensor suite for the Mars Science Laboratory rover. Space Sci. Rev. 170(1-4), 583-640, doi: 10.1007/s11214-012-9921-1
Greeley, R., 2002. Saltation impact as a means for raising dust on Mars. Planet. Space Sci. 50, 151–5.
Greeley, R., Iversen, J.D., 1985. Wind as a Geological Process on Earth, Mars and Venus. Cambridge Planetary Science Series. Cambridge Univ. Press., Cambridge
Greeley, R., Williams, R., 1987. Experiments in planetary and related science and the space station. NASA conference publication 2494.
Greeley, R. Iversen, J.D., Pollack, J.B., 1974. Wind tunnel studies of Martian Aeolian processes. Prodeecings of the Royal Society London 341, 331-360.
Greeley, R., Leach, R., White, B.R., Iversen, J.D., Pollack, J.B., 1980. Threshold windspeeds for sand on Mars – Wind-tunnel simulations. Geophys. Res. Lett. 7, 121–124.
Greeley, R., *et al.* , 2006. Gusev crater: Wind-related features and processes observed by the Mars Exploration

Rover Spirit. J. Geophys. Res. 111, E02S09, doi:10.1029/2005JE002491
Greeley, R., *et al.*, 2008. Columbia Hills, Mars: Aeolian features seen from the ground and orbit. J. Geophys. Res. 113, E06S06, doi:10.1029/2007JE002971
Grott, M., Breuer, D. 2010. On the spatial variability of the Martian elastic lithosphere thickness: Evidence for mantle plumes? J. Geophys. Res., 115, E03005, doi:10.1029/2009JE003456.
Gudmundsson, A., 2000. Dynamics of volcanic systems in Iceland: example of tectonism and volcanism at juxtaposed hot spot and mid-ocean ridge systems. Ann. Rev. Earth Planet. Sci. 28,107-140.
Gudmundsson, G., 2011. Respiratory health effects of volcanic ash with special reference to Iceland. A review. Clinic. Respir. J. 5, 2-9. doi: 10.1111/j.1752-699X.2010.00231.
Gudmundsson, M.T., *et al.*, 2012. Ash generation and distribution from the April-May 2010 eruption of Eyjafjallajökull, Iceland. Nature. Doi: 10.1038/srep00572
Gunnarsson, B., Marsh, B.D., Taylor Jr., H.P., 1998. Generation of Icelandic rhyolites: Silicic lavas from the Torfajökull central volcano. J. Volcanol. Geotherm. Res. 83, 1-45.
Guzzetti, F., Peruccacci, S., Rossi, M., Stark, C.P., 2008. The rainfall intensity–duration control of shallow landslides and debris flows: an update. Landslides 5, 3-17.
Hall, K., 1999. The role of thermal stress fatigue in the breakdown of rock in cold regions. Geomorphology 30, 47-63.
Haberle, R.M., *et al.*, 1999. General circulation model simulations of the Mars Pathfinder atmospheric structure investigation/meteorology data. J. Geophys. Res. 104, E4, 8957-8974.
Haberle, R.M., Murphy, J.R., Schaeffer, J., 2003. Orbital change experiments with a Mars general circulation model. Icarus 161, 66–89.
Hamilton, N., Owens, W.H., Rees, A.I. 1968. Laboratory experiments on the production of grain orientation in shearing sand. J. Geol., 76(4), 465-472.
Hansen,C.J., *et al.*, 2011. Seasonal Erosion and Restoration of Mars' Northern Polar Dunes. Science 331, 575-578.
Hansen, C.J., *et al.*, in press. Observations of the northern seasonal polar cap on Mars: I. Spring sublimation activity and processes. Icarus, doi: 10.1016/j.icarus.2012.09.024
Hartmann, W.K., 2005. Martian cratering 8: isochron refinement and the chronology of Mars. Icarus 174:294–320.
Hartmann, W.K., Neukum, G., 2001. Cratering chronology and the evolution of Mars. Space Sci. Rev. 96, 165-194.
Hartmann, W.K., Thorsteinsson, T., Sigurdsson, F., 2003. Martian hillside gullies and Icelandic analogs. Icarus 162, 259-277.
Hassanpour, A., 2011. The use of ArcGIS for determination of quartz optical axis orientation in thin section images. Journal of Microscopy, Volume 245, Issue 3, pages 276–287, March 2012 DOI: 10.1111/j.1365-2818.2011.03571.x
Hayward, R.K. *et al.*, 2008. Mars global digital dune database: Distribution in north polar region and comparison to equatorial region. Lunar Planet. Sci. 39. Abstract #1208.
Head III, J.W., Mustard, J.F., Kreslavsky, M.A., Milliken, R.E., Marchant, D.R., 2003a. Recent ice ages in Mars. Nature. 426, 797-802.
Head III, J.W., Wilson, L., Mitchell, K.L., 2003b. Generation of recent massive water floods at Cerberus Fossae, Mars by dike emplacement, cryospheric cracking, and confined aquifer groundwater release. Geophys. Res. Lett. 30, 1577, doi:10.1029/2003GL017135
Head III, J.W., Wilson, L., 2007. Heat transfer in volcano–ice interactions on Mars: synthesis of environments and implications for processes and landforms. Annal. Glaciol. 45, 1-13(13)
Heiken, G., 1972. Morphology and petrography of volcanic ashes. Geol. Soc. Am. Bull. 83, 1961–1988.
Heiken, G., Wohletz, K.H., 1985. Volcanic Ash. University of California Press, Berkeley.
Heilbronner, R., 2000. Automatic grain boundary detection and grain size analysis using polarization micrographs or orientation images. J. Struc. Geol. 22, 969-981.
Heilbronner, R.P. & Pauli, C. 1993. Integrated spatial and orientation analysis of quartz c-axes by computer aided microscopy. J. Struct. Geol. 15, 369–382.
Heine, K., Reuther, A.U., Thieke, H.U., Schulz, R., Schlaak, N., Kubik, P.W., 2009. Timing of Weichselian ice marginal positions in Brandenburg (northeastern Germany) using cosmogenic *in situ* 10Be. Zeitschrift für Geomorphologie 53 (4), 433-454.
Herkenhoff, K.E., *et al.*, 2003. Athena Microscopic Imager investigation, J. Geophys. Res., 108(E12), 8065, doi:10.1029/2003JE002076
Hess, S.L., Henry, R.M., Leovy, C.B., Ryan, J.A., Tillman, J.R., 1977. Meteorological results from the surface of Mars: Viking 1 and 2. J. Geophys. Res. 82, 4559-4574.
Hilgers, A., 2007. The chronology of Late Glacial and Holocene dune development in the northern Central European lowland reconstructed by optically stimulated luminescence (OSL) dating. PhD thesis, University of Köln, 353 pp. http://kups.ub.uni-koeln.de/2178/
Hinkel, K.M., 1997. Estimating seasonal values of thermal diffusivity in thawed and frozen soils using temperature time series. Cold Reg. Sci. Techol. 26, 1-15.
Holstein-Rathlou, C., *et al.* 2010. Winds at the Phoenix landing site. J. Geophys. Res. 115, E00E18, doi:

10.1029/2009JE003411
Horgan, B., Bell, J.F. 2012a. Widespread weathered glass on the surface of Mars. Geology 40, 391-394.
Horgan, B.H.N., Bell III, J.F., 2012b. Seasonally active slipface avalanches in the north polar sand sea of Mars: Evidence for a wind-related origin, Geophys. Res. Lett., 39, L09201, doi:10.1029/2012GL051329.
Horwell, C.J., 2007. Grain-size analysis of volcanic ash for the rapid assessment of respiratory health hazard. J. Environ. Monitor. 9, 1107-1115. doi: 10.1039/b710583p
Horwell, C.J., Baxter, P.J., 2006. The respiratory health hazards of volcanic ash: a review for volcanic risk mitigation. Bull. Volcanol. 69, 1-24. doi: 10.1007/s00445-006-0052-y
Hovius, N., Lea-Cox, A., Turowski, J.M., 2008. Recent volcano-ice interaction and outburst flooding in a Mars polar cap re-entrant. Icarus 197:24–38.
Hugenholtz, C.H., 2008. Frosted granular flow: A new hypothesis for mass wasting in Martian gullies. Icarus 197, 65–72.
Hunter, R.E., 1977. Basic types of stratification ins small eolian dunes. Sedimentology, 24, 361-387.
Hutton, S.R., Forsyth, A.J., Rhodes, M.J., Osborne, C.F., 2004. Effect of interparticle force on mixing and segragation of dry granular materials. Phys. Rev. E. 70, 031301, doi:10.1103/PhysRevE.70.031301
Ibrahim, A.H., Dunn, P.F., 2006. Effects of temporal flow acceleration on the detachment of microparticles from surfaces. Aerosol Sci. 37, 1258–1266.
Innes, J.L., 1983. Debris flows. Prog. Phys. Geogr. 7, 469–501.
Iversen, J.D., White, B.R., 1982. Saltation threshold on Earth, Mars and Venus. Sedimentology. 29, 111-119.
Jackson, K.A., Chalmers, B., 1958. Freezing of Liquids in Porous Media with Special Reference to Frost Heave in Soils. J. Appl. Phys. 29, 1178-1181. doi: 10.1063/1.1723397
Jakobsson, S.P., Gudmundsson, M.T., 2008. Subglacial and intraglacial volcanic formations in Iceland. Jökull 58, 179-196.
Jarosch, A., Gudmundsson, M.T., Högnadóttir, T., Axelsson, G., 2008. Progressive cooling of the hyaloclastite ridge at Gjálp, Iceland, 1996–2005. J. Volcanol. Geotherm. Res. 170, 218–229.
Jenkinson, G., 1989. An introduction to the operation and capabilities of image analysis systems. International Labmate. Londen, 12 (3/4), 12.
Jónasson, K., 2007. Silicic volcanism in Iceland: Composition and distribution within the active volcanic zones. J.Geodyn. 43, 101-117.
Jones, J.G., 1969. Intraglacial volcanoes of the Laugarvatn region, south-west Iceland, I. Quarterly J. Geol. Soc. London 124, 197–211.
Jones, J.G., 1970. Intraglacial volcanoes of the Laugarvatn region, south-west Iceland, II. J. Geol. 78, 127–140.
Jones, R., Pollock, H.M., Cleaver, J.A.S., Hodges, C.S., 2002 Adhesion Forces between Glass and Silicon Surfaces in Air Studied by AFM: Effects of Relative Humidity, Particle Size, Roughness, and Surface Treatment. Langmuir 18, 8045-8055.
Jull, M., Mackenzie, D., 1996. The effect of deglaciation of mantle melting beneath Iceland. J. Geophys. Res. 101, 21815–21828.
Juschus, O., 2001. Das Jungmoränenland südlich von Berlin - Untersuchungen zur jungquartären Landschaftsentwicklung zwischen Unterspreewald und Nuthe. Berliner Geographische Arbeiten 95, 152 pp. http://nbn-resolving.de/urn:nbn:de:kobv:11-10014402
Kaitna, R., Rickenmann, D. 2007. A new experimental facility for laboratory debris flow investigation. J. Hydro. Res. 45, 797-810. doi: 10.1080/00221686.2007.9521817
Kass, D.M. and Yung, Y.L., 1995. Loss of atmosphere from Mars due to solar wind-induced sputtering. Science 268, 697-699.
Kass, D.M., Yung, Y.L., 1996. The loss of atmosphere from Mars. Science 274, 1932-1933.
Katainen, J., Paajanen, M., Ahtola,E., Poreb,V., Lahtinena, J., 2006. Adhesion as an interplay between particle size and surface roughness. J. Colloid and Interface Sci. 304, 524–529.
Keszthelyi, L.P., Jaeger, W.L., Dundas, C.M., Martínez-Alonso, S., McEwen, A.S., Milazzo, M.P., 2010. Hydrovolcanic features on Mars: Preliminary observations from the first Mars year of HiRISE imaging. Icarus 205, 211–229. doi:10.1016/j.icarus.2009.08.020
Keunen, Ph.H., 1960. Experimental abrasion 4: Eolian action. J. Geol. 68, 427-449.
Kieffer, H.H. and Zent A.P., 1992. Quasi-periodic climate change on Mars, in: Kieffer, H.H., *et al.*, (Eds.) Mars, pp. 1180-1218, Univ. of Ariz. Press, Tucson.
Kjartansson, G., 1943. Geology of Árnessýsla. In: Árnesingasaga I, 1–250. (In Icelandic)
Kleinhans, M.G., 2005. Grain-size sorting in grainflows at the lee side of deltas, Sedimentology, 52, 291–311.
Kleinhans, M.G., 2010. A tale of two planets: geomorphology applied to Mars' surface, fluvio-deltaic processes and landforms. Earth Surf. Proc. Landf. 35, 102-117.
Kleinhans, M.G., Markies, H., De Vet, S.J., In 't Veld, A.C., Postema, F.N., 2011, Static and dynamic angles of repose in loose granular materials under reduced gravity, J. Geophys. Res. 116, E11004, doi:10.1029/2011JE003865
Kok, J.F., 2010a. An improved parameterization of wind-blown sand flux on Mars that includes the effect of hysteresis. Geophys. Res. Lett. 37, L12202, doi: 10.1029/2010GL043646.
Kok, J.F., 2010b. Difference in the wind speeds required for initiation versus continuation of sand transport on Mars: implications for dunes and dust storms. Phys. Rev. Lett. 104, 074502, doi: 10.1103/PhysRevLett.104.074502

Kok, J.F., Parteli, E.J.R., Michaels, T.I., Karam, D.B., 2012. The physics of wind-blown sand and dust. Rep. Prog. Phys. 7510, 106901, doi:10.1088/0034-4885/75/10/106901
Komatsu, G., Ori, G.G., Ciarcelluti, P., Litasov, Y.D., 2004. Interior layered deposits of Valles Marineris, Mars: analogous subice volcanism related to Baikal Rifting, Southern Siberia. Planet. Space Sci. 52, 167-187.
Kueppers, U., Putz, C., Spieler, O., Dingwell, D.B., 2012. Abrasion in pyroclastic density currents: Insights from tumbling experiments. Phys. Chem. Earth. Parts A/B/C. 45-46,33-39. doi: 10.1016/j.pce.2011.09.002
Laithy, J.E., 2009. Landforms, landscapes and processes of Aeolian Erosion. In : Parsons, A.J., Abrahams, A.D. (Eds.), Geomorphology of Desert Environments. Springer, p. 597-628.
Lancaster, N., Greeley, R., 1990. Sediment volume in the north polar sand seas of Mars. J. Geophys. Res. 95, 10921–10927.
Land, L.S., 1964. Eolian Cross-Bedding in the Beach Dune Environment, Sa. J. Sediment Petro. 34(2), 389-394.
Lanza, N.L., Meyer, G.A., Okubo, C.H., Newsom, H.E., Wiens, R.C., 2010. Evidence for debris flow gully formation initiated by shallow subsurface water on Mars. Icarus 205, 103-112, doi:10.1016/j.icarus.2009.04.014
Laskar. J., *et al.*, 2004. Long term evolution and chaotic diffusion of the insolation quantities of Mars. Icarus. 170, 343-364.
Leadbetter, S.J., Hort, M.C., Von Löwis, S., Weber, K., Witham, C.S. 2012. Modeling the resuspension of ash deposited during the eruption of Eyjafjallajökull in spring 2010. J. Geophys. Res. 117. doi: doi:10.1029/2011JD016802
Levy, J.S., Marchant, D.R., Head, J.W., 2010. Thermal contraction crack polygons on Mars: a synthesis from HiRISE, Phoenix, and terrestrial analog studies. Icarus 206:229–252.
Li, Y., Onasch, C.M. and Guo, Y., 2008. GIS-based detection of grain boundaries. J. Struct. Geol. 30, 431–443.
Licciardi, J.M., Kurz, M.D., Curtice, J.M., 2007. Glacial and volcanic history of Icelandic table mountains from cosmogenic 3He exposure ages. Quart. Sci. Rev. 26, 1529–1546.
Lippitsch, R., White, R.S., Soosalu, H., 2005. Precise hypocentre relocation of microearthquakes in a high-temperature geothermal field: the Torfajökull central volcano, Iceland. Geophys. J. Int. Volcanol. 160, 370-387.
Litt, T., Behre, K.-E., Meyer, K.-D., Stephan, H.-J., Wansa, S., 2007. Stratigraphical Terms for the Quaternary of the North German Glaciation Area. In: Litt, T. (Ed.), Stratigraphie von Deutschland – Quartär. Eiszeitalter & Gegenwart Quaternary Science Journal 56 (1/2), 7-65.
Maclennan, J., Jull, M., Mackenzie, D., Slater, L., Grönvold, K., 2002. The link between volcanism and deglaciation in Iceland. Geochem. Geophys. Geosys. 3. doi:10.1029/2001GC000282 Art. No. 1062.
Macpherson, G.J. 1984. A Model for Predicting the Volumes of Vesicles in Submarine Basalts. J. Geol. 921, 73-82.
Magelhães, J.A., Schofield, J.T., Seiff, A., 1999. Results of the Mars Pathfinder atmospheric structure investigation. J. Geophys. Res. 104, E4, 8943-8955.
Magnússon E., *et al.*, 2012. Ice-volcano interactions during the 2010 Eyjafjallajökull eruption, as revealed by airborne imaging radar. J. Geophys. Res. Lett. 117, B07405, doi:10.1029/2012JB009250
Major, J. 1998. Pebble orientation on large, experimental debris flow deposits. Sediment Geol. 117, 151-164.
Makse, H.A., Havlin, S., King, P.R., Stanley, H.E., 1997. Spontaneous stratification in granular mixtures. Nature 386, 379–381.
Mangold, N., Baratoux, D., Arnalds, O., Bardintzeff, J-M., Platevoet, B., Grégoire, M., Pinet, P., 2011. Segregation of olivine grains in volcanic sands in Iceland and implications for Mars. Earth Planet. Sci. Lett. 310, 233-243. doi: 10.1016/j.epsl.2011.07.025
Manukyan. E., Prigozhin, L., 2009. Formation of aeolian ripples and sand sorting. Phys. Rev. E. 79, 031303, doi: 10.1103/PhysRevE.79.031303
Marshall, J.R., Bull, P.A., Morgan, R.M., 2012. Energy regimes for aeolian sand grain surface textures. Sediment. Geol. 253-254, 17-24. doi: 10.1016/j.sedgeo.2012.01.001
Martel, C., Dingwell, D.B., Spieler, O., Pichavant, M., Wilke, M., 2000. Fragmentation of foamed silicic melts: an experimental study. Earth Planet. Sci. Lett. 178, 47-58.
Martin, E., Sigmarsson, O., 2007. Crustal thermal state and origin of silicic magma in Iceland: the case of Torfajökull, Ljósufjöll and Snæfellsjökull volcanoes. Contrib Mineral Petrol (2007) 153, 593–605, doi:10.1007/s00410-006-0165-5
Martini, I. P., 1971. A test of validity of quartz grain orientation as a paleocurrent and paleoenvironmental indicator. J. Sedi. Res. 41, 60-68.
Martínez-Alonso, S., Mellon, M.T., Banks, M.E., Keszthelyi, L.P., McEwen, A.S., and the HiRISE team, 2011. Evidence of volcanic and glacial activity in Chryse and Acidalia Planitiae, Mars. Icarus 212, 597-62, doi:10.1016/j.icarus.2011.01.004
Matoza, R.S. *et al.*, 2011. Long-range acoustic observations of the Eyjafjallajökull eruption, Iceland, April–May 2010. J. Geophys. Res. Lett. 388, L06308, doi:10.1029/2011GL047019
Matsuoka, N., Murton, J., 2008. Frost Weathering: Recent Advances and Future Directions. Permafrost Periglac. 19, 195–210. doi: 10.1002/ppp.620
McGarvie, D.W., 1984. Torfajökull — a volcano dominated by magma mixing. Geology 12, 685–687.
McGarvie, D., 2009. Rhyolitic volcano-ice interactions in Iceland. J. Volcanol. Geotherm. Res. 4, 367-389.
McGarvie, D.W., Burgess, R., Tindle, A.G., Tuffen,H and Stevenson, J.A., 2006. Pleistocene rhyolitic volcanism at

Torfajökull, Iceland: eruption ages, glaciovolcanism, and geochemical evolution. Jökull, 56, 57-75.
McGarvie, D.W., Stevenson, J.A., Burgess, R., Tuffen, H., Tindle, A.G., 2007. Volcano–ice interactions at Prestahnúkur, Iceland: rhyolite eruption during the last interglacial–glacial transition. Annals of Glaciology 45, 38–47.
McSween, H.Y., Taylor, G.J., Wyatt, M.B., 2009. Elemental composition of the Martian crust. Science, 324, 736-739.
Melosh, J.H., 2011. Planetary Surface Processes. Cambridge University Press, Cambridge. pp.348-379.
Merrison, J.P., Gunnlaugsson, H.P., Nørnberg, P., Jensen, A.E., Rasmussen, K.R., 2007. Determination of the wind induced detachment threshold for granular material on Mars using wind tunnel simulations. Icarus 191, 568-580.
Merrison, J.P., Bechtold, H., Gunnlaugsson, H., Jensen, A., Kinch , K., Nørnberg, P., Rasmussen, K., 2008. An Environmental Simulation Wind Tunnel for Studying Aeolian Transport on Mars. Planet. Space Sci. 56, 426-437.
Merrison, J.P., Gunnlaugsson, H.P., Jensen, S.K., Nørnberg, P. 2010. Mineral alteration induced by sand transport: A source for the reddish color of martian dust. Icarus 205, 716-718. doi: 10.1016/j.icarus.2009.09.004
Merrison, J.P., *et al.*, 2011. Factors affecting the electrification of wind-driven dust studied with laboratory simulations. Planetary and Space Science 60, 328-335.
Michaels, T.I., Rafkin, S.C.R., 2008. Large eddy simulation of the convective boundary layer of Mars Q. J. R. Meterol. Soc. 130, 1251–1274.
Moore, J. G. and L. C. Calk 1991. Degassing and differentiation in intraglacial volcanoes, Iceland. J. Volcanol. Geotherm. Res. 46, 157–180.
Mork, M.B.E., 1984. Magma mixing in the post-glacial Veidivötn fissure eruption, southeast Iceland: a microprobe study of mineral and glass variations. Lithos 17, 55-75.
Mouginis-Mark, P.J., 1985. Volcano/Ground Ice Interactions in Elysium Planitia, Mars. Icarus 64, 265-284.
Mueller, S., Scheu, B., Kueppers, U., Spieler, O., Richard, D., Dingwell, D.B. 2011. The porosity of pyroclasts as an indicator of volcanic explosivity. J. Volcanol. Geoth. Res. 203, 168-174. doi: 10.1016/j.jvolgeores.2011.04.006
Mustard, J.F., *et al.*, 2008. Hydrated silicate minerals on Mars observed by the Mars Reconnaissance Orbiter CRISM instrument. Nature 454, 305-309.
Nesbitt, H.W., Young, G.M., 1984. Prediction of some weathering trends of plutonic and volcanic rocks based on thermodynamic and kinetic considerations. Geochem. Cosmochim. Acta. 48, 1523-1534.
Neukum, G., Jaumann, R., Hoffmann, H., Hauber, E., Head, J.W., Basilevsky, A.T., Ivanov, B.A., Werner, S.C., van Gasselt, S., Murray, J.B., McCord, T., and the HRSC Co-Investigator Team, 2004. Recent and episodic volcanic and glacial activity on Mars revealed by the High Resolution Stereo Camera. Nature 432:971–979.
Neukum, G., *et al.*, 2010. The geologic evolution of Mars: Episodicity of resurfacing events and ages from cratering analysis of image data and correlation with radiometric ages of Martian meteorites. Earth. Planet. Sci. Lett. 294, 204-222.
Nickling, W.C., 1988. The initiation of particle movement by wind. Sedimentology, 35, 499-511.
Nino, Y., Lopez, F., Garcia, M., 2003. Threshold for particle entrainment into suspension. Sedimentology 50, 247–263.
Owen, J., Tuffen, H., McGarvie, D.W., 2012. Using dissolved H_2O in rhyolitic glasses to estimate palaeo-ice thickness during a subglacial eruption at Bláhnúkur Torfajökull, Iceland. Bull. Volcanol. 74, 1355–1378, doi: 10.1007/s00445-012-0601-5
Pálmason, G., Friedman, J.D., Williams Jr., R.S., Jónsson, J., Saemundsson, K., 1970. Aerial infrared surveys of Reykjanes and Torfajökull thermal areas, Iceland, with a section on cost of exploration surveys.
Parteli, E.J.R., Herrmann, H.J., 2007a. Saltation transport on Mars. Phys. Rev. Lett. 98, 198001, doi:0.1103/PhysRevLett.98.198001
Parteli, E.J.R. Herrmann, H.J., 2007b. Dune formation on the present Mars. Phys. Rev. E. 76, 041307, doi: 10.1103/PhysRevE.76.041307
Passchier C.W., Trouw R.A.J., 2005. Microtectonics. 2nd edn. Springer, Berlin, 366 pp.
Peacock, M.A., 1926. The vulcano-glacial palagonite formation of Iceland. Geol. Mag. 6, 385–399
Pedersen, G.B.M., Head, J.W., Wilson, L., 2010. Formation, erosion and exposure of early Amzonian dikes, dike swarms and possible subglacial eruptions in the Elysium Rise/Utopia Basin Region, Mars. Earth Planet. Sci. Lett. 294, 424-439.
Pelletier, J.D., Kolb, K.J., McEwen, A.S., Kirk, R.L., 2008. Recent bright gully deposits on Mars: Wet or dry flow? Geology 36, 211-214.
Peltier, L.C., 1950. The geographic cycle in periglacial regions as it is related to climatic geomorphology. Ann. Assoc. Am. Geogr. 40, 214-236.
Phillips, R.J., *et al.*, 2008. Mars north polar deposits: stratigraphy, age, and deodynamical response. Science, 320, 1182-1185, doi:10.1126/science.1157546
Phillips, R.J., *et al.*, 2011. Massive CO_2 Ice Deposits Sequestered in the South Polar Layered Deposits of Mars. Science. 332, 838-841.
Pjetursson, H., 1900. The glacial palagonite formation of Iceland. Scottish Geograph. Mag. 16, 265–293.
Prins, M.A., Vriend, M., Nugteren, G., Vandenberghe, J., Lu, H., Zheng, H., Weltje, G.J., 2007, Late Quaternary

aeolian dust flux variability on the Chinese Loess Plateau: Inferences from unmixing of loess grain-size records. Quaternary Science Reviews, v. 26, p. 230-242.
Pollack, J.B., Kasing, J.F., Richardsoon, S.M., Poliakoff, K., 1987. The case for a wet, warm climate on early Mars. Icarus 71, 203-224.
Pommerol, A., *et al.* in press. Observations of the northern seasonal polar cap on Mars III: CRISM/HiRISE observations of spring sublimation. Icarus, doi:10.1016/j.icarus.2012.08.039
Portyankina, G., *et al.* in press. Observations of the northern seasonal polar cap on Mars II: HiRISE photometric analysis of evolution. Icarus, doi:10.1016/j.icarus.2012.10.017
Potts, A.S., 1970. Frost Action in Rocks: Some Experimental Data. T. I. Brit. Geogr. 49, 109-124.
R Development Core Team, 2011. R: A language and environment for statistical computing. R Foundation for Statistical Computing, Vienna, Austria. URL http://www.R-project.org/.
Rapp, A., 1959. Avalanche Boulder Tongues in Lappland. Geografiska Annaler, 41, 34-48.
Rasmussen, K.R., Iversen, J.D., Rautahemio, P., 1996. Saltation and wind-flow interaction in a variable slope wind tunnel. Geomorphology 17, 19-28.
Rasmussen, K.R., Kok, J.F., Merrison, J.R. 2009. Enhancement in wind-driven sand transport by electric fields. Planet. Space Sci. 57, 804–8.
Rees, A.I., 1968. The production of preferred orientation in a concentrated dispersion of elongated and flattened Grains. J. Geol. 76(4), 457-465.
Renno, N.O., Kok, J.F., 2008. Electrical activity and dust lifting on Earth, Mars, and beyond. Space Sci. Rev. 137, 419–34.
Rice, J.W., Edgett, K.S., 1997. Catastrophic flood sediments in Chryse Basin, Mars, and Quincy Basin, Washington: application of sandar facies model. J Geophys Res 102:4185–4200.
Ringrose, T.J., Towner, M.C., Zarnecki, J.C., 2003. Convective vortices on Mars: A reanalysis of Viking lander 2 meteorological data, sols 1–60. Icarus 163, 78–87.
Rouquerol, F., Rouquerol, J., Sing, K., 1999. Adsorption by powders & porous solids; principles, methodology and applications. Academic press, London
Rubin, D.M., Hunter, R.E., 1987. Bedform alignment in directionally varying flows. Science 237, 276–78.
Rusnak, G.A., 1957. The Orientation of Sand Grains under Conditions of "Unidirectional" Fluid Flow: 1. Theory and Experiment. J. Geol. 65(4), 384-409.
Sæmundsson, K., 1974. Fissure swarms and central volcanoes of the neovolcanic zones of Iceland. Crustal Evolution of NWBritain and Adjacent Regions. Geological Journal Special Issue, vol. 10, pp. 415–432.
Sæmundsson, K., 1979. Outline of the geology of Iceland. Jökull 29, 7–28.
Sass, O., Krautblatter, M., 2007. Debris flow-dominated and rockfall-dominated talus slopes: Genetic models derived from GPR measurements. Geomorphology 86, 176-192.
Scherer, G.W., 1999. Crystallization in pores. Cement Concrete Res. 29, 1347-1358.
Scherer, G.W., Valenza II, J.J., 2005. Mechanisms of Frost damage. In: Young, F., Skalny, J.P., (Eds.), Materials Science of Concrete VII, 1st edn. Wiley, New York, pp 209-246
Schofield, J.T., *et al.*, 1997. The Mars Pathfinder Atmospheric Structure Investigation/Meteorology (ASI/MET) experiment. Science 278, 1752-1758.
Schopka, H.H., Gudmundsson, M.T., Tuffen, H., 2006. The formation of Helgafell, southwest Iceland, a monogenetic subglacial hyaloclastite ridge: Sedimentology, hydrology and volcano-ice interaction. J. Volcanol. and Geotherm. Res. 152, 359-377.
Schwan, J. 1989. Grain fabrics of natural and experimental low-angle aeolian sand deposits. Geologie en Mijnbouw. 68, 211 – 219.
Schwarzacher, W. 1951. Grain orientation in sands and sandstones. J. Sedi. Petro. 21(3), 162-172.
Selby, M.J., 2000. Hillslope materials and processes. 2nd ed. Oxford University Press, Oxford.
Shao, Y., Lu, H., 2000. A simple expression for wind erosion threshold friction velocity. J. Geophys. Res. 105, 22437–22443.
Shelby, J.E. 2005. Introduction to glass science and technology. The royal society of chemistry, Cambridge, p.291
Sigmundsson F., *et al.*, 2010. Intrusion triggering of the 2010 Eyjafjallajökull explosive eruption. Nature 468, 426-432. doi:10.1038/nature09558
Sigurðsson, O., Williams Jr., R.R., 1991. Rockslides on the terminus of "Jökulsárgilsjökull", Southern Iceland. Geogr. Annal. 73, 129-140.
Silvestro, S., Fenton, L.K., Vaz, D.A., Bridges, N.T., Ori, G.G., 2010. Ripple migration and dune activity on Mars: Evidence for dynamic wind processes. J. Geophys. Res. Lett. 37, L20203, doi:10.1029/2010GL044743
Silvestro, S., Vaz, D.A., Fenton, L.K., Geissler, P.E., 2011. Active aeolian processes on Mars: A regional study in Arabia and Meridiani Terrae, Geophys. Res. Lett., 38, L20201, doi:10.1029/2011GL048955.
Sime, L.C., Ferguson, R.I., 2003. Information on grains sizes in gravel-bed rivers by automates image analysis. J. Sedi. Res. 73(4), 630-636.
Simmons, G., Cooper, H.W., 1978. Thermal cycling cracks in three igneous rocks. Int. J. Rock. Mech. Min. Sci. Geomech. 15, 145-148.
Sindowski, K.-H., 1957, Die synoptische Methode des Kornkurvenvergleichs: Geol. Jb., v. 73, 235-275. (in German)

Skilling, I.P., 2009. Subglacial to emergent basaltic volcanism at Hlöðufell, south-west Iceland: A history of ice-confinement. J. Volcanol. Geotherm. Res. 185, 276-289.
Slater, L., Jull, M., Mackenzie, D., Grönvold, K., 1998. Deglaciation effects on mantle melting beneath Iceland: results from the Northern Volcanic Zone. Earth Planet. Sci. Lett. 164, 151–164.
Smellie, J.L., 2006. The relative importance of supraglacial versus subglacial meltwater escape in basaltic subglacial tuya eruptions: An important unresolved conundrum. Earth Sci. Rev. 74, 241–268.
Smellie, J.L., 2007. Quaternary volcanism: subglacial landforms. in: Encyclopedia of Quaternary Sciences, eds: S.A. Elias, Elsevier, Amsterdam, pp 784–798.
Smellie, J.L., 2008. Basaltic subglacial sheet-like sequences: Evidence for two types with different implications for the inferred thickness of associated ice. Earth-Sci. Rev. 88, 60-88.
Smellie, J.L., Skilling, I.P., 1994. Products of subglacial volcanic eruptions under different ice thicknesses: two examples from Antarctica. Sediment.Geol. 91, 115–129.
Smith, D.E., Zuber, M.T., Neumann, G.A., 2001. Seasonal variations of snow depths on Mars. Science 294, 2141-2146, doi: 10.1126/science.1066556
Soosalu, H., Einarsson, P., 2004. Seismic constraints on magma chambers at Hekla and Torfajökull volcanoes, Iceland. Bull. Volcanol. 66, 276–286.
Soosalu, H., Lippitsch, R., Einarsson, P., 2006. Low frequency earthquakes at the Torfajökull volcano, south Iceland. J. Volcanol. Geotherm. Res. 153, 187–199.
Spotts, J.H., 1964. Grain orientation and imbrication in Miocene turbidity current sandstones, California. J. Sedi. Petro. 34(2), 229-253.
Starokon, E.V., Dubkov, K.A., Pirutko, L.V., Panov, G.I., 2003. Mechanisms of iron activation on Fe-containing zeolites and the charge of α-oxygen. Topics in Catalysis 23, 137-143.
Statham, I., 1973. Scree slope development under conditions of surface particle movement. Transactions of the Institute of British Geographers 59, 41–53.
Sullivan, R., *et al.*, 2005. Aeolian processes at the Mars Exploration Rover Meridiani Planum landing site. Nature 436, 58–61.
Sullivan, R., *et al.*, 2008. Wind-driven particle mobility on Mars: Insights from Mars Exploration Rover observations at "El Dorado" and surroundings at Gusev Crater, J. Geophys. Res., 113, E06S07, doi:10.1029/2008JE003101
Sutton, J.L., Leovy, C.B., Tillman, J.E., 1978. Diurnal variation of the Martian surface layer meteorological parameters during the first 45 sols at two Viking lander sites. J. Atm. Sci. 35, 2346-2355.
Tanaka, K.L., Scott D.H., 1987. Geologic map of the polar regions of Mars, USGS Misc. Invest. Ser. Map, I-1802-C, U.S. Geological Survey, Reston, VA.
Taylor, G. I., 1935. Distribution of velocity and temperature between concentric rotating cylinders, Proc. Royal Soc. London, Series Al51, 494-512.
Thodarson T., Larsen, G., 2007. Volcanism in Iceland in historical time: Volcano types, eruption styles and eruptive history. J. Geodyn. 43, 118-152.
Thomson, B. J., Bridges, N. T., Greeley, R., 2008. Rock abrasion features in the Columbia Hills, Mars, J. Geophys. Res. 113, E08010, doi:10.1029/2007JE003018.
Treiman, A.H., 2003. Geologic settings of Martian gullies: Implications for their origins. J. Geophys. Res. 108, 8031.
Trimble, 2011. eCognition Developer 8.7 Reference Book. Trimble Germany GmbH, Trappentreustr. 1, D-80339 München, Germany.
Tuffen, H., 2007. Models of ice melting and edifice growth at the onset of subglacial basaltic eruptions, J. Geophys. Res., 112, B03203, doi:10.1029/2006JB004523.
Tuffen, H., Gilbert, J. McGarvie, D., 2001. Products of an effusive subglacial rhyolite eruption: Bláhnúkur, Torfajökull, Iceland. Bull. Volcanol. 63, 179-190.
Tuffen H., Pinkerton, H., McGarvie, D.W., Gilbert, J.S., 2002a. Melting of the glacier base during a small-volume subglacial rhyolite eruption: evidence from Bláhnúkur, Iceland. Sediment. Geol. 149, 183-198.
Tuffen, H., McGarvie, D.W., Gilbert, J.S., Pinkerton, H., 2002b. Physical volcanology of a subglacial-to-emergent rhyolitic tuya at Rauðfossafjöll, Torfajökull, Iceland. in: Smellie, J.L., Chapman, M.G. (Eds.), Volcano-Ice Interaction on Earth and Mars, Geological Society, London, Special publications 202, 213-236.
Tuffen, H., McGravie, D.W., Pinkerton, H., Gilbert, J.S., Brooker, R.A., 2008. An explosive-intrusive subglacial rhyolite eruption at Dalakvísl, Torfajökull, Iceland. Bull. Volcanol. 70, 841-860.
Tuffen, H., Owen, J., Denton, J. 2010. Magma degassing during subglacial eruptions and its use to reconstruct palaeo-ice thickness. Earth. Sci. Rev. 99, 1-18.
Urbanski, J., Wochna, A., Herman, A., 2011. Automated granulometric analysis and grain-shape estimation of beach sediments using object-based image analysis. J. coastal res. 64, 1745-1749.
van Asselen, S., Seijmonsbergen, A.C., 2006. Expert-driven semi-automated geomorphological mapping for a mountainous area using a laser DTM. Geomorphology 78, 309–320.
van Bemmelen, R.W., Rutten, M.G., 1955. Tablemountains of Northern Iceland. E. J. Brill, Leiden, 217 pp.
van Steijn, H., Brederode, L.E. van, Goedheer, G.J., 1984. Stratified Slope Deposits of the grèze-litée Type in the Ardèche Region in the South of France. Geogr.Annal. 66, 295-305.
van Steijn, H., Bertan, P., Francou, B., Hétu, B., Texier, J-P., 1995. Models for the genetic and environmental

interpretation of stratified slope deposits: review. Permafr. Periglac. Proces. 6, 125-146.
van Steijn, H., Hétu, B., 1997. Rain-generated overland flow as a factor in the development of some stratified slope deposits: a case study from the Pays du Buëch (Préalpes, France). Géogr. Phys. Quat. 51, 3–15.
van Steijn, H., Boelhouwers, J., Harris, S., Hétu, B., 2002. Recent research on the nature, origin and climatic conditions of blocky and stratified slope deposits. Prog. Phys. Geograph. 26, 551–575.
Vilmundardóttir, E.G., 1997. Bedrock geology of Möðrudalsfjallgarðar and adjacent areas. (In Icelandic). Orkustofnun, Report OS-97066, 37 pp.
Walder, J.S., Hallet, B., 1986. The Physical Basis of Frost Weathering: Toward a More Fundamental and Unified Perspective. Arctic Alpine Res. 181, 27-32.
Walker, G.P.L. 1965. Some aspects of Quaternary volcanism in Iceland. Transact. Leicester Lit. Philosoph. Soc. 59, 25–40.
Walker, G.P.L., 1966. Acid volcanic rocks in Iceland. Bull. Volcanol. 29, 376–402.
Warren, A., Kay, S., 1987. Dune networks, Geol. Soc. Spec. Pub. 35, 205– 212.
Wayland, R.G., 1939. Optical Orientation in elongate clastic quartz. Am. J. Sci. 237(2), 99-109, doi: 10.2475/ajs.237.2.99 AJS Online
Werner, S.C., 2009. The global martian volcanic evolutionary history. Icarus 201:44–68.
Werner, R., Schmincke, H.-U., Sigvaldason, G.E., 1996. A new model for the evolution of table mountains: volcanological and petrological evidence from Herdubreid and Herdubreidartögl volcanoes (Iceland). Geol. Rundsch. 85, 390–397.
Werner, R. and Schmincke, H.-U., 1999. Englacial vs lacustrine origin of volcanic table mountains: evidence from Iceland. Bull. Volcanol. 60, 335–354.
Whalley, W.B., 1984. Rockfalls. In: Brunsden, D., Prior, D.B. (Eds.), Slope Instability. Wiley and Sons, London, pp. 217–256.
Whalley, W.B., Douglas, G.R., Jonsson, A., 1983. The magnitude and frequency of large rockslides in Iceland in the postglacial. Geogr. Annal. 65, 99-110.
White, B.R., Davis, C.A., Leach, R.N., Greeley, R., Iversen, J.D., 1987. Saltation threshold experiments conducted under reduced gravity conditions. In: AIAA 25th Aerospace Science Meeting. AIAA-87-0621.
White, F.M., 2006. Viscous Fluid Flow. McGraw-Hill, New York.
Wieczorek, G.F., Nishenkod, S.P., Varnes, D.J., 1995. Analysis of rockfalls in the Yosemite Valley, California. In Daemen, J.J.K. and Schultz, R.A. (Eds.), Rock mechanics: proceedings of the 35th US symposium. Balkema, Rotterdam, pp. 85–89.
Wieczorek, G.F., *et al.*, 2000. Unusual July 10, 1996, Rock fall at Happy Isles, Yosemite National Park, California. Geol. Soc. Am. Bull. 112, 75–85.
Willetts, B., Rice, M.A., Swaine, S.E., 1982. Shape effects in aeolian grain transport. Sedimentology 29, 409-417.
Wilson, L., Head, J.W., 2002. Heat transfer and melting in subglacial basaltic volcanic eruptions: implications for volcanic deposit morphology and meltwater volumes, in: Smellie, J.L., Chapman, M.G. (Eds.), Volcano-Ice Interaction on Earth and Mars, Geological Society, London, Special publications 202, pp.5-26.
Wilson, L., Head, J.W., 2007. Explosive volcanic eruptions on Mars: Tephra and accretionary lapilli formation, dispersal and recognition in the geologic record. J. Volcanol. Geotherm. Res. 163, 83-97.
Wurm, G., Teiser, J., Reiss, D., 2008. Greenhouse and thermophoretic effects in dust layers: the missing link for lifting of dust on Mars Geophys. Res. Lett. 35 L10201, doi: 10.1029/2008GL033799
Yang, R.Y., Yu, A.B., McElroy, L., Bao, J., 2008. Numerical simulation of particle dynamics in different flow regimes in a rotating drum. Powder Techol. 188, 170-177.
Zaniewski, K. 2001. Plasmic fabric analysis of glacial sediments using quantitative image analysis methods and GIS techniques. PhD dissertation, University of Amsterdam.
Zealey, W.J., 2009. Glacial, periglacial and glacio-volcanic structures on the Echus plateau, upper Kasei Valles. Planet. Space Sci. 57, 699-710.
Ziskind, G., Fichman, M., Gutfinger, C., 1995. Resuspension of particulates from surfaces to turbulent flows – review and analysis., J. Aerosol. Sci. 26, 613-644.
Zeeberg, J. 1998. The European sand belt in eastern Europe – and comparison of Late glacial dune orientation with GCM simulation results. Boreas 27, 127-139, doi:10.1111/j.1502-3885.1998.tb00873.x
Zuber, M.T., *et al.*, 2007. Density of Mars' South Polar Layered Deposits. Science, 137, 1718-1719, doi: 10.1126/science.1146995

Summary in English

In keywords: *glaciovolcanism · hyaloclastite (volcanic glass) · granular avalanching · grain-size analysis · porosity · ice · fracturing · wind · deflation · atmosphere dynamics · boundary layer · rolling · sand grains · Mars' surface environment · object-based image analysis · imbrication · wind direction*

Volcano-ice interactions have been studied since 1900. Subsequent refinements in our understanding of a volcano's response to the overlying ice mass have shown the complex dynamics of these eruption environments and interrelationships with material properties. Iceland is a prominent location where young landscape features such as *tuyas* (emergent sub-ice volcanoes that have melted upwards trough the ice) and *tindars* (subglacially formed ridges) can be studied. On planet Mars similar surface features have been identified as early as 1979 based on topographic features that are comparable to Icelandic tuyas and tindars. Landforms on Earth and Mars are composed of glassy breccias that are known as 'hyaloclastites' and these glasses are a unique material for these eruption environments. Recent spectral evidence from the surface of Mars shows that glaciovolcanic glass is highly abundant in the circumpolar aeolian sediments and the large sand sea on Mars. Substantial work on the environmental dynamics of these eruption products is still lacking for understanding the mechanisms and thresholds that control the erosion, mobility and modification rates of these materials on Mars. Subglacial eruptions in Iceland and on Mars have occurred under similar glaciostatic and water-ice dominated conditions. These parallels between the formation environments make terrestrial hyaloclastites an ideal physico-mechanical analogue material in field studies and experiments to study the behaviour of glassy sediments on Mars.

The aim of this dissertation was firstly to fill the gap in the knowledge of physical erosion mechanisms and transport thresholds of glaciovolcanic glass. Secondly, this dissertation aims to investigate if the role and effects of atmospheric pressure and wind flow in these geomorphological processes differ on Mars. The selection of a suitable analogue material was driven by the physico-mechanical properties as these are determined by the subglacial eruption environment (rather than by the geochemical or mineralogical properties). These criteria resulted in the selection of the rhyolitic particle population from the Bláhnúkur edifice in the Torfajökull area in Iceland. The edifice is globally the best-studied location which means that the well-characterised formation and material properties of the particle population give an ideal basis to the process-oriented studies in this dissertation.

The erosion characteristics of an edifice composed of hyaloclastites are studied in chapter 2. While the erosion of steep-sided slopes in the Grænagil gorge show that numerous processes drive the erosion of the overlying slope, only a few processes are dominantly reflected in the sedimentary record. The sediment influx of sedimentary landforms such as scree slopes is primarily driven by freeze-thaw erosion and deflation of the overlying slopes. Particle transport is therefore mostly confined to dry and cold conditions when discrete avalanches can form foot slopes with high angles of repose. These processes are also reflected in the stratigraphy of the scree slopes, as these show stratification (layering) from dry avalanching and depletion in small size fractions by winds. Deflation of small particles and effects of freeze-thaw cycles are therefore considered to be the prime mechanisms for the erosion of poorly cohesive glass deposits.

The insights at a landscape scale are complemented in chapter 3 with the effects that these erosion processes have on a particle scale. Samples from the Bláhnúkur hyaloclastites were used in experimental simulation to study transport-induced abrasion of sand-sized fractions. Abrasion from aeolian and gravity transport was simulated by subjecting 300-600 μm sized particles for 15 weeks to continuous rolling and avalanching, which corresponds to transport distances of 500-715 km. Physico-mechanical properties of larger particles, such as porosity and tensile strength, were measured using high-pressure mercury intrusion and uniaxial loading to understand the scale effects of freezing of water inside pores. Similar particles were simultaneously subjected to 10% of the yearly amount of freeze-thaw cycles. Damage to the material in the experiments was then related to the measured physico-mechanical properties of the glass. These analyses show that rolling of particles during avalanching and by wind is only marginally modifying sediments. Effects of ice nucleation during freeze-thaw cycles are more effective in modifying larger particles and it forms new, finer sediment textures. This fracturing was increased the amount of respirable particle sizes (<10 μm, or PM_{10}) which increases the risk to respiratory health hazards.

In chapter 4 and 5 the transition is made to the planet Mars in order to understand how the observed processes in Iceland influence the transport and modification of volcanic glass in the different surface conditions. Here, wind appears to play an important role. However, wind transport is very paradoxical on Mars. Wind speeds in the thin atmosphere are insufficient to frequently meet the threshold conditions for particle mobilisation, while planet-wide migration of dunes has been observed with speeds that are comparable to terrestrial dunes. The most common and lowest threshold for particle detachment and mobility is by rolling. Wind tunnel simulations in chapter 4 were therefore used to determine a realistic range for the rolling of sediments at fluid threshold conditions. Using removal experiments under different atmospheric pressures allowed the fitting of a semi-empirical model to describe these rolling processes. Different particle properties such as shape, specific surface area and density were measured to assess the dependence of the model on variations in material properties per particle fraction. Although no clear dependences were found, the analysis confirmed that particle density and diameter also control the detachment threshold for wind-induced rolling. This validated the use of the semi-empirical model for predicting the removal of volcanic glass by rolling on Mars. The model predicts an upper limit for rolling that falls within the range of known wind speeds on Mars. Rolling of sand grains may be further enhanced as the structure of the boundary layer promotes rolling in the Martian atmosphere. Rolling as a means of particle mobility is therefore proposed as an important precursor to saltation as it can contribute to the lowering of the threshold that is responsible for the observed migration of dunes.

Despite the detection of extensive glass deposits on Mars, little is known about the exact properties and the rate at which this material has been physically modified by exposure to the local environment. The initially angular grains in these glass-rich dune systems may have been gradually abraded over geologic time by the impacts of other grains during saltation, which produces well-rounded particles. Many of the sand grains observed by Marslanders in aeolian sediment indeed have these well-rounded shapes. The obtained streamlined shape leads to interesting phenomenon; sand grains can orient their long-axis to the local wind flow. This causes aeolian sediments to record near-surface wind flow patterns in a measurable entity known as the 'imbrication' of the sediment. In chapter 5 a new method is developed that makes it possible to measure sand grain orientation using Object-Based Image Analysis

(OBIA). In this process images are decomposed into smaller image segments. These segments are reclassified to delineate the boundaries of individual sand grains and allow the calculation of the orientation. This strategy was first applied to thin-sections (~30 μm thick microscope slides) of terrestrial inland dunes where pre-existing studies also determined palaeowinds with different techniques. Good agreement was found with the directions determined in these studies and it validated the applicability of the OBIA technique for other settings. The method was then applied to images of sand grains at three sites along the traverse of Mars Exploration Rover 'Spirit' trough the Columbia Hills. Winds in this area are highly variable due to topographic forcing, but inferred directions using the OBIA method give an additional type of data for reconstructing the genetic wind directions of aeolian bedforms in this area. Inferred wind directions correlate well to headings determined using oriented features such as dunes and ripples. As sand grains orient easily to the local wind flow, their orientation reflects the most recent high-energy wind events in an area. Detachment of particles by rolling and subsequent transport by saltation allows wind flow patterns to be measured at the smallest possible physical and temporal scale possible in the present surface environment on Mars.

Chapter 6 provides a synthesis of the preceding chapter in this dissertation in order to characterise the behaviour of volcanic glass on Mars. Dry environmental processes are dominant in regulating the weathering of glass deposits in Iceland and on Mars. Unlike Earth, effects of frost weathering are very limited as the atmospheric deposition of CO_2 ice in polar dunes systems lacks the expansive force of water during freezing. This makes erosion related to aeolian processes by far the most important for the modification on glass grains on Mars. Although the physico-mechanical properties of angular glass cause the wind thresholds for removal to be higher than for well-rounded sediments, both extremes in particle shape can be mobilised by rolling during high-energy wind events such as storms and thermal vortices. Cryogenic induration of dunes near the pole substantially reduces aeolian mobilisation to only a short period of the Martian year. Physical weathering of glass is therefore highly dependent on latitude. The possible presence of geologically young glaciovolcanic glass associated to north polar tuyas suggests that these materials may have retained their original properties due to frequent seasonal induration and lower rates of aeolian transport (and modification). Future geochemical surface studies on Mars may therefore be able to use these glasses for inferring subglacial formation conditions and reconstructions of past glaciers.

This dissertation has addressed several questions for understanding the environmental fate of glaciovolcanic glass on two contrasting planetary surfaces. At the same time, new niches for further work on the environmental characterisation of glaciovolcanic glasses have been identified to aid the future investigation of this part of the Martian particle population. From the aeolian studies in chapter 4 and 5 the most promising direction is the further amelioration of interparticle adhesion and the associated threshold response. Low-gravity wind tunnel studies may therefore shed important light on these aspects of the force balances for particle removal on Mars.

Samenvatting in het Nederlands

In steekwoorden: *glaciovulkanisme · hyaloklastiet (vulkanisch glas) · granulaire lawines · korrelgrootte analyse · porositeit · ijs · versplintering · wind · deflatie · atmosfeer dynamica · grenslaag · rollen · zandkorrels · Mars' oppervlakte milieu · object-gebaseerde beeldanalyse · imbricatie · windrichting*

Vulkaanijsinteracties worden al bestudeerd sinds het jaar 1900. De stapsgewijze verbetering van ons begrip van subglaciale vulkaanuitbarstingen in relatie tot de bovenliggende ijsmassa laat zien dat de complexe dynamiek belangrijke gevolgen heeft voor de materiaaleigenschappen van het gevormde materiaal. IJsland is een belangrijke locatie waar relatief jonge landschapsvormen zoals *tuyas* en *tindars* in het landschap voorkomen. Tuyas zijn kenmerkende tafelvormige bergen, die ontstaan doordat een subglaciale vulkaanuitbarsting door de gletsjer omhoog is gesmolten, terwijl tindars dit maar deels gedaan hebben en daardoor nu als heuvels herkenbaar zijn. Deze landschapvormen bestaan voor een groot deel uit glasrijke breccias die 'hyaloklastiet' worden genoemd. Dit glaciovulkanische glas wordt tijdens subglaciale vulkaanuitbarstingen gevormd waardoor het diagnostisch is voor dit unieke vormingsmilieu. Op de planeet Mars zijn vergelijkbare landschapsvormen waargenomen die veel kenmerken delen met de IJslandse tuyas en tindars. Recente spectrale meting van het Marsoppervlakte laten zien dat zandafzettingen rondom het Noordpoolgebied en zandzeeën in de noordelijke laaglanden op Mars voor een groot gedeelte bestaan uit glaciovulkanisch glas. Uitvoerig onderzoek naar de erosie van deze glasrijke zandafzettingen, transport van korrels en verandering van het materiaal ontbreekt. Deze karakterisering is belangrijk om te begrijpen hoe vulkanisch glas zich in het afwijkende oppervlaktemilieu van de planeet Mars gedraagt. Een interessant gegeven is dat de uitbarstingen op IJsland en Mars plaatsvonden onder vergelijkbare omstandigheden qua glaciostatische druk (de druk van de bovenliggende ijsmassa) en afkoeling van het magma door smeltwater van gletsjerijs. Deze parallellen maken het mogelijk om het vulkanische glas in IJsland als substituut voor het glas op Mars te gebruiken aangezien het vergelijkbare fysisch-mechanische eigenschappen heeft. Veldstudies en experimenten met dit aardse materiaal kunnen daarom nieuwe en potentieel belangrijke inzichten geven in het gedrag van vulkanisch glas op Mars.

Het doel van dit proefschrift is om dit gat in kennis aan te vullen, vooral daar waar nog weinig bekend is over de fysische verwering alsmede de drempelwaarden die het transport van dit type materiaal bepalen. Daarbij stelt dit proefschrift zich ook ten doel om de invloeden van de lage luchtdruk en lage zwaartekracht op Mars te karakteriseren in relevante geomorfologische processen. Hiertoe is eerst een glas op IJsland geselecteerd op basis van fysisch-mechanische eigenschappen die afkomstig en gedomineerd zijn door een subglaciale vulkaanuitbarsting (in tegenstelling tot een geochemisch- of mineralogisch georiënteerde selectie). Het geselecteerde rhyolitisch glas werd gevormd in de laatste ijstijd tijdens de uitbarsting van de Bláhnúkur vulkaan die gelegen is in het Torfajökull gebied in de zuidelijke centrale hooglanden in IJsland. Deze vulkaan is wereldwijd de best bestudeerde locatie van zijn soort en dit betekent dat de gekarakteriseerde vormings- en materiaaleigenschappen een goede uitgangspositie geven aan het procesonderzoek in dit proefschrift.

De erosie-eigenschappen van een subglaciale vulkaan die is opgebouwd uit glasrijke

afzettingen wordt bestudeerd in hoofdstuk 2. Alhoewel de erosie van de hellingen in de Grænagilkloof het gevolg is van verschillende processen, zijn er slechts een paar processen die hierbij een dominante rol vervullen. De flux van sediment die sedimentaire landschapseenheden vormt, bijvoorbeeld puinhellingen, bestaat vooral uit materiaal dat losgemaakt wordt tijdens vries-dooicycli en door deflatie (winderosie) van materiaal op de bovenliggende hellingen. Het transport van dit materiaal is vooral beperkt tot droge en koude omstandigheden waardoor individuele lawines van sediment zorgen voor een karakteristieke gelaagdheid en hoge rusthoeken van het sediment in de puinhellingen. Deflatie van fijnstof door de wind en de effecten van vries-dooi cycli zijn de belangrijkste mechanismen ten aanzien van de erosie van deze glasrijke en tevens slecht gecompacteerde hellingen.

De voorgaande inzichten op landschappelijke schaal worden in hoofdstuk 3 aangevuld met een studie naar de effecten van deze processen op de schaal van de zandkorrels zelf. Monsters van het Bláhnúkur hyaloklastiet zijn daarom gebruikt in experimenten om de schurende werking tussen korrels tijdens transport te meten. Transport door wind en zwaartekracht werd gesimuleerd door het materiaal gedurende vijftien weken continu te laten rondrollen in draaiende trommels; met een equivalente transportafstand van 500-715 km. Daarnaast werden fysisch mechanische eigenschappen van grotere brokstukken glas bepaald. Oppervlakteporiën van de glasbrokken werden gemeten aan de hand van kwikintrusie onder hoge druk en de breeksterkte werd bepaald op een trekbank. Hiermee was het mogelijk om de te begrijpen welke processen ten grondslag lagen aan de versplintering die werden gemeten in vries-dooi experimenten waaraan vergelijkbare brokstukken werden blootgesteld. De schade aan het materiaal was bijzonder laag na het gesimuleerde wind- en zwaartekrachttransport terwijl de gevolgen van vries-dooicycli aanzienlijk groter waren. Beide processen leiden in verschillende mate tot de vorming van nieuw sediment waaronder een fijnstoffractie (<10 μm, of PM_{10}). Dit fijne materiaal kan bij inademing schadelijke gevolgen hebben voor de gezondheid.

In hoofdstukken 4 en 5 wordt de overstap gemaakt naar de planeet Mars om te begrijpen welke rol de waargenomen processen op IJsland spelen in het transport en de modificatie van vulkanisch glas op Mars. Daar lijkt vooral een belangrijke rol te zijn weggelegd voor eolische (windgedreven) processen. Zandtransport door de wind is op Mars echter paradoxaal; de atmosfeer is te ijl om grootschalig zandtransport bij de gemiddelde dagelijkse windsnelheden toe te staan, terwijl er zandduinen worden waargenomen die migreren met snelheden die vergelijkbaar zijn met aardse zandduinen. De meest voorkomende en laagdrempeligste transportvorm van korrels door de wind is in de vorm van rollen. In hoofdstuk 4 worden windtunnelexperimenten gebruikt om realistisch drempelwaarden te bepalen waarbij vulkanisch glas door de wind op Mars in beweging gezet kan worden. Experimenten onder verschillende luchtdrukken maakten het mogelijk om een semi-empirisch model te ontwikkelen dat het wegrollen van korrels beschrijft. Per korreldiameter werden hiertoe verschillende korreleigenschappen gemeten zoals vorm, specifiek oppervlak en dichtheid om te bepalen hoe de nauwkeurigheid van het model werd beïnvloed door de natuurlijke variatie in deze korreleigenschappen. Deze gevoeligheidsanalyse bevestigde dat alleen de massadichtheid en diameter van de korrel de drempelwaarden voor het wegrollen beïnvloeden, en hiermee kon het model gevalideerd worden om zo het gedrag van rollende korrels op Mars te bepalen. Het model toont aan dat het zeer hoekige vulkanische glas op Mars onder de hedendaagse windsnelheden verplaatst kan worden. Dit rollen lijkt bovendien versterkt te worden door de structuur van de turbulente grenslaag van de ijle Marsatmosfeer.

Wegrollen van zand is daarom op Mars een belangrijke vorm van sedimenttransport. Het draagt bovendien bij aan het verlagen van de drempelwaarden waarbij het roltransport overgaat in de saltatieprocessen die zandduinen laten migreren.

Ondanks de detectie van vulkanisch glas op Mars is er weinig bekend over de exacte eigenschappen van vulkanische glaskorrels en daarmee ook de mate waarin het materiaal fysisch is veranderd door de blootstelling aan het heersende milieu. Het van oorsprong hoekige glas kan op geologische tijdschalen langzaam verweren naar afgeronde korrels als gevolg van de herhaaldelijke inslagen van zandkorrels tijdens windtransport. Veel zandkorrels die door Marsrovers zijn waargenomen in zandduinen hebben inderdaad dergelijke afgeronde vormen. Deze gestroomlijnde vorm leidt tot een bijzonder fenomeen; korrels kunnen zich met de langere lengteas oriënteren langs de richting van de locale windstroming. Dit zorgt ervoor dat eolisch sediment de lokale windrichting vastlegt in een meetbare eigenschap. In hoofdstuk 5 is een nieuwe methode ontwikkeld waarmeer het mogelijk is om deze oriëntaties te meten aan de hand van Object-Gebaseerde BeeldAnalyse (afgekort 'OBIA' in het Engels). In dit proces wordt een foto onderverdeeld in kleine beeldsegmenten. Deze beeldsegmenten kunnen vervolgens aan de hand van strikte regels geclassificeerd worden om de individuele zandkorrels te herkennen. Na het samenvoegen van de geclassificeerde segmenten ontstaan polygonen van de korrelomtrek waarmee de oriëntatie van de korrel kan worden berekend. Deze strategie werd eerste toegepast op slijpplaatjes (~30 μm dikke microscooppreparaten) van zandafzettingen in Duitsland waar andere studies met oudere microscooptechnieken de paleowindrichtingen al eerdere bepaald hadden. De OBIA techniek leverde vergelijkbare korreloriëntaties en windrichtingen op, waarmee de techniek breder toepasbaar wordt in andere omgevingen. De methode werd vervolgens ook toegepast op beeldmateriaal van zandkorrels dat door de Mars Exploration Rover 'Spirit' werd gemaakt tijdens de doorkruising van de Columbia Hills. De windrichtingen in deze regio zijn erg variabel als gevolg van topografische effecten, maar de metingen met de OBIA methode geven een nieuwe kijk op de atmosferische stroming die de zandafzettingen in dit gebied gevormd heeft. De afgeleide windrichtingen met de nieuwe methode kwamen goed overeen met de richtingen die afgeleid zijn uit de grootschalige oriëntatie van eolische landschapsvormen zoals duinen en windribbels. Doordat zandkorrels op Mars zich net als op aarde oriënteren naar de wind, is het mogelijk om met deze oriëntatie de windrichting van de meest recente stormen af te leiden. De oriëntatie van korrels maakt het daarom mogelijk om op de kleinst mogelijke schaal van het Marslandschap de windrichtingen te meten.

Hoofdstuk 6 geeft een synthese van de verschillende hoofdstukken in deze dissertatie om het gedrag van glas op Mars verder te karakteriseren. 'Droge' processen reguleren de erosie van glasafzettingen op IJsland en Mars. Het opvriezen van sediment rond de polen op Mars vindt echter plaats met CO_2-ijs. Doordat dit ijs niet dezelfde expansie-eigenschappen als water heeft, zal vorstverwering op Mars zeer gering zijn. Hierdoor heeft de wind op Mars een belangrijk aandeel in de erosie en modificatie van vulkanisch glas. De fysisch-mechanische eigenschappen zorgen er weliswaar voor dat de drempelwaarden voor transport en erosie boven die van goed afgerond zand zullen liggen, maar beide extremen kunnen tijdens stormen of thermische vortexen ('dust devils') verplaatst worden. De cryogene (ijsgedomineerde) oppervlakteverharding van duinen rond de polen zorgt voor een drastische reductie van windgedreven mobilisatie van dit sediment. Dit beperkt de modificatie van het glas door eolische processen tot een zeer korte ijsvrije periode in het Marsjaar. Fysische verwering is zodoende sterk breedtegraadafhankelijk. De mogelijke

aanwezigheid van geologisch jong glaciovulkanisch glas dat geassocieerd is met de vorming van recentere tuyas suggereert dat deze korrels hun oorspronkelijke materiaaleigenschappen deels hebben behouden. Dit is het gevolg van de langdurige immobilisatie die ontstaat door seizoenmatige variaties in ijsbedekking en als gevolg daarvan een veel lagere modificatie door de wind dan op breedtegraden waar geen ijs voorkomt. Geochemische metingen van dit glas door toekomstige Marslanders kunnen deze glassoorten daarom gebruiken voor reconstructies van gletsjers om zo de uitbarstingsomstandigheden ten tijde van de vorming van het glas af te leiden.

Dit proefschrift richt zich vooral op het beantwoorden van een aantal vragen om het gedrag van vulkanisch glas op twee contrasterende planeetoppervlakten nader te karakteriseren. Tegelijkertijd zijn er een aantal nieuwe onderzoeksniches te definiëren om het glas op Mars verder te karakteriseren. Uit de eolische studies in hoofdstuk 4 en 5 blijkt dat meer kennis nodig is om beter te begrijpen wat de rol is van de krachten tussen individuele korrels in transportprocessen en de daaruit voortvloeiden modificatie van het glas. Windtunnelexperimenten onder gereduceerde zwaartekracht kunnen daarom belangrijke inzichten geven in deze processen en daarmee het gedrag van zandkorrels op Mars.

Acknowledgements

It certainly helps that my field site is a Technicolor™ revelation in an otherwise monochromatic landscape. Many people are awestruck by the colourful vistas in Landmannalaugar and I wish I had more time during my stays to enjoy this tremendously exciting part of Iceland. Perhaps sometime in the near future I can wonder around a bit and enjoy the vistas as any 'first-time visitor' would do. With a thermos or two of well-brewed coffee, of course. Unfortunately, the damage has been done. Working on this PhD has changed my perception of this rugged Icelandic landscape for sure. It is one of the many 'occupational hazards' that we geomorphologists face. Each sand grain, glass shard and tuya now takes me on an adventure to Mars; although I also suspect there are still many new ones to come. The last time I left Torfajökull was on foot and with fond memories. I thank the Icelandic Environment Agency and the Icelandic Institute of Natural History for their permission to carry out fieldwork and collecting samples in the Fjallabak Nature Reserve. The area has recently been proposed as a future UNESCO world heritage site and I hope that the unique geology, nature and wildlife will be preserved for many generations of hikers and scientists to come.

I am indebted to various persons who have supported me in the preparation of this PhD dissertation and I want to take some time here to properly acknowledge them.

First I would like to thank my promotor Karsten Kalbitz, co-promotor Erik Cammeraat and IBED-director Peter van Tienderen for their support and vote of confidence to carry out this PhD research within the allotted time. A few words I want to dedicate to Erik in particular. We, "the students", know you as a 'field guy' with a passion for the science (and adventure) that is found in the field. You started this planetary adventure and have giving me the freedom to develop my own scientific interests and ideas. For this I owe you my deepest thanks.

Writing lies at the heart of any dissertation and this work was made a bit easier by the feedback and various discussions with my co-authors; Niels Anders, Thijs de Boer, Jochem Braakhekke, Erik Cammeraat, Marjo Mittelmeijer-Hazeleger, Emiel van Loon and Jon Merrison. I also thank the patience and diligence of my proofreaders for their feedback and contributions that helped to improve parts of this dissertation: Jaap van der Meer, Hester Jiskoot, Kenneth Rijsdijk, Chiara Cerli, Gillian Kopitte, Christiaan Eschauzier, Ellen Schuurink, Vivienne Hoyng-Geel and Wanda Remijn.

I have met or spoken with many people during my work on the various studies that comprise this dissertation. In no particular order I want to mention: Leo Hoitinga, Bert de Leeuw, Martine Hagen, Jan van Arkel (for his spectacular photography of volcanic glasses), Ruben Abellon (UV/VIS spectroscopy), Arjen Markus, Briony Horgan, Dave McGarvie, Hugh Tuffen, Jaqueline Owen, Peter Baxter, Jim Shelby (for his help with interpreting UV/VIS spectra) and George Scherer (for his notes on frost weathering and porosity). My field days in the pouring rain and under much rarer clear skies were made much more enjoyable by the hospitality and in company of Lilja-Rut Víðisdóttir and Helga Garðarsdóttir from Ferðafélag Íslands (Icelandic Hiking Association). Budgets were not approved for a field trip to Mars and images of Martian sand grains were therefore retrieved from NASA's PDS imaging archive. I kindly thank Susan LaVoi from the PDS Imaging Node and the NASA JPL lander imagery team for their support and suggestion for finding 'true north' on Mars.

From 2010-2012 I had the pleasure and privilege to work on the highly successful education programme 'Space Ship Earth', launched as part of the PromISSe mission of ESA astronaut André Kuipers. A core team of educators and scientists started in 2010 under the auspices of the Netherlands Space Office and we continued well into 2012 together with the education office of the Human Space Flight directorate from the European Space Agency to finalise the programme. Again in no particular order or preference I want to mention: Jack van Loon, Jasper Wamsteker, Wendy van den Putte, Hans Tuinenberg, Sander Koenen, Rob van den Berg, Hans van der Lande, Shamim Hartevelt, Nigel Savage, Elisabeth Celton, Anneke Le Floc'h, Jennifer Hordijk, Erwin van der Kroon, Rigo Kok, Leo Timmermans, Zeholy Pronk and those I might have forgotten. Thank you for the exciting times we shared during the development of Space Ship Earth ('Ruimteschip Aarde'), the PromISSe mission and the launch and operations of the 'EPO Convection' experiment on board the International Space Station.

I am bound to have forgotten to mention someone here, but you know who you are and my thanks also go to you.

Finally, mom and dad. You are doing your little share to make this planet a better place for those that have been less fortunate in their home situation. I know this foster care is demanding at times, but it also earns you the genuine respect of many. You are an inspiration and have been a great support during these busy times. Thank you.

Delft, June 2013

Curriculum Vitae

Sebastiaan de Vet was born on July 13th 1984 in the city of Maarssen. He finished his high-school at VWO-level with the profile 'science and technology' (N&T) at the Niftarlake College in 2003. From 2003-2004 he briefly studied Aerospace Engineering at the Technical University of Delft before he switched to a bachelor in Liberal Arts and Sciences (Bèta-Gamma) in Amsterdam. After majoring in Earth Sciences and his graduation in 2007 he continued with a master in Earth Sciences that took him to the fields in Tenerife and the high-alpine cordilleras of Peru. For his master thesis he studied the aeolian erosion of glass breccias in Iceland and independently set-up various experimental studies to translate the field processes in Iceland to conditions on planet Mars. These experiments covered wind tunnel simulations of particle removal and a Mars parabolic flight campaign to study granular avalanching. During his master he was awarded a research-grant by the education office of the European Space Agency (ESA) to study soil water repellency processes in microgravity during the 54th ESA parabolic flight campaign. In September 2010 he graduated *cum laud*e (with distinction) for his master degree with the specialisation 'Earth Surface Processes and Materials'. Before starting with his PhD research he briefly worked as programme manager of the bachelor and master Earth Sciences at the Education Service Centre of the University of Amsterdam.

During his master and PhD he (co)supervised 10 BSc theses, tutored several undergraduate workgroups in process-modelling and lectured on the physics, geology and hazards of impact cratering. He has been an educator for more than a decade at the astronomical observatory 'Sonnenborgh' where he tours and lectures the public on the history of science, astronomy and space flight. Space has become interwoven in his 'academic upbringing' since he flew his first experiment to the International Space Station in 2004 and when he contributed to the educational experiments on the PromISSe and NEEMO16 missions in 2012.

He is currently a member of the European Low Gravity Research Association (ELGRA), the IAVCEI/IACS Joint Commission on Volcano-Ice Interactions, the Dutch Space Association (NVR) and the Netherlands Platform for Planetary Research (NPP).

Appendices

Appendix A (chapter 1) – Tuyas at the North Pole (a) and the South Pole (b) on Mars. Solid black dots mark locations of tuyas identified by Ghatan and Head (2002), Hovius *et al.* (2008) and Fagan *et al.* (2010), while open circles are other volcanic features.

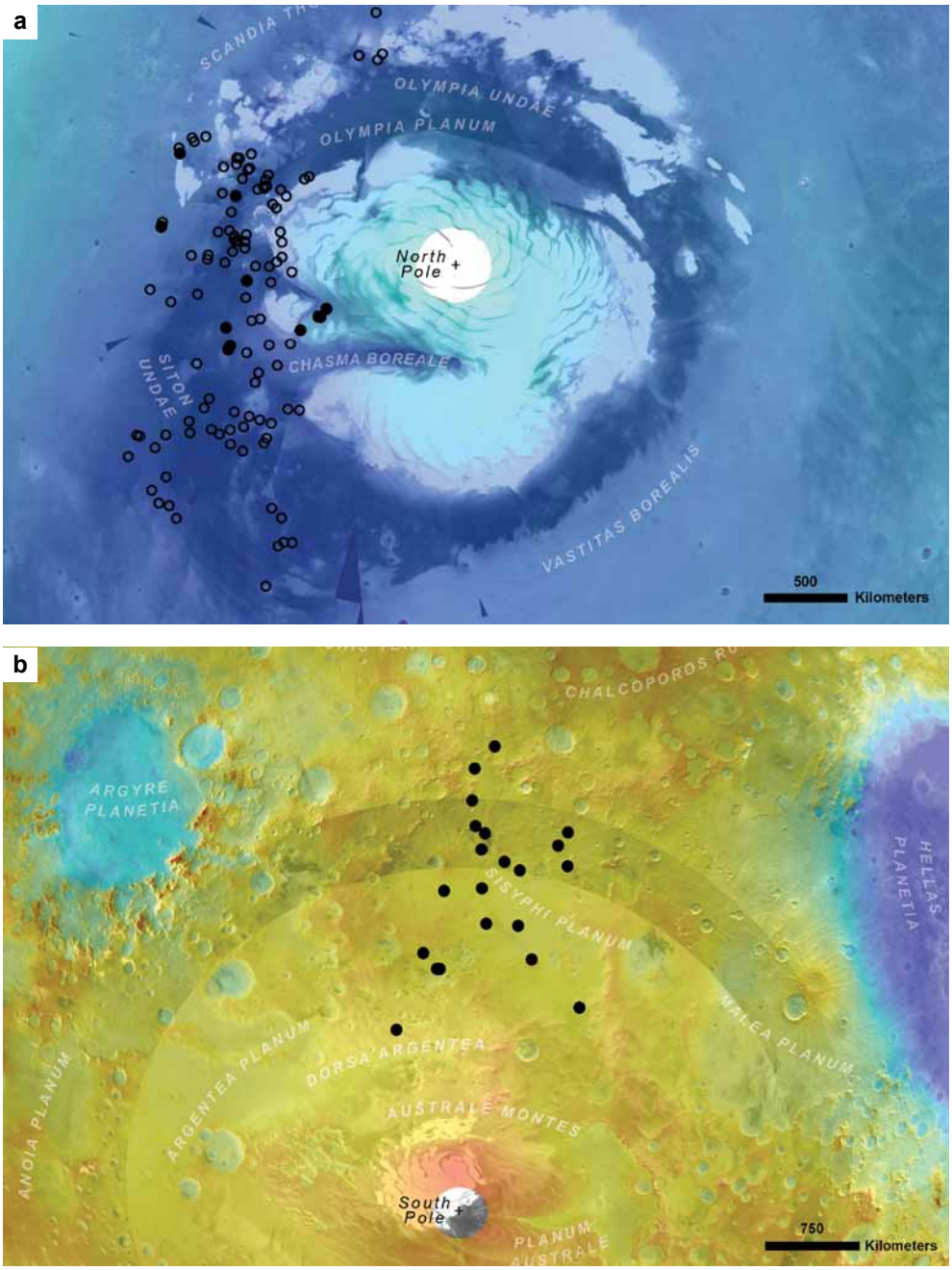

Appendix B (chapter 1) – Locations of putative glaciovolcanic surface features (based on: Cousins and Crawford, 2011). Black dots locate the general areas of tuyas formed by subglacial volcanism, tindars formed by magma intrusions in ice-rich subsurface layers and geomorphological features related to volcanism-induced catastrophic floods. Also see Fig. 3 for a geological time line. The map consists of MOLA topography data draped over MOC (red band) imagery of the Martian surface.

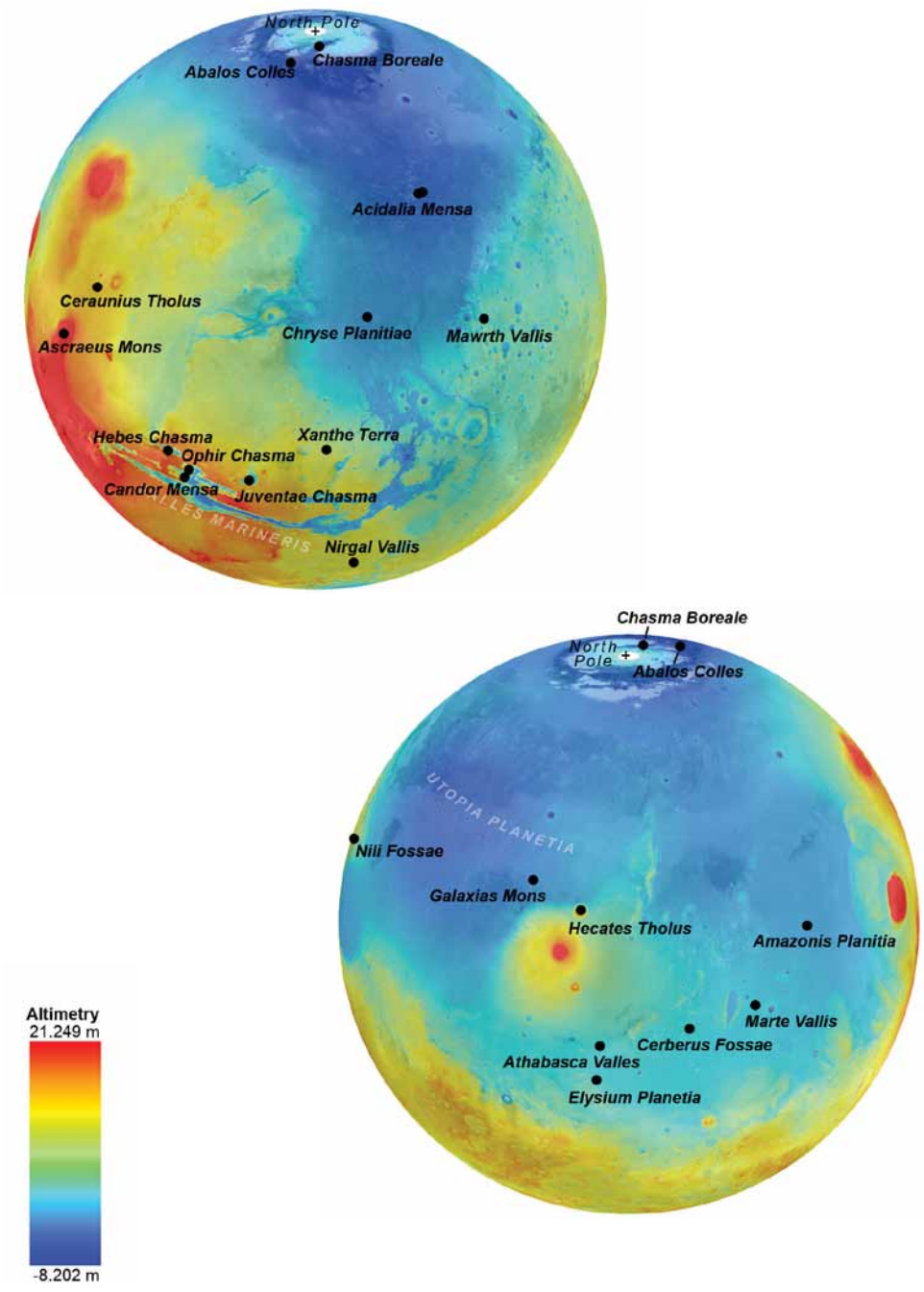

Appendix C (chapter 1) – Jökulhlaup-resembling catastrophic flood channels draining from tindar features inside Valles Marineris and surrounding area. Locations with signs for glaciovolcanism are marked by black dots and are similar to those listed in Fig. 3 and appendix B. Arrows represent flow directions of catastrophic floods. Similar to Earth, Amsterdam and surroundings are situated below 'sealevel'. The map consist of MOLA topography data draped over MOC imagery of the Martian surface.

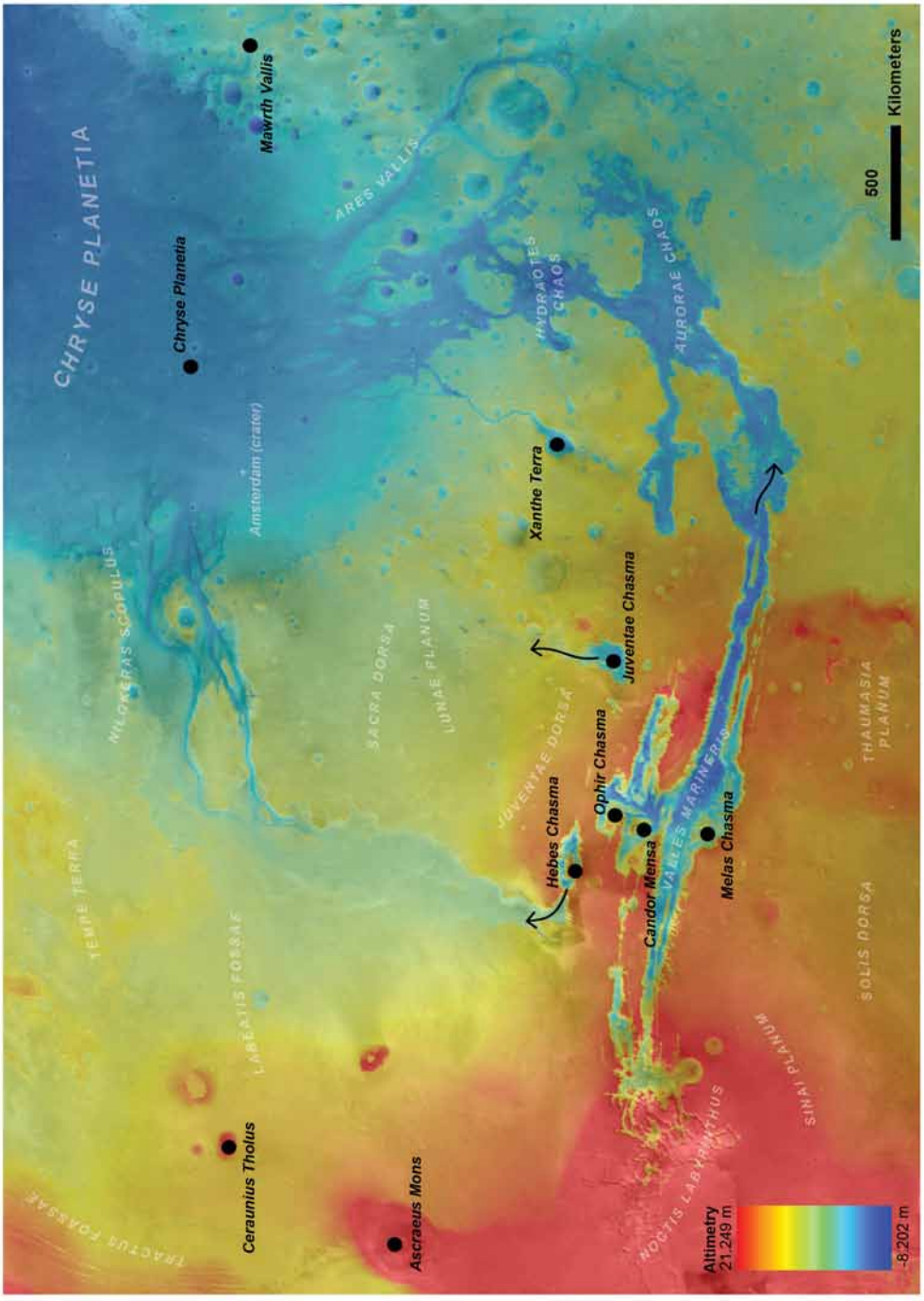

Appendix D (chapter 1 and 4) – A comparison of subglacial eruption pressures in Iceland and on planet Mars. Tuyas on Mars are shown as solid circles in appendix A, while those in Iceland are shown below (a) in map subsets from Fig.1. Summit heights were respectively obtained from Fagan *et al.* (2010) and those in Iceland from van Bemmelen and Rutten (1955) and Licciardi *et al.* (2007). The glaciostatic pressure (p_{ice}) is given by $p_{ice} = \rho_{ice} \cdot g \cdot h$, with ρ_{ice} the ice density, g the gravitational acceleration and h the overlying ice thickness. Maximum subglacial pressures in (b) were calculated using the summit heights for h and the gravitational acceleration (g) for each of the two planets (3.71 m s^{-2} for Mars, 9.81 m s^{-2} for Earth). Some caution is required as confining pressures are often lower than the ones calculated by the edifice summit heights. Nevertheless, pressures regimes are very comparable and indicate similar pressure controls on magma fragmentation on the two planets.

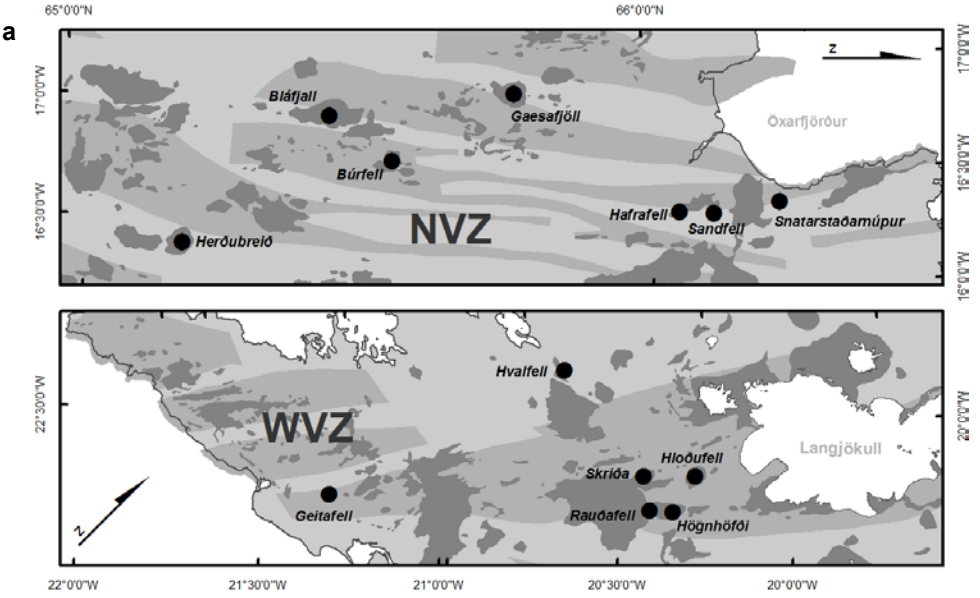

b

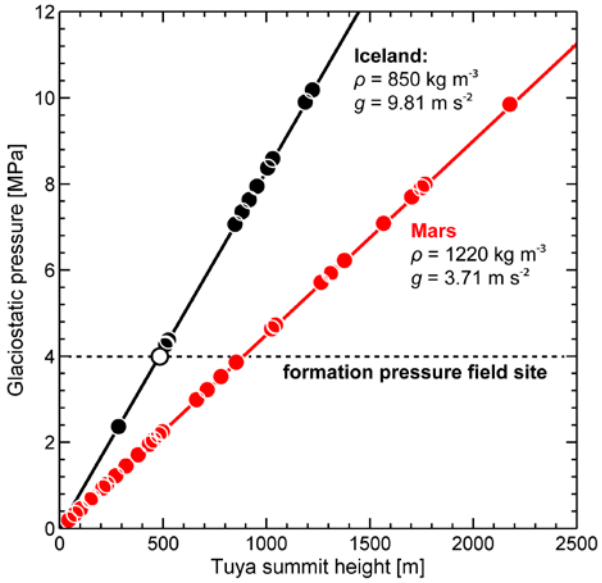

Appendix E (chapter 2) - Overview of the grain-size analyses and Sedigraph measurements of the samples of the ten source areas (RS-series, their locations are marked in Fig. 8) and of the twelve scree cone sediment samples (SC-series and their numbers corresponds to the positions marked in Fig. 10.

Sample	Moments (µm)				Percentile diameters (µm)			Fractions (%)				
	Mean	Sorting	Skewness	Kurtosis	D_{10}	D_{50}	D_{90}	Very coarse	Coarse	Medium	Fine	Very fine
RS1	252	290	1,60	4,43	88	199	1738	21,1	12,8	11,7	21,8	32,6
RS2	378	279	0,93	3,07	118	344	1038	11,0	21,9	32,5	23,4	11,2
RS3	314	276	1,05	3,45	110	354	1439	19,2	17,8	27,2	22,4	13,4
RS4	320	277	1,22	3,77	107	299	1237	15,3	15,9	27,3	27,2	14,4
RS5	346	306	0,95	2,85	102	359	1310	18,1	20,6	23,3	21,4	16,6
RS5	308	310	1,19	3,25	94	297	1461	20,6	16,8	17,3	22,8	22,4
RS7	291	241	1,45	4,74	94	242	888	8,4	13,7	26,5	29,2	22,2
RS8	282	229	1,43	4,84	93	239	824	7,8	13,4	27,0	28,1	23,7
RS9	296	316	1,18	3,24	101	391	1960	28,1	16,4	16,8	21,5	17,2
RS10	279	281	1,48	4,22	90	223	1280	15,7	13,8	17,3	26,0	27,2
SC1A	324	277	0,88	3,21	152	416	1606	23,2	19,3	30,7	19,7	7,2
SC1B	205	352	1,47	3,59	369	1138	30223	73,2	13,6	6,8	4,6	1,7
SC1C	411	309	0,51	2,34	184	498	1373	21,3	28,6	30,0	16,8	3,3
SC1D	431	400	0,18	1,47	429	966	2410	48,1	36,9	10,1	3,4	1,6
SC2A	294	318	1,02	3,00	163	643	2839	38,9	17,5	21,7	16,0	5,9
SC2B	206	341	1,43	3,57	366	1140	22621	71,1	14,6	8,6	4,1	1,6
SC2C	349	370	0,64	1,98	235	935	3205	47,2	25,3	16,2	9,3	2,0
SC2D	328	374	0,70	2,03	293	1082	4307	53,2	24,4	14,7	6,0	1,7
SC3A	431	306	0,48	2,38	196	487	1290	19,6	29,2	33,3	14,9	3,1
SC3B	369	321	0,68	2,40	150	508	1624	25,9	24,7	24,2	17,8	7,4
SC3C	327	312	0,89	2,78	129	482	1861	28,3	20,5	23,0	18,7	9,4
SC4C	286	300	1,09	3,33	159	524	2423	34,8	16,4	22,6	20,4	5,8

Appendix F (chapter 4) - Illustration of the Aarhus Wind Tunnel Simulator (AWTS-I) that was used for the wind tunnel simulations described in chapter 4. The turbulent flow wind tunnel is a recirculating design; the test section is enclosed inside a 3 m long pressure hull (a) that allows the atmospheric density to be varied by lowering the pressure, or by altering the ambient temperature. Removing the hull exposes the main flow section of the tunnel (b) that has a length of 1.5 m and a diameter of 0.4 m. Sample placement is possible through the porthole above the test section that, once closed off by a 5 cm thick optically clear polycarbonate plate, allows images to be taken of wind-induced particle removal.

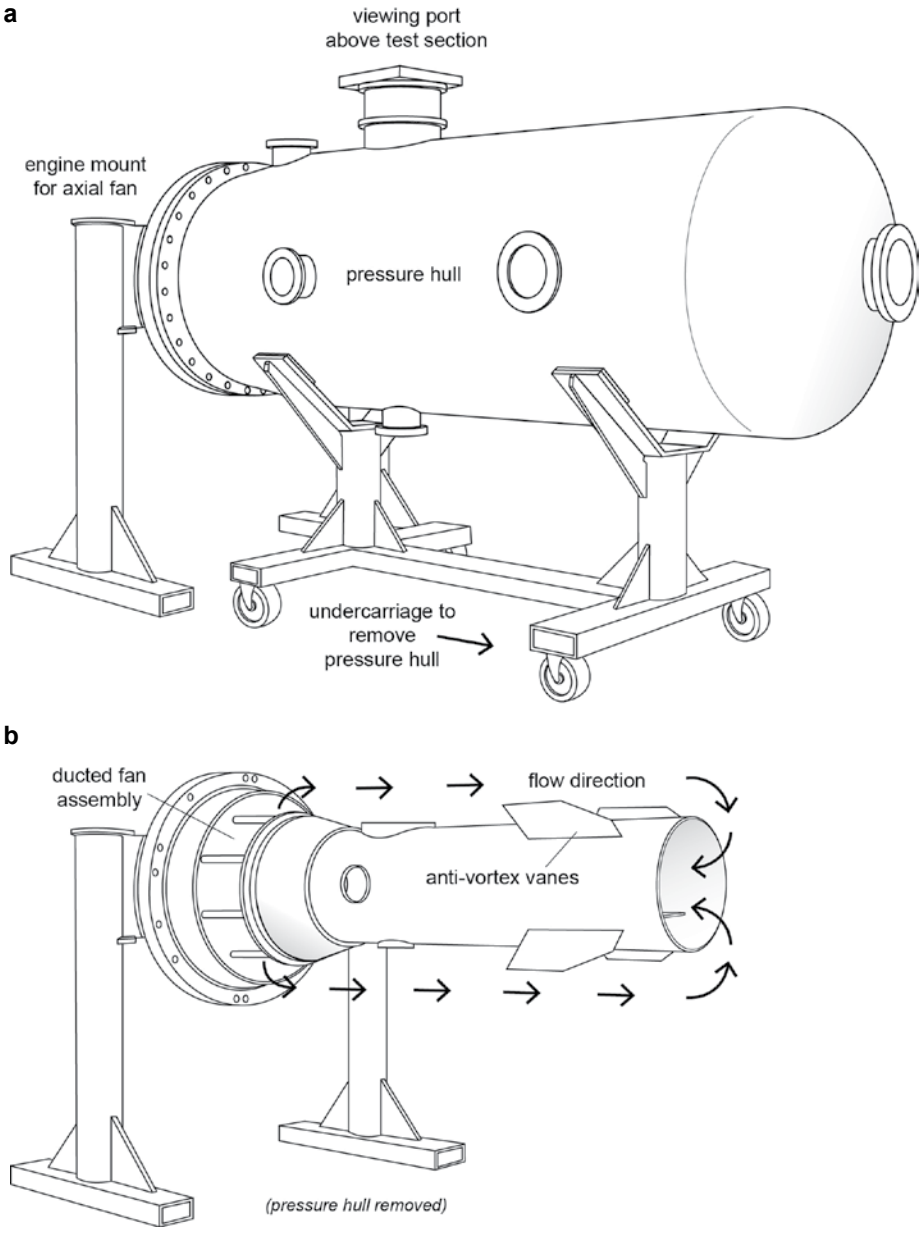

Appendix G (chapter 4) - Extracted shape parameters and standard deviations for describing the morphology of particles using segmentation in eCognition of 50 individual particles contained in microscope imagery. Mathematical descriptions of these shape properties are described in detail in Trimble (2011).

Shape property	Particle size (µm)							
	<63	63-75	106-150	150-212	212-300	300-425	425-600	850-1190
Asymmetry (mean)	0.44	0.38	0.41	0.38	0.35	0.42	0.32	0.31
std	0.20	0.21	0.20	0.18	0.15	0.17	0.15	0.16
Border index (mean)	1.51	1.46	1.44	1.56	1.40	1.51	1.43	1.39
std	0.24	0.23	0.20	0.24	0.16	0.21	0.15	0.12
Elliptic fit (mean)	0.70	0.74	0.77	0.74	0.81	0.78	0.80	0.82
std	0.11	0.12	0.10	0.10	0.08	0.08	0.07	0.06
Length/Width ratio (mean)	1.52	1.50	1.50	1.43	1.40	1.50	1.33	1.34
std	0.40	0.51	0.41	0.29	0.25	0.29	0.25	0.27
Radius incl. ellipse (mean)	1.39	1.36	1.31	1.39	1.26	1.31	1.29	1.24
std	0.15	0.16	0.13	0.17	0.12	0.10	0.12	0.08
Radius encl. ellipse (mean)	0.60	0.67	0.71	0.61	0.75	0.69	0.71	0.77
std	0.16	0.17	0.18	0.17	0.12	0.13	0.13	0.09
Rectangular fit (mean)	0.83	0.85	0.86	0.85	0.88	0.87	0.87	0.88
std	0.05	0.05	0.05	0.05	0.04	0.03	0.03	0.03
Roundness (mean)	0.79	0.69	0.61	0.78	0.51	0.61	0.58	0.48
std	0.27	0.31	0.29	0.27	0.21	0.20	0.21	0.15

Appendix H (chapter 4) - Data of the detachment thresholds and particle properties of the eight fractions studied in the wind tunnel simulations. Measured properties are given in most commonly used units. Chemical compositions of volcanic glass are given for of the average of 10 randomly selected particles per size fraction.

Parameter	Particle size (µm)							
	<63	63-75	106-150	150-212	212-300	300-425	425-600	850-1190
shear stress (240 mbar) [Nm^{-2}]	0.540	0.452	0.206	0.206	0.220	0.220	0.220	0.230
std	0.015	0.015	0.015	0.015	0.015	0.015	0.015	0.015
shear stress (480 mbar) [Nm^{-2}]	0.554	0.470	0.215	0.215	0.215	0.215	0.215	0.229
std	0.030	0.030	0.030	0.030	0.030	0.030	0.030	0.030
shear stress (920 mbar) [Nm^{-2}]	0.539	0.495	0.230	0.201	0.211	0.211	0.211	0.211
std	0.030	0.030	0.030	0.030	0.030	0.030	0.030	0.030
shear stress (1024 mbar) [Nm^{-2}]	0.535	0.445	0.214	0.185	0.199	0.199	0.190	0.190
std	0.033	0.033	0.033	0.033	0.033	0.033	0.033	0.033
skeletal density [g cm^{-3}]	2.3236	2.3195	2.3524	2.3602	2.3533	2.3248	2.3099	2.3381
std	0.0034	0.0034	0.0033	0.0041	0.0052	0.0089	0.0030	0.0040
Sa [m^2/g]	1.52	1.00	0.69	0.47	0.68	0.45	0.46	0.53
C [wt%]	-[b]	38.0 [a]	-[b]	26.2 [a]	11.1 [a]	25.3 [a]	27.0 [a]	-[b]
std	-[b]	3.0	-[b]	1.5	1.5	1.8	3.1	-[b]
N [wt%]	-[b]	1.7	-[b]	0.0	0.0	0.0	0.0	-[b]
std	-[b]	2.9	-[b]	0.0	0.0	0.0	0.0	-[b]

[a] *high C(wt%) is indicative for dissolved CO_2 in Bláhnúkur volcanic glasses (Denton et al., 2009)*
[b] *not measured*

appendix H (continued)

O [wt%]	-[b]	43.5	-[b]	46.0	51.7	46.5	45.0	-[b]
std	-[b]	2.4	-[b]	2.8	2.5	2.0	4.5	-[b]
Na [wt%]	-[b]	1.2	-[b]	2.2	2.8	2.4	2.1	-[b]
std	-[b]	0.3	-[b]	0.2	0.6	0.4	0.4	-[b]
Mg [wt%]	-[b]	0.7	-[b]	0.0	0.3	0.0	0.0	-[b]
std	-[b]	1.1	-[b]	0.0	1.0	0.0	0.0	-[b]
Al [wt%]	-[b]	2.0	-[b]	5.4	6.7	5.5	4.8	-[b]
std	-[b]	1.3	-[b]	0.4	1.5	0.5	0.8	-[b]
Si [wt%]	-[b]	8.6	-[b]	14.6	22.5	15.2	13.6	-[b]
std	-[b]	0.9	-[b]	1.6	2.0	1.8	3.1	-[b]
Cl [wt%]	-[b]	0.6	-[b]	0.3	0.0	0.3	0.3	-[b]
std	-[b]	0.1	-[b]	0.2	0.0	0.0	0.1	-[b]
K [wt%]	-[b]	1.1	-[b]	2.0	3.1	2.1	1.9	-[b]
std	-[b]	0.3	-[b]	0.3	0.8	0.4	0.6	-[b]
Ca [wt%]	-[b]	0.9	-[b]	0.3	0.2	0.2	0.2	-[b]
std	-[b]	1.7	-[b]	0.0	3.0	0.2	0.3	-[b]
Fe [wt%]	-[b]	1.6	-[b]	2.9	1.9	2.2	4.6	-[b]
std	-[b]	1.6	-[b]	4.6	2.8	2.5	6.5	-[b]

[b] *not measured*

Room for notes

Use these pages for making notes during reading, or during the defense of this dissertation.

Index

N

O

P

Q

R

S

T

U

V

W

X

Y

Z

Colophon

Cover design:
Višnja Ostojic (visnjaostojic.com)

Content layout:
Sebastiaan de Vet

Printed by:
GVO drukkers & vormgevers B.V., Ede, The Netherlands

Printed on FSC and PEFC certified paper.

Figures:
All figures and photos in this dissertation were made by the author using data obtained in the various presented studies. Some photos were taken on request of the author, or were used with permission of the following contributors:

J. van Arkel: p.11, 23, 51, 74
D. Bergmann: p.24-25
L.H. Cammeraat: p.39
NASA/ESA, NEEMO16 crew, p.85
NASA PSD imaging node: p.86, 96, 98
NASA/JPL/University of Arizona, p.110

Cover story:
Melting of glacial ice is of great importance during volcano-ice interactions for the explosive fragmentation of magma and the production of glaciovolcanic glass. The front cover shows a mixed-media artistic rendering of a melting glacial surface, caused by what appears to be a subglacial eruption located in the lower left-hand corner of the back cover.